



Pesko, Bogumila Katarzyna (2017) *Estimation of time since death using comparative proteomic and metabolomic approaches*. PhD thesis.

<http://theses.gla.ac.uk/8179/>

Copyright and moral rights for this work are retained by the author

A copy can be downloaded for personal non-commercial research or study, without prior permission or charge

This work cannot be reproduced or quoted extensively from without first obtaining permission in writing from the author

The content must not be changed in any way or sold commercially in any format or medium without the formal permission of the author

When referring to this work, full bibliographic details including the author, title, awarding institution and date of the thesis must be given

Enlighten:Theses  
<http://theses.gla.ac.uk/>  
theses@gla.ac.uk

# **Estimation of time since death using comparative proteomic and metabolomic approaches**

**Bogumila Katarzyna Pesko**

**BSc (Hons) MSc MRes**

**Submitted in fulfilment of the requirements for the  
Degree of Doctor of Philosophy**

**School of Life Sciences  
College of Medical, Veterinary and Life Sciences  
Institute of infection, Immunity & Inflammation  
University of Glasgow**

**May 2017**

## Abstract

The success of forensic investigation very often depends on the establishment of the correct timeline of events. In the investigation of fatalities, this depends greatly on the estimation of the time since death of the victim. Current methods lead to inaccurate results and depend greatly on the experience of the investigator. Pathologists estimate the time since death based on visual inspection of the bodies as well as body temperature measurement. Only very short post-mortem intervals (PMIs) can be evaluated with some degree of certainty.

This investigation used untargeted proteomic and metabolomic approaches to identify potential molecular markers (proteins, metabolites) which could help to quantify post-mortem changes and aid PMI estimation.

Animal models were used in the initial stages of the project. Aged beef meat (stored at 4°C for 13 days) and rat muscle samples (intact cadavers stored at ambient temperature for 3 days) were sampled at 24 h time intervals. In the final stages of the project, human tissue samples were collected at the Forensic Anthropology Centre at Texas State University (San Marcos, Texas). Muscle samples were collected at various times post-mortem from 6 different subjects over the period of two weeks. For the proteomics experiment, 0.5g of tissue was homogenized in extraction buffer consisting of urea, thiourea and 3-((3-cholamidopropyl) dimethylammonio)-1-propanesulfonate (CHAPS). Protein separation was carried out using two-dimensional gel electrophoresis. Protein identification was performed using liquid chromatography-tandem mass spectrometry. For the metabolomics experiment, 0.5g of tissue was homogenized in chloroform/methanol/water solution. The extracted samples were analysed using liquid chromatography-mass spectrometry as well as gas chromatography - mass spectrometry.

The investigation allowed the identification of potential biomarker candidates. The proteins of interest varied between the sampled mammals. However, myosin and actin appear as promising candidates for all three species. The metabolomics experiments yielded a large number of possible biomarker candidates. Both liquid and gas chromatography approaches were successfully

applied, pointing towards various compounds. Proteogenic amino acids were identified as main compounds of interest in all species using both methods.

The study has shown that both proteomic and metabolomic approaches can be successfully applied in forensic medical science and can help to find PMI markers. Using the untargeted approach gives the advantage of looking at a whole range of detected molecules and choosing the most appropriate ones for the task. Furthermore, the combination of these two approaches gives a deeper insight into the post-mortem biological processes. The biomarker candidates proposed in this study require further validation in a larger cohort of subjects.

# Table of Contents

Abstract.....	2
List of Tables.....	7
List of Figures.....	9
List of Equations.....	14
List of Accompanying Materials .....	15
Acknowledgement.....	17
Dedication.....	18
Author’s Declaration.....	19
Definitions/Abbreviations .....	20
1 INTRODUCTION .....	24
1.1 Human decomposition .....	24
1.2 Estimation of Post-mortem Interval (PMI) .....	25
1.2.1 Vitreous humour chemistry .....	27
1.2.2 Electrolytes.....	30
1.2.3 Creatinine.....	30
1.2.4 Amino acids.....	31
1.2.5 Biogenic amines.....	31
1.2.6 Adenosine triphosphate (ATP) .....	32
1.2.7 DNA/RNA .....	32
1.2.8 Metabolites .....	33
1.2.9 Proteins .....	34
1.2.10 Other markers .....	35
1.2.11 Examples of other methods.....	35
1.3 Muscle composition and structure .....	37
1.4 Proteomics.....	43
1.4.1 Proteomic techniques: gel-based vs. gel-free.....	44
1.4.2 Two-dimensional gel electrophoresis (2DE) .....	46
1.5 Metabolomics.....	49
1.5.1 Liquid Chromatography - Mass Spectrometry (LC-MS).....	53
1.5.2 Gas Chromatography - Mass Spectrometry (GC-MS) .....	56
1.6 Aims .....	58
2 METHODOLOGY .....	60
2.1 Sample collection.....	60

2.1.1	Beef.....	60
2.1.2	Rat .....	60
2.1.3	Human.....	61
2.2	Proteomic studies .....	64
2.2.1	Commonly used reagents.....	64
2.2.2	Protein extraction .....	64
2.2.2.1	Method development.....	64
2.2.2.2	Finalized protocol .....	67
2.2.3	Protein precipitation.....	67
2.2.4	Protein assay .....	68
2.2.5	Two dimensional gel electrophoresis (2DE).....	68
2.2.5.1	Gel preparation and casting .....	68
2.2.5.2	Protein separation - trial experiment .....	69
2.2.5.3	Finalised protein separation protocol .....	72
2.3	Metabolomics experiments.....	78
2.3.1	Sample preparation .....	78
2.3.2	Liquid Chromatography - Mass Spectrometry (LC-MS) analysis .....	79
2.3.3	Gas Chromatography - Mass Spectrometry (GC-MS) analysis .....	80
2.3.3.1	Preparation of calibrators, quality control standards (QC) and internal standards.....	80
2.3.3.2	Sample derivatisation .....	80
2.3.3.3	Sample analysis .....	81
2.3.3.4	Data analysis .....	81
2.3.4	Phenylalanine assay .....	83
2.3.4.1	Preparation of standards and reagents.....	83
2.3.4.2	Sample preparation .....	83
3	PROTEOMICS .....	89
3.1	Introduction .....	89
3.2	Methodology.....	90
3.3	Results .....	90
3.3.1	Beef tissue.....	90
3.3.2	Rat muscle.....	99
3.3.3	Human tissue.....	106
3.3.3.1	Subject selection .....	107
3.3.3.2	Subject 2.....	107
3.3.3.3	Subject 5.....	114
3.4	Discussion.....	118
3.5	Conclusion .....	125
4	METABOLOMICS (LC-MS) .....	126

4.1	Introduction .....	126
4.2	Methodology.....	127
4.3	Results .....	127
4.3.1	Beef tissue .....	128
4.3.1.1	Decomposition products .....	129
4.3.1.2	Amino acids.....	130
4.3.2	Rat tissue .....	133
4.3.2.1	Amino acids.....	135
4.3.2.2	Decomposition products .....	137
4.3.2.3	Other metabolites .....	138
4.3.3	Human tissue .....	139
4.3.3.1	Amino acids.....	140
4.3.3.2	Phenylalanine assay .....	143
4.3.3.3	Other metabolites .....	147
4.3.4	PMI calculations.....	150
4.4	Discussion .....	151
4.5	Conclusion .....	156
5	METABOLOMICS (GC-MS) .....	157
5.1	Introduction .....	157
5.2	Methodology.....	158
5.2.1	Peak identification, average response calculation and presentation for relative quantification .....	158
5.3	Results .....	159
5.3.1	Rat tissue .....	159
5.3.1.1	Amino acids.....	162
5.3.1.2	Other metabolites .....	166
5.3.2	Human tissue .....	169
5.3.2.1	Relative quantification .....	169
5.3.2.2	Absolute quantification.....	175
5.4	Discussion .....	185
5.5	Conclusion .....	191
6	GENERAL DISCUSSION.....	192
	Appendices .....	199
	List of References .....	201

## List of Tables

Table 1-1. Overview of mammalian decomposition. (Swann et al. 2010).....	25
Table 2-1. Basic information of the individuals included in the study. ....	62
Table 2-2. Experimental set up of the first trial 2DE experiment (beef tissue)..	70
Table 2-3. Example of an experimental set up of multiplex 2DE experiment (rat tissue). ....	70
Table 2-4. IEF instrument parameters (total time - 26 h).....	73
Table 2-5. Amino acid retention times and quantification ion used for concentration calculation. ....	82
Table 2-6. Volumes of the phenylalanine standard used to prepare the calibration curve. ....	84
Table 2-7. Volumes of reagents used to develop the assay. ....	84
Table 2-8. Tecan instrument settings used for fluorescence intensity measurement. ....	84
Table 2-9. Readings of the trial phenylalanine assay test.....	85
Table 2-10. The weight of tissue used for each subject and time point for the assay.....	86
Table 2-11. Layout of a 96-well plate showing the positions of all of the samples tested with the phenylalanine assay. ....	87
Table 3-1. Summary of the changes observed for proteins of interest at different time points. ....	91
Table 3-2. List of proteins of interest identified using a single multiplex 2DE experiment in beef tissue. ....	95
Table 3-3. List of proteins identified using a single multiplex 2DE experiment in rat muscle tissue. ....	102

Table 3-4. List of confidently identified proteins using a single multiplex 2DE experiment in human muscle tissue. ....	109
Table 4-1. List of all identified metabolites of interest in rat and human tissue. ....	128
Table 4-2. Phenylalanine assay reading of samples obtained from human subjects 2 and 5. ....	144
Table 4-3. The amount of phenylalanine present in the samples (subjects 2 and 5), calculated using the standard curve. ....	145
Table 4-4. The concentration of phenylalanine present in samples collected from subject 5. ....	146
Table 4-5. Sampling times for rat and human subjects included in this study as Post-Mortem Interval (PMI) and Cumulative Degree Hours (CDH). ....	151
Table 5-1. List of metabolites of interest as PMI biomarkers selected in rat tissue. ....	160
Table 5-2. Metabolites of interest selected in human tissue. ....	171
Table 5-3. Actual vs calculated concentrations of the calibrators. ....	183

## List of Figures

Figure 1-1. The hierarchy of muscle organisation. ....	38
Figure 1-2. A molecular view of muscle structure. ....	39
Figure 1-3. The organisation of the sarcomere. ....	40
Figure 1-4. Overview of the cross-bridge cycle. ....	42
Figure 1-5. Overview of a gel-based proteomics workflow (2DE). (Dhingra et al. 2005) .....	45
Figure 1-6. Overview of a shotgun workflow. (Ahmad & Lamond 2014).....	46
Figure 1-7. Gel analysis workflow (Decyder software). ....	48
Figure 1-8. Overview of an untargeted metabolomics approach workflow. ....	52
Figure 1-9. Basic components of a liquid chromatography (LC) system. ....	54
Figure 1-10. Basic components of a mass spectrometer. ....	55
Figure 1-11. Basic components of gas chromatography (GC) system. ....	57
Figure 2-1. Rat muscle anatomy. ....	61
Figure 2-2. Human leg anatomy. ....	62
Figure 2-3. Scanned images of fluorescently labelled samples. ....	66
Figure 2-4. An example of DiGE and preparative gels for the same sample. ....	71
Figure 2-5. Diagram illustrating the two-dimensional gel electrophoresis protocol. ....	74
Figure 2-6. Example of a Mascot search results page. ....	77
Figure 2-7. An example of Mascot search result, showing a list of matched peptides. ....	78
Figure 2-8. Image showing the observed colour change in the trial phenylalanine assay. ....	85
Figure 2-9. Images representing already developed phenylalanine assay. ....	88

Figure 3-1. Image of a DiGE gel showing the proteins of interest and their corresponding spot numbers (beef).....	94
Figure 3-2. Proteins of interest identified through 2DE experiments in beef tissue. ....	96
Figure 3-3. Comparison of images obtained for all of the investigated beef samples. ....	98
Figure 3-4. Image of a DiGE gel showing all of the 46 proteins of interest and their spot numbers (rat tissue). ....	101
Figure 3-5. Graphs representing changes in proteins identified as myosin-binding protein C.....	103
Figure 3-6. Graphs illustrating differences in trends between same proteins...	103
Figure 3-7. Representation of the change in spot abundance in gels with different PMI. ....	104
Figure 3-8. Proteins of interest identified through 2DE experiment in rat tissue. ....	106
Figure 3-9. Image of a DiGE gel showing all of the 45 proteins of interest and their spot numbers (human tissue, subject 2). ....	108
Figure 3-10. Proteins of interest identified through 2DE experiment in human tissue (subject 2). ....	110
Figure 3-11. Overview of the two types of protein found in all of the investigated species. ....	112
Figure 3-12. Protein sequence alignment of alpha-actin identified in three different species.....	113
Figure 3-13. Image of a DiGE gel showing all of the 78 proteins of interest and their spot numbers (human tissue, subject 5). ....	115
Figure 3-14. Proteins of interest identified through 2DE experiment in human tissue (subject 5). ....	116

Figure 3-15. Graphs representing change in protein abundance of spots identified as actin and tropomyosin in human tissue (subject 5). .....	117
Figure 3-16. General representation of how molecular weight and pH are distributed in a standard 2DE gel. ....	121
Figure 4-1. Examples of metabolites identified in trial beef study. ....	129
Figure 4-2. Decomposition products identified in beef tissue. ....	130
Figure 4-3. Patterns of change observed in the identified amino acids (beef tissue). ....	131
Figure 4-4. Graph representing the classes of compounds identified through the pHILIC method in rat tissue. ....	134
Figure 4-5. Graph representing the classes of compounds identified through the HILIC method in rat tissue. ....	134
Figure 4-6. Change in levels of eleven amino acids with increasing time since death in rat tissue. ....	136
Figure 4-7. Amino acids which show similar instrument response for two rats sampled at the same PMI. ....	137
Figure 4-8. Patterns of change of identified decomposition products with increasing time since death in rat tissue. ....	138
Figure 4-9. Metabolites that increase in rat tissue with increasing PMI. ....	139
Figure 4-10. An example of how the levels of a single metabolite (leucine) change over time for all of the investigated subjects. ....	140
Figure 4-11. Amino acids which show similar trend of increase over time for different subjects at the same PMI. ....	142
Figure 4-12. Amino acids which show similar trend of increase over time for three different subjects at the same PMI. ....	143
Figure 4-13. Graph representing the standard curve for the phenylalanine enzymatic assay. ....	144

Figure 4-14. Comparison of phenylalanine levels measured using two different methods (subject 5).....	146
Figure 4-15. Comparison of phenylalanine levels measured using two different methods (subject 2).....	147
Figure 4-16. Graphs showing PMI changes in human cadavers of levels of metabolites of interest (n-acetylneuraminate, 1-methylnicotinamde, choline phosphate, xanthine and uracil). ....	149
Figure 5-1. Comparison of TICs obtained from analysis of rat tissue samples collected at each time point. ....	161
Figure 5-2. Comparison of selected peaks in the TIC's of samples collected at each time point (rat tissue).....	162
Figure 5-3. Change in levels of thirteen proteogenic amino acids with increasing time since death in rat tissue. ....	163
Figure 5-4. Change in levels of Alanine detected using two different methods, GC-MS (a) and LC-MS (b).....	164
Figure 5-5. Change in levels of non-proteogenic amino acids of interest with increasing time since death in rat tissue. ....	165
Figure 5-6. Non-proteogenic amino acids of interest compared with LC-MS results. ....	165
Figure 5-7. Metabolites that increased in rat tissue with increasing PMI. ....	167
Figure 5-8. Adenine showed a decreasing trend in rat tissue with increasing PMI. ....	167
Figure 5-9. Comparison of changes in metabolites of interest based on GC-MS and LC-MS results. ....	168
Figure 5-10. Trends of change of the six metabolites of interest for subjects 2, 3, 5 and 6. ....	172
Figure 5-11. Metabolites showing increasing trend with PMI for subject 4. ....	172

Figure 5-12. Levels of leucine detected in human tissue by GC-MS.....	174
Figure 5-13. Levels of leucine detected in human tissue by LC-MS. ....	174
Figure 5-14. Extracted ion chromatograms of selected amino acid standards. .	176
Figure 5-15. Graph representing the pooled standard response across the batch. .....	179
Figure 5-16. The responses of internal standards shown across the whole batch (batch 1). ....	181
Figure 5-17. The responses of internal standards shown across the whole batch (batch 2). ....	182
Figure 5-18. Comparison of results obtained with absolute and relative quantification. ....	184
Figure 5-19. Scheme showing two reactions involved in cysteine synthesis (Kanehisa 1995). ....	186

## List of Equations

Equation 4-1. Formula used to calculate the concentration of phenylalanine in the sample.....	145
---	-----

## List of Accompanying Materials

### Appendices

- I. Supplementary data: List of proteins identified in the trial proteomics experiment (beef tissue) - Excel spreadsheet
- II. Supplementary data: List of proteins identified in the second proteomics experiment (beef tissue) - Excel spreadsheet
- III. Supplementary data: List of proteins identified in the 2DE proteomics experiment (rat tissue) - Excel spreadsheet
- IV. Supplementary data: List of proteins identified in the 2DE proteomics experiment (human tissue, subject 2) - Excel spreadsheet
- V. Supplementary data: Metabolomic dataset comparing all beef samples collected at various times post-mortem (LC-MS, pHILIC separation) - IDEOM macro-enabled spreadsheet
- VI. Supplementary data: Metabolomic dataset comparing all beef samples collected at various times post-mortem (LC-MS, HILIC separation) - IDEOM macro-enabled spreadsheet
- VII. Supplementary data: Metabolomic dataset comparing all rat samples collected at various times post-mortem (LC-MS, pHILIC separation) - IDEOM macro-enabled spreadsheet
- VIII. Supplementary data: Metabolomic dataset comparing all rat samples collected at various times post-mortem (LC-MS, HILIC separation) - IDEOM macro-enabled spreadsheet
- IX. Supplementary data: Metabolomic dataset comparing all samples collected from subject 1 (LC-MS, pHILIC separation) - IDEOM macro-enabled spreadsheet
- X. Supplementary data: Metabolomic dataset comparing all samples collected from subject 1 (LC-MS, HILIC separation) - IDEOM macro-enabled spreadsheet
- XI. Supplementary data: Metabolomic dataset comparing all samples collected from subject 2 (LC-MS, pHILIC separation) - IDEOM macro-enabled spreadsheet
- XII. Supplementary data: Metabolomic dataset comparing all samples collected from subject 2 (LC-MS, HILIC separation) - IDEOM macro-enabled spreadsheet
- XIII. Supplementary data: Metabolomic dataset comparing all samples collected from subject 3 (LC-MS, pHILIC separation) - IDEOM macro-enabled spreadsheet

- XIV. Supplementary data: Metabolomic dataset comparing all samples collected from subject 3 (LC-MS, HILIC separation) - IDEOM macro-enabled spreadsheet
- XV. Supplementary data: Metabolomic dataset comparing all samples collected from subject 4 (LC-MS, pHILIC separation) - IDEOM macro-enabled spreadsheet
- XVI. Supplementary data: Metabolomic dataset comparing all samples collected from subject 4 (LC-MS, HILIC separation) - IDEOM macro-enabled spreadsheet
- XVII. Supplementary data: Metabolomic dataset comparing all samples collected from subject 5 (LC-MS, pHILIC separation) - IDEOM macro-enabled spreadsheet
- XVIII. Supplementary data: Metabolomic dataset comparing all samples collected from subject 5 (LC-MS, HILIC separation) - IDEOM macro-enabled spreadsheet
- XIX. Supplementary data: Metabolomic dataset comparing all samples collected from subject 6 (LC-MS, pHILIC separation) - IDEOM macro-enabled spreadsheet
- XX. Supplementary data: Metabolomic dataset comparing all samples collected from subject 6 (LC-MS, HILIC separation) - IDEOM macro-enabled spreadsheet
- XXI. Supplementary data: Metabolites of interest detected in rat tissue using the GC-MS approach - Excel spreadsheet
- XXII. Supplementary data: Metabolites of interest detected in human tissue using the GC-MS approach - Excel spreadsheet

## Acknowledgement

Firstly, and most importantly, I would like to thank my parents Barbara and Stanislaw Pesko, who have continuously supported me throughout the years and did everything in their power to help me achieve this goal. I could not have done it without you. I would also like to thank the rest of our family; all of you have been supporting me throughout my time in Glasgow.

Najpierw, chciałabym szczególnie podziękować moim rodzicom Barbarze i Stanislawowi Pesko, którzy bezustannie wspierali mnie przez lata i czynili wszystko co w ich mocy, aby pomóc mi osiągnąć ten cel. Bez was nie dałabym rady. Chciałabym również podziękować reszcie naszej rodziny, która wspierała mnie podczas mojego pobytu w Glasgow.

Secondly, I would like to thank all of my supervisors Dr Richard Burchmore, Dr Karl Burgess and Dr Hazel Torrance. Thank you all for your time, support and patience. You have consistently helped me throughout this PhD, especially at times when I doubted myself.

I would especially like to thank Dr Mark McLaughlin from the Veterinary School at the University of Glasgow and Dr Daniel Wescott from FACTS at Texas State University. Thanks to your help I was able to source samples which were crucial for this project and allowed me to take it much further than I anticipated.

I would also like to thank Dr Stefan Weidt, who patiently answered hundreds of my questions and helped me numerous times with software and instrumentation, Suzanne McGill, Alan Scott, Lorraine Brown and Dr Christina Naula for their help, support and encouragement, our small group of Polyomics PhD students: Laurence Stipetic, Jennifer Haggarty and James Newton, as well as Lauren Meckel from Texas State University - it was great working with you guys.

Finally, I would like to thank the Engineering and Physical Sciences Research Council (EPSRC) which funded the project, Glasgow Polyomics where I have carried out my research and Doctoral Training Centre in Technologies at the interface between Engineering and the Physical Sciences and the Life Sciences (previously Cell and Proteomic Technologies) which made this project possible.

## **Dedication**

I would like to dedicate this thesis to my parents.

Chcialabym zadedykowac te prace moim rodzicom.

## **Author's Declaration**

I declare that this thesis has been written by myself. I declare that, except where specific reference is made to the contribution of others, this dissertation is the result of my own work and has not been submitted in any previous application for a higher degree at the University of Glasgow or any other institution.

Signature:

Printed name: Bogumila Katarzyna Pesko

## Definitions/Abbreviations

$^1\text{H}$  NMR -  $^1\text{H}$  nuclear magnetic resonance spectroscopy

2DE - two-dimensional gel electrophoresis

$^{31}\text{P}$  MRS -  $^{31}\text{P}$  magnetic resonance spectroscopy

3-MT - 3-methoxytyramine

%CV - coefficient of variation

ADD - accumulated degree days

ADP - adenosine-5'-diphosphate

AMP - adenosine-5'-monophosphate

APCI - atmospheric pressure chemical ionisation

APS - ammonium persulfate

ATP - adenosine triphosphate

BSA - bovine serum albumin

CaMKII - calmodulin-dependent kinase II

CDH - cumulative degree hours

cDNA - complementary DNA

CHAPS - 3-((3-cholamidopropyl) dimethylammonio)-1-propanesulfonate

CI - chemical ionisation

CnA - calcineurin A

COD - cause of death

CSF - cerebrospinal fluid

CT - computed tomography

cTnI - cardiac troponin I

cTnT - cardiac troponin T

DIGE - difference gel electrophoresis

DNA - deoxyribonucleic acid

DTT - 1,4-dithiothreitol

EI - electron ionisation

ELISA - enzyme-linked immunosorbent assay

emPAI - exponentially modified protein abundance index

ESI - electrospray ionisation

FACTS - Forensic Anthropology Centre at Texas State University

FasL - fas ligand

fTMA - free trimethylammonium

GABA - gamma aminobutyric acid

GC - gas chromatography

GC-MS - gas chromatography-mass spectrometry

GSH - glutathione

GSW - gunshot wound

h - hours

HILIC - hydrophilic interaction chromatography

HMDB - the Human Metabolome Database

HMGB1 - high mobility group box-1 protein

HPLC - high performance liquid chromatography

HSP - heat shock protein

Hx - hypoxanthine

HxR - inosine

IEF - isoelectric focusing

IMP - inosine-5'-monophosphate

IPG - immobilised pH gradient

KEGG - the Kyoto Encyclopedia of Genes and Genomes

LC - liquid chromatography

LC-MS - liquid chromatography-mass spectrometry

m/z - mass to charge ratio

MALDI - matrix-assisted laser desorption/ionisation

MARCKS -myristoylated alanine-rich C-kinase substrate

MCP - multicatalytic proteinase complex

miRNA - micro RNA

MOWSE - molecular weight search

mRNA - messenger RNA

MS - mass spectrometry

MS/MS - tandem mass spectrometry

MSTFA - N-methyl-N-(trimethylsilyl) trifluoroacetamide

MW - molecular weight

NADH - nicotinamide adenine dinucleotide (reduced)

NIST - the National Institute of Standards and Technology

NPN - non-protein nitrogen

NWS - National Weather Service

P<sub>i</sub> - inorganic phosphorus

pI - isoelectric point

PM -post-mortem

PMI - post-mortem interval

PP2A - protein phosphatase 2A

Prep gel - preparative gel

PTEN - phosphate and tensin homologue detected chromosome 10

QC - quality control

RNA - ribonucleic acid

RT - retention time

RT-PCR - real time polymerase chain reaction

SDS - sodium dodecyl sulfate

SDS-PAGE - sodium dodecyl sulfate polyacrylamide gel electrophoresis

SEB - strip equilibration buffer

SIDS - sudden infant death syndrome

TBS - total body score

TEMED - N,N,N',N'-Tetramethylethylenediamine

TIC - total ion chromatogram

TMA-N - trimethylamine-nitrogen

TMCS - trimethylchlorosilane

TMS - trimethylsilyl group

TnT - troponin T

UPLC/Q-TOF MS - ultra performance liquid chromatography coupled with quadrupole time-of-flight mass spectrometry

VOC - volatile organic compound

X - xanthine

# 1 INTRODUCTION

## 1.1 Human decomposition

Decomposition begins rapidly after death and is driven by the process of autolysis. Once there is no more oxygen delivered to tissues, levels of carbon dioxide increase in the blood, pH decreases and waste products begin to accumulate, poisoning the cells. The integrity of lipid membranes is disrupted once there is insufficient energy to maintain transmembrane ion gradients and cellular and subcellular organisation is corrupted. Proteolytic enzymes are no longer controlled by sequestration and start degrading proteins. During this process the body cools down to ambient temperature (algor mortis), blood settles in lower parts of the body, which causes skin discolouration (livor mortis) and muscles become stiff due to increased acidity and depletion of ATP (rigor mortis). Eventually, putrefaction begins, where soft tissues are destroyed due to microbial action (Gill-King 1997). Decay is a continuous process which is inherently disorder; however, many studies have attempted to classify mammalian decomposition into certain stages. Various numbers of distinctive stages were proposed, varying between 1 and 9 (Goff 2009), but discrimination of 4 main stages seems to be the most popular (Swann et al. 2010; Vass 2011). These 4 stages include fresh, bloated, active decay and dry phases of decomposition. Table 1-1 describes these stages in more detail. Human decomposition is a complicated process, subject to many influencing factors, which make it very difficult to relate the stage of the decomposition to the time that passed since death occurred. Nevertheless, living tissue is highly organised and is protected from microbial activity by the immune system. Thus the early stages of decomposition (autolysis) result from the activity of endogenous processes such as proteolysis, and are followed in later stages by the activity of exogenous players, such as bacteria and fungi (putrefaction).

**Table 1-1. Overview of mammalian decomposition. (Swann et al. 2010)**  
 Permission to reproduce this table has been granted by Elsevier publishing company,  
 license Number: 3946500286695.

Stage of decomposition	Description
Fresh	Commences immediately after death Autolysis Fluid filled blisters on the skin, skin slippage Marbling of skin due to livor mortis
Bloating	Putrefaction - destruction of soft tissues by microorganisms Greenish discolouration of the skin Gas and fluid accumulation followed by purging Anaerobic fermentation
Active decay	Bloating has ceased Skin usually broken in one or more places Rapid leaching from body Large numbers of aerobic and anaerobic bacteria Extensive insect activity Possible carnivore activity Collapse of abdominal activity Loss of internal organs through insect activity or autolysis Possible adipocere formation
Dry	Diagenesis No carrion fauna remaining Small amount of decaying tissue Mummification of remaining skin Bone exposure and skeletonisation

## 1.2 Estimation of Post-mortem Interval (PMI)

Estimation of the time of death is central to the course of many forensic investigations. Knowing when death occurred may help to clarify the circumstances of a death and to assess the alibis of any potential suspects (Kaliszan et al. 2009). However, estimation of the post-mortem interval (PMI) may only be accurate up until 24-48 hours post-mortem (Fatteh 1973). Currently used methods include temperature measurement (algor mortis), assessment of rigor mortis, lividity (livor mortis) and morphological changes of the body (Swift 2006). The first description of body temperature changes as a means of time of death estimation was published by Rainy in 1868 (Rainy 1868). This method has been successfully applied in forensic cases over the years; however, its usefulness is limited to a very short PMI before the temperature of the body equilibrates with the temperature of the surroundings. Furthermore, it has very

little use in places with high average temperatures, as the body temperature can increase after death. Similarly to algor mortis, rigor mortis and livor mortis reach a steady state before 48 h after death (Ith et al. 2002). Observation of rigor mortis also dates back to the 19<sup>th</sup> century where it was first investigated by Pierre-Hubert Nysten (Swift 2006). Rigor mortis describes a state of constant muscle contraction, which is caused by the depletion of ATP source in post-mortem tissue (this phenomenon will be described in detail in section 1.3 of this chapter). Living muscle contracts through the formation of the actin-myosin complex, which requires ATP to release the contraction. After death ATP is no longer produced and the actin-myosin complex cannot be broken - muscles remain contracted, up until the process of autolysis starts degrading the muscle tissue (Henssge et al. 2002). Livor mortis, or otherwise hypostasis, describes the purplish-blue discolouration of the skin resulting from the cessation of the blood circulation and gravitational settling of the blood in the lower parts of the body. However, it will not form in cases where the deceased suffered a significant blood loss (Perper 2006). The final method of time since death estimation is the assessment of morphological changes of the body. This method relies solely on the experience and knowledge of the forensic investigator. Furthermore, it can be quite subjective as the rate of decomposition depends on many ante mortem factors (as, for example, the health of the deceased) as well as the circumstances surrounding death and the environmental conditions in which the body had been discovered (Swift 2006).

Four main factors can affect the rate of the decomposition process: temperature, moisture, pH and partial pressure of oxygen (Clark et al. 1997). The pH determines the type of chemical reactions that occur during decomposition. An alkaline environment is usually created when aerobic surface decomposition takes place and an acidic environment is formed when anaerobic decomposition occurs (due to bacterial fermentation). Lack of oxygen slows down the decomposition process. Other minor factors affecting the rate of decomposition include the presence or lack of clothing, injuries, carnivore activity, insect activity, disease, percent body fat, introduction of chemicals etc. (Vass 2011). Recent studies have shown that also the size of the individual influences the decomposition rate (Sutherland et al. 2013; Matuszewski et al. 2014).

Currently used methods of time of death prediction depend greatly on the experience of the medical examiner. Aydin and colleagues tested this by asking 56 pathologists and forensic medicine specialists to estimate PMI in various cases based on the same set of information (post-mortem changes, time, environment and geographical information where the individual was found) and found that the estimations varied greatly between specialists, especially in cases of advanced decomposition (Aydin et al. 2010). Finding a more objective, laboratory based method would allow removing human perception from the task, potentially making the estimation more accurate. A large amount of research has been dedicated over the last hundred years to finding new methods to estimate PMI. However, there is still much room for improvement. Margins of error are still very significant, even when using a few of the methods combined. The longer the PMI the bigger the error: a 6 hour PMI can have an error of at least 2 hours, rising to a 4.5 hour error for a 10 hour PMI (Kaliszan et al. 2009).

Increasing numbers of researchers are trying to find a more accurate way of estimating the time since death, for example through biochemical indicators (biomarkers). Biomarkers are molecules which indicate a certain biological state, for example a diseased state. It has been previously suggested that certain substances could serve as post-mortem biomarkers, helping to estimate time of death. Chemical methods, which are used for this purpose, fall under the name of thanatochemistry (Madea 2005). The following literature review has been divided into different groups of possible biomarkers presented in the past.

### **1.2.1 Vitreous humour chemistry**

Potassium is one of the elements thoroughly researched in this area. It has been known for years that the potassium concentration  $[K^+]$  in vitreous humour increases post-mortem and that those levels can be correlated with PMI (Sturner 1963). Vitreous humour is a forensic specimen of choice due to its isolated and confined anatomy, which slows down the metabolic and autolytic processes with respect to other specimens such as blood (Madea 2005). Various studies have correlated the relationship between the PMI and potassium levels in vitreous humour by linear regression (Sturner 1963; Adelson et al. 1963; Sturner & Gantner 1964; Madea et al. 1990; Lange et al. 1994). However, as Muñoz *et al.* suggested, previously proposed equations contain some major flaws, which lead

to erroneous results. This group proposed a correction to the existing formulae by switching the variables (Muñoz et al. 2001) as well as including the cause of death as a variable (Muñoz Barús et al. 2002). Up until that point, the PMI was used as the independent variable and potassium as the dependent one in the linear regression models. Muñoz suggested using potassium as the independent value, as a means of reducing the margins of error in the calculations. This hypothesis was tested by Madea and Rödiger, who showed that changing the variables does in fact increase the accuracy of the result, reducing the error from  $\pm 25.96$  h to  $\pm 23.27$  h (over a post-mortem interval up to 130 h) (Madea & Rödiger 2006). The increase in accuracy is small, however it is statistically significant. The authors concluded that this method is correct for statistical analysis.

Muñoz and colleagues did not stop there and tried to improve the PMI calculations from vitreous potassium even further. Instead of using linear regression models, they have applied flexible regression models to data obtained from 201 cadavers (Muñoz Barús et al. 2008). They have shown that the relationship of potassium levels and time since death is not linear and concluded that it was a false assumption. Flexible regression, which models nonlinearities, should be used instead of linear regression. Authors showed that using two flexible regression models: generalized additive models (GAMs) and support vector machines (SVMs) brought the mean square error of 0.20 for linear regression down to 0.16 for flexible regression models. GAMs are an extension of traditional linear models, but more flexible than them. The researcher does not need to assume a parametric form for the effects of the continuous covariates, but only assumes that these effects can be represented by unknown smooth functions (Muñoz Barús et al. 2008). SVMs (also support vector networks) are supervised learning models, which given a set of training samples belonging to one of two categories, builds a model which then can assign new samples to one of the given categories (Cortes & Vapnik 1995). On that basis they have produced R-based software, which can be used to calculate the time since death from potassium and hypoxanthine levels in vitreous humour - PMICALC (Muñoz-Barús et al. 2010).

Potassium is not the only element being investigated for the time of death estimation in vitreous humour. The changes in levels of sodium, calcium and

chloride were also investigated. Jashnani *et al.* found a linear relationship between potassium levels and PMI as well as inverse relationship between sodium/potassium ratio and PMI (Jashnani *et al.* 2010). Sodium alone, as well as calcium and chloride levels showed no relationship. Chandrakanth *et al.* confirmed these findings, as their research showed no correlation between PMI and sodium, chloride, or even potassium levels (Chandrakanth *et al.* 2013), while Siddamsetty *et al.* like many other researchers found a relationship with vitreous potassium, as well as weak correlation with levels of sodium and glucose (Siddamsetty *et al.* 2014). Hypoxanthine is also believed to be a good marker for PMI estimation in vitreous (Rognum *et al.* 1991; Muñoz Barús *et al.* 2002; Muñoz Barús *et al.* 2008; Muñoz-Barús *et al.* 2010), in some cases considered more suitable than potassium (Rognum *et al.* 1991). Other substances shown to have a relationship with PMI include free amino acids (Patrick & Logan 1988b; Girela *et al.* 2008), especially taurine, glutamate and aspartate (Girela *et al.* 2008), lactate (Mihailovic *et al.* 2011) and iron (Santos Júnior *et al.* 2014). Odriozola *et al.* investigated the miRNA content in vitreous humour and while no relationship was found with time elapsed since death, the investigators were able to distinguish whether the individual died during day or night time (Odriozola *et al.* 2013). Similar finding was later presented by Corradini *et al.* (Corradini *et al.* 2015). Considerable amount of research has shown the value of vitreous humour and its chemistry as an indicator of PMI. However, some researchers raise concern over this method of PMI estimation. Balasooriya *et al.* found differences in levels of potassium, sodium and urate measured in the right and the left eye of the same individual (Balasooriya *et al.* 1984), while other studies raised concerns over different sample preparation methods (Thierauf *et al.* 2009; Camba *et al.* 2014) and low precision and high standard deviation when measurements were repeated (Thierauf *et al.* 2009). Being aware of these issues, researchers carry on re-evaluating and testing new and existing approaches to improve this methodology (Bocaz-Beneventi *et al.* 2002; Passos *et al.* 2009; Bortolotti *et al.* 2011; Lendoiro *et al.* 2012). Moreover, Tumram *et al.* published a comparative study of post-mortem analysis in vitreous humour and synovial fluid (Tumram *et al.* 2011). Both substances were analysed for potassium, chloride, calcium, creatinine, glucose and urea. Levels of potassium and glucose were comparable in both vitreous humour and synovial fluid. The authors concluded that post-mortem analysis of synovial fluid is as accurate as

vitreous humour. Swain *et al.* carried out a very similar comparison in vitreous humour and cerebrospinal fluid; however, this time vitreous was deemed a much better medium for PMI estimation (Swain *et al.* 2015).

### 1.2.2 Electrolytes

Changes in levels of electrolytes post-mortem were also investigated in other media than vitreous humour. Querido showed a linear relationship between the log of sodium/potassium concentration ratio and log of PMI (Querido 1990a) as well as log of chloride concentration and log of PMI (Querido 1990b), both in rat plasma. Yadav *et al.* found correlations between sodium, potassium as well as sodium/potassium ratio and PMI in cerebrospinal fluid (Yadav *et al.* 2007). Potassium, sodium/potassium ratio as well as phosphorus levels were also found to be correlated with PMI in pericardial fluid by Singh *et al.* (Singh *et al.* 2006), while Kawamoto *et al.* did not find these or other electrolytes (chloride, calcium and magnesium) to be useful in PMI estimation in this post-mortem specimen (Kawamoto *et al.* 2013). However, the levels of these electrolytes did seem to correlate with the cause of death, which might be very useful in its determination. Tavichakorntrakool *et al.* reported an increase of potassium, sodium, magnesium and calcium levels over time in post-mortem muscle tissue (Tavichakorntrakool *et al.* 2008).

### 1.2.3 Creatinine

Gallois-Montbrun *et al.* showed a relationship between creatinine concentration and PMI in bird muscle (Gallois-Montbrun *et al.* 1988). This theory was later tested and confirmed by Brion *et al.* in human psoas muscle (Brion *et al.* 1991). The authors suggested that creatinine concentration measurement could be a useful tool in estimating longer PMIs (weeks). On the other hand, Donaldson *et al.* suggested that this compound could be a useful marker in a shorter PM period of 96 h measured in rat plasma (Donaldson & Lamont 2014). However, two other studies of creatinine levels in post-mortem synovial fluid and vitreous humour (Tumram *et al.* 2011), as well as pericardial fluid (Kawamoto *et al.* 2013) did not find it a useful marker.

### 1.2.4 Amino acids

Over 30 years ago, Perry *et al.* determined that the levels of most proteogenic amino acids increased over time in PM brain (Perry *et al.* 1981). However, this work did not concern PMI estimation. Later, Patrick and Logan showed a relationship between the levels of amino acids and PMI in vitreous humour in cases of sudden infant death syndrome (SIDS) (Patrick & Logan 1988b). A few years later, Kärkelä and Scheinin documented the increase of tryptophan in post-mortem cisternal fluid (Kärkelä & Scheinin 1992). Girela *et al.* also investigated how free amino acids behaved in PM vitreous humour and cerebrospinal fluid (CSF) (Girela *et al.* 2008). The CSF results were inconclusive, as the fluid was contaminated with blood, however, in vitreous humour, the levels of most amino acids increased, especially aspartate, glutamate and taurine. Vass *et al.* investigated amino acid levels in various post-mortem organs and tissues (liver, kidney, heart, brain, muscle) (Vass *et al.* 2002). He found different amino acids to be useful biomarkers for each organ, with proline and methionine being useful in all organs tested. Finally, two very recent studies presented various amino acids as useful markers in PMI estimation using rat plasma (Donaldson & Lamont 2014; Sato *et al.* 2015).

### 1.2.5 Biogenic amines

Biogenic amines, especially putrescine, cadaverine, indole and skatole (3-methylindole), are well known decomposition products, associated with the post-mortem process of putrefaction (Vass 2001; Janaway *et al.* 2009). They seem to be likely candidates for PMI estimation, as they are produced post-mortem. Many studies regarding detection of volatile organic compounds (VOCs) released from decomposing bodies have investigated these amines (Statheropoulos *et al.* 2005; Statheropoulos *et al.* 2007; Statheropoulos *et al.* 2011; Zang *et al.* 2009; Dekeirsschieter *et al.* 2012). However, they remained undetected. In two other studies, only indole was successfully detected (Hoffman *et al.* 2009; Dekeirsschieter *et al.* 2009). This is most probably due to the low volatility of these amines. Vass *et al.* detected these compounds in various organs using gas chromatography, however, concluded that they were not useful as PMI biomarkers.

### 1.2.6 Adenosine triphosphate (ATP)

Sun *et al.* presented a relationship between ATP and PMI in post-mortem rabbit blood (Sun *et al.* 2013; Sun *et al.* 2014). The ATP level increased in the first few hours after death and then showed a steady decrease over the period of 72 h. Mao *et al.* investigated the relationship between the levels of ATP and its degradation products (adenosine-5'-diphosphate (ADP), adenosine-5'-monophosphate (AMP), inosine-5'-monophosphate (IMP), inosine (HxR), hypoxanthine (Hx) and xanthine (X)) (Mao *et al.* 2013). The authors used a parameter called *K* which measures the speed of ATP degradation based on the concentration of ATP itself and its degradation products. As a result they found that the *K* value could be a potential indicator of PMI. Liu *et al.* showed a relationship between microbial ATP and PMI in various tissues of rats (muscle, liver, spleen and kidney) (Liu *et al.* 2009) and Schmidt *et al.* suggested the ratio between the signal intensities of  $\alpha$ -ATP and inorganic phosphorous ( $\alpha$ -ATP/ $P_i$ ) as means of PMI estimation (Schmidt *et al.* 2014). The authors used  $^{31}\text{P}$  magnetic resonance spectroscopy ( $^{31}\text{P}$  MRS) to scan human muscle tissue every hour, over the period of 4.5 to 24 h after death.

### 1.2.7 DNA/RNA

Deoxyribonucleic acid (DNA) and ribonucleic acid (RNA) are essential components of any organism and their degradation post-mortem was also suggested as means of PMI estimation. Larkin *et al.* investigated the changes in the yield (amount measured) of skeletal muscle DNA of pigs (Larkin *et al.* 2010). The authors attempted to use the relationship between accumulated degree days (ADD, the cumulative total of average daily temperatures) to estimate PMI. However, no clear trend between the DNA yield and ADD was found. Initial decrease in DNA yield was observed and the authors concluded that after further testing, this could potentially be used for PMI estimation. The RNA route appears to be the more successful one in PMI estimation. Inoue *et al.* studied the degradation of messenger RNA (mRNA) post-mortem in rat brain, lung, heart and liver; however, PMI estimation was not the end goal of the study (Inoue *et al.* 2002). The authors concluded that mRNA is most stable in the brain and therefore, it would be best to study mRNA degradation in this organ and also that real time polymerase chain reaction (RT-PCR) is a reliable method of

measuring the levels of mRNA post-mortem. Later Bauer *et al.* showed that mRNA degradation could be used as a method of PMI estimation (Bauer et al. 2003). The group investigated the change in levels of mRNA in whole blood collected from live individuals stored *in vitro* over a particular length of time as well as post-mortem blood and brain samples collected during autopsies. In the case of both types of blood samples they found a relationship between mRNA and the time elapsed since death or collection. Additionally, they concluded that brain tissue can be equally useful in the absence of blood. However, the method requires further research due to large confidence intervals. Sampaio-Silva *et al.* investigated the total RNA instead of mRNA in post-mortem heart, muscle and liver (Sampaio-Silva et al. 2013). The authors found a significant correlation between PMI and RNA degradation in all three tissue types. The degradation was organ dependent. Additionally, they synthesised complementary DNA (cDNA, from the extracted RNA) and discovered 4 genes in muscle tissue that correlated with PMI. This finding was then used to create a mathematical model for PMI estimation. The relationship between RNA and PMI was linear, which was not the case in the study carried out by Li *et al.* However, this group investigated the relationship between 18S-rRNA (main ribosomal RNA) and microRNA with regards to PMI estimation (Li et al. 2014). Their results showed a parabolic relationship between RNAs and PMI, which according to authors could potentially be used in PMI estimation. However, a parabolic curve could result in the same marker level at two different time points, which might make the result of the estimation unclear.

### **1.2.8 Metabolites**

“Metabolites” is a general term describing any compounds involved in metabolism, whether in a role of a product or an intermediate. It is also used to collectively describe any number or kind of small molecules present in an organism. Various metabolites have been suggested as possible PMI markers over the years. Harada *et al.* investigated metabolite changes in rat liver, spleen, brain, heart and dorsal muscle (Harada et al. 1984). The authors concluded that lactate and pyruvate could be related to PMI in heart and muscle tissue. Post-mortem changes in brain metabolites were extensively studied by three different groups (Ith et al. 2002; Scheurer et al. 2005; Banaschak et al. 2005; Ith et al. 2011; Musshoff et al. 2011). Free trimethylammonium was suggested as a

suitable marker in all but one of the five studies carried out by these groups. Other common metabolites included propionate, butyrate, alanine and acetate. Less common ones included lactate, creatine, succinate, GABA, myo-inositol and some amino acids. Meanwhile, Donaldson and Lamont looked at changes in post-mortem blood and suggested lactic acid, hypoxanthine, uric acid, ammonia, NADH and formic acid as potential markers (Donaldson & Lamont 2013). Over the recent years, the study of metabolites evolved into a unique branch of science, called metabolomics, which attempts to characterise the metabolome of any given organism (described in more detail later on in this chapter). This approach, very often untargeted and termed metabolic profiling, has also been applied to PMI estimation through the means of various techniques  $^1\text{H-NMR}$  (Hirakawa et al. 2009), LC-MS/MS (Kang et al. 2012) and GC-MS (Donaldson & Lamont 2014; Sato et al. 2015; Kaszynski et al. 2016). Due to the nature of the untargeted approach, large numbers of metabolites have been identified and suggested as PMI markers using these techniques; therefore, they will be discussed in detail in the metabolomics section of this thesis (chapters 4 and 5) as relevant.

### **1.2.9 Proteins**

Post-mortem protein degradation has been extensively studied in animal tissue, with regards to meat production and tenderisation (Yates et al. 1983; Anderson et al. 2012; Picard et al. 2014; Koohmaraie & Geesink 2006; Nowak 2011). The change in levels and activity with PMI of various proteins and proteases was studied as a result. Some of these changes were also suggested as possible indicators of PMI. Main protein markers of interest are troponin (Sabucedo & Furton 2003; Kumar, Ali, Bhattacharya, et al. 2015; Kumar, Ali, Singh, et al. 2015; Pittner et al. 2015; Pittner et al. 2016), actin (Xiao & Chen 2005; Y. Liu et al. 2008) and calmodulin binding proteins (Kang et al. 2003; Poloz & O'Day 2009). Various other protein markers were suggested (Kominato et al. 1989; Kikuchi et al. 2010; Zapico et al. 2014; Finehout et al. 2006), as well as certain enzymes (Gos & Raszeja 1993) and lipids (Shirley & Wood 2013). These protein markers and post-mortem protein degradation will be discussed in detail in the proteomics chapter of this thesis (chapter 3).

### 1.2.10 Other markers

Various biological markers have been proposed over the years, as can be seen above. However, some of them are quite unique and difficult to classify within a general group. Sasaki *et al.* investigated the changes in non-protein nitrogen (NPN) in human brain, lung, liver and kidney (Sasaki *et al.* 1983). He found that the correlation of NPN and PMI was best in brain tissue in comparison to other tissues and this could potentially become a method of PMI estimation. Liu *et al.* investigated trimethylamine-nitrogen (TMA-N) content in rat muscle, liver and kidneys and found that it is positively correlated with PMI (Q. Liu *et al.* 2008). Kimura *et al.* suggested the use of the biological clock to estimate PMI (Kimura *et al.* 2011). RT-PCR analysis of certain gene expressions was carried out in mouse and human. The circadian oscillation of these gene expressions was detectable up to 48 h post-mortem. The ratio of hRev-ErbA/hBmal1 was found useful in PMI estimation. Bilheux *et al.* found a correlation between hydrogen abundance levels in tissue and PMI (Bilheux *et al.* 2015). Muscle tissue, lung and bone collected from canine cadavers were tested using neutron radiography. Wehner *et al.* investigated the immunohistochemical response of insulin in pancreatic  $\beta$ -cells; however, the method can only be used for PMI delimitation and not estimation (Wehner *et al.* 1999). Various types of cells were also suggested as possible PMI indicators. Alibegović suggested that cartilage cells (chondrocytes) could be used as their viability gradually decreases post-mortem (Alibegović 2014). Dokgöz *et al.* investigated the morphological changes in white blood cells post-mortem and concluded that cellular changes in leukocytes can help to estimate PMI until 120 h (Dokgöz *et al.* 2001). Finally, Boehm *et al.* investigated the post-mortem loss of enzymatic activity in bone marrow osteoclasts (Boehm *et al.* 2012). However, the results were very variable and the authors concluded that it does not correlate with PMI.

### 1.2.11 Examples of other methods

As can be seen from the above review, most of the research regarding PMI estimation is looking for an endogenous element, molecule or cell which could be correlated with the progression of human decomposition. However, various other, non-biomarker methods, have also been proposed. Estracanhalli *et al.* suggested in situ tissue optical fluorescence, where the fluorescence of the skin

in the abdominal area of rat cadavers was measured at various PMIs (Estracanholti et al. 2009). Prieto-Bonete *et al.* investigated morphological and histological changes in the eye lens and reported that the loss of structure, sphericity and absorbance of the rabbit eye lens decreased with PMI (Prieto-Bonete et al. 2015). Hauther *et al.* suggested the use of certain strains of gut microbial communities, which decreased in abundance with time (Hauther et al. 2015), while Ishikawa *et al.* showed by means of computed tomography (CT) imaging that the abdominal aorta is gradually narrowing post-mortem (Ishikawa et al. 2013). Electrical impedance tissue measurement was also suggested for PMI estimation. Querido and Phillips measured electrical impedance of intact rat abdomen (Querido & Phillips 2001) and Mao *et al.* used electrical impedance spectroscopy to test rat spleens at various temperatures and PMIs (Mao et al. 2011). In both cases the measured impedance decreased with time. Warther *et al.* suggested idiomuscular contraction (muscle contraction following a mechanical stimulation) as means of PMI estimation, however, this method can only be applied within the first 13 h post-mortem (Warther et al. 2012). A slightly more unusual method presented by Romanelli *et al.* involved the measurement of the ciliary motility in the nasal cavity: the movement of the cilia decreased over time (Romanelli et al. 2012). Megyesi *et al.* published a PMI estimation method based on ADD and total body score (TBS) (Megyesi et al. 2005). TBS is a point based system which allows a numerical description of the extent of decomposition and ADD is a unit of PMI which accounts for the daily temperatures which the cadaver has been exposed to. This method was later tested by Myburgh *et al.* using pig cadavers, but poor results led the authors to conclude that the method had a very limited use (Myburgh et al. 2013). The use of ADD as a PMI estimation tool was also investigated by Dabbs, who tested the use of temperature data collected by a National Weather Service (NWS) station (Dabbs 2010). The author compared data from two nearby stations with the data collected by instruments on the research site and found significant differences between the readings. She also showed how a seemingly small difference in temperature introduces error into the final estimation. Meanwhile, Arpad Vass suggested that PMI can be estimated based solely on two mathematical formulas (Vass 2011). He created two formulas derived from empirical data collected over 20 years of research, one for bodies decomposing on the surface and another for buried cadavers. The formulae are based on temperature, moisture and partial

pressure of oxygen and he claimed that these universal formulae can be applied anywhere in the world. This was later disputed by Cockle and Bell, who tested these formulae using a set of 42 bodies decomposing on the surface and 22 buried (Cockle & Bell 2015). Neither of the formulae performed well and the authors suggested that 'universality' cannot be applied to PMI estimation.

Finally, it should be noted that the current research is not only focused on new ways of PMI estimation, but also on improving the well-established methods, which have been used for years. For example, the nomogram method created by Henssge (Henssge 1988) based on the two-exponential term of Marshall and Hoare (Marshall & Hoare 1962), which estimates PMI using a rectal temperature measurement, was further evaluated by the author (Henssge et al. 2000) as well as other researchers, in the case of sudden temperature increase (Bisegna et al. 2008) and the error associated with the model (Hubig et al. 2011; Hubig et al. 2015). Other researchers also attempted to improve PMI estimation based on body cooling by multiple measurement sites (Morgan et al. 1988), creating new algorithms (Nelson 2000) and reference databases (Muggenthaler et al. 2012). Anders *et al.* further investigated the re-establishment of rigor mortis and re-evaluated the time span in which this phenomenon can occur (Anders et al. 2013), while Vanezis and Trujillo used colorimetry to assess the advancement of post-mortem hypostasis (Vanezis & Trujillo 1996) and Usumoto *et al.* used spectrophotometric analysis on lividity to estimate PMI (Usumoto et al. 2010).

As can be seen from the above literature review, the list of proposed methods of PMI estimation is extensive and a considerable amount of work has already been done. However, all of the methods so far still have a large error and are limited in their use. Much of the work described is targeted to specific classes of molecules, but emerging proteomic and metabolomics approaches permit the comparative analysis of large numbers of molecules, originating from diverse areas of metabolism, and might be exploited to screen for new, previously unobserved changes that are correlated with PMI.

### **1.3 Muscle composition and structure**

Muscle tissue is one of the main components of the human body. It makes up about 40 to 50% of the total body weight and fulfils three very important

functions: movement, posture support and heat production. Three types of this tissue are distinguished: skeletal (attached to bones), cardiac (within the walls of the heart) and smooth (making up hollow organs, such as the intestinal tract and vasculature) (Wingerd 2014). This section will refer to skeletal muscle only, which was used as a specimen in the study described in this thesis.

Skeletal muscle (also known as voluntary muscle) is composed of muscle fibers encased in a plasma membrane called the sarcolemma. Sarcolemma can be electrically excited and therefore, receive a nerve impulse to initiate the process of contraction. The muscle fibers are made up of myofibrils, which are further divided into sarcomeres that repeat along the length of the fibril (Zubay et al. 1995). A detailed schematic of muscle organisation is shown in Figure 1-1.

*Figure has been removed due to Copyright restrictions.*

**Figure 1-1. The hierarchy of muscle organisation.**

**A voluntary muscle such as the bicep is a composite of many fibers connected to tendons at both ends. Each muscle fiber is composed of several myofibrils that are surrounded by an electrically excitable membrane (sarcolemma). Myofibrils exhibit longitudinally repeating structures called sarcomeres. (Zubay et al. 1995)**

Muscle tissue is mainly composed of proteins; the most important ones include actin, myosin, troponin and tropomyosin. These proteins make up filaments, which in turn, make up the sarcomeres. Two types of filaments are present, thin (made of actin, troponin and tropomyosin) and thick (made of myosin). Actin molecules form a double helix with repeating subunits. Each actin unit is connected with troponin on each side and surrounded by tropomyosin molecules along the length of each unit. The thick filaments are composed of two identical heavy chain myosin molecules and two different light chain myosin molecules (Zubay et al. 1995). Figure 1-2 shows the structure of those two filaments, as

well as how they are organised within the sarcomere. The thick and thin filaments are arranged interchangeably along the length of the myofibril, which gives it the striated look which can be seen in Figure 1-1. Thick filaments create a dark band and thin filaments alone a light band (Figure 1-3).

*Figure has been removed due to Copyright restrictions.*

**Figure 1-2. A molecular view of muscle structure.**

**Image a) segment of actin-tropomyosin-troponin, b) segment of myosin, c) integration of thin filaments (actin) and thick filaments (myosin) in a muscle fiber. (Zubay et al. 1995)**

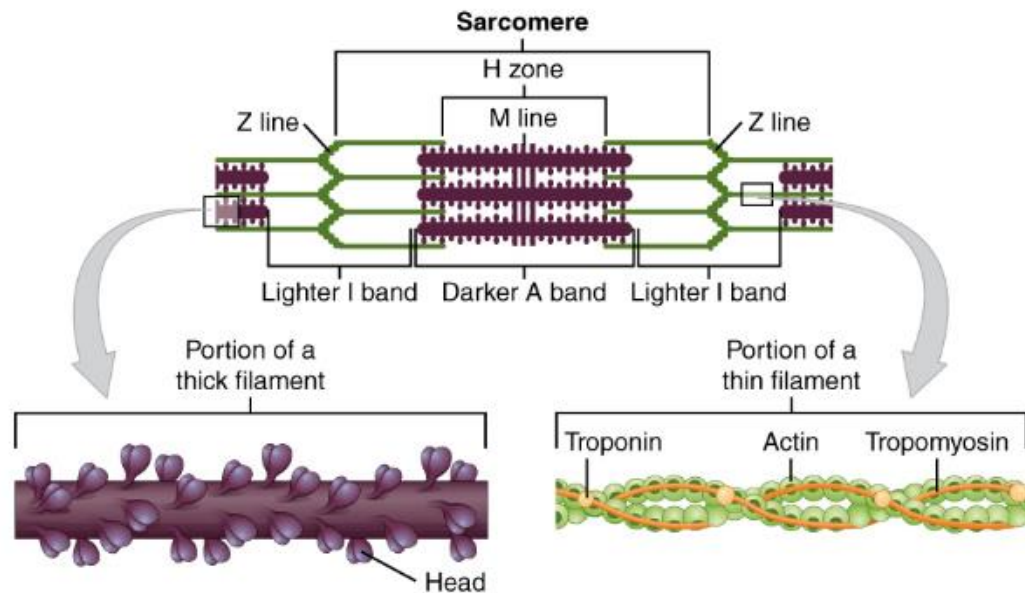


**Figure 1-3. The organisation of the sarcomere.**

The sarcomere is the region between one Z line and another. This is the functional unit of muscle tissue. When the contraction occurs, the Z lines are brought closer together and the A band region remains the same. Thick filament: myosin, thin filament: actin, troponin and tropomyosin (OpenStax 2013). Image licensed under a Creative Commons Attribution 4.0 International License.

Figure 1-3 shows a more detailed organisation of the sarcomere. Two lines are highlighted in that schematic, Z line, which defines the start and the end of each sarcomere unit and M line, which is located in the centre of the unit. These lines are made up of two other proteins, myomesin (M) and  $\alpha$ -actinin (Z) (Zubay et al. 1995). The A band describes the region in the middle of the sarcomere, where the thick filament is extended on both sides of the M line, including the area where the thick and thin filaments overlap. When contraction occurs the thin filaments move along the thick filaments and pull the Z lines closer towards the centre. The A band remains the same, i.e. the thick filament does not move (OpenStax 2013).

Figure 1-4 illustrates the sequence of events involved in muscle contraction, also known as the cross-bridge cycle. The muscle cell needs to receive a nerve impulse from the central nervous system, in order to contract. That signal is received by the sarcolemma, which triggers the sarcoplasmic reticulum to release  $\text{Ca}^{2+}$  ions. Calcium binds to troponin in the troponin-tropomyosin complex, which surrounds the actin molecule (thin filament). This causes the complex to expose myosin binding sites on the actin molecule (which are unavailable in the state of muscle rest). Then, the myosin heads bind to actin, at the same time releasing inorganic phosphate ( $\text{P}_i$ ), which is bound to myosin,

allowing a stronger bond between actin and myosin (Figure 1-4 a, b). Next, so called power stroke occurs, where the myosin head pulls the actin molecule closer to the M line of the sarcomere, causing the filaments to slide and the cell to contract. At the same time, the ADP molecule is released and the ATP binding site on the myosin head is exposed (Figure 1-4 c). The myosin will not detach from actin in the absence of ATP. If there is ATP available, it attaches to myosin and causes the contraction to release (Figure 1-4 d). The hydrolysis of ATP into ADP and  $P_i$  reconfigures myosin heads position and it is available for another binding cycle (Figure 1-4 e). As long as there is calcium and ATP available to make and break the binding between actin and myosin molecules the cycle will repeat and the muscle contractions will continue. It should be noted that many myosin heads are present in a muscle cell; therefore, many cross-bridges form simultaneously (OpenStax 2013).

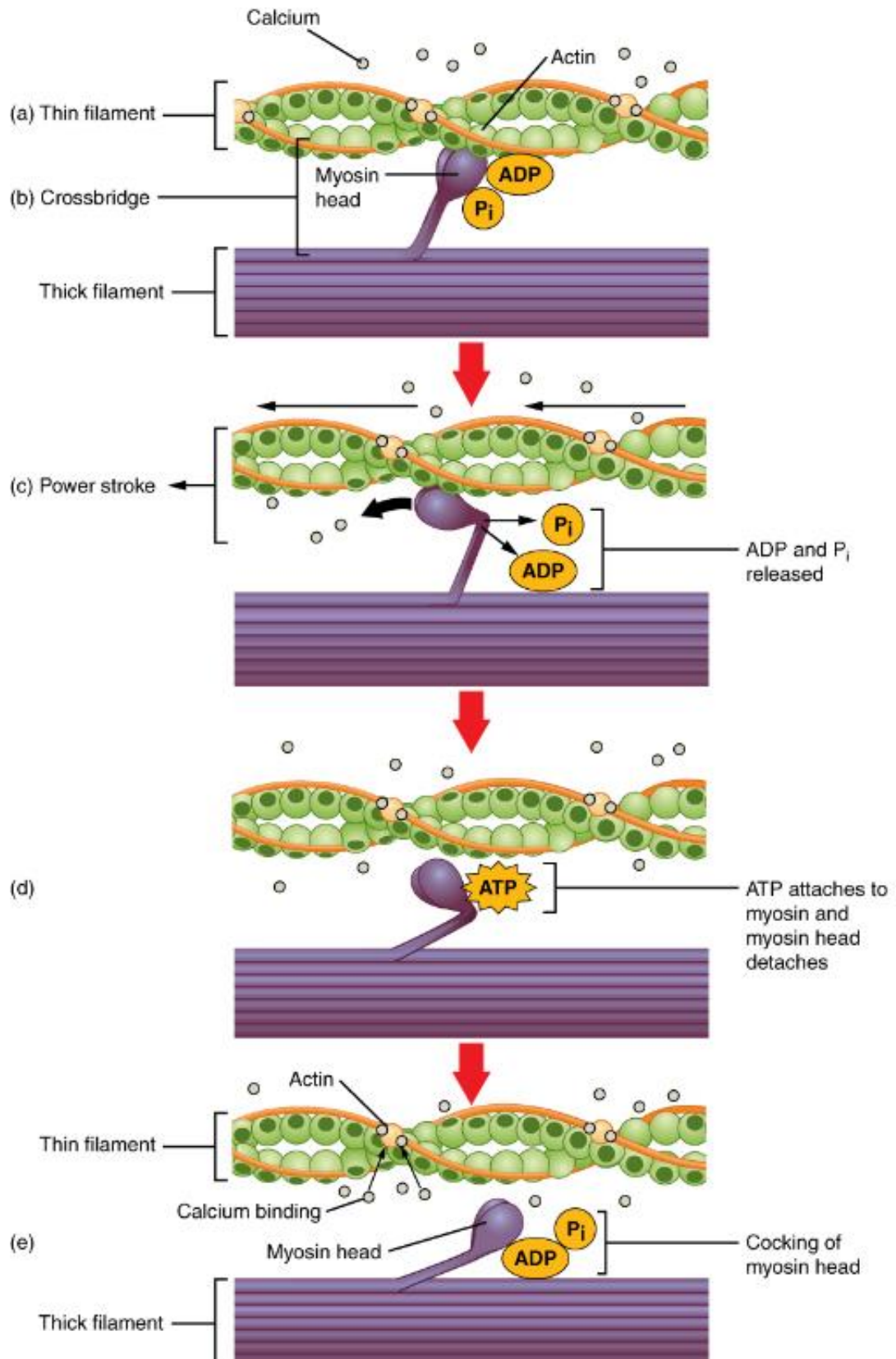


**Figure 1-4. Overview of the cross-bridge cycle.**

(a) The active site on actin is exposed as calcium binds to troponin. (b) The myosin head is attracted to actin, and myosin binds actin at its actin-binding site, forming the cross-bridge. (c) During the power stroke, the phosphate generated in the previous contraction cycle is released. This results in the myosin head pivoting toward the centre of the sarcomere, after which the attached ADP and phosphate group are released. (d) A new molecule of ATP attaches to the myosin head, causing the cross-bridge to detach. (e) The myosin head hydrolyses ATP to ADP and phosphate, which returns the myosin to the cocked position. (OpenStax 2013) Licensed under a Creative Commons Attribution 4.0 International License.

In the absence of ATP, the muscle will remain contracted. This is the process which causes the state of post-mortem rigor mortis, briefly mentioned in section 1.2 of this chapter. As the cellular compartmentalisation disintegrates and the normal cellular processes and safety mechanisms cease in a decomposing body, the calcium sequestered in the sarcoplasmic reticulum is released and causes the muscles to contract. No more ATP is available to release the contraction after death; therefore, the muscles remain contracted until the process of proteolysis, i.e. protein breakdown, will cleave the proteins that are involved in the contraction.

## 1.4 Proteomics

Proteomics “*is the study of protein properties (expression level, post-translational modification, interactions etc.) on a large scale to obtain a global, integrated view of disease processes, cellular processes and networks at the protein level*” (Blackstock & Weir 1999). In other words, this branch of science aims to characterise all the proteins that comprise a given system at a given time. The term “proteome” was first introduced by Wilkins *et al.* and is defined as “the entire PROTein complement expressed by a genOME, or by a cell or tissue type” (Wilkins *et al.* 1995). It is a relatively new branch of science, emerging and fast-developing over the past 20 years. Proteomics has a very challenging task of defining the whole proteome, which, as of yet, has not been achieved (Nesvizhskii *et al.* 2007). This is due to the fact that the proteome is a very dynamic and complex entity, which rapidly changes depending on the environment, through various processes of protein transcription, translation, turnover and post-translational modification. There is only one genome in an organism, but it is coding for many different proteomes (Abdallah *et al.* 2012). Proteins are directly involved in many functions of the body; hence, many researchers think that proteomic analysis of an organism presents more useful knowledge about the underlying biological processes than genomic information (Anderson & Anderson 1998; Blackstock & Weir 1999; Abdallah *et al.* 2012). Proteomic studies help us understand protein function, protein interaction, as well as their involvement in many processes and pathways within a cell (Dhingra *et al.* 2005). Most drug targets are proteins (Blackstock & Weir 1999) and various proteomic studies, presented in recent years, have discovered prognostic and diagnostic indicators of a disease state (Pena *et al.* 2015) as well as new therapy

targets (Satelli & Li 2011). The proteomic approaches that are employed to characterise living organisms, or to highlight markers for disease state or progression, might also be applied to look at changes occurring post-mortem, with a view to discovering markers for PMI.

#### **1.4.1 Proteomic techniques: gel-based vs. gel-free**

Various proteomic approaches are currently available. They can be divided into two general categories, gel-based and gel-free approaches. A standard gel-based proteomic workflow includes sample preparation, where the proteins are extracted from a tissue or cell. Then the proteins are separated using a one-dimensional (according to molecular weight) or two-dimensional (according to isoelectric point and molecular weight) polyacrylamide gel. The proteins of interest are then excised from the gel and digested into peptides with an appropriate enzyme (most commonly trypsin) and analysed using mass spectrometry (MS). This is illustrated in Figure 1-5. Sodium dodecyl sulfate polyacrylamide gel electrophoresis (SDS-PAGE, one dimension separation) and two-dimensional gel electrophoresis (2DE, two dimension separation) are the main gel-based approaches used. The latter will be discussed in more detail in the next section, as this approach was used in this study.

The gel free approach is quite similar, with the exclusion of the gel-based separation. Proteins are extracted from a tissue or cell and the whole protein content extracted from the sample is digested prior to MS analysis. Optionally, to reduce the complexity of the sample, a gel-free fractionation method can be applied prior to analysis to separate out different classes of proteins (i.e. membrane proteins etc.). This is illustrated in Figure 1-6. The main difference between these two approaches is that in the gel-based approach a resolved, intact protein is digested into peptides which are then matched back to that protein. In a gel free approach a pool of various peptide spectra, coming from different proteins has to be analysed and matched back to them. The digestion is a very important step which makes the MS analysis of the proteins possible. The protein molecules are otherwise too large to be analysed using this instrumentation.

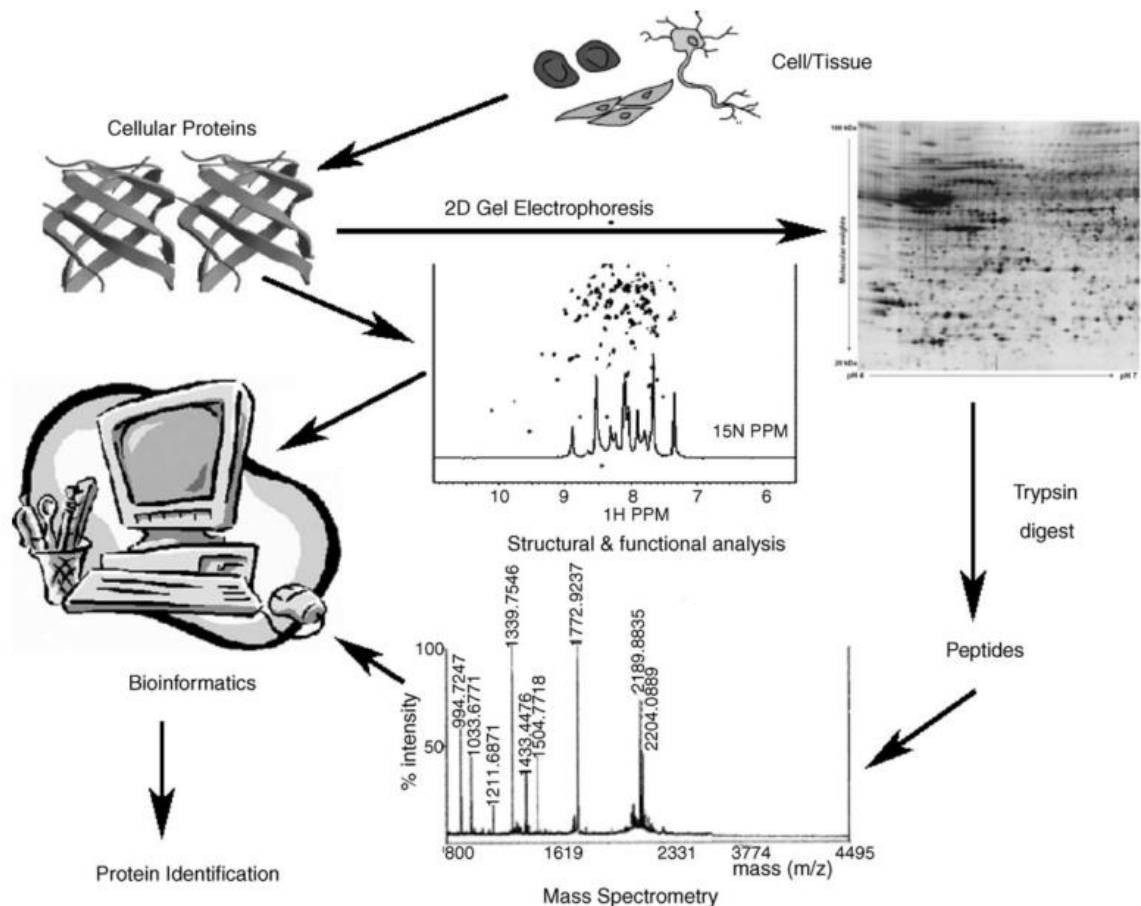


**Figure 1-5. Overview of a gel-based proteomics workflow (2DE). (Dhingra et al. 2005)**  
 Permission to reproduce this image has been granted by Elsevier publishing company,  
 license Number: 3944091100757.

One of the most popular gel-free strategies employed, is so called “shotgun proteomics”. Tandem mass spectrometry is required in this approach: the first analysis is a survey scan which detects all of the features in the sample and then the instrument automatically selects a few precursor ions for fragmentation, usually the most abundant ones. However, this is also one of the drawbacks of the method as the complexity of the sample makes it impossible to fragment all of the ions present and only a few are selected. In this setting low abundance ions that could be of interest can be missed from the analysis. This also causes issues with the reproducibility between analyses. Both of these issues can be improved upon when using one of the other two known approaches, direct or targeted. In a direct approach the principle is the same, however at least two analyses are performed. First analysis is again a survey scan which creates a list of all peptides, from which a list of peptides of interest is created and only the peptides present on the list are selected for fragmentation. In the targeted approach a prior knowledge of the sample is required, as this method is hypothesis driven. No survey scan is performed in this approach, as the

instrument is set up to target particular ions, pre-selected based on the created hypothesis (Domon & Aebersold 2010). The selection of the approach used, depends greatly on the resources available, as well as the purpose of the research conducted.

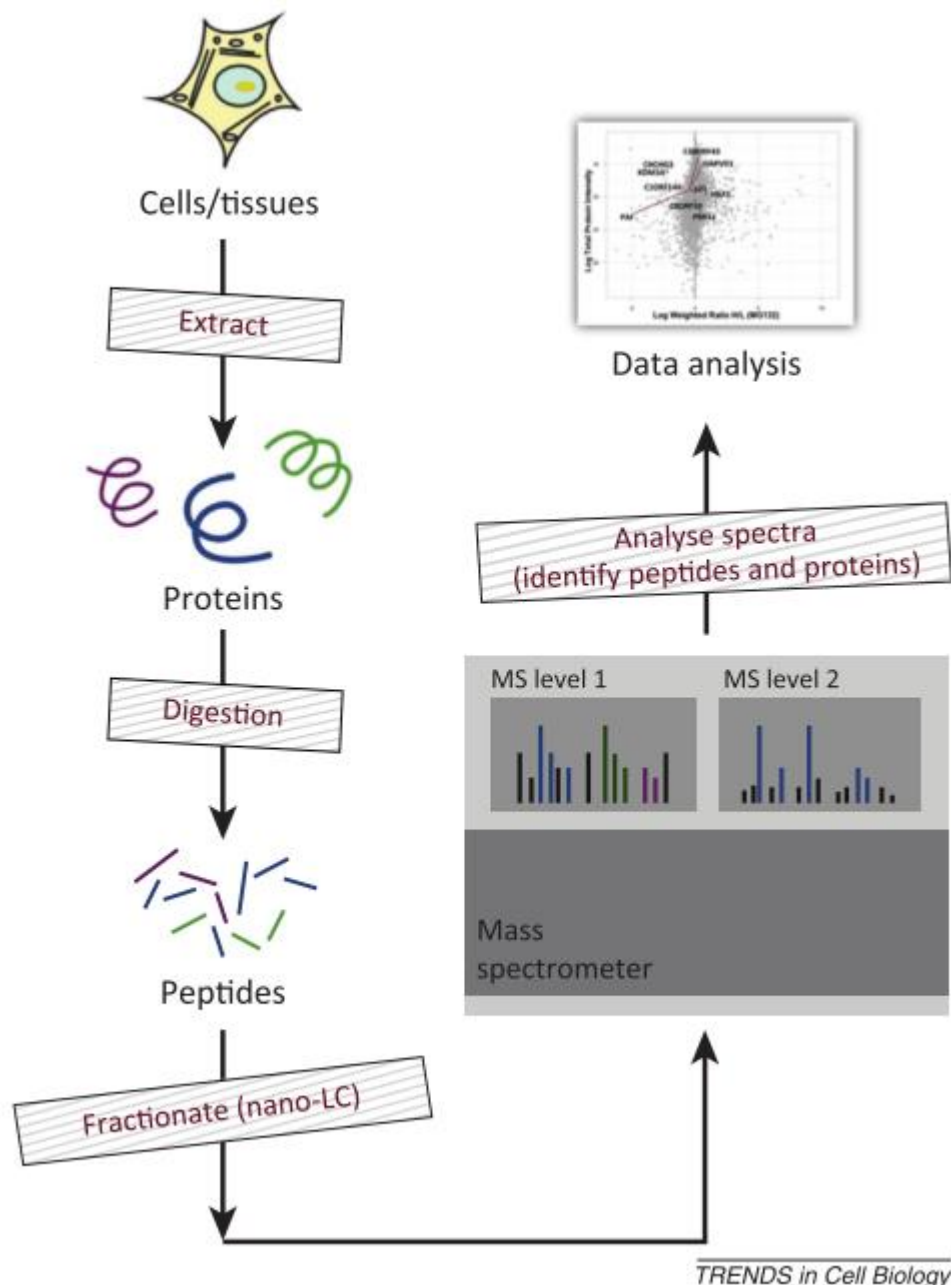


Figure 1-6. Overview of a shotgun workflow. (Ahmad & Lamond 2014)  
Image licensed under a Creative Commons Attribution 4.0 International License (CC BY 4.0)  
<https://creativecommons.org/licenses/by/4.0/>

### 1.4.2 Two-dimensional gel electrophoresis (2DE)

Since this technique was developed by O'Farrell in 1975 (O'Farrell 1975), it has remained one of the most popular protein separation methods until today. It is

most often chosen to analyse differential protein expression (Abdallah et al. 2012). As mentioned in the previous section, this technique separates the proteins in two steps, based on two characteristics, isoelectric point (pI) and molecular weight. An extracted and cleaned up protein sample is first added to an electrofocusing strip (of a certain pH range), where an electric potential is applied and the proteins align along the strip based on their pI (first dimension). Next, the strip is secured on a polyacrylamide gel and the second separation step is carried out as proteins travel down the gel at varying speed dependent on their molecular weight (a detailed protocol is described in chapter 2). This method was initially used for protein separation of a single sample per gel. However, in 1997, Unlü *et al.* modified the method enabling a comparison of two different samples on one gel (Unlü et al. 1997). This was achieved by fluorescently tagging the samples with two different dyes and running them together on one gel. Two images of the gel are then created, visualising each of the samples separately. The images can be superimposed and compared to pinpoint the differences between the samples. The dyes do not affect the protein separation, which means that proteins common to both samples will be resolved in the same parts of the gel. This modification improves the reproducibility between the samples and significantly simplifies this technique for comparative studies. The approach was given the name of difference gel electrophoresis (DIGE). A few years later, this technique was further improved by Alban *et al.*, by the inclusion of an internal standard in the DIGE experiment (Alban et al. 2003). The modification involves adding an aliquot of a pooled standard (created by mixing equal amounts of all of the samples to be analysed) to each gel. The standard is also labelled with a fluorescent dye, different from the two dyes used to label the samples. As a result, two samples and the pooled standard are loaded onto each gel, differentially labelled. Up until this modification was introduced, only two samples could be compared on one gel and comparing more samples between the gels was quite difficult and unreliable due to experimental variability between the gels. This improvement allows for normalization between separate gels and reduces the error associated with experimental variation. The software, used to process the gel images, compares the abundance of spots on each gel with the abundance of the corresponding spot from the pooled standard, and these differences are then compared between gels. For schematic of this workflow see Figure 1-7. This allows detecting the

biological variation between the spots in a more reliable way. This modification enables the comparison of multiple samples within a single DIGE experiment and reduces the number of gels required to complete this task.

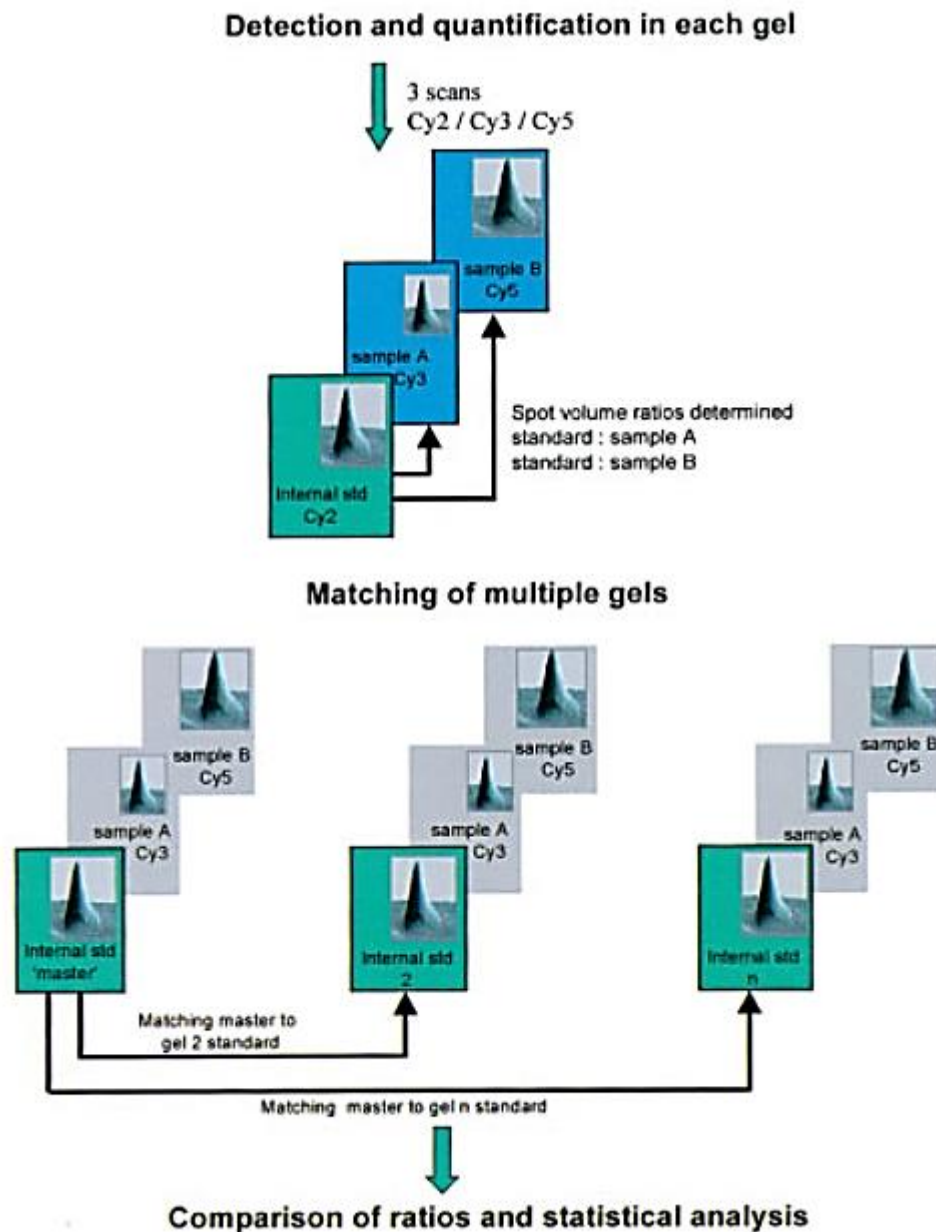


Figure 1-7. Gel analysis workflow (Decyder software).

Spot detection is carried out on image pairs consisting of the pooled standard and a sample from the same gel. The two images overlay perfectly allowing direct measurement of volume ratios of spots between the standard and a sample. The standard spot maps are matched together and the standard: sample volume ratio values are compared enabling the calculation of abundance ratio between samples from different gels, followed by the application of statistical tests. (Alban et al. 2003). Permission to reproduce this image has been granted by John Wiley and Sons publishing group, license Number: 3944071191832.

The 2DE approach is a perfect methodology to separate proteins in a complex mixture. Additionally, it makes the protein identification slightly easier as intact proteins are separated within the gel and (at least in theory) those single

proteins are excised from the gel, digested and analysed by mass spectrometry. Trying to identify proteins from a single protein peptide mix is more straightforward than a multiple protein mix. Furthermore, no prior knowledge of the sample is required and the differences in protein expression can be easily found, with the MS analysis limited to the proteins of interest. Finally, since the approach separates the proteins based on their pI, post-translational protein modifications can be detected using 2DE (Jensen 2004). The method has significantly improved over the years in efficiency, reproducibility and decreased experimental variation, through the modifications in experimental set-up. However, this method is not without its limitations. This approach is quite expensive, due to requirement of high quality reagents and many pieces of equipment. Moreover, the approach is time consuming, a single experiment can take up to a week, if not more to complete, and there is not much room for automation (aside from robotically picking the gel spots). Additionally, proteins of low abundance, highly hydrophobic, acidic or basic, as well as very large proteins will not be well represented on a 2DE gel. Finally, proteins might co-elute and merge into detected protein spots, which can introduce an error to the measured protein abundance and complicate the protein identification (Abdallah et al. 2012). Nevertheless, this method, with its many advantages, still remains a method of choice for many researchers, as it was in the case of this research project. The proteins of interest discovered using this approach were analysed by LC-MS/MS, which is described in detail in section 1.5.1 of this chapter. Chapter 3 describes the results of the proteomic part of this study and how protein research was previously applied in PMI estimation.

## 1.5 Metabolomics

“Occasionally, a new idea emerges that has the potential to revolutionize an entire field of scientific endeavour. It is now within our grasp to be able to detect subtle perturbations within the phenomenally complex biochemical matrix of living organisms. The discipline of metabolomics promises an all-encompassing approach to understanding total, yet fundamental, changes occurring in disease processes, drug toxicity and cell function.” (Mitchell et al. 2002)

Metabolomics (or metabolonomics) is a large scale study, aiming to measure the whole metabolome of a given organism at a given point of time, under given circumstances - a metabolic snapshot, so to speak. It is a relatively new branch

of science, even though many researchers have investigated various metabolites in the past; they did not look at the metabolism from a global perspective. Metabolic profiling (term often used for metabolomics studies) has been discussed in the literature since the 1950s. However, it developed very slowly and only in the last decade or so it has become a major research interest. Numbers of publications involving metabolomics saw a sudden escalation around the years 2003-2005 (Rochfort 2005). Metabolomics followed on from other global approaches: genomics, transcriptomics and proteomics and complements the other 'omics' datasets.

The term metabolome was first introduced by Oliver *et al.* in 1998 (Oliver *et al.* 1998) as the quantitative total of all small molecules present in cells at a particular developmental or physiological state. However, Beecher later stated, that the metabolome only includes the native small molecules, which partake in general metabolism and are necessary for cellular functions (Beecher 2003). Slight discrepancies also occurred when it comes to name the science of investigating the metabolome. Two terms are used, metabolomics and metabonomics. Some researchers use these terms interchangeably, while others see a particular distinction, where metabonomics deals with a metabolic response occurring due to a pathophysiological stimuli or genetic modification (Nicholson *et al.* 1999; Lindon *et al.* 2003), while metabolomics deals with any changes in the metabolome. There is an overlap between both definitions and the metabolomics terminology includes the specifics of metabonomics testing, therefore, in this thesis the term 'metabolomics' will be used to define this approach.

As mentioned above, metabolomics aims to detect compounds of low molecular weight (up to ~1000 Da), which include amino acids, oligopeptides, sugars, bile acids, simple fatty acids, and intermediates of many biochemical pathways (Clarke & Haselden 2008). The size of the entire metabolome is debatable, as it would require a specific definition of which small molecules should be included or not. Numbers ranging from a few thousand to tens of thousands of compounds have been suggested (Kaddurah-Daouk *et al.* 2008). This makes this task quite difficult as various molecules, with various chemistries need to be detected, ideally, with a single analytical method. Even though the analytical platforms available are fast developing, it is still not possible to measure the entire

metabolome using a single analytical platform. This is why, where possible, scientists combine different methods in order to increase the possible coverage of the metabolome. Three main analytical platforms are available for metabolomics experiments: Nuclear Magnetic Resonance (NMR) Spectroscopy and Mass Spectrometry (MS), the latter coupled either to Liquid (LC-MS) or Gas (GC-MS) Chromatography. The choice of the analytical method often depends on the available resources, but more importantly, it depends on the type of sample (Goodacre et al. 2004). NMR spectroscopy is often used in metabolic profiling of biofluids (e.g. urine or plasma) and does not require any complicated sample preparation steps, as an intact sample can be analysed using this approach (Lenz & Wilson 2007). Additionally, it has an advantage of being non-destructive; the sample is not used up in the analysis and can be later used for other analyses. However, mass spectrometry is capable of creating a more comprehensive metabolic profile, especially when combined with chromatographic techniques. Liquid and gas chromatography coupled to MS will be discussed in more detail in the following sections.

Metabolomics analysis can be divided into untargeted (discovery) and targeted approach. An untargeted approach is used in cases where there is no prior knowledge of how the metabolome will be affected in given circumstances. For example, in comparative studies, disease state versus healthy control. This gives an insight into which pathways (if any) are affected. It is often called a hypothesis-generating approach. This knowledge can be then used to focus on particular aspects of the biological question. A diagram of typical untargeted approach workflow is presented in Figure 1-8. Targeted approach, as the name suggests, is used when a particular target (compound, pathway) is investigated. The same methodologies are used for both approaches, with the differences in sample preparation (extraction of specific components of the sample, fractionation) and how the data is acquired at the sample analysis stage (e.g. looking for particular ions as opposed to collecting a general sample spectrum in MS) This approach usually requires prior knowledge of the subject and a specific hypothesis to be tested. In the study described in this thesis, an untargeted metabolomics approach was used to discriminate the metabolites affected by the decomposition process.

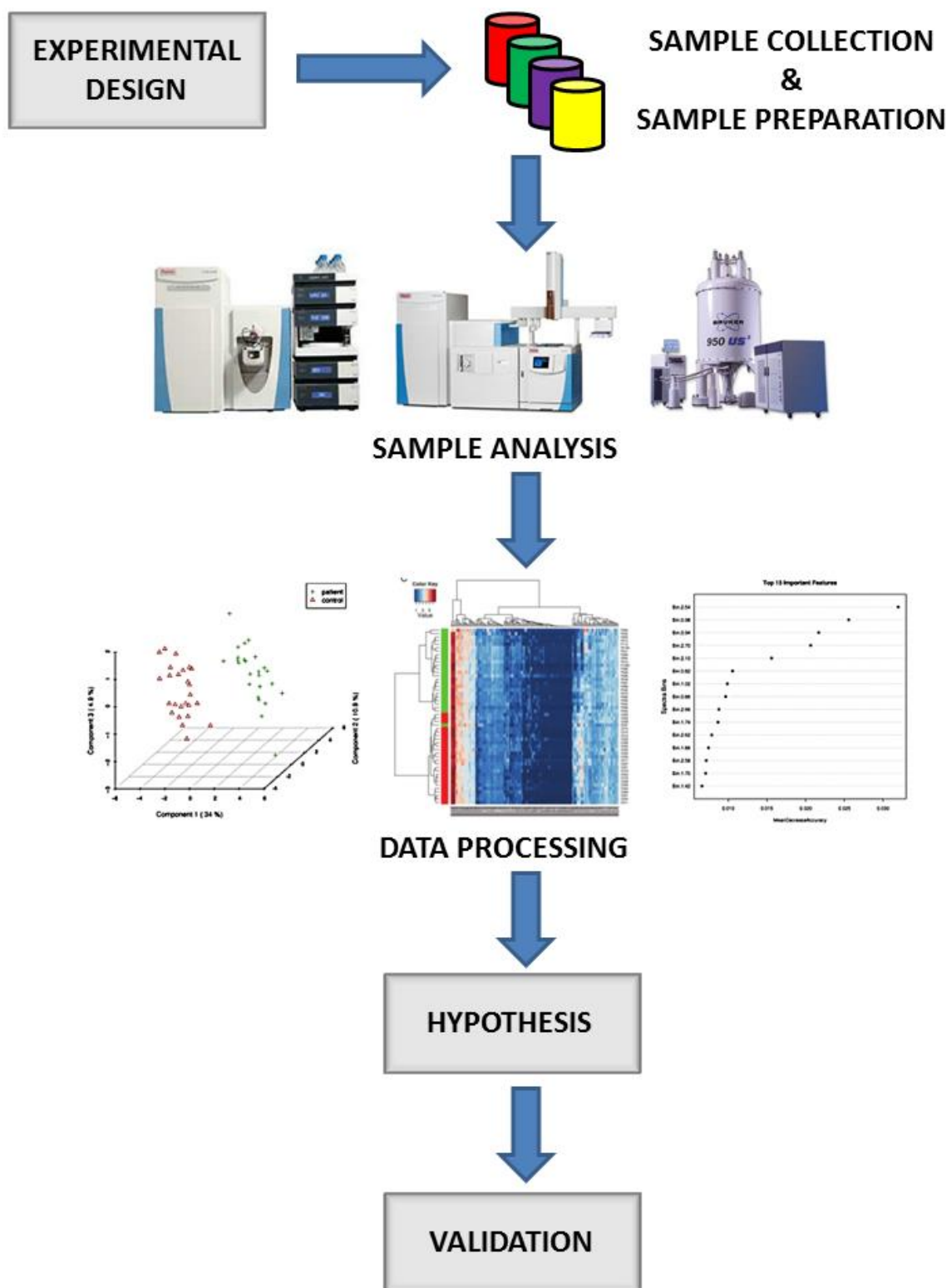


**Figure 1-8. Overview of an untargeted metabolomics approach workflow.** The examples of the graphical outcomes of data analysis were from MetaboAnalyst software (Xia et al. 2009). Permission to reproduce these images has been granted by Oxford University Press, license Number: 3944100710749.

Data analysis is a very important aspect of metabolomics experiments. Especially, when dealing with an untargeted approach. A vast amount of data is collected and bioinformatics tools are required to simplify it. Bioinformatics is a fast developing branch of science, where informatics is used to understand

biological data. It is an integral part of all of the 'omics' sciences and many computational platforms have been developed to help understand the metabolomics data collected, for example MetaboAnalyst (Xia et al. 2009; Xia et al. 2012), ASCA (Smilde et al. 2005) or IDEOM (Creek et al. 2012). The latter program was used in this study. These bioinformatics tools can process, normalize and perform statistical analysis, as well as graph and map metabolomics data onto pathways. More importantly, with the help of various databases (e.g. HMDB (Wishart et al. 2007), KEGG (Kanehisa & Goto 2000) or MetaCyc (Karp et al. 2002)), they also identify the detected metabolites.

Metabolomics approach is very universal and can be applied in many areas of study. One of the most popular ones is medicine. Metabolomics is a perfect tool for this task, as a metabolomics approach shows a broad image of the changes and the pathways affected under certain circumstances. Diet, illness, lifestyle and many more factors affecting living systems can be detected at the metabolic level. Therefore, a lot of metabolomics research is dedicated to health and nutrition (Watkins & German 2002; German et al. 2003; Arab 2004; German et al. 2004), prognostic and diagnostic biomarker discovery (Hunter et al. 2016; Fan et al. 2016), drug development, as well as their effects and toxicity (Cuperlovic-Culf & Culf 2016; Hoerr et al. 2016; Dinis-Oliveira 2016). However, metabolomics approach is versatile and is applied in many other areas, as for example food, plant and agricultural studies (Eloh et al. 2016; Gillis et al. 2016).

### **1.5.1 Liquid Chromatography – Mass Spectrometry (LC-MS)**

Liquid chromatography is a separation technique, where compounds present in the sample are separated between two phases: a mobile phase and a stationary phase. The compounds are separated based on their varying chemistries and as a result, different affinity for the stationary phase. The sample analytes, in solution, are passed through the column, where they can interact with the stationary phase. Analytes will be retained by the stationary phase according to their chemistry, so that separation of mixed analytes can be achieved. Typical solvents include acetonitrile, methanol, or dichloromethane, often mixed with particular buffers, for example trifluoroacetic acid or formic acid. The process by which analytes are released from the column is called elution. Different compounds elute at different times, referred to as retention time (RT). The RT

of a compound in a specific chromatographic configuration is one of the criteria used to identify it. A schematic of an LC system is presented in Figure 1-9.

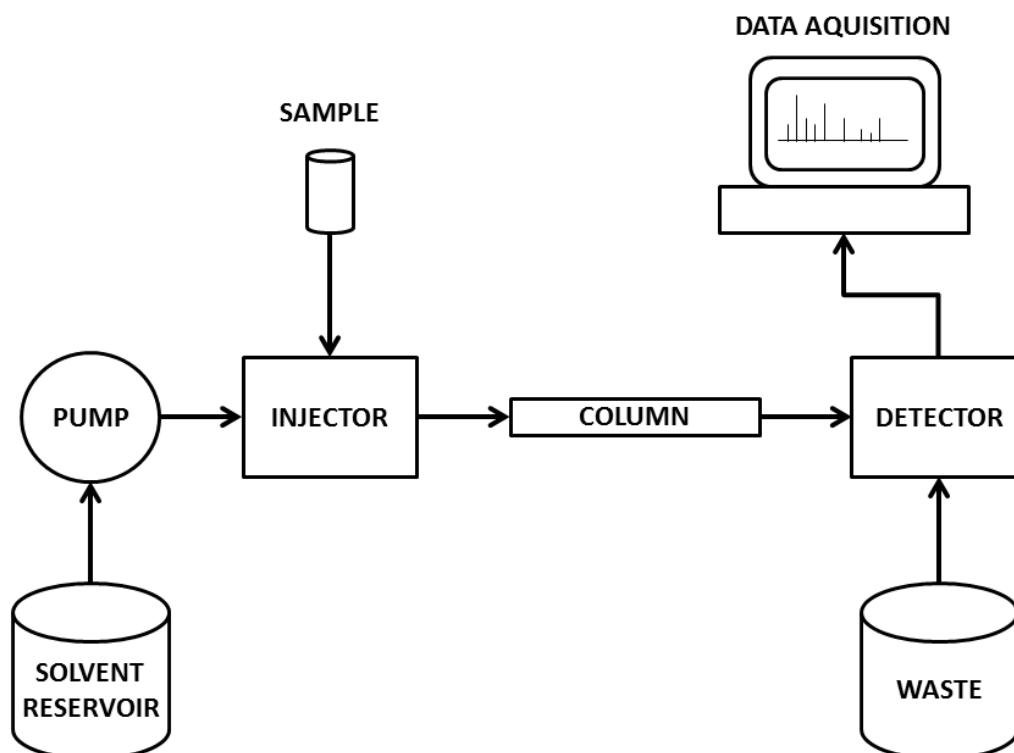


**Figure 1-9. Basic components of a liquid chromatography (LC) system.**

The most commonly used type of chromatography in metabolomics experiments is reversed phase chromatography (Lenz & Wilson 2007), used for separation of non-polar compounds (Tolstikov & Fiehn 2002) (also used for the proteomic analysis in this study). In this setting the solid phase lining the chromatographic column is hydrophobic, with a polar mobile phase. As a result, hydrophobic compounds present in the sample are bound to it and hydrophilic ones just pass through the column. The compounds are eluted by decreasing the polarity of the mobile phase. This is opposed to ‘normal’ phase chromatography, where hydrophilic stationary phase is used and hydrophilic compounds bind to the column. In this case, they are eluted by increasing the polarity of the mobile phase. The separation of polar compounds, has been significantly improved with the development of hydrophilic interaction chromatography (HILIC) (Tolstikov & Fiehn 2002), which has been used in the metabolomics part of this study. This is a special type of normal phase chromatography, where hydrophilic stationary phase is used together with eluents normally used in reversed phase chromatography. However, in contrast to reversed phase, the mobile phase

starts with a solvent of low polarity and elutes the compounds by increasing the polarity of the mobile phase (Cubbon et al. 2007).

In LC-MS, following separation using the LC system, the sample is introduced to a mass spectrometer. The mass spectrometer measures the mass to charge ratio ( $m/z$ ) of ions in a gas phase (Griffiths & Wang 2009). The molecules introduced into the MS by coupling to an LC system are in a liquid phase, therefore, they have to be vaporised and ionised in an ion source. Then they are sorted according to their  $m/z$  ratios in the mass analyser and finally detected in the mass detector. A plot of ion abundance against  $m/z$  is created from the collected data, which is called the mass spectrum of the sample. A schematic of the basic components of a mass spectrometer are presented in Figure 1-10. Tandem MS is often used (MS/MS) in the 'omics' sciences. It typically includes two mass analysers, separated with a collision cell. MS/MS is capable of collecting a much more detailed mass spectrum of the sample, which aids compound identification in cases of unknown metabolites.

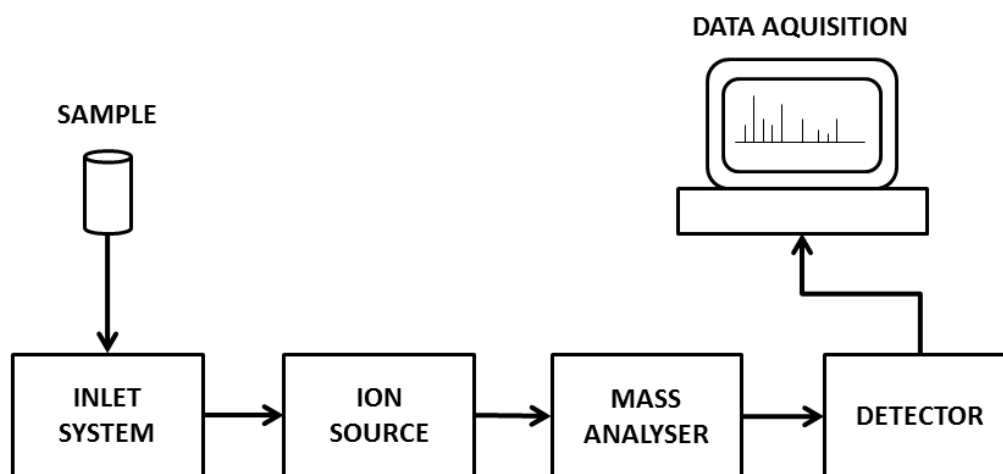


**Figure 1-10. Basic components of a mass spectrometer.**

The most commonly used ionisation method in LC-MS metabolomics is electrospray ionisation (ESI) (Lenz & Wilson 2007), however, atmospheric pressure chemical ionisation (APCI) or matrix-assisted laser desorption/ionisation (MALDI) can also be used (Griffiths & Wang 2009). ESI, as the name suggests, uses an electrospray which converts the mobile phase into aerosol and at the same time adds charge to the analyte particles by applying voltage as they are sprayed out. The droplets evaporate until only charged particles are left. In the

APCI ionisation, the analyte solution is first, vaporised and desolvated, then, the particles are ionised by a corona pin (discharge electrode). In MALDI technique, an appropriate matrix must be added to the sample, which is placed on a metal plate. Then, a laser is used for ablation and desorption of the sample and finally hot gas ionises the analyte and directs it to the mass analyser.

By carefully choosing the chromatography method, various analytes can be detected using the LC-MS based metabolomics. Therefore, it is often the method of choice of many scientists. However, there is one major drawback of this method, ion suppression (Lenz & Wilson 2007). Ion suppression occurs when compounds co-elute and as a result affect each other's ionisation potential. In this case the signal detected for some molecules can be decreased (or increased) causing an error in the metabolite's abundance. Therefore, scientists must be wary of this issue when analysing data collected using LC-MS.

### **1.5.2 Gas Chromatography – Mass Spectrometry (GC-MS)**

Gas chromatography, works on a similar separation principle as liquid chromatography, however, in this case, the mobile phase is a carrier gas instead of liquid. Typical carrier gases used are helium, nitrogen or hydrogen. The column is very thin and long (up to 60m) and available with varying degrees of polarity of the stationary phase. The polarity selected should be similar to the polarity of the analyte for a better separation. The analytes present in the sample adsorb to the column as the sample passes through the column. How well they are absorbed depends on the chemistry of the compound and just like in the LC separation, different compounds take different lengths of time to pass through the column (retention time). The column in a GC system is situated in an oven, and the conditions of separation can be altered by the length of the column, oven temperature and gas flow rate. A schematic of basic components of a GC system is presented in Figure 1-11.

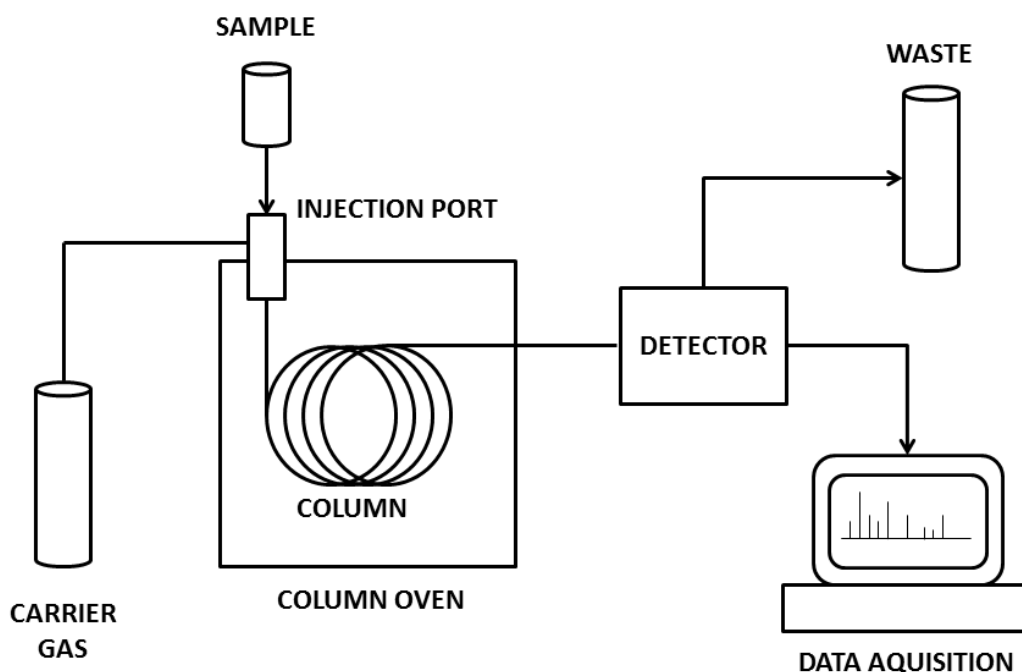


**Figure 1-11. Basic components of gas chromatography (GC) system.**

The capabilities of GC as a separation technique have been significantly improved with the development of multidimensional GC (GC x GC) (Lenz & Wilson 2007). In this setting two GC columns are used, usually one 30m long and the second 1.5m long, with different selectivities. The analytes elute from the first column and then they are quickly separated and eluted from the other column.

Different ionisation techniques are used in GC-MS compared to LC-MS, as the sample is introduced into the mass spectrometer in a gaseous and not liquid form, as well as the fact that the ion source operates under a vacuum and not at atmospheric pressure. Two most commonly used methods of ionisation for GC instruments are electron ionisation (EI) and chemical ionisation (CI) (Lenz & Wilson 2007). In the EI source, a heated filament is present, with voltage applied to it, which creates a flow of high energy electrons. This distorts the electric field of the analyte molecules passing through it, resulting in ionisation through the loss of an electron. The unstable molecules undergo fragmentation to achieve a more stable state. This process depends on the molecule and the fragmentation pattern is very predictable. It is a higher degree of fragmentation than in the LC-MS ionisation sources and more structural information about the compound can be obtained. CI ionisation uses a reagent gas (for example methane) to ionise the analyte. The ionisation occurs through collisions of the

analyte molecules with the ionised reagent gas molecules. In comparison with EI, very little or no fragmentation occurs in CI. However, this method is useful to detect parent ions, which can sometimes be missed in the EI fragmentation.

This technique has a major drawback, as it is limited to the analysis of volatile compounds. If the intended analytes are not naturally volatile, additional derivatisation steps must be included in sample preparation, which makes it more complicated and can introduce error. Additionally, as the sample is in many cases injected in a liquid form, it must be immediately vaporised, which can be quite problematic and result in sample loss. However, GC-MS offers great sensitivity, high resolving power and is not susceptible to ion suppression. Additionally, the fragmentation patterns of the same compounds are highly reproducible, even between different laboratories, which allows for the creation of international compound databases, which aid metabolite identification (Garcia & Barbas 2011).

## **1.6 Aims**

The human decomposition process is a complex biological phenomenon. It is known that after death, when normal physiological processes cease, there is a loss of homeostasis. This leads to a cascade of biological changes, inactive during life, which result in the breakdown of human tissue and other components of the body. Although this process was thoroughly studied in the past, it is still very difficult to assess the PMI. Other available PMI estimation methods (i.e. temperature measurement) can only be accurately used in a very short window of time after death. Studying the progression of post-mortem decomposition on a molecular level could yield the discovery of a biomarker or a panel of biomarkers, the levels of which change in a predictable manner with increasing time since death (for example, protein breakdown in muscle tissue). The discovery of a possible PMI biomarker could permit the development of an accurate, laboratory based method of PMI estimation. To test this hypothesis, this PhD project was set out with the following aims:

- ✓ To apply state of the art proteomic and metabolomics technologies in forensic research for estimation of the PMI

- ✓ To optimise the analytical methods available for protein and metabolite extraction and analysis in post-mortem tissue
- ✓ To use untargeted proteomic and metabolomics approaches to find potential biomarker candidates for the estimation of the PMI
- ✓ To use animal tissue as model and test the PMI biomarker discovery approaches
- ✓ To test the hypotheses developed using animal tissue, in human tissue
- ✓ To test the capabilities of commercially available metabolic or protein assays in PMI estimation (according to the results of the study).

## **2 METHODOLOGY**

### **2.1 Sample collection**

#### **2.1.1 Beef**

A sample of cow muscle (sternomandibularis) was collected from an abattoir by the project supervisor - Richard Burchmore and chilled over ice immediately post-slaughter (<5min). It was transported to the lab immediately after (<1 h). The time of death of the animal was recorded. First sample (time point 0) was collected immediately upon arrival. A small piece of the muscle was cut off using a scalpel and placed in a 50 mL Falcon tube (Corning, UK) and immediately frozen by placing it in a -80°C freezer. The time delay between the time of death of the cow to freezing the first sample was about 1.5 h. The rest of the meat was stored in a Tupperware container in a cold room at 4°C. Further samples were collected at daily intervals - a piece of the muscle was cut off and immediately frozen every 24 hours. Thirteen samples were collected in total, over thirteen days. Samples were labelled from T0 (time point/day 0) to T12 (time point/day 12).

#### **2.1.2 Rat**

Eight male Wistar rats (283-309g, average weight 296.5g) were sacrificed through carbon dioxide asphyxiation. Two of the rats were immediately dissected and the biceps femoris muscle tissue (see Figure 2-1) was collected from both left and right side of the body. First, only one rat was sacrificed separately from the remaining seven and dissected. Then, the remaining rats were sacrificed and one of those was dissected. This was done in order to be able to dissect two of the rats immediately after their death. The six remaining rats were stored in a Tupperware box at room temperature. The remaining rats were dissected at 24 h intervals during three consecutive days (two rats per day). Tissue samples were collected from each rat, both left and right biceps femoris. The collected tissue was weighed and cut into 0.5g portions, placed in separate cryogenic vials (Nunc CryoTubes, 1.8 ml, Sigma-Aldrich, Dorset, UK) and immediately snap frozen in liquid nitrogen. Samples were then stored at -80°C until analysis.

*Figure has been removed due to Copyright restrictions.*



**Figure 2-1. Rat muscle anatomy.**

**A. Lateral view of superficial muscles of the rat (Wingerd & Stain 1988), B. Biceps femoris muscle exposed prior to dissection (author's own photo).**

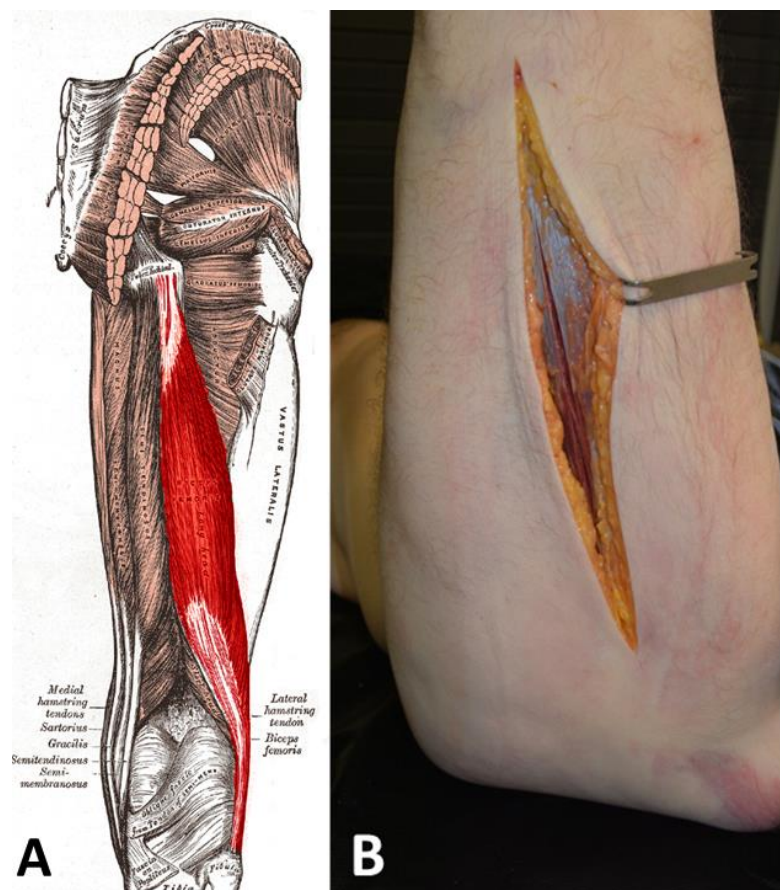
### **2.1.3 Human**

Human tissue samples were collected from individuals who donated their bodies to Forensic Anthropology Centre at Texas State University (FACTS) in San Marcos, Texas, US. Six donations were included in this study (see Table 2-1 for details). The post-mortem interval of each individual differed depending on the particular case. Medical examinations had to be carried out in some of the cases before the bodies were received at FACTS. Tissue samples were collected at regular daily intervals for a period of 2-5 days starting as soon as possible after the receipt of the bodies.

**Table 2-1. Basic information of the individuals included in the study.**

Abbreviations: COD – cause of death, GSW – gunshot wound, PMI – post-mortem interval (at the time of sampling).

Subject no	Gender	Age	COD	Sampling period (days)	PMI (days)
1	Male	60	Haemorrhagic stroke	4	7,8,9,10
2	Male	62	Pulmonary embolism	4	11,12,13,14
3	Female	69	Suicide - GSW (chest)	5	11,12,13,14,15
4	Male	59	Acute respiratory distress syndrome	3	3,4,5
5	Male	69	Metastatic non-small cell lung cancer	5	12,13,14,15,16
6	Male	60	Cardiovascular disease	2	18,19

**Figure 2-2. Human leg anatomy.**

A. Posterior view of leg muscle - biceps femoris highlighted in red (by Mikael Häggström, used with permission), B. Biceps femoris muscle exposed prior to sampling (author's own photo).

Four of the six cadavers (subjects 1, 2, 3 and 5) were refrigerated (in body bags) throughout the period of sampling in a cooler set to 7.2<sup>0</sup>C (45<sup>0</sup>F). The lower

limbs of two of these subjects were incomplete. Subject 1 was a tissue donor (leg bone and skin), therefore the skin and bones from his legs were removed, leaving the intact muscle supported on wooden sticks (in place of bones) and wrapped in bandages. Subject 3 had incisions made at the back of her legs, all along their length, exposing muscle tissue. However, the documentation did not explain why that was done. Shortly before sampling, the bodies were removed from the cooler, the right leg of the cadaver was lifted up and a single incision was made at the back of the leg, along the biceps femoris muscle line (see Figure 2-2). The female was placed in the cooler facing down for an easier access to the tissue. The underlying muscle tissue (biceps femoris) was exposed and a piece of the muscle was cut out using a scalpel. The collected tissue was then weighed into six 1g (approximately) portions and put into separate screw top vials (micro tubes 2ml, PP - Sarstedt, Leicester, UK). The bodies were returned to the cooler immediately after sampling. Sample vials were labelled and placed in a container with dry ice to be transported to FACTS, where they were stored in a  $-80^{\circ}\text{C}$  freezer until shipment. Mistakenly, a wrong type of muscle tissue was collected for subject 5 for the first 2 days of the sampling.

The other two individuals (subjects 4 and 6) were placed outdoors, out in the field belonging to the facility. The bodies were placed facing down (for an easy access to the sampling site) and covered with a cage (to protect from vulture activity). Subject 4 was first sampled two days after placement outdoors and subject 6 was first sampled indoors before it was placed outdoors. An incision was made to expose the muscle and a piece of biceps femoris was collected. The tissue was immediately wrapped in a piece of aluminium foil and placed in a plastic Ziploc bag, to be transported to the lab (5-10min drive). The incision site was covered up with tape to prevent the development of insect activity in the wound. Back in the lab, the tissue was cut up and weighed into six portions of approximately 1g and placed in the vials. The vials were labelled and placed on dry ice together with other samples collected on that day and transported to the main university campus to be placed in the freezer.

Once all of the samples were collected, they were shipped on dry ice to University of Glasgow using a courier service (CitySprint, UK). The muscle tissue was processed and analysed at the University of Glasgow.

## **2.2 Proteomic studies**

### **2.2.1 Commonly used reagents**

The reagents required for the two dimensional gel electrophoresis were acquired from two suppliers GE Healthcare, Buckinghamshire, UK (CHAPS, DTT, APS, TEMED, IPG-Buffer, agarose, glycine, Cy5 Dyes - yellow, blue and red) and Sigma-Aldrich, Dorset, UK (thiourea, SDS, BSA, Bromophenol Blue, glycerol, phosphoric acid, Coomassie Brilliant Blue, sypro orange stain). Urea and tris base were ordered from Fisher Scientific, Leicestershire, UK. Acrylamide and Bradford assay reagent were obtained from Bio-Rad, Hertfordshire, UK. Trypsin was provided by Promega, Southampton, UK. Solvents (methanol, ethanol, acetonitrile, chloroform, HPLC grade water) and acetic acid were acquired from VWR, Bedford, UK.

### **2.2.2 Protein extraction**

#### **2.2.2.1 Method development**

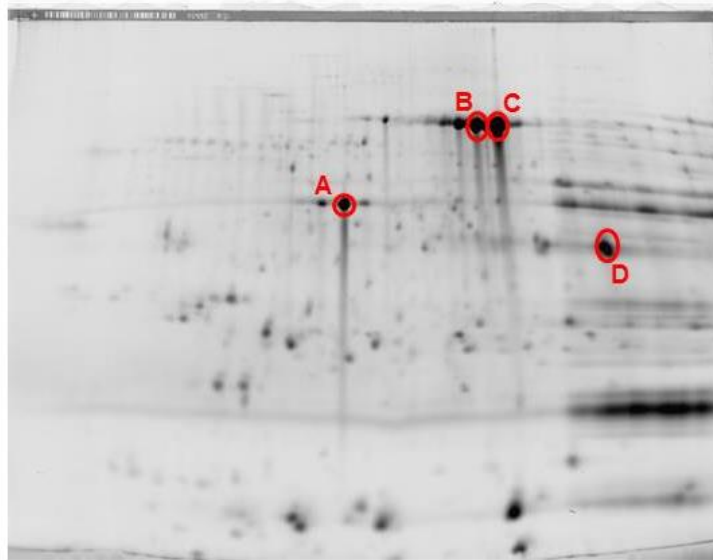
The first stage of the proteomics investigation involved developing an appropriate extraction method for the proteins present in muscle tissue. Initially, it was not possible to obtain post-mortem human or laboratory animal tissue to work with, due to ethical restrictions. Therefore, a sample of cow muscle was obtained from a slaughter house and used to optimise a protein extraction method from muscle tissue.

Two extraction methods found in the literature were initially tested: deionised water extraction (volume of 20x weight of the sample) (Michalczyk et al. 2012) and buffer extraction (urea, thiourea, CHAPS) (Montowska & Pospiech 2012). Four out of thirteen samples were selected for the 2DE proteomics experiment. This was due to the limitation of the gel based separation approach - only two samples can be compared on one gel. Comparison of four samples results in an eight gel experiment, which significantly increases the complexity of the experiment. Tissue samples from time points 0, 3, 7 and 11 were selected to investigate the changes at equal time intervals across the length of the time course. In order to perform a successful 2DE experiment the protein concentration in the extracted sample should be equal to 5mg/ml. The water

extraction did not yield the required protein concentration. Three of the extracted samples contained only 1mg/ml of protein. The fourth sample contained 4mg/ml, which is significantly better than the others, however, still too low to carry on with the experiment. The samples were re-precipitated in acetone and re-suspended in a smaller amount of lysis buffer to increase the concentration of protein, resulting in the following concentrations: 4.46, 2.71, 4.85, 1.33mg/ml for T0, T3, T7 and T11 respectively. It was decided to go ahead with the separation and analysis of samples T0 and T7 (highest protein concentrations) to test if the proteins can be successfully resolved using the 2DE approach. The two selected samples were labelled with two different fluorescent labels - Cy3 (T0) and Cy5 (T7) and compared on one gel (labelling protocol described in section 2.2.5.3 on page 71). Figure 2-3 shows two images obtained by scanning the gel using two different wavelengths, appropriate for each dye.

The two dimensional separation of the proteins in the trial samples worked very well, therefore a few spots were picked for mass spectrometry analysis to complete the workflow of this experiment and check all of the steps involved. As the spots were excised by hand, the most visible (abundant) spots were picked for the analysis (see Figure 2-3).

T0 Cy3



T7 Cy5

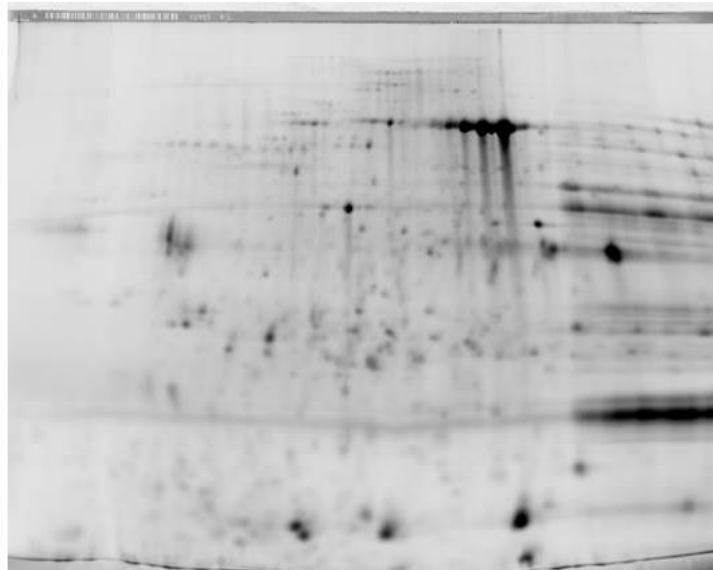


**Figure 2-3. Scanned images of fluorescently labelled samples. Differences in the spot intensities between the images can be observed. Protein spots circled in the top image were excised from the gel and identified through mass spectrometry: A – actin, B and C – serum albumin, D – lactate dehydrogenase B.**

The amount of the precipitated proteins was initially very low, most probably due to the low efficiency of the water extraction method. To test this assumption, the precipitation step was repeated with another aliquot of the homogenised sample. Again, the concentration of the protein was not high enough. In conclusion, this extraction method is not suitable for 2DE experiments as most proteins are not water-soluble. Additionally, the water extraction described by Michalczyk *et al* was used on ground beef samples, which is most probably the reason why the method worked in their investigation. It is possible that the mincing process would cause an initial break down of the proteins. Further grinding and denaturation steps would add to the initially released proteins. However, the authors did not state the protein concentration

in the samples following the extraction so it is difficult to say how well their method worked. Furthermore, they carried out their protein separation using SDS-PAGE for which the loading amount varies from 0.5 to 4 $\mu$ g of protein for purified samples (Grabski & Burgess 2001). This is significantly less than the 50 $\mu$ g required for 2DE gels.

The buffer extraction performed much better and yielded much higher amounts of extracted protein - concentrations in the samples varied between 7.4 and 8.2mg/ml. Therefore, it was selected as the extraction method for the proteomics workflow. However, the samples extracted with buffer were very viscous and gelatine-like in appearance, which put the accuracy of the measured protein concentration into question, as parts of the sample were hard to pipette. This was most probably due to presence of DNA in the samples, which should have been removed during the protein precipitation step of sample preparation. In order to break up any remaining DNA residues, the samples were sonicated using a probe sonicator. Following the sonication, the protein concentration measurement was repeated and more lysis buffer was added to adjust the concentration to the required 5mg/ml for 2DE analysis.

#### **2.2.2.2 Finalized protocol**

Tissue portions of 0.5g (for each time point) were used for each analysis. If tissue was weighed prior to freezing, it was homogenized while still frozen to minimise protein degradation. If it was not possible to weigh the tissue portions accurately before freezing, the samples had to be quickly thawed and weighed. The tissue was homogenized over ice, in 10 x weight volume (i.e. 5 ml) of the extraction buffer (7M urea, 2M thiourea and 4% CHAPS (Montowska & Pospiech 2012)), until a uniform mixture was achieved. A handheld homogenizer was used for this process (LabGEN 7, 220 VAC - Cole-Parmer, IL, USA). Homogenized samples were then centrifuged at 3000rpm to remove any insoluble matter. Extracts were kept on ice at all times.

#### **2.2.3 Protein precipitation**

250 $\mu$ l aliquots of the extracts were pipetted into fresh Eppendorf tubes (Reaction tubes, 1.5ml, PP - Greiner Bio-One, Frickenhausen, Germany) and 1ml

(4 x sample volume) of 100% acetone was added and placed in a -20°C freezer for an overnight precipitation. Next day, the samples were centrifuged (10 min, 13,000rpm) to pellet the precipitated protein. The pellet was then washed twice using 80% acetone (centrifuging the samples for 10 min at 13,000 rpm after each wash) and re-suspended in 200-250µl of the lysis buffer (6M urea, 2M thiourea 4% CHAPS and 25mM tris).

### **2.2.4 Protein assay**

The protein concentration was measured using the Bradford protein assay. Protein standards of the following concentrations were used: 0, 0.1, 0.2, 0.3, 0.4, and 0.5 mg/ml. 10µl of each of the standards and diluted samples (1:100) were pipetted onto a 96-well plate and 200µl of the diluted (1:5) Bio-Rad Bradford reagent was added to each. Plate was then shaken briefly and incubated for 30 min in the dark. A Tecan Genios plate reader and XFluor4 software were used to measure sample absorbance. Finally, a calibration curve was created, using the absorbance values of the standards, which was used to calculate the protein concentrations of the tissue extracts.

For the 2DE analysis the sample protein concentration was adjusted to 5mg/ml.

### **2.2.5 Two dimensional gel electrophoresis (2DE)**

#### **2.2.5.1 Gel preparation and casting**

Polyacrylamide gels were prepared freshly for each experiment. To prepare 6 gels (550ml solution) the following reagents were required: 171.5ml acrylamide, 137.5ml Tris, 5.5ml APS, 5.5ml SDS and 230ml H<sub>2</sub>O. All of the solutions were filtered prior to mixing. 77µl of TEMED was added to initiate the polymerisation reaction. The gels were poured into plate assemblies immediately after TEMED addition, then overlaid with 1ml of water-saturated butanol to ensure that each gel polymerised with a flat upper surface. The gels were prepared by laboratory technician - Alan Scott. Two types of gels were casted for each experiment: DiGE and preparative (prep) gels. Both types are prepared as described above; however, prep gels are secured to the glass plates with bind-silane. This is carried out, so that the prep gels can be safely handled and stained after the separation step. Additionally, prep gels contain unlabelled portions of the

sample mixture as these are later used for the mass spectrometric analysis of the proteins. DiGE gels contain sample mixtures labelled with fluorescent labels (cye dyes). Proteins of interest are selected using DiGE gels; corresponding spots are matched between DiGE and prep and excised from prep gels for analysis.

#### **2.2.5.2 Protein separation – trial experiment**

First, a trial proteomics experiment was carried out using four samples out of the 13-day time course. The trial 2DE experiment had a simpler set up, which was later modified (see Table 2-2 and Table 2-3). Initially, there was no internal standard used, only two samples were loaded onto each gel. This made it quite difficult to compare the samples across the gels. All of the gels were run in one tank at the exactly same conditions. However, that did not guarantee that the results were comparable between the gels. The sample mixture was separately labelled and prepared for each gel and also the protein spots had varying intensities between them. This created certain issues with data analysis as the software could not quantify or compare these changes without any normalisation method, e.g. (reference standard added to each gel). As a result, it was only possible to see and quantify the changes between the two samples compared within one gel. In order to analyse the protein spots, the images of all of the gels were printed off in 1:1 scale and compared by eye to match the same protein spots from the same samples on different gels (see Figure 2-4). The spots of interest were excised from the corresponding prep gels, i.e. if a significant change was observed between samples T0 and T3 the corresponding spot was cut out of the prep gel with sample T0 or T3. This was a very time-consuming process and mistakes could be made with the identification of the same protein spots in the corresponding gels.

Table 2-2. Experimental set up of the first trial 2DE experiment (beef tissue).

GEL	SAMPLE ID	Cy Dye	IEF STRIP NO
1 DiGE	T0	Cy3	84237
	T3	Cy5	
2 DiGE	T3	Cy3	84238
	T7	Cy5	
3 DiGE	T7	Cy3	84239
	T11	Cy5	
4 DiGE	T11	Cy3	84240
	T0	Cy5	
5 Prep	T0	N/A	84241
6 Prep	T3	N/A	84242
7 Prep	T7	N/A	84243
8 Prep	T11	N/A	84244

Table 2-3. Example of an experimental set up of multiplex 2DE experiment (rat tissue).

GEL	SAMPLE ID	Cy Dye	IEF STRIP NO
1 DiGE	T0	Cy3	68534
	T1	Cy5	
	Pooled std	Cy2	
2 DiGE	T1	Cy3	68535
	T2	Cy5	
	Pooled std	Cy2	
3 DiGE	T2	Cy3	68536
	T3	Cy5	
	Pooled std	Cy2	
4 DiGE	T3	Cy3	68537
	T0	Cy5	
	Pooled std	Cy2	
5 Prep	Pooled std	N/A	68538
6 Prep	Pooled std	N/A	68539

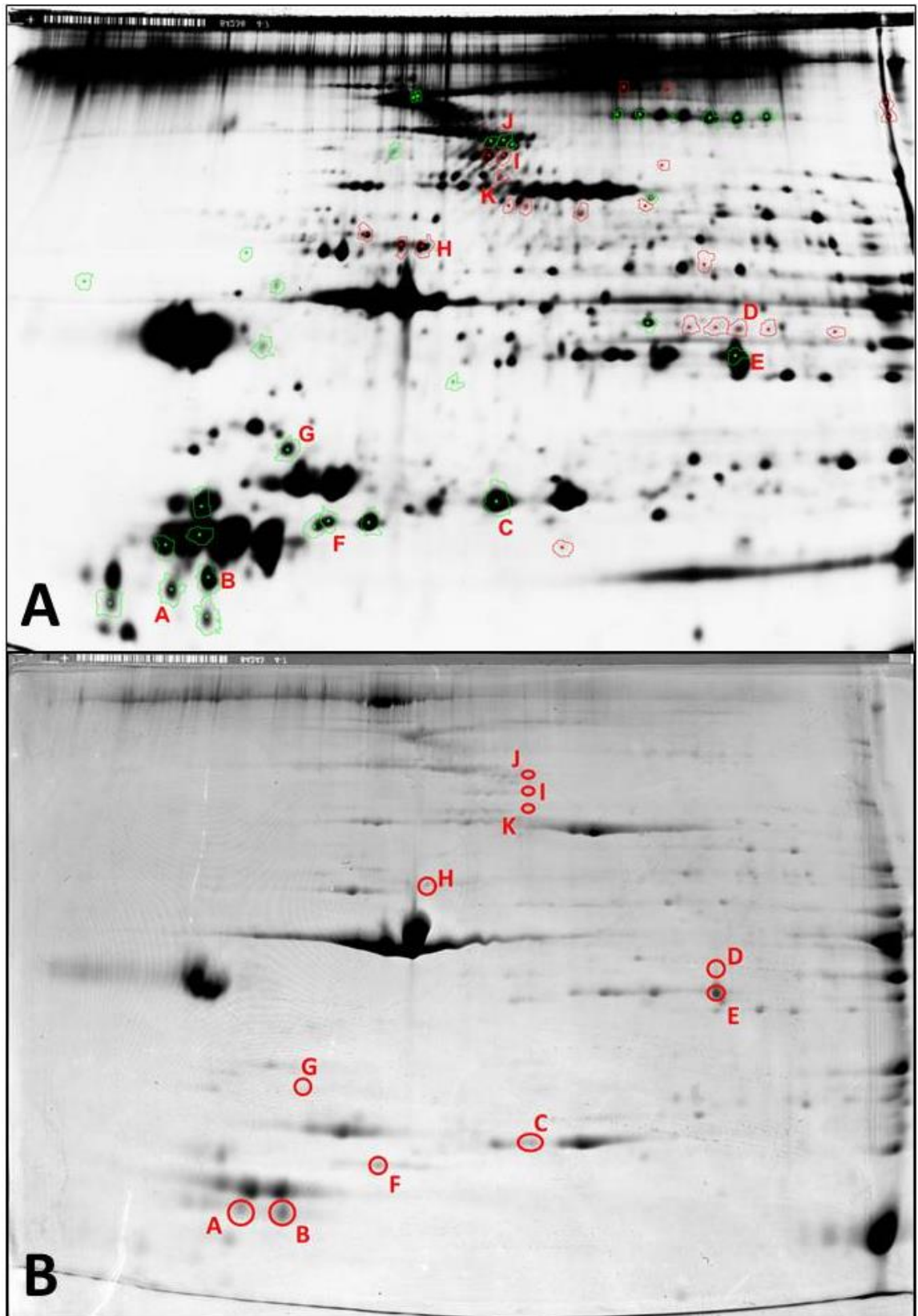


Figure 2-4. An example of DiGE and preparative gels for the same sample. Image A – DiGE gel where samples T3 and T7 were separated. Image B – preparative gel where unlabelled T7 sample was separated. Protein spots highlighted in image A were selected as proteins of interest. Red spots show proteins that decreased in abundance between the two samples and green show ones that increased. Protein spots A-J were picked from the preparative gel by comparing and matching corresponding spots by eye.

The problems with processing and interpretation of the data from this experiment proved that it should include a way of normalizing the data across the separate gels. A multiplex 2DE experiment solves that issue, as it allows comparing multiple gels and at the same time, multiple samples, through the inclusion of a pooled standard. A pooled standard is created by mixing equal amounts of each of the tested samples. Therefore, this experiment was repeated using a slightly different set-up, where a pooled standard was run alongside the samples on each gel (see Table 2-3). The pooled standard (labelled with a third dye) allowed normalising the spot intensities between separate gels using the Decyder software. This significantly increased the accuracy of the matching. Additionally, in the first experiment, four different prep gels were used - one for each of the tested samples (see Table 2-2). This was amended to include only one prep gel, containing the pooled standard, i.e. a single mix of all of the tested samples. This simplified the process of excision and identification of the proteins of interest. Finally, an automated spot-picker was purchased, which allowed for a far more precise excision of spots of interest. The amended protocol is described in detail in the next section.

### **2.2.5.3 Finalised protein separation protocol**

Two samples were compared on each 2D gel. To allow comparison between separate gels, a pooled standard was added to each gel. All three components of each gel were differentially labelled with fluorescent Cy5 dyes: yellow (pooled standard) and red and blue (samples). 1 $\mu$ l of dye was mixed with 10 $\mu$ l of sample (which is equivalent to 50 $\mu$ g of protein) and incubated in the dark for 30 min. Next, 1 $\mu$ l of 1mM lysine solution was added to stop the cross-linking reaction between the Cy5 dyes and proteins contained in the sample. The solution was still kept in the dark for another 10 min after adding the lysine. Finally, the differentially labelled samples were mixed according to which samples were to be compared on which gels (see Table 2-3) and made up to 460 $\mu$ l with rehydration buffer (7M Urea, 2M Thiourea, 4% CHAPS, 10mg/ml DTT, 5 $\mu$ l/ml IPG-Buffer pH 4-7, 0.002% Bromophenol blue). Furthermore, 100 $\mu$ l of an unlabelled portion of pooled standard was also made up to 460 $\mu$ l with strip rehydration buffer to be run separately on preparative gels, which were used to excise gel spots with proteins of interest and identify them.

Once all of the samples were mixed with rehydration buffer, 450µl of each was pipetted onto an isoelectrofocusing (IEF) coffin. Then, an IEF strip was placed on top of each sample and allowed to mix. After 30 min 1ml of oil was added on top of the strips to seal them off and finally, the coffins were placed in an IEF instrument (IPGphor, Pharmacia Biotech, Buckinghamshire, UK) and set to run overnight. The instrument settings are shown in Table 2-4.

**Table 2-4. IEF instrument parameters (total time – 26 h).**

Voltage applied (V)	Setting	Time (h)
30	Step and hold	10
300	Step and hold	2
600	Gradient	2
1000	Gradient	2
8000	Gradient	1
8000	Step and hold	9
1000	Step and hold	-

The IEF instrument separates the proteins out on the IEF strip based on their isoelectric point (pI). pI is defined as the pH value at which a molecule has no net charge (McNaught & Wilkinson 1997). Different proteins are differentially charged, therefore their pI values differ. Furthermore, the pI of a particular protein can change if the structure of the protein is modified in any way. The pH of the strip varies from pH 4 to 7 and the proteins line up accordingly along the strip. The pI values of most of the proteins lie within this pH range. This process is illustrated in Figure 2-5.

Next day the strips were removed from the coffins and washed. First they were very briefly immersed in 0.1% SDS to wash off any remaining oil residue. Next the strips were washed twice with 10ml each of 10mg/ml DTT in SEB solution (Strip Equilibration Buffer - 6M Urea, 75mM Tris pH 8.8, 29.3% glycerol, 2% SDS, 0.002% Bromophenol Blue) and 25 mg/ml iodoacetamide in SEB solution. Each of the four washes took 15 min. The strips were then secured on top of the gels with 1ml of agarose (0.5% in 1x SDS running buffer (1x Laemmli SDS electrophoresis buffer - 25mM Tris base, 192mM glycine, 0.1% SDS, 10L)). Finally, the gels were placed in an electrophoresis tank (Ettan Dalt II System, Amersham Biosciences, Buckinghamshire, UK) filled with x1 (lower chamber) and x2 (upper chamber) running buffer and run overnight at 1W per gel.

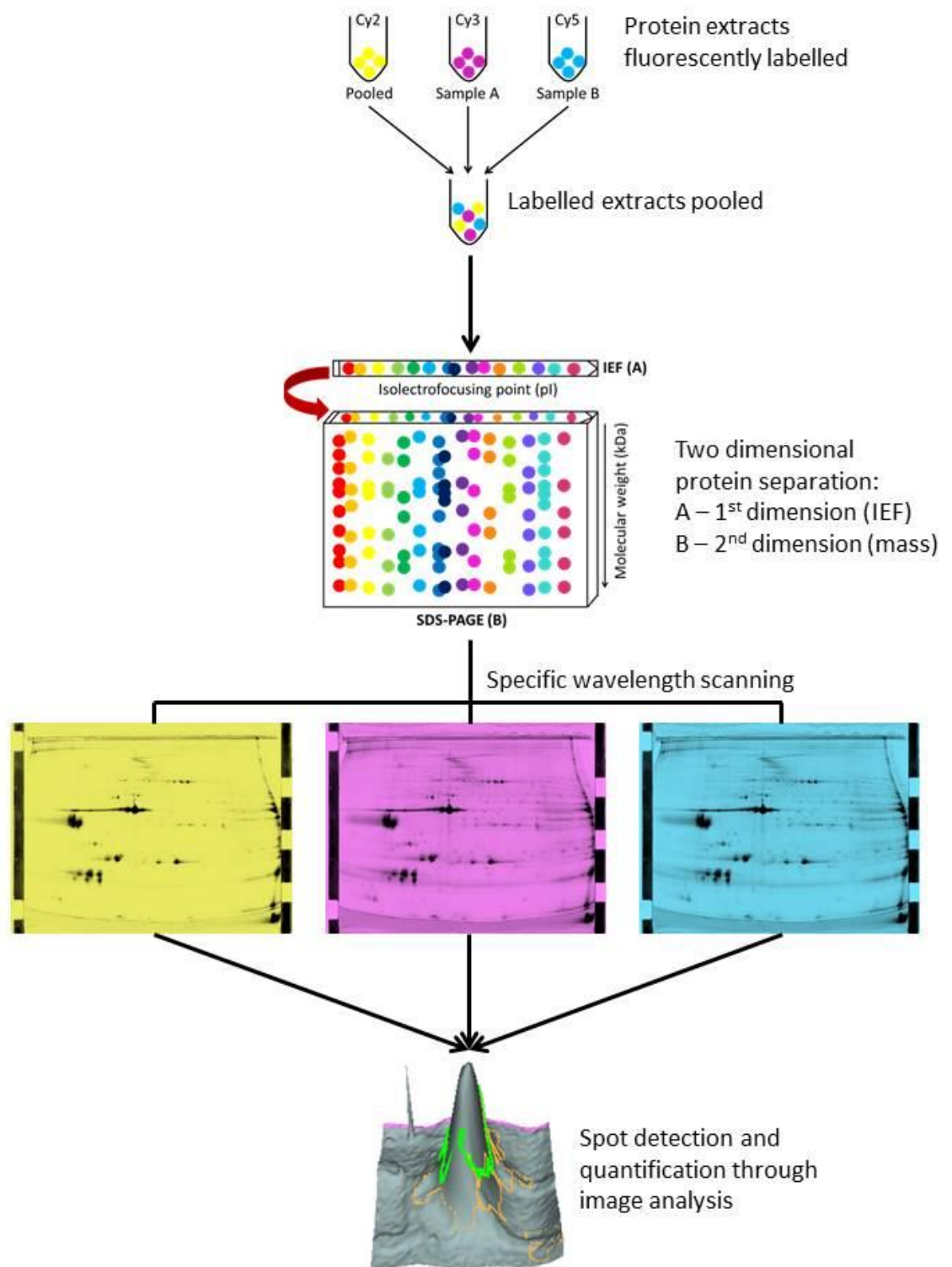


**Figure 2-5. Diagram illustrating the two-dimensional gel electrophoresis protocol.**

This is the second step (the second dimension) of the 2DE process. In this part the proteins separated out on the IEF strip undergo a further separation based on their molecular weight (MW). Proteins travel down the polyacrylamide gel with various speeds. The larger proteins move through the gel much slower than the smaller proteins, resulting in the smaller ones travelling to the bottom of the

gel and larger ones remaining nearer the top. This process occurs when power is supplied to the tank (see Figure 2-5).

The following day, all of the gels were removed from the tank. The DiGE gels were imaged on the same day. Meanwhile, the preparative gels were stained using two different stains: non-colloidal Coomassie stain (200ml of Coomassie Dye stock with 50ml of methanol added; Coomassie dye stock: 50g ammonium sulphate, 6ml 85% phosphoric acid, made up to 490 with deionised water and 10ml of Coomassie blue stain added) and sypro orange fluorescent stain (0.0001% sypro stain in 7% acetic acid). Before staining, the gels were fixed to stop protein diffusion and preserve the state of the gel. The Coomassie stained gel was fixed for 1.5 h in a solution of 40% ethanol and 10% acetic acid in water (500ml per gel). The sypro stained gel was fixed in for 1 h in a solution of 7% acetic acid and 10% methanol in water (500ml per gel). After that 500ml of appropriate stain was added to each gel. Sypro orange staining time was 2 h and in the case of Coomassie blue the staining time was 4 days. Following the staining procedure, the gels were imaged using a fluorescence scanner (Typhoon 9400, GE Healthcare, Buckinghamshire, UK), as were the unstained DiGE gels. Cy2 stained samples were scanned using the blue laser (488nm), Cy3 using green laser (532nm) and Cy5 using red laser (633nm). The obtained images were processed using DeCyder software (version 7, GE Healthcare, Buckinghamshire, UK). The above described protocol is illustrated in Figure 2-5.

Protein spots of interest were selected from the software processed images and a map of these spots was created. With the help of the spot map, protein spots of interest were excised from the prep gels using a scalpel for beef samples and using an automated spot picker (Ettan, Amersham Biosciences, Buckinghamshire, UK) for rat and human samples. The gel pieces were then washed in 100mM ammonium bicarbonate and 50% acetonitrile/ammonium bicarbonate solutions respectively. Next, they were digested in trypsin solution overnight. The following day the digest (liquid surrounding the gel pieces) was transferred onto a new 96-well plate and the remaining gel pieces were washed in 5% formic acid and acetonitrile. The liquid from the gels was collected and added to the second plate with previously transferred gel digests. The plate containing the liquid extracted from the gel pieces was dried down in a vacuum centrifuge (Savant SPD1010, Thermo Scientific) and analysed using mass spectrometry; peptides

were solubilized in 2% acetonitrile with 0.1% trifluoroacetic acid and fractionated on a nanoflow uHPLC system (RSLCnano Thermo Scientific, Hemel Hempstead, UK) before online analysis by ESI mass spectrometry on an Amazon Speed ion trap MS/MS (Bruker Daltonics, Coventry, UK). First, peptides were desalted and concentrated using a trap column (for 4 min). This was followed by peptide separation performed on a Pepmap C18 reversed phase column (Thermo Scientific): an acetonitrile gradient (in 0.1% v/v formic acid) (3.2 - 32% v/v 4 - 27 min, 32% to 80% v/v 27 - 36 min, held at 80% v/v 36 - 41 min and re-equilibrated to 3.2%) for a total time of 45 min. A fixed solvent flow rate of 0.3 $\mu$ l/min was used for the analytical column. The trap column solvent flows at a flow rate of 25 $\mu$ l/min using 2% acetonitrile with 0.1% v/v trifluoroacetic acid. MS analysis was performed using a continuous duty cycle of survey MS scan. 10 most abundant ions were selected for fragmentation in each survey scan, which is then continuously repeated. Only multiply charged peptides were chosen, with dynamic exclusion for 120 s. This means that each selected ion was added to an exclusion list for this length of time.

MS data were processed using Data Analysis software (Bruker) and the automated Matrix Science Mascot Daemon server (v2.5.1). Protein identifications were assigned using the Mascot search engine used to interrogate protein sequences in the NCBI Genbank database, allowing a mass tolerance of 0.4Da for both MS and MS/MS analyses.

Mascot software (Perkins et al. 1999) compared the experimental masses of peptides or fragment ions present in the sample with the calculated masses available in the database. By using specific algorithms the software could find the closest match or matches with the unknown. Furthermore, the algorithm employed a scoring system which reflected the confidence of the match (MOWSE<sup>®</sup> score, for MOlecular Weight SEarch). As a result, it created a list of proteins which were matched to the MS identified peptides. An example of a Mascot search result page can be seen in Figure 2-6.


**Mascot Search Results**

```

User          :
Email         :
Search title  : Bony Vertebrates Search NCBI
MS data file  : \\130.209.53.48\share\Amazon\Bogusia_150213\Output_MGF\Bogusia_RH1_01_3821.mgf
Database      : NCBIInr 20130219 (23214025 sequences; 7977717942 residues)
Taxonomy      : Bos Taurus (Cattle) (43982 sequences)
Timestamp     : 20 Feb 2013 at 15:52:54 GMT
Enzyme        : Trypsin
Fixed modifications : Carbamidomethyl (C)
Variable modifications : Oxidation (M)
Mass values   : Monoisotopic
Protein Mass  : Unrestricted
Peptide Mass Tolerance : ± 0.4 Da
Fragment Mass Tolerance: ± 0.4 Da
Max Missed Cleavages : 1
Instrument type : ESI-TRAP
Number of queries : 2693
Protein hits  :
  gi|4501881   actin, alpha skeletal muscle [Homo sapiens]
  gi|4501885   actin, cytoplasmic 1 [Homo sapiens]
  gi|116004449 aminoacylase-1 [Bos taurus]
  gi|297474460 PREDICTED: keratin, type II cytoskeletal 1 [Bos taurus]
  gi|358421417 PREDICTED: keratin, type II cytoskeletal 3 [Bos taurus]
  gi|4838363   creatine kinase M chain [Bos taurus]
  gi|60097925  creatine kinase M-type [Bos taurus]
  gi|56710317  keratin, type II cytoskeletal 5 [Bos taurus]
  gi|262118301 keratin, type I cytoskeletal 14 [Bos taurus]
  gi|115495957 keratin, type I cytoskeletal 25 [Bos taurus]
  gi|195963439 nuclear pore complex protein Nup205 [Bos taurus]
  gi|296485337 TPA: interleukin 9-like [Bos taurus]
  gi|329663591 gametogenetin-binding protein 2 [Bos taurus]
  gi|115496716 uncharacterized protein C19orf60 homolog [Bos taurus]
  gi|297474454 PREDICTED: keratin, type II cytoskeletal 2 oral [Bos taurus]
  gi|115495113 keratin, type II cytoskeletal 71 [Bos taurus]
  gi|297474456 PREDICTED: keratin, type II cytoskeletal 2 oral [Bos taurus]
  gi|296475269 TPA: ZBTB42 protein-like [Bos taurus]
  gi|329663345 telomerase-binding protein EST1A [Bos taurus]
  gi|329664586 UPF0639 protein [Bos taurus]
  gi|89399     argininosuccinate lyase (EC 4.3.2.1) - bovine (tentative sequence) (fragments)
  gi|358415263 PREDICTED: plectin-like [Bos taurus]
  gi|28603800  ATP synthase subunit delta, mitochondrial precursor [Bos taurus]

```

### Select Summary Report

Format As	Select Summary (protein hits) ▾	<a href="#">Help</a>
Significance threshold p<	<input type="text" value="0.05"/>	Max. number of hits <input type="text" value="AUTO"/>
Standard scoring	<input type="radio"/> MudPIT scoring <input checked="" type="radio"/>	Ions score or expect cut-off <input type="text" value="0"/>
Show pop-ups	<input checked="" type="radio"/> Suppress pop-ups <input type="radio"/>	Show sub-sets <input type="text" value="0"/>
Preferred taxonomy	<input type="text" value="All entries"/> ▾	
<input type="button" value="Re-Search"/> <input checked="" type="radio"/> All queries <input type="radio"/> Unassigned <input type="radio"/> Below homology threshold <input type="radio"/> Below identity threshold		

**Figure 2-6. Example of a Mascot search results page.**

Since different proteins can contain similar peptide chains, the software matches them to various possible proteins and ranks them in terms of probability. Matches containing the highest scores have the highest probability of being correctly identified. Only matches with a significance threshold of 0.05 or lower are displayed, which means the matches are fairly confident. However, in cases where proteins had not been well resolved on the gel, more abundant protein spots could contain more than one protein. In this case, another parameter assigned to each match could be examined - emPAI value (Exponentially Modified Protein Abundance Index). This is an indication of how abundant the protein was in the spot - the higher the number, the higher the abundance of the protein. Therefore, matches with the highest scores and

highest emPAI values were most likely to be the correct identifications for the protein spots in question. The parameters discussed above are highlighted in Figure 2-7 showing another part of the Mascot search result page including a list of matched peptides.



Figure 2-7. An example of Mascot search result, showing a list of matched peptides.

## 2.3 Metabolomics experiments

### 2.3.1 Sample preparation

For the purpose of statistical analysis, 4 separate pieces of rat tissue (two rats, right and left leg) and 3 separate pieces of beef and human tissue were used for each time point.

Tissue samples (0.5g) were homogenized in 5ml of chloroform/methanol/water solution 20:60:20 (v/v/v) (T'Kindt et al. 2010) using a handheld homogenizer (Cole-Palmer) and shaken on ice for 1h using a rocking table (150 rpm, Lab-

Shaker LS-X, Kuhner, Switzerland). Following extraction, samples were centrifuged at 3000 rpm for 30 min. 1ml of the supernatant was transferred into an Eppendorf tube and centrifuged again at 13 000 rpm for 10 min. Samples were then transferred to fresh Eppendorf tubes and stored at -80 °C until analysis.

### **2.3.2 Liquid Chromatography – Mass Spectrometry (LC-MS) analysis**

10µl of each sample was used for analysis using hydrophilic interaction liquid chromatography-mass spectrometry (UltiMate 3000 RSLC (Thermo Scientific, San Jose, California, USA) with a 150 x 4.6mm ZIC-pHILIC analytical column (Merck SeQuant, Umea, Sweden) running at 300µl/min, coupled to an Exactive mass spectrometer (Thermo Scientific, Waltham, Massachusetts, USA) for MS detection. Buffers consisted of A: 20mM ammonium carbonate (Sigma Aldrich) in H<sub>2</sub>O (LC-MS Grade, Rathburn, Walkerburn) and B: acetonitrile (LC-MS Grade, Rathburn, Walkerburn). The gradient ran from 80% B 20% B in 15 min, followed by a wash at 5% B for 3 min, and equilibration to initial conditions for 5 min. The Exactive mass spectrometer was used to detect ions using a HESI-II interface with a source temperature of 150 °C and capillary temperature of 270 °C. Sheath gas flow rate was set at 40, auxiliary gas flow rate was 5 and sweep gas was 1. Each sample was analysed using alternating detection in positive ion and negative ion using polarity switching mode, the spray voltage was 4.5 kV and 3.5kV respectively. Full scan MS detection was acquired for the range 70 to 1400 m/z at 50000 (at 400 m/z) resolution for each polarity.

For better detection and identification of different groups of compounds, the samples were also analysed using a ZIC-HILIC analytical column (150 x 4.6mm, Merck SeQuant) coupled to the same LC-MS system. Method parameters were the same as above with the exception of the buffers used - A: 0.1% formic acid and B: 0.08% formic acid, both in acetonitrile.

Raw mass spectrometry data was processed using the Glasgow University Polyomics pipeline, consisting of XCMS (Smith et al. 2006) (for peak picking), MzMatch (Scheltema et al. 2011) (for filtering and grouping) and IDEOM (Creek et al. 2012) (for further filtering, post-processing and identification). Core

metabolite identifications were validated against a panel of unambiguous standards by accurate mass and retention time. Additional putative identifications were assigned by accurate mass along with a retention time prediction algorithm (Creek et al. 2011). Mean intensity relative to the control group (i.e. earliest time point in the given analysis) and standard errors of the mean were generated for all groups of picked peaks.

### **2.3.3 Gas Chromatography – Mass Spectrometry (GC-MS) analysis**

GC-MS analysis was carried out by a Glasgow University Polyomics mass spectrometry specialist - Stefan Weidt.

#### **2.3.3.1 Preparation of calibrators, quality control standards (QC) and internal standards**

Eight concentrations ranging from 4.6nmole to 23pmole of amino acid standard mixture were prepared for calibration series calculation. Two QC amino acid concentrations were prepared at 1.6nmole and 160pmole. Internal standards  $^{13}\text{C}_6$ -glucose (2nmole),  $^2\text{H}_{27}$ -myristic Acid (2nmole) and scyllo-inositol (1nmole) were added to each sample aliquot, calibration standard and quality control standard. All of the above were purchased from Sigma-Aldrich, UK.

#### **2.3.3.2 Sample derivatisation**

10 $\mu\text{l}$  of extracted sample along with a pooled standard was transferred into a 9mm screw cap borosilicate glass 1.5ml vial. Samples were then dried in a Savant SPD1010 SpeedVac concentrator (Thermo Scientific) for 120 min. 50 $\mu\text{l}$  of 20mg/ml (w/v) methoxyamine HCL in pyridine was added to each dried vial, vortexed for 10 s and incubated at 80°C for 15 min. Following the methoximation step, 50 $\mu\text{l}$  of N-Methyl-N-(trimethylsilyl) trifluoroacetamide + 1% trimethylchlorosilane (MSTFA + 1% TMCS) was added, followed by a further 30 s of vortexing. Silylation was performed by incubation at 80°C for a further 15 min. Samples were cooled to room temperature and were then ready for injection on the GC-MS instrument.

### 2.3.3.3 Sample analysis

The acquisition sequence started with one matrix blank injection of the derivatisation reagents, followed by 6 injections of the pooled standard. Samples, calibration standards and QC samples were injected in randomised order with a pooled standard injection every 6 injections. 1µl of derivatised sample was injected into a split/splitless (SSL) injector at 280°C using a 1 in 10 split flow using a Trace 1310 gas chromatograph (Thermo Scientific). Helium carrier gas at a flow rate of 1.0ml/min was used for separation on a TraceGOLD TG-5SILMS 30m length × 0.25mm inner diameter × 0.25µm film thickness column (Thermo Scientific). The initial oven temperature was held at 70°C for 4 min, followed by a temperature gradient of 20°C/min ramp rate to 300°C, which was held for 4 min. Eluting peaks were transferred through an auxiliary transfer temperature of 240°C into a QExactive-GC mass spectrometer (Thermo Scientific), with EI ionisation at 70 eV energy, emission current of 50µA and an ion source temperature of 250°C. A filament delay of 4.5 min was used to prevent excess reagents from being ionised. High resolution EI fragment spectra were acquired using 120,000 resolution with a mass range of 50-750 *m/z*. The best internal lock mass from the background peaks at *m/z* 207.0324, 281.0511 or 355.0699 was used to maintain mass accuracy throughout the chromatogram.

### 2.3.3.4 Data analysis

Data processing was carried out using TraceFinder 4.0 General Quan (Thermo, UK). Untargeted screening was performed using a forward library search for unknown compound discovery. This involved a peak deconvolution step using a peak threshold of 2,000.000 with *m/z* signal-to-noise threshold of 20. National Institute of Standards and Technology (NIST) 2014 'mainlib' and 'replib' low resolution libraries were used to annotate the peaks with a search index threshold of 500. Chemical formulae were then assigned to the accurate mass of each deconvoluted fragment ion measured from the Q Exactive GC making use of the molecular formula of the match to the NIST low resolution library hits. Deconvoluted samples are then retention time aligned and peaks grouped for comparison.

The rat data was analysed without the inclusion of calibration standards, therefore, the amino acid concentrations were calculated from ion chromatogram peak areas matched to the reference standards included in the analysis (detailed in section 5.2.1). The retention times and quantification ions used for concentration calculations are shown in Table 2-5. In the case of human tissue, the analysis included a set of calibrators (see section 2.3.3.1) which were used to create a calibration curve and calculate the amino acid concentrations.

**Table 2-5. Amino acid retention times and quantification ion used for concentration calculation.**

Amino Acid	RT (min)	Quan Ion ( <i>m/z</i> )
Glycine	9.28	174.1128
L-Alanine	10.11	116.089
L-Asparagine	11.64	231.1343
L-Aspartatic Acid	10.72	232.1184
L-Cysteine	10.97	220.1006
L-Cystine	14.78	411.1442
L-Glutamic Acid	11.33	246.134
L-Glutamine	12.23	156.0839
L-Histidine	13.02	218.1027
L-isoleucine	9.18	158.136
L-Leucine	9.00	158.136
L-Lysine	12.70	174.1129
L-Methionine	10.75	176.0924
L-Ornithine and L-Arginine	12.15	348.2079
L-Phenylalanine	11.44	192.1203
L-Proline	11.14	142.1047
L-Serine	9.65	204.1234
L-Threonine	9.83	219.1105
L-Tryptophan	14.46	202.1047
L-Tyrosine	13.12	218.1027
L-Valine	8.54	218.1027
Hydroxy-L-Proline	10.78	230.1391
L-Homoserine	10.27	218.1391

## **2.3.4 Phenylalanine assay**

### **2.3.4.1 Preparation of standards and reagents**

Phenylalanine was one of the potential PMI markers. Therefore, a commercially available assay kit (Sigma-Aldrich, Dorset, UK) was used to quantify the amount of this amino acid in muscle tissue, to test it as a potential method of PMI estimation. The assay used was a coupled enzyme assay, which detects enzymatic activity by coupling of two enzymatic reactions. In the case of this particular assay, the first reaction was phenylalanine deamination, which results in production of the reduced form of nicotinamide adenine dinucleotide (NADH). Then the NADH reacts with the assay resulting in a fluorimetric product (not specified), which is proportional to the amount of phenylalanine. The kit included all of the reagents necessary to carry out the assay - assay buffer, phenylalanine standard 10 $\mu$ mole, enzyme mix, tyrosinase (used to control interference, which might be caused by tyrosine present in the sample) and assay developer. The enzyme mix and developer were prepared according to manufacturer's guidelines by reconstituting in 220 $\mu$ l of the assay buffer. According to the provided method the phenylalanine standard was supposed to be reconstituted in 100 $\mu$ l of water to give 10nmole/ $\mu$ l solution. However, the standard was re-suspended in 1 ml of water by mistake with resulting concentration of 1nmole/ $\mu$ l solution. The standard was further diluted before carrying out the assay to a final concentration of 0.1nmol/ $\mu$ l, therefore the initially reconstituted standard was diluted 1 in 10 instead of 1 in 100 as the protocol dictates.

### **2.3.4.2 Sample preparation**

Samples were prepared according to manufacturer's guidelines - 20mg of tissue sample (exact weight 21mg) was homogenized in 100 $\mu$ l of the phenylalanine assay buffer. The tissue was homogenized in Eppendorf tubes by mashing it with a special pestle designed for this purpose. Finally, the samples were centrifuged at 13,000 rpm to remove any insoluble material. As the concentration of phenylalanine in the muscle tissue was unknown, various sample dilutions had to be tested to ensure the reading was within the range measured by the assay. To do this, different amounts of the sample, i.e. 1, 2, 5 and 10 $\mu$ l were pipetted onto a 96-well plate along with the standard (see Table 2-6) and made up to 50 $\mu$ l

with the assay buffer. All of the standards were pipetted in duplicate as stated in the guidelines. Samples were pipetted in quadruplicate to test the necessity of a sample blank (enzyme mix not added) required to correct for background signal coming from NADH and NADPH present in the sample.

**Table 2-6. Volumes of the phenylalanine standard used to prepare the calibration curve.**

Standard	1	2	3	4	5	6
Volume used ( $\mu\text{l}$ )	0	2	4	6	8	10
Resulting concentration (nmole)	0	0.2	0.4	0.6	0.8	1.0

Once all of the standards and samples were pipetted onto the plate, the volumes of reagents added were as shown in Table 2-7.

**Table 2-7. Volumes of reagents used to develop the assay.**

Reagent	Sample blank	Samples and Standards
Phenylalanine assay buffer	48 $\mu\text{l}$	46 $\mu\text{l}$
Enzyme mix	-	2 $\mu\text{l}$
Developer	2 $\mu\text{l}$	2 $\mu\text{l}$

Once all of the standards, samples and reagents were pipetted on to the plate, it was incubated for 20 min at 37°C. The fluorescence intensity was then measured using an Infinite 2000 Pro plate reader (Tecan, Switzerland). The instrument settings used are shown in Table 2-8.

**Table 2-8. Tecan instrument settings used for fluorescence intensity measurement.**

Mode	Fluorescence top reading
Excitation wavelength	535nm
Emission wavelength	587nm
Excitation bandwidth	9nm
Emission bandwidth	20nm
Gain	76 optimal (100%)
Number of flashes	25
Integration time	20 $\mu\text{s}$
Lag time	0 $\mu\text{s}$
Settle time	0ms
Z-position (Manual)	20000 $\mu\text{m}$

**Table 2-9. Readings of the trial phenylalanine assay test.**

<>	1	2	3	4	5	6	7	8	9	10	11	12
A	1312	1092	3817	4110	6325	6629	9249	9266	11219	11238	13753	13608
B	27758	24571	28979	32346	1	2	2	2	2	1	2	2
C	33661	38932	40418	39820	2	1	3	2	2	2	2	2
D	40154	37858	41263	37469	2	2	1	2	2	1	2	1
E	36140	38033	37654	39215	2	1	2	2	2	1	2	2
F	3	2	3	2	2	2	3	2	1	1	1	2
G	2	3	2	1	3	2	2	3	2	2	2	2
H	3	3	2	2	2	2	2	2	3	2	2	2

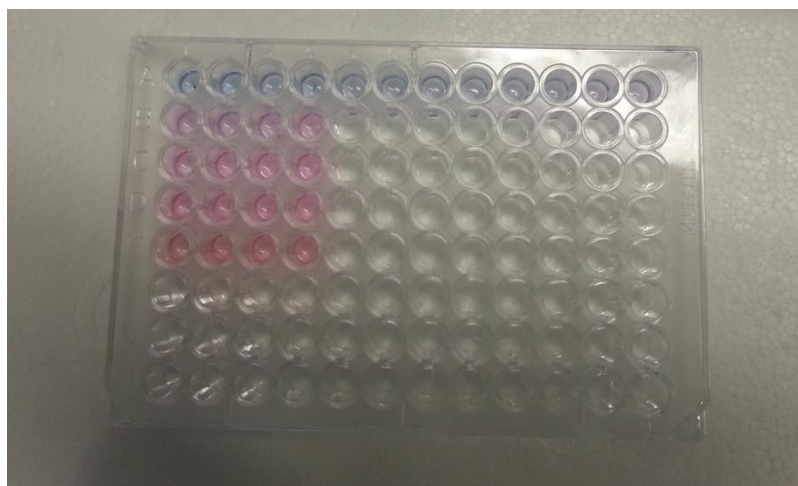


**Figure 2-8. Image showing the observed colour change in the trial phenylalanine assay. Top row contains the phenylalanine standard at various concentrations. The 4 rows below contain different aliquots of the homogenized tissue sample. Pink colour indicates that the concentration of phenylalanine is too high in comparison with the calibration standards in the top row.**

The phenylalanine levels were too high to be measured within the range of the calibration curve (see Table 2-9 and Figure 2-8). Therefore, the test was repeated using different dilutions of the homogenized tissue. 22mg of tissue was homogenized and 10 $\mu$ l of neat, 1 in 10, 1 in 100, 1 in 1000 and 1 in 10,000 dilutions of the homogenate were pipetted onto the plate along with the standards and made up to 50 $\mu$ l with assay buffer. In this case no sample blank was used as the test was carried out just to work out the appropriate dilution of the sample. The neat and 1 in 10 dilutions were too concentrated, whereas 1 in 1000 and 1 in 10,000 were too low to be measured. The 1 in 100 dilution was within the range of the calibrators, however, at the very low end (calculating at 0.03nmole on a scale from 0 to 1nmole). Since only 10 $\mu$ l of the dilution was used, the addition of the assay buffer to make it up to 50 $\mu$ l would have diluted it further, resulting in a final dilution of 1 in 500. Therefore, to carry out the assay, the sample was diluted 1 in 100 with the buffer, and 50 $\mu$ l of that was pipetted onto the 96-well plate.

After the initial testing, the amount of reagents left was only sufficient to carry out one experiment involving tissue samples from two of the human subjects (the amount of phenylalanine tested at each time point). Subjects 2 and 5 were selected as they were both male, with overlapping PMI at the time of sampling.

Table 2-10 shows the amount of tissue weighed out for each time point.

**Table 2-10. The weight of tissue used for each subject and time point for the assay.**

PMI (days)	Subject 2	Subject 5
11	21mg	N/A
12	21mg	22mg
13	21mg	20mg
14	21mg	22mg
15	N/A	20mg
16	N/A	20mg

Three 50 $\mu$ l aliquots of each sample (1 sample blank and 2 including the enzyme mix) were pipetted onto the plate along with the two aliquots of each of the calibration standards. Only one sample blank was used, as there was not enough developer solution left for 4 aliquots of each time point (only one kit was purchased). Ideally, each blank, standard and sample should be measured in duplicate to give an average end result. Table 2-11 shows how the samples were situated in the 96-well plate.

**Table 2-11. Layout of a 96-well plate showing the positions of all of the samples tested with the phenylalanine assay.**

**Abbreviations used: Blk – blank, Std – standard, S2 – subject 2, S5 – subject 5, D followed by a number – indicates PMI (days since death), subject/day number followed by Blk – indicates sample blank for this particular sample, X – unused, empty wells.**

	1	2	3	4	5	6	7	8	9	10	11	12
<b>A</b>	Blk	Blk	Std 1	Std 1	Std 2	Std 2	Std 3	Std 3	Std 4	Std 4	Std 5	Std 5
<b>B</b>	S2 D11 Blk	S2 D11	S2 D11	X	S5 D15 Blk	S5 D15	S5 D15	X	X	X	X	X
<b>C</b>	S2 D12 Blk	S2 D12	S2 D12	X	S5 D16 Blk	S5 D16	S5 D16	X	X	X	X	X
<b>D</b>	S2 D13 Blk	S2 D13	S2 D13	X	X	X	X	X	X	X	X	X
<b>E</b>	S2 D14 Blk	S2 D14	S2 D14	X	X	X	X	X	X	X	X	X
<b>F</b>	S5 D12 Blk	S5 D12	S5 D12	X	X	X	X	X	X	X	X	X
<b>G</b>	S5 D13 Blk	S5 D13	S5 D13	X	X	X	X	X	X	X	X	X
<b>H</b>	S5 D14 Blk	S5 D14	S5 D14	X	X	X	X	X	X	X	X	X

The standards, samples and appropriate reaction mix were added to the plate and after 20 min incubation the fluorescence intensity was measured. However, the buffer used for the assay became very foamy during the pipetting stage and it was impossible to remove the air bubbles by neither mixing it with a pipette tip nor shaking the plate using a plate shaker. As the accuracy of the plate reading could have been affected by the presence of the air bubbles in the wells, all of the samples were pipetted onto a new plate, avoiding the air bubbles and the plate was measured again. However, this could have affected the sample volume pipetted onto the second plate, which in turn could have had an effect on the obtained readings (see Figure 2-9). The results of this assay are presented in chapter 4.

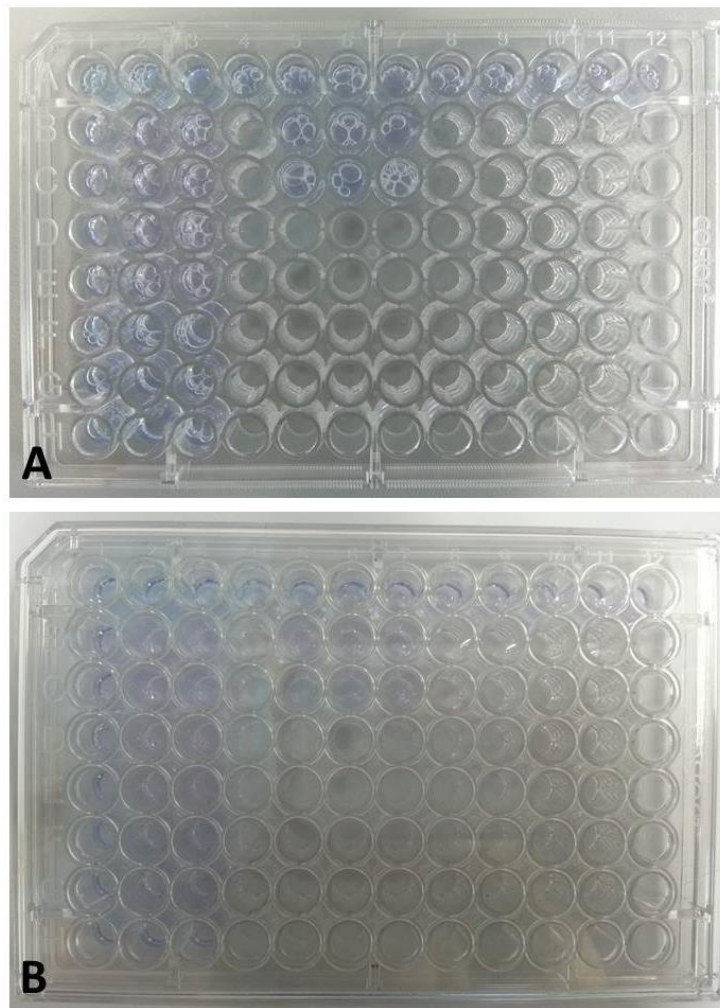


**Figure 2-9. Images representing already developed phenylalanine assay. Image A shows the air bubbles created via addition of the buffer mixture. Image B shows the samples after they were pipetted onto a new 96-well plate. The top row contains various concentrations of phenylalanine standard. Both standards and samples are of light blue/purple colour which blends in with the background.**

## 3 PROTEOMICS

### 3.1 Introduction

Proteomics is a branch of science which belongs under the umbrella of “omics” approaches. It aims to identify and characterise the proteins that comprise a given biological system. The proteome is very complex, consisting of many large molecules, and requires protein separation or digestion steps in order to identify components by means of mass spectrometry. In untargeted approaches, the most commonly used protein separation techniques are SDS-PAGE or for more complex samples, 2DE (used in this study). These are often combined with liquid chromatography separation of peptides and mass spectrometry for protein identification. Other approaches, like western blotting, allow for a targeted analysis using protein-specific antibodies and also serve as protein identification confirmation techniques. The proteome is also very dynamic and would be expected to change rapidly and progressively once homeostasis breaks down upon death.

Researchers have suggested various protein markers for PMI estimation over the years, with varying degrees of success. In 1986, Pla *et al.* measured the activities of rate limiting enzymes of glycolysis in post-mortem rat brains (Pla *et al.* 1986). However, they found that phosphofructokinase and hexokinase have very little value in PMI determinations. Not long after, Kominato *et al.* suggested the cleavage of the third component of complement (C3) as means of PMI estimation (Kominato *et al.* 1989). The percentage of C3 cleavage was positively correlated with PMI. A few years later, Gos and Raszeja investigated the activity of lactate and malate dehydrogenase in human liver up to 35 days post-mortem and reported a time dependent decrease (Gos & Raszeja 1993). More recently, Kikuchi *et al.* investigated post-mortem changes in high mobility group box-1 protein (HMGB1) in rat serum up to 7 days post-mortem (Kikuchi *et al.* 2010). They reported that the protein levels increased throughout the investigated period when rat cadavers were stored at 4°C. Different trends were seen at higher temperatures. Another two independent studies, by Kang *et al.* (Kang *et al.* 2003) and Poloz and O’Day (Poloz & O’Day 2009) investigated the use of calmodulin binding proteins in both lung and skeletal muscle tissue of rats and mice, respectively. In both cases the PMI investigated was up to 96 h. The first

group reported that the levels calmodulin-dependent kinase II (CaMKII) did not change in either muscle or lung, however, myristoylated alanine-rich C-kinase substrate (MARCKS) and calcineurin A (CnA) showed a PMI dependent decrease in lung. MARCKS was not detected and CnA levels were very variable in muscle tissue. The second group did not find lung tissue to be useful for the purpose of PMI estimation and suggested that CnA could potentially be used as a marker for short PMI of up to 24 h and protein phosphatase 2A (PP2A), not included in the first study, for longer PMI. Recently, Zapico *et al.* looked at mRNA expression of Fas Ligand (FasL) and phosphatase and tensin homologue detected chromosome 10 (PTEN) in rat muscle, however for a very short time period of up to 8 h post-mortem (Zapico *et al.* 2014). They reported that expression of mRNA of both FasL and PTEN increased up to 6 h post-mortem. In the same year, Santos Junior *et al.* investigated the levels of metals and metallo-proteins in human vitreous humour (Santos Júnior *et al.* 2014). The authors reported a correlation between iron levels and PMI.

This chapter presents the results of the application of an untargeted proteomics approach, to identify possible protein markers of PMI in skeletal muscle tissue. Initial experiments and method development were carried out using beef steak, followed by a controlled experiment using muscle tissue collected from rat. Finally, human cadavers were investigated as a preliminary test for PMI markers highlighted in the rat study.

## **3.2 Methodology**

All of the methods used in the proteomics experiments, including method development and optimisation, were described in detail in Chapter 2.

## **3.3 Results**

### **3.3.1 Beef tissue**

An initial experiment included four samples: T0, T3, T7 and T11. A pairwise comparison using a 2DE approach was carried out. Proteins that showed a significant change in magnitude of volume ratios (at least 2-fold) between the time points were selected for identification using mass spectrometry. Volume

ratio is a normalized ratio between the co-detected spots (more specifically, pixel spot volumes) in separate gel images. Twelve proteins of interest were selected. These included various forms of myosin, troponin and heat shock protein, as well as desmin, malate dehydrogenase, lactate dehydrogenase, NADH-ubiquinone and C->U-editing enzyme APOBEC-2. A full list of these proteins, including the links to the Mascot search results is attached in Appendix I. The changes occurring across the range of time points are presented in Table 3-1. As this initial experiment was carried out without the inclusion of a pooled standard, the protein spots between the gels were compared and matched by naked eye. The protein spots were highlighted in DiGE gels and corresponding spots were excised from the appropriate prep gel. Each of the four samples was separated on a separate prep gel. Therefore, in order to see the change across all of the time points for a particular protein, this protein should be matched and identified in all four gels. Unfortunately, none of the spots of interest were successfully identified and matched in all four gels, which resulted in the missing data in Table 3-1. Additionally, it can be seen from the table that in some cases there are two trends noted for one time point. For example lactate dehydrogenase B in the T0→T3 column shows both decreasing (D) and no significant change (NSC) trend (volume ratio less than 2-fold). This occurred when the same protein was identified in two separate spots on one gel which showed different trends. In that case both results were presented. The spots with insignificant result were also included, as they were matched to corresponding spots that showed a significant result.

**Table 3-1. Summary of the changes observed for proteins of interest at different time points.**

D – decreasing, I – increasing, NSC – no significant change. Protein spot matching between gels was carried out by naked eye as no standard was included between gels. The data shown below is for proteins which were identified through MS. Some of the protein spots remained unmatched and weren't picked, which resulted in missing data – indicated by the grey areas in the table. Two numbers and results are presented where the same protein has been identified in two spots on the same gel – results are presented for both spots.

Protein ID	Accession no	T0 → T3		T3 → T7		T7 → T11		T0 → T11	
		Change	Fold change	Change	Fold change	Change	Fold change	Change	Fold change
Myosin regulatory light chain 2	gi 115497166	D	2.28	I/I	28.88/12.67			I	35.14
Troponin T (slow type)	gi 21039010	D/D	2.38/2.42	I	2.58			D/D	2.14/3.01
Lactate dehydrogenase B chain	gi 118572666	D/NSC	2.57/1.67	I	2.58			D	2.95
Probable C->U-editing enzyme APOBEC-2	gi 77735661			I	19.56			D	2.24
Myosin light chain 6B	gi 115496556	D/NSC	2.24/1.67	I/I	2.55/33.84	I	2.86		
Myosin-7	gi 41386711			D/I	3.11/2.23	I/I	2.67/2.15		
Myosin regulatory light chain 2, ventricular/cardiac muscle isoform	gi 296478466							I/I	13.33/24.01
Troponin T (fast type)	gi 21038998							D	4.40
Heat shock protein beta-1	gi 85542053							D	2.02
Heat shock protein beta-6	gi 115496724							D	4.11
Malate dehydrogenase	gi 77736203	D	2.07						
Myosin-2	gi 261245063	D	2.81						
Heat shock cognate 71 kDa protein	gi 148887198	D/D	2.17/2.12						
Desmin	gi 2959452			D	2.54				
NADH-ubiquinone oxidoreductase 75 kDa subunit	gi 27807355			D	5.73				
Tripartite motif-containing protein 72	gi 119917044					I	2.26		
Myosin heavy chain (fetal)	gi 22335457					I	2.57		

This initial experiment served to establish an appropriate protocol for sample preparation and for 2DE separation, but the experimental design made it quite difficult to look at the overall change across all of the time points. Therefore this experiment was repeated with the addition of a pooled standard to each gel. This allowed normalising the results across all of the gels. Based on this, the Decyder software can graph the changes between the matched protein spots across all of the gels and show a general trend throughout the different time points. So in this case, the protein spots of interest were picked based on a graphical representation of how the levels of the protein change with time. The experiment yielded 105 protein spots of interest. Twenty-five of these, showing the most consistent trend of change, were excised from the gels and identified by mass spectrometry (see Table 3-2). Additional information on these identifications, including links to Mascot search results are attached in Appendix II. Figure 3-1 shows an image of one of the gels with the selected proteins of interest and their corresponding spot numbers (software assigned). The image only displays 14 out of the 25 of proteins of interest. This is due to the fact that not all of the proteins have been matched in all of the gels. The software does not always assign the spots in the same way on different gels. Poorly resolved or low intensity spots might be missed or incorrectly assigned. This is also the reason why some of the statistical data was not available for some of the proteins (Table 3-2). The proteins have to be matched in more than one gel, i.e. software needs data for more than one spot of each protein to be able to carry out the statistical analysis for it (mean protein volume at each time point and student's t-test between time points). Figure 3-2 shows graphs of nine selected proteins of interest, which showed the most promising patterns of change over time.

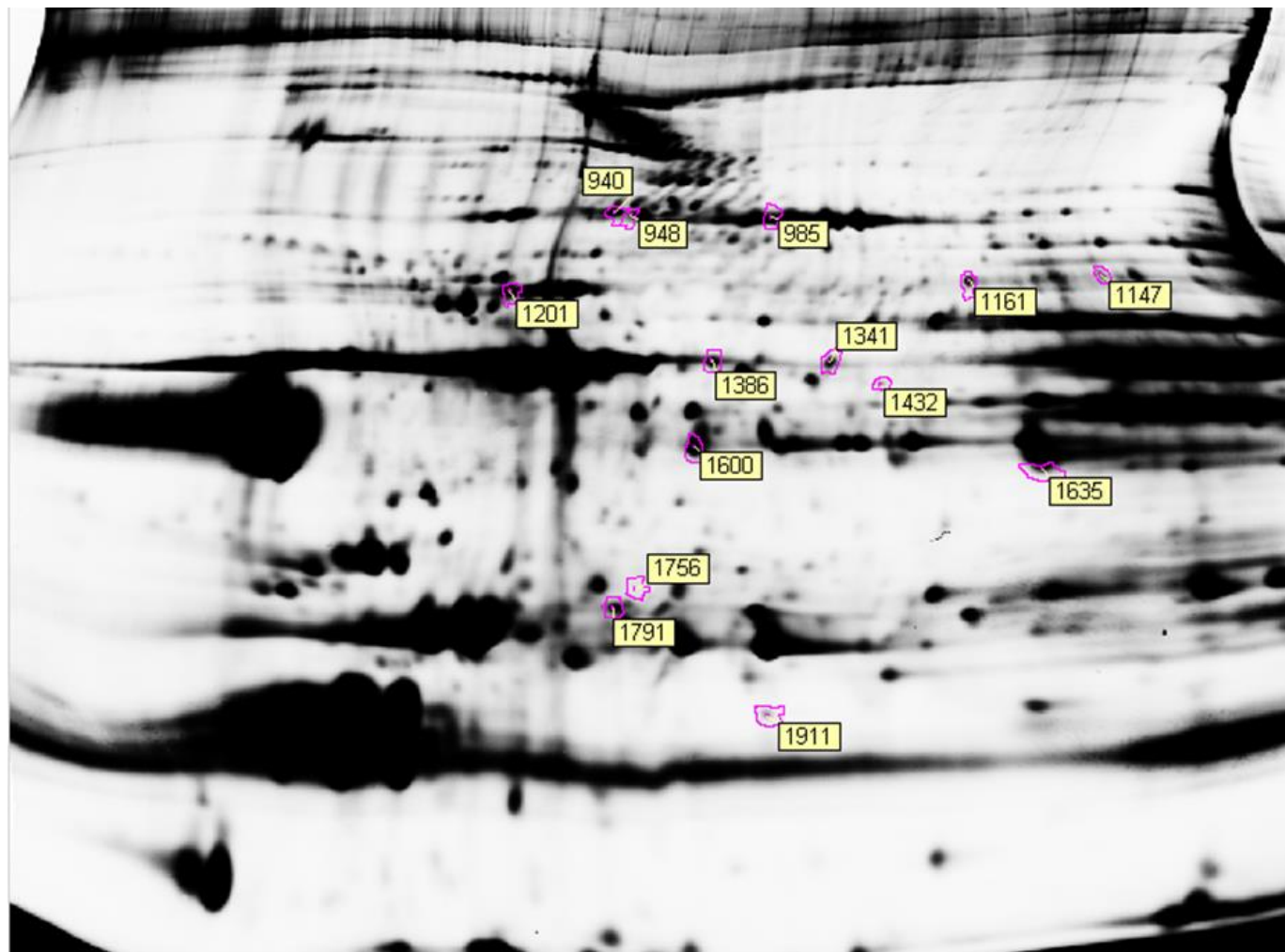
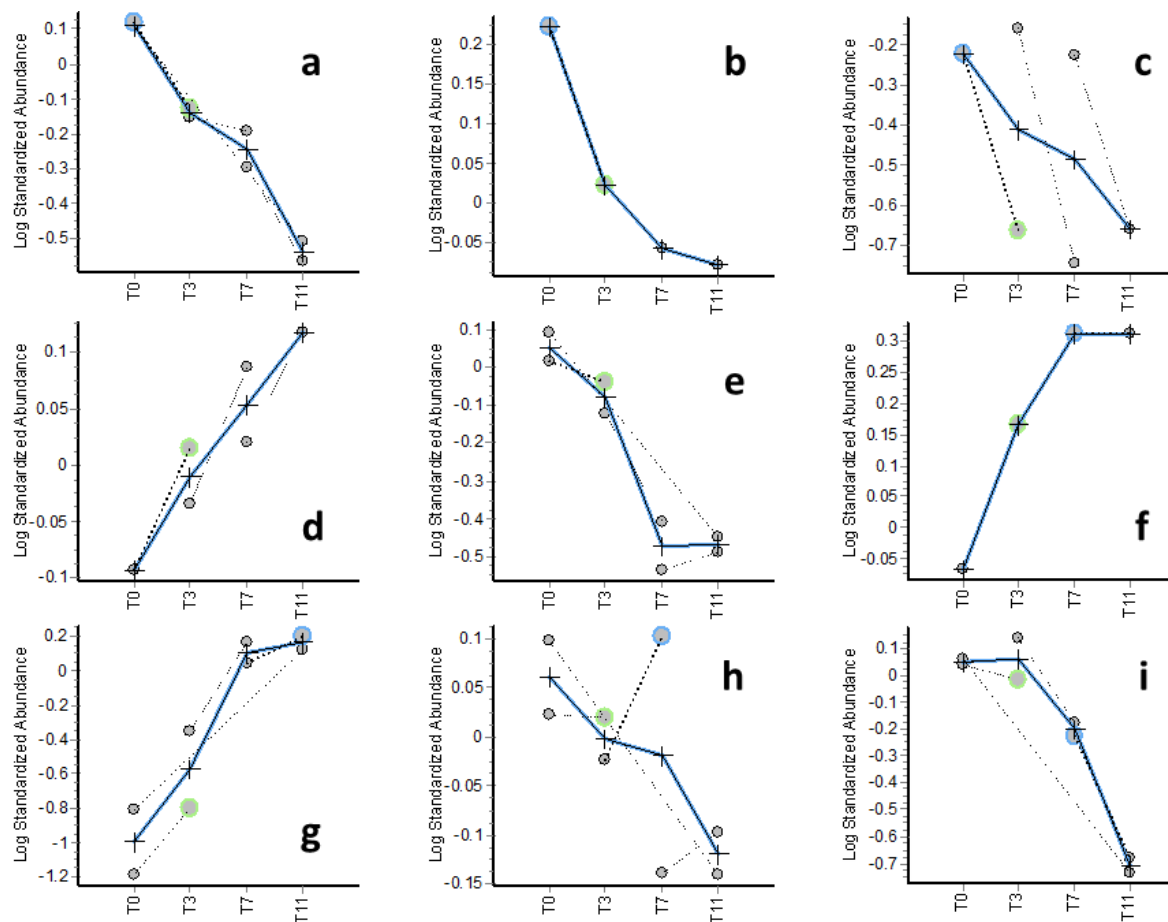


Figure 3-1. Image of a DiGE gel showing the proteins of interest and their corresponding spot numbers (beef). One of four DiGE gels included in this experiment. This particular image represents sample T7 (7 days PM), labelled with Cy5 and scanned with red laser (633nm). 14 out of 25 proteins of interest were matched in this particular gel. Proteins were separated using pH gradient 4-7 (from left to right).

**Table 3-2. List of proteins of interest identified using a single multiplex 2DE experiment in beef tissue.**

Spot numbers correspond to Figure 3-1 (software assigned by Decyder software). NCBI database was used for Mascot search. Accession number given in the NCBI database. T-test indicates the significance of the change observed. Mascot search result shows the ID assigned by Mascot search engine and its corresponding MOWSE probability score. A score of 36 or higher indicates a significant match, with the significance threshold of  $p < 0.05$ . N/A – not available.

Spot no	Accession no	T-test	Mascot search result	MOWSE score
910	gi 119917044	N/A	tripartite motif-containing protein 72	124
938	gi 157832112	0.35	Chain A, Structural Basis Of The 70-kilodalton Heat Shock Cognate Protein	1180
940	gi 157832110	0.55	Chain A, Structural Basis Of The 70-Kilodalton Heat Shock Cognate Protein	983
948	gi 157832110	0.84	Chain A, Structural Basis Of The 70-Kilodalton Heat Shock Cognate Protein	588
975	gi 157832112	N/A	Chain A, Structural Basis Of The 70-kilodalton Heat Shock Cognate Protein	619
985	gi 1351907	0.78	serum albumin	338
1141	gi 116004023	0.54	phosphoglucosyltransferase-1	769
1147	gi 27806321	0.36	retinal dehydrogenase 1	1168
1161	gi 41386711	0.25	myosin-7	1498
1161	gi 119917044	0.25	tripartite motif-containing protein 72	1738
1201	gi 2959452	0.25	desmin	428
1341	gi 27819614	0.6	actin, alpha skeletal muscle	284
1341	gi 296481810	0.6	succinyl-CoA ligase [ADP-forming] subunit beta, mitochondrial	139
1386	gi 27819614	N/A	actin, alpha skeletal muscle	662
1386	gi 296482731	N/A	actin, gamma-enteric smooth muscle	681
1432	gi 21038992	0.13	troponin T fast skeletal muscle type	844
1495	gi 115497482	0.097	prostaglandin reductase 2	175
1591	gi 164420789	0.2	pyruvate dehydrogenase E1 component subunit beta, mitochondrial precursor	876
1591	gi 77735405	0.2	four and a half LIM domains protein 3	72
1597	gi 41386697	0.1	troponin T, slow skeletal muscle	410
1600	gi 164420789	0.13	pyruvate dehydrogenase E1 component subunit beta, mitochondrial precursor	335
1635	gi 41386697	N/A	troponin T, slow skeletal muscle	2020
1648	gi 528940817	0.28	F-actin-capping protein subunit beta isoform X1	2106
1756	gi 296482731	N/A	actin, gamma-enteric smooth muscle	1255
1756	gi 71037405	N/A	heat shock protein beta-1	2463
1791	gi 529007450	0.045	heat shock protein beta-1 isoform X1	268
1888	gi 115496556	0.072	myosin light chain 6B	469
1897	gi 115496556	0.027	myosin light chain 6B	416
1911	gi 115496724	0.024	heat shock protein beta-6	324
2012	gi 27819614	N/A	actin, alpha skeletal muscle	111



**Figure 3-2. Proteins of interest identified through 2DE experiments in beef tissue.**

Mascot database search resulted in the following identifications: a – heat shock protein beta 6, b – troponin T, c – myosin 7, d – actin, e - heat shock protein beta 1, f – actin, g – myosin light chain 6B, h – pyruvate dehydrogenase E1, i – desmin. The x-axis represents PMI, T0, T3, T7 and T11 correspond to 0, 3, 7 and 11 days PM, respectively. Y-axis shows the log standardised pixel volume of the protein spots (only spots which were included in the statistical evaluations were included in the graph). The dots represent the volume of each protein spot. The dashed lines connect the spots compared on 1 gel. The + sign shows the mean value between samples from the same time point, which are connected with a line to show the trend across the time course.

The proteins displayed in Figure 3-2 provide a good example of the purpose of using an untargeted proteomics approach to look for protein markers for time since death. A number of proteins were separated and identified in this experiment. Different proteins show different trends with increasing time since death and this way we can look for proteins which show steadily increasing or decreasing patterns. Of particular interest, heat shock protein  $\beta 6$  and actin (Figure 3-2 a and d respectively) show nearly linear decrease and increase, respectively, over the PMI studied. Heat shock protein and troponin T were also identified in the trial experiment.

Figure 3-3 shows gel images for each of the samples included in the experiment. They appear distorted as Decyder software warps the images to improve matching. The proteins of interest were selected from various parts of the gel; however, none of the gels contained all of the 25 protein spots of interest. The gels look very similar; however, differences can be seen between them in the intensity and resolution of the spots. The longer the PMI, the more 'messy' the image looks. Poorly resolved regions of the gel appear in the later PMIs, which are absent or a lot smaller at earlier PMIs. More apparent and abundant protein spots could indicate a build-up of protein fragments. These would accumulate as the proteins break down with tissue degradation over time.

The results of the experiments carried out using beef tissue were very promising. However, the decomposition process in an intact cadaver would proceed in a different way than in an isolated tissue fragment. Therefore, subsequent studies were directed to intact cadavers.

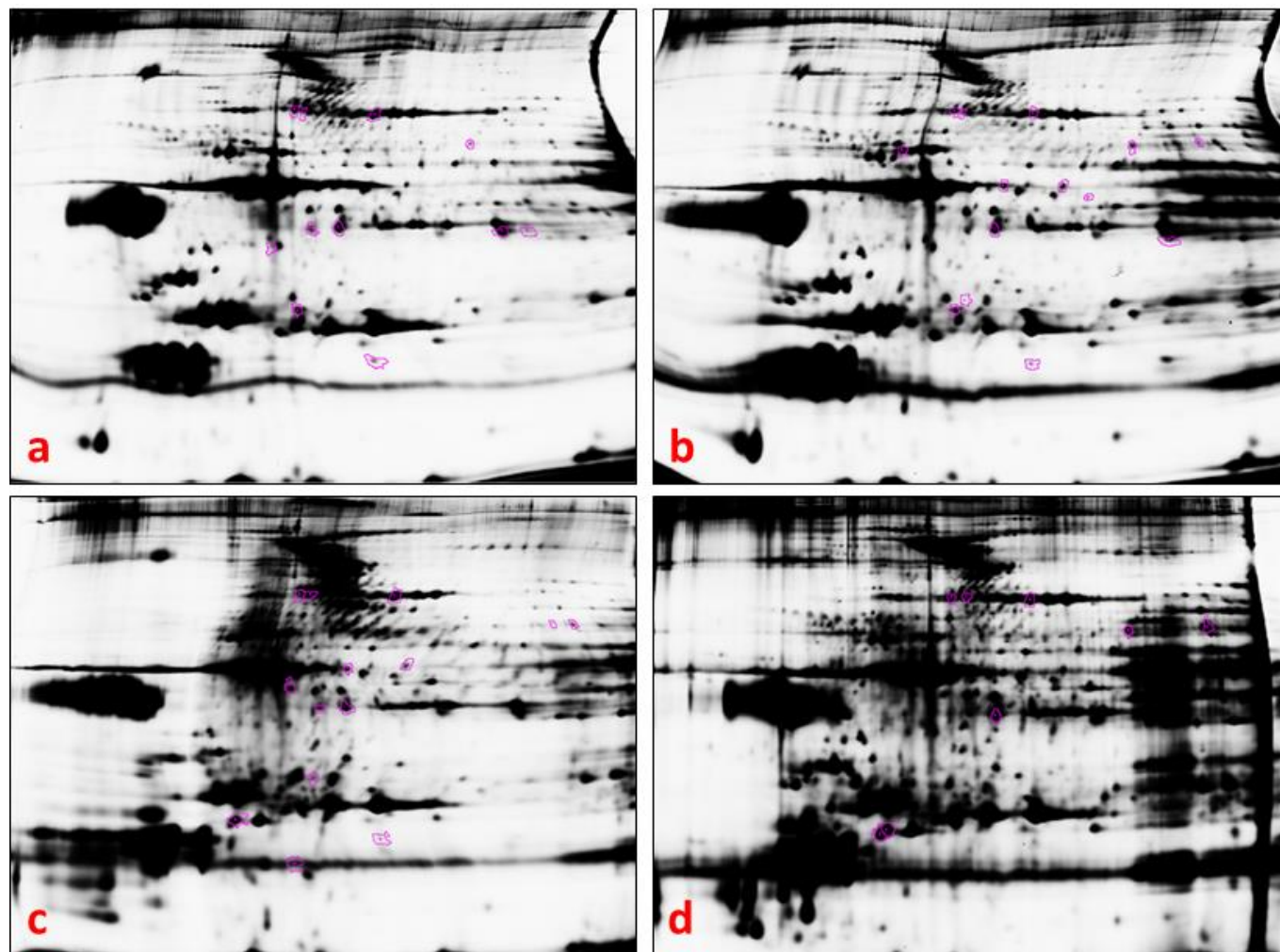


Figure 3-3. Comparison of images obtained for all of the investigated beef samples. Images correspond to the following samples: a – T0 (0 days PM), b – T3 (3 days PM), c – T7 (7 days PM), d – T11 (11 days PM). All of the gels were run together under the same conditions; all above images represent samples labelled with Cy5 and scanned with red laser (633nm). The images look 'messier' with increasing time since death. Tissue in more advanced stages of decomposition seems to be poorly resolved using 2DE separation technique.

### 3.3.2 Rat muscle

The rat was selected as an appropriate animal model in which to discover potential markers of PMI. Rats were euthanized and allowed to decompose intact. Biceps femoris samples were collected from different rats at different post-mortem intervals (0, 24, 48 and 72 h). In this case the post-mortem period under investigation was much shorter than in the case of beef, due to the limited number of rats used and practicalities of storing cadavers at room temperature.

The multiplex 2DE experimental design that had proved effective in the trial study with beef was applied to rat tissue. This time, an automated spot picker was used to pick the spots, allowing for more accurate matching and picking of the selected spots, as well as the identification of a larger number of potential biomarker candidates. Forty-six gel spots were selected for picking (see Figure 3-4) and 40 were successfully picked. Table 3-3 shows a list of proteins that were identified in the 40 spots that were picked. Additional information about them can be found in Appendix III. They were selected on the basis of how the protein levels changed over time, irrespective of their proximity to each other on the gel. Therefore, some of the spots were picked from the same area of the gel and were subsequently identified as the same protein. Twenty-two unique proteins were identified, though their appearance at different positions on the 2D gels is consistent with the presence of multiple isoforms. These may arise through different post-translational modification events, which might have occurred during life or post-mortem, as the result of dysregulation of the pathways for protein synthesis, modification or degradation. The biological relevance of post-translational modification may be to alter the structure, function or localisation of proteins, through the regulated addition of phosphates, sugars, lipids etc., or through proteolytic cleavage (Brooker et al. 2014, p.431). Post-translational modification is a major source of complexity in a proteome, as there is the potential for each gene product to be present as many proteoforms. In post-mortem tissue, modifications may occur in an unregulated manner, and proteolysis will accumulate over time. Most different proteoforms will have chemical features that alter mass or charge, and these may thus be evident in 2DE separation. This can be observed in Figure 3-4 - protein spots with numbers 1256, 1274, 1279, 1284, 1287 and 1290 were all identified as

myosin-binding protein C, slow type (Table 3-3). These spots are aligned horizontally across the gel, as they all have a similar MW but different pI value. This reinforces the correct identification of the protein and, although it reduces the number of gene products that are candidate markers of PMI, it highlights specific pathways that show modifications after death. Furthermore, even though the properties of the modified proteins differ, all of them behave in a similar way post-mortem. All of the proteins identified as myosin-binding protein C gradually increase with time since death (see Figure 3-5), however at various rates. For example, protein in spot 1274 increased nearly 15-fold but protein in spot 1256 only 3-fold. However, this is not the case for two other proteins identified in multiple gel spots in this experiment. Different proteoforms of myosin-4 and alpha-actinin-3 show both decreasing and increasing trends (see Figure 3-6).

The change in levels of the proteins can also be seen by direct comparison of the gel images. Figure 3-7 shows how three selected spots can be seen appearing or disappearing with increasing time since death. The images of the gels containing each of the different samples (labelled with the same dye - Cy3) were aligned with increasing time since death. The samples were taken at 24 h intervals, therefore there is not much difference in the general appearance of the gels. However, certain spots show clear differences in intensity between the images.

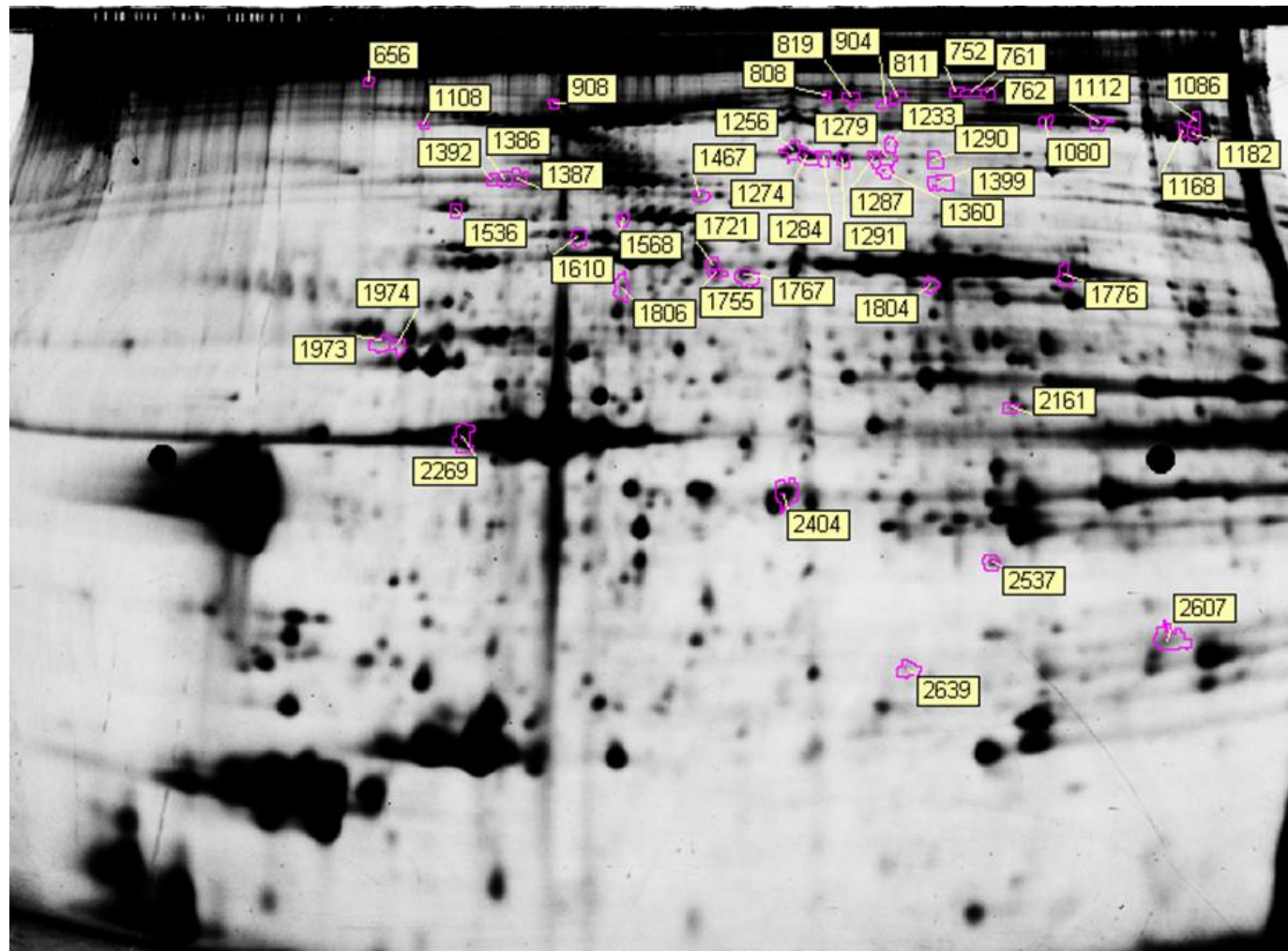
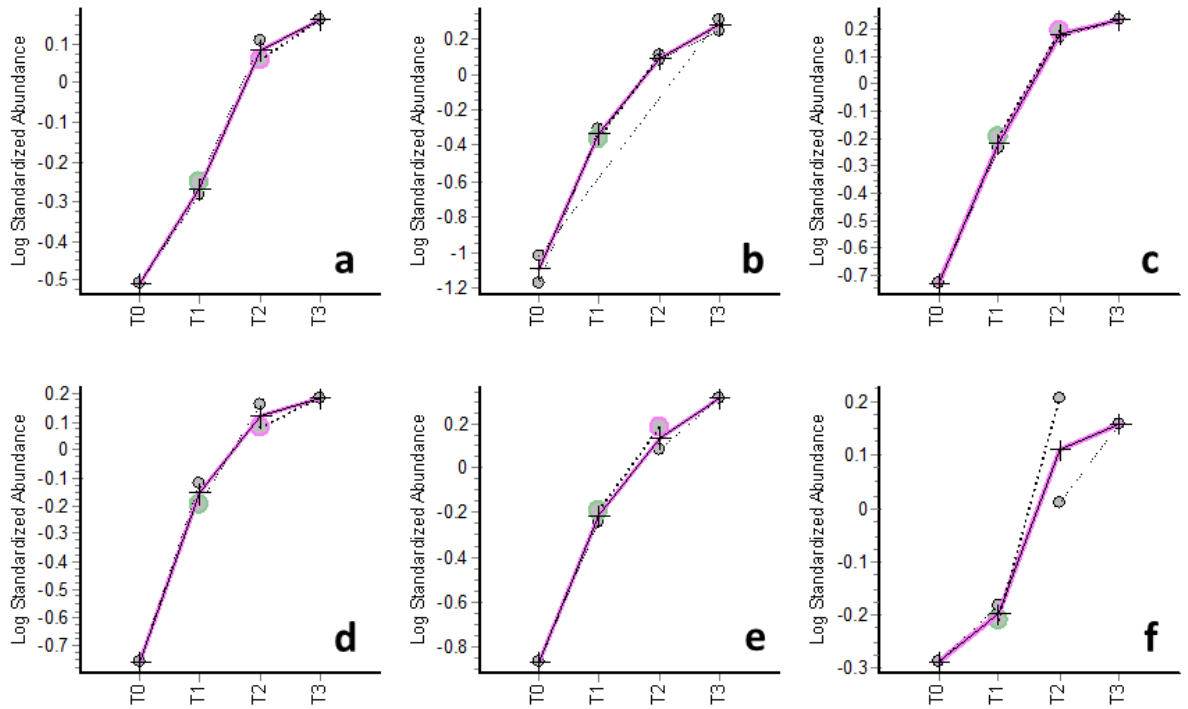


Figure 3-4. Image of a DiGE gel showing all of the 46 proteins of interest and their spot numbers (rat tissue). One of four DiGE gels included in this experiment. This particular image represents the pooled standard (contains equal amounts of all 4 samples included in the experiment), labelled with Cy2 and scanned with blue laser (488nm). Spots with the following numbers, 1108, 1291, 1387, 1610, 1776 and 1974 were not successfully picked. Proteins were separated using pH gradient 4-7 (from left to right)

**Table 3-3. List of proteins identified using a single multiplex 2DE experiment in rat muscle tissue.**

Spot numbers correspond to Figure 3-4. NCBI database was used for Mascot search. Accession number given in the NCBI database. T-test indicates the significance of the change observed. Fold change for each protein across the time course, minus sign indicates a decreasing trend. Mascot search result shows the ID assigned by Mascot search engine and its corresponding MOWSE probability score. A score of 35 or higher indicates a significant match, with the significance threshold of  $p < 0.05$ . N/A – data not available.

Spot no	Accession no	T-test	Fold change	Mascot search result	MOWSE score
656	gi 106879208	0.087	-1.44	myosin-4	826
752	gi 300797519	0.029	-1.61	myomesin-1	443
761	gi 300797519	N/A	-1.48	myomesin-1	292
762	gi 300797519	0.045	-1.63	myomesin-1	455
808	gi 281306803	0.26	-1.18	myomesin 2	1155
811	gi 564319841	N/A	1.34	histone H3.3-like	38
819	gi 281306803	0.019	-1.65	myomesin 2	1550
904	gi 106879208	0.0056	3.33	myosin-4	51
908	gi 149043182	N/A	1.19	actin, alpha 1, isoform CRA_a	64
1080	gi 157823379	0.13	-1.63	myosin-binding protein C, fast-type	857
1086	gi 157821545	N/A	-1.55	uncharacterized protein LOC362455	37
1112	gi 157823379	0.005	-2.99	myosin-binding protein C, fast-type	333
1168	gi 157823379	N/A	-2.29	myosin-binding protein C, fast-type	497
1182	gi 157823379	N/A	-2.87	myosin-binding protein C, fast-type	621
1233	gi 40849900	0.0033	3.91	plectin 8	88
1256	gi 281604187	N/A	3.18	myosin-binding protein C, slow-type	355
1274	gi 281604187	0.002	14.81	myosin-binding protein C, slow-type	1100
1279	gi 281604187	N/A	6.39	myosin-binding protein C, slow-type	363
1284	gi 281604187	N/A	6.38	myosin-binding protein C, slow-type	249
1287	gi 281604187	N/A	8.84	myosin-binding protein C, slow-type	306
1290	gi 281604187	N/A	2.07	myosin-binding protein C, slow-type	110
1360	gi 19071449	N/A	1.31	organic anion transporter K8	37
1386	gi 19173800	N/A	-1.25	alpha-actinin-3	177
1392	gi 19173800	N/A	-1.38	alpha-actinin-3	318
1399	gi 564323684	N/A	2.07	girdin-like isoform X1	38
1467	gi 564332022	N/A	2.77	glycogen phosphorylase, isoform X1	851
1536	gi 51859516	N/A	-2.79	heat shock protein 90kDa alpha	1091
1568	gi 19173800	N/A	2.05	alpha-actinin-3	385
1721	gi 347019	0.28	1.42	dnaK-type molecular chaperone hsp72-ps1	107
1755	gi 347019	0.0075	4.14	dnaK-type molecular chaperone hsp72-ps1	290
1767	gi 149047633	0.11	1.22	rCG35722, isoform CRA_b	63
1804	gi 38303941	0.11	-1.85	myosin binding protein H	94
1806	gi 77917546	0.14	2.26	mitochondrial membrane protein	66
1973	gi 40018568	0.2	-1.48	tubulin beta-4B chain	74
2161	gi 58865384	0.026	1.19	NADH dehydrogenase [ubiquinone] iron-sulfur protein 2	347
2269	gi 4501881	0.14	-1.13	actin, alpha skeletal muscle	1166
2404	gi 149041699	0.023	1.22	isocitrate dehydrogenase 3 (NAD+) alpha, isoform CRA_a	290
2537	gi 20304123	0.13	1.3	3-mercaptopyruvate sulfurtransferase	142
2607	gi 538426	0.049	1.28	triosephosphate isomerase	46
2639	gi 51948506	0.025	1.38	adenylate kinase 8	38



**Figure 3-5.** Graphs representing changes in proteins identified as myosin-binding protein C. The graphs show spots with the following numbers: a – 1256, b – 1274, c – 1279, d – 1284, e – 1287 and f – 1290. All of the proteins show similar trends, however their rates of increase differ. The x-axis represents PMI, T0, T1, T2 and T3 correspond to 0, 1, 2 and 3 days PM, respectively. Y-axis shows the log standardised pixel volume of the protein spots. The dots represent the volume of each protein spot. The dashed lines connect samples from same gel. The + sign is the mean value between samples from the same time point.

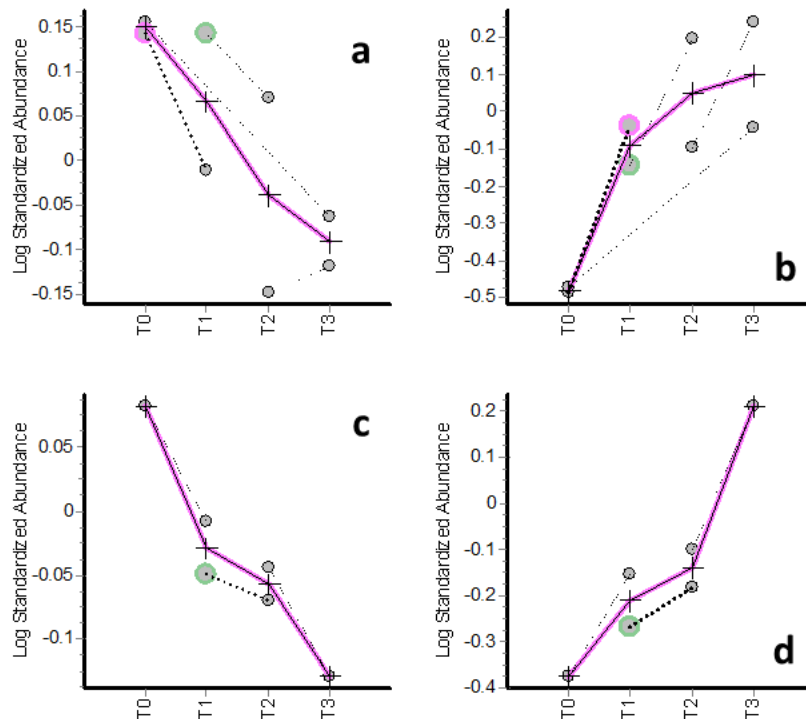


**Figure 3-6.** Graphs illustrating differences in trends between same proteins. Proteins excised from separate gel spots and identified as the same proteins. Graphs a and b show myosin-4 and c and d show alpha-actinin-3. The x-axis represents PMI, T0, T1, T2 and T3 correspond to 0, 1, 2 and 3 days PM, respectively. Y-axis shows the log standardised pixel volume of the protein spots. The dots represent the volume of each protein spot. The dashed lines connect samples from same gel. The + sign is the mean value between samples from the same time point.

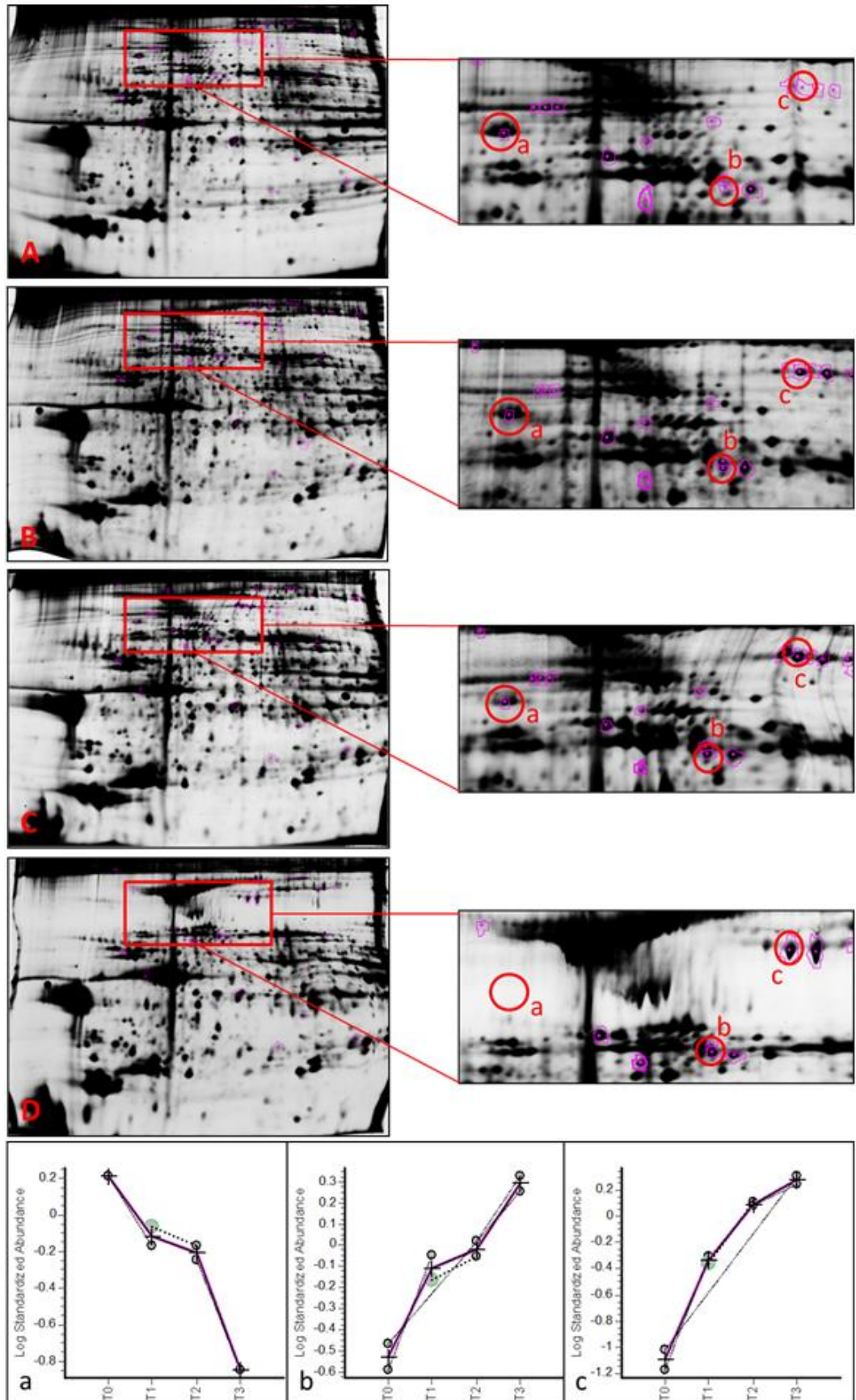


**Figure 3-7. Representation of the change in spot abundance in gels with different PMI. Images correspond to the following samples: A – T0 (day 0), B – T1 (1 day PM), C – T2 (2 days PM), D – T3 (3 days PM). All samples in the above images were labelled with Cy3 and scanned with green laser (532nm). Selected protein spots were identified as a – Heat shock protein 90kDa alpha (spot 1536), b – dnaK-type molecular chaperone hsp72 (spot 1755) and c – myosin-binding protein C (spot 1274). The graphs show the change in log standardised protein volume (y-axis) over time in days (x-axis, T0 – T3 as above).**

Of the 22 identified proteins, 9 were selected as potential PMI markers. These are shown in Figure 3-8. These proteins were selected based on two criteria. First, they showed a clear, steady increasing or decreasing trend, and secondly, the levels of these proteins were comparable between replicate samples. The graph is based on the mean of the values obtained between two different gels (each sample was separated in duplicate - on two different gels). If the discrepancy between the protein levels was large, the graphical representation of how the protein levels changed was not accurate. An example of this can be seen in graphs a and b in Figure 3-6. Since both aliquots come from the same sample extract and they are matched at the same position in both gels, it can be assumed that it is the same protein. Therefore, they should be present in similar levels on both gels. However, this is assessed based on the intensity of the spot measured in the gel image, which can be affected by the efficiency of the dye labelling.

The proteins of interest differ in the case of rat and beef tissue. An untargeted approach was applied in both studies and the best candidates were selected in each case. There are however, some similarities: members of actin, myosin and heat shock protein families were identified in both cases.

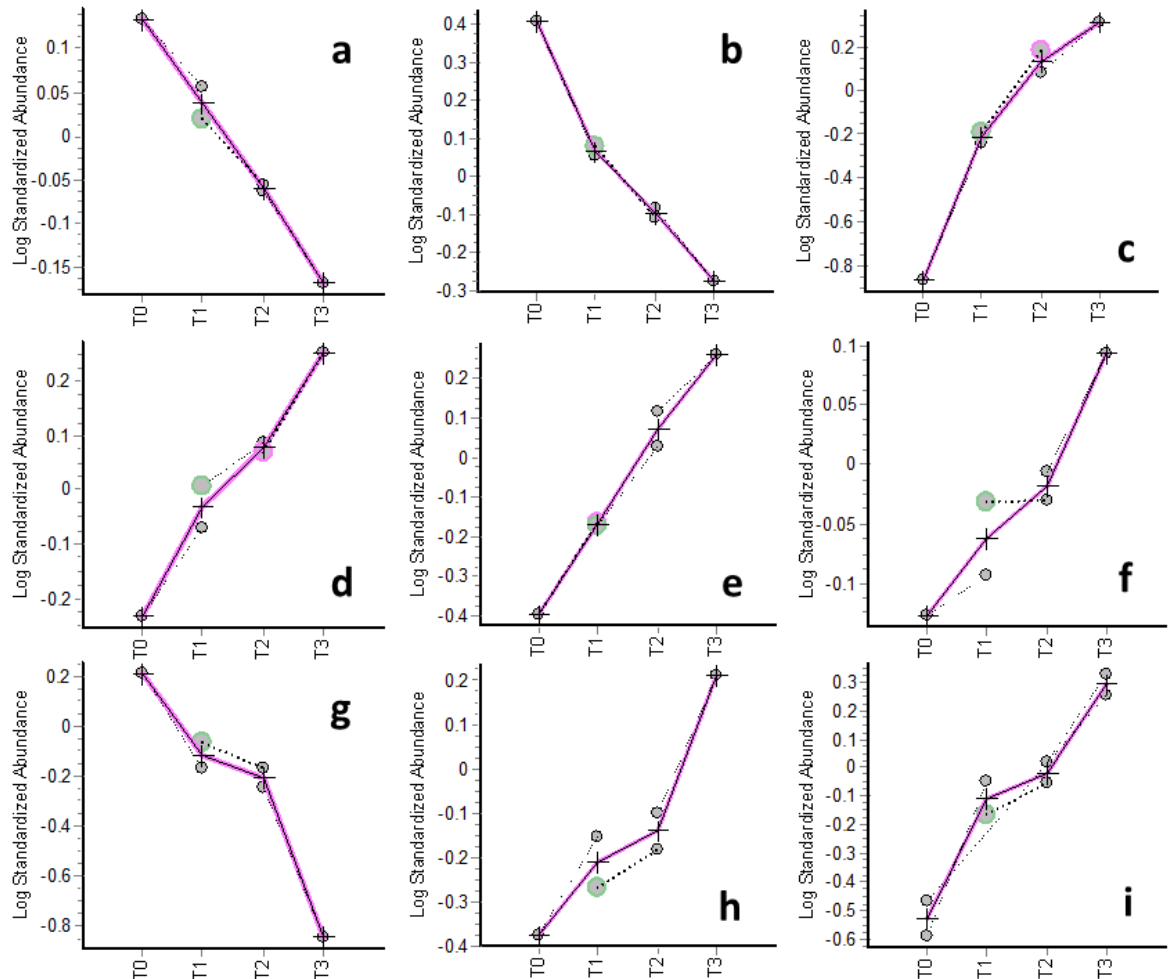


**Figure 3-8. Proteins of interest identified through 2DE experiment in rat tissue. Mascot database search resulted in the following identifications: A – myomesin-1, B – myosin-binding protein C (fast-type), C – myosin-binding protein C (slow-type), D – girdin-like isoform X1, E – glycogen phosphorylase, F – organic anion transporter K8, G – heat shock protein 90kDa alpha, H – alpha-actinin-3, I – dnaK-type molecular chaperone hsp72-ps1. The x-axis represents PMI, T0, T1, T2 and T3 correspond to 0, 1, 2 and 3 days PM, respectively. Y-axis shows the log standardised pixel volume of the protein spots (only spots which were included in the statistical evaluations were included in the graph). The dots represent the volume of each protein spot. The dashed lines connect the spots compared on 1 gel. The + sign shows the mean value between samples from the same time point, which are connected with a line to show the trend across the time course.**

### 3.3.3 Human tissue

The experiments carried out using animal tissue demonstrated that proteomic methodology can be used to monitor changes in protein levels post-mortem. Additionally, these experiments showed that some protein changes are reproducible and could potentially be used as PMI markers. However, it was of interest to verify the relevance of this approach in human cadavers. Therefore, further experiments were carried out using human tissue. Human biceps femoris tissue, the same muscle that was investigated in rats, was collected at various times PM. This muscle was chosen for consistency and because it is convenient to sample, with limited disruption to the cadaver. Due to limited facilities where

the sampling took place, four of the cadavers were stored in refrigerated conditions and two of them were placed outdoors. It was not possible to control the PMI of the cadavers included in this study, but the time of death was known in each case. Basic information about the subjects including PMI, age, sex and cause of death are detailed in chapter 2.

### **3.3.3.1 Subject selection**

Tissue samples from six different people were collected, but it would be very impractical to try to compare all of them using a single 2DE experiment, as it would involve running a very large number of gels at once. Therefore, initially, only tissue collected from subject 2 was tested. This particular subject was selected, for three main reasons: first of all, the body was stored in refrigerated conditions (constant temp). Secondly, this individual's legs were still intact, contrary to subjects 1 and 3 (also refrigerated). Subject 1 was a tissue donor, so the bone and tissue from his legs were removed, leaving just the muscle wrapped in bandages. Additionally, there was an incision made along the back of the legs of subject 3. This would significantly influence the rate of decomposition of the tissue, as it was exposed to the surrounding environment. In the case of subject number 5, the wrong portion of muscle was mistakenly sampled for the first two days. Finally, the metabolomics analysis (explained in detail in chapter 4) of the human tissue was carried out before the proteomics investigations and the results obtained for subject 2 were the most promising out of all of the subjects.

### **3.3.3.2 Subject 2**

Four samples were collected for this individual at PMIs of 11, 12, 13 and 14 days and all of these were included in the 2DE experiment. Forty-five proteins of interest were selected. Figure 3-9 shows a gel image with the selected spots and their corresponding spot numbers. Mass spectrometry analysis failed to generate a confident identification for 14 of these 45. A list of confident protein IDs obtained for the remaining 31 spots is displayed in Table 3-4. The confidence was assigned based on a MOWSE score equal or higher than the confidence threshold, in this case 38 (associated with a match probability of  $p < 0.05$ ). A full list of the analysed spots, including Mascot links, is attached in Appendix IV.

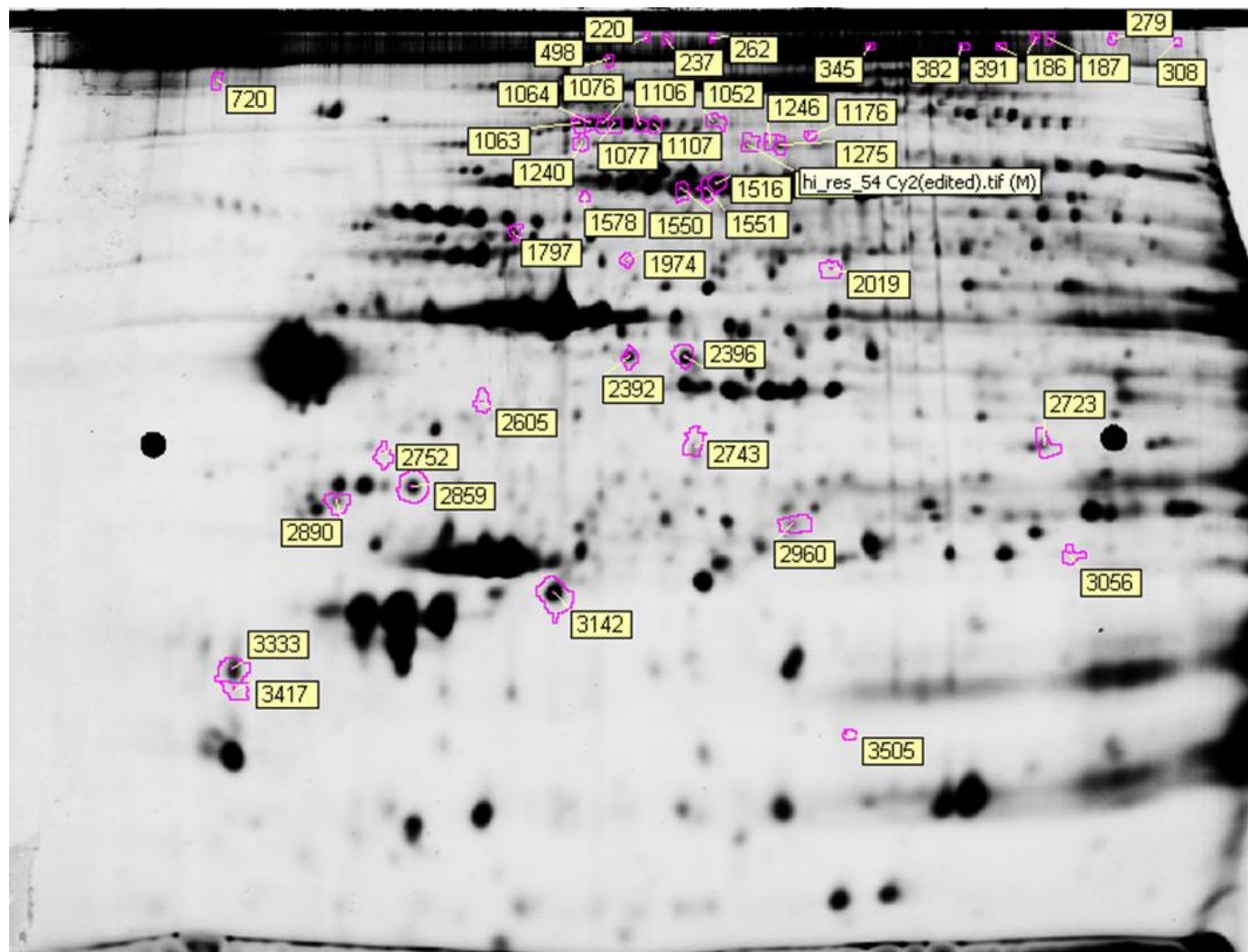


Figure 3-9. Image of a DiGE gel showing all of the 45 proteins of interest and their spot numbers (human tissue, subject 2). One of four DiGE gels included in this experiment. This particular image represents the pooled standard (contains equal amounts of all 4 samples included in the experiment), labelled with Cy2 and scanned with blue laser (488nm). Proteins were separated using pH gradient 4-7 (from left to right).

**Table 3-4. List of confidently identified proteins using a single multiplex 2DE experiment in human muscle tissue.**

Spot numbers correspond to Figure 3-9. NCBI database was used for Mascot search. Accession number given in the NCBI database. T-test indicates the significance of the change observed. Fold change for each protein across the time course, minus sign indicates a decreasing trend. Mascot search result shows the ID assigned by Mascot search engine and its corresponding MOWSE probability score. A score of 38 or higher indicates a significant match, with the significance threshold of  $p < 0.05$ . N/A – data not available.

Spot no	Accession no	T-test	Fold change	Mascot search result	MOWSE score
237	gi 29727	0.11	1.46	cardiac beta myosin heavy chain	100
262	gi 179508	0.29	1.15	beta-myosin heavy chain	124
498	gi 115496169	0.51	-1.06	myosin-7	908
1052	gi 189209	0.013	1.34	nidogen	42
1063	gi 4501893	0.0071	-1.17	alpha-actinin-2 isoform 1	418
1064	gi 4501893	0.029	-1.18	alpha-actinin-2 isoform 1	113
1076	gi 4501893	0.03	-1.21	alpha-actinin-2 isoform 1	393
1077	gi 4501893	0.035	-1.2	alpha-actinin-2 isoform 1	375
1106	gi 4501893	0.045	1.58	alpha-actinin-2 isoform 1	128
1107	gi 4501893	0.028	1.98	alpha-actinin-2 isoform 1	97
1240	gi 17066105	0.013	1.61	Titin	99
1271	gi 4504165	0.089	-1.15	gelsolin isoform a precursor	48
1275	gi 38044288	0.042	-1.21	gelsolin isoform b	57
1516	gi 395759492	0.034	-1.33	Chain A, Crystal Structure Of A Heat Shock 70kda Protein 2 (Hspa2)	380
1550	gi 190613719	0.033	-1.2	Chain B, Crystal Structure Of A Complex Of Sse1p And Hsp70	728
1551	gi 23307793	0.081	1.58	serum albumin	92
1797	gi 23506465	0.0014	-1.49	mutant desmin	434
1974	gi 4502111	0.16	-1.15	annexin A7 isoform 1	52
2019	gi 499719	0.02	-1.33	mitochondrial dihydrolipoamide succinyl transferase	235
2392	gi 426252759	0.017	1.18	alpha-actin	154
2396	gi 178027	0.15	1.11	alpha-actin	260
2605	gi 6841302	0.088	-1.66	HSPC326	64
2723	gi 119626083	0.026	1.19	albumin, isoform CRA_t	50
2743	gi 4505773	0.022	1.15	prohibitin isoform 1	291
2752	gi 178027	0.0027	1.93	alpha-actin	97
2859	gi 178027	0.35	1.05	alpha-actin	282
2890	gi 4507949	0.25	-1.08	14-3-3 protein beta/alpha	96
2960	gi 4504517	N/A	1.25	heat shock protein beta-1	184
3142	gi 5453559	0.036	1.1	ATP synthase subunit d, mitochondrial isoform a	208
3333	gi 34846	0.0035	2.18	cardiac ventricular myosin light chain-2	59
3417	gi 49259004	0.0048	2.08	Chain A, Crystal Structure Of The Paz Domain Of Human Eif2c1 In Complex With A 9-Mer Sirna-Like Duplex	40

Among the 31 identified proteins, 24 unique proteins were found, with alpha-actin and alpha-actinin identified in a number of spots. Different types of the myosin and heat shock proteins were identified (Table 3-4). Nine proteins were selected as possible biomarker candidates and the graphs of how their levels change with increasing time since death can be seen in Figure 3-10.

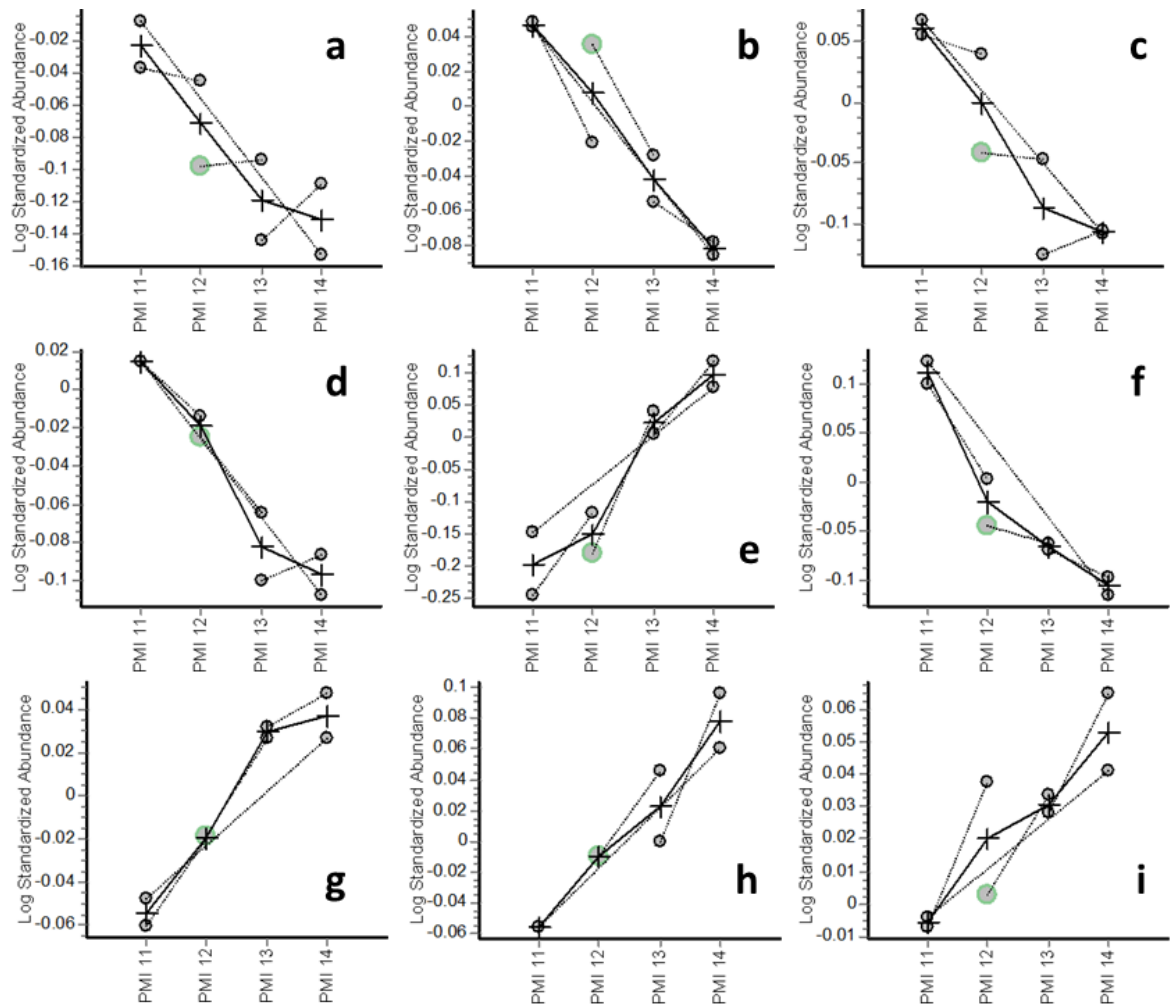


**Figure 3-10. Proteins of interest identified through 2DE experiment in human tissue (subject 2).**

Mascot database search resulted in the following identifications: **A** – alpha-actinin-2 isoform 1, **B** – gelsolin isoform b, **C** – Chain A, Crystal Structure Of A Heat Shock 70kda Protein 2, **D** – Chain B, Crystal Structure Of A Complex Of Sse1p And Hsp70, **E** – serum albumin, **F** – mutant desmin, **G** – alpha-actin, **H** – heat shock protein beta 1, **I** – ATP synthase subunit d, mitochondrial isoform a. The x-axis represents PMI, PMI\_11, PMI\_12, PMI\_13 and PMI\_14 correspond to 11, 12, 13 and 14 days PM, respectively. Y-axis shows the log standardised pixel volume of the protein spots (only spots which were included in the statistical evaluations were included in the graph). The dots represent the volume of each protein spot. The dashed lines connect the spots compared on 1 gel. The + sign shows the mean value between samples from the same time point, which are connected with a line to show the trend across the time course.

Figure 3-11 shows two proteins, which were identified in all three investigated species, alpha actin and myosin. Alpha actin seems to be a promising candidate. The changes in the levels of this protein follow similar increasing patterns over time in all of the mammals (see Figure 3-11). However, according to the Mascot search, it is not exactly the same protein - as mentioned previously, different forms of the same protein occur, especially when it comes to different species. Both alpha actins identified in the beef and human tissue have 377 residues and very similar, yet not identical protein sequence. The rat alpha actin, on the other hand, has been identified as isoform CRA\_a of alpha actin with 465 residues. The peptide sequence is very similar to the other two, but is longer (see Figure 3-12). However, considering that none of the peptides unique to the CRA\_a isoform were detected and matched in the protein sequence, it cannot be said for certain that this is a different isoform. The peptides matched can also be matched to other actin proteins with similar sequences. Moreover, this should not make much difference to the end result, given that in all cases it is alpha actin and it behaves in a similar manner in all three cases. Myosin does not show the same trends between all species, but it shows a similar trend between rat and human samples. Heat shock proteins have also been identified in all three species, but their sequences vary to a much larger extent, therefore they are not considered to be similar and were not included in the comparison in Figure 3-11. The similarities between the sequences of the actin and myosin proteins identified gave rise to this comparison.

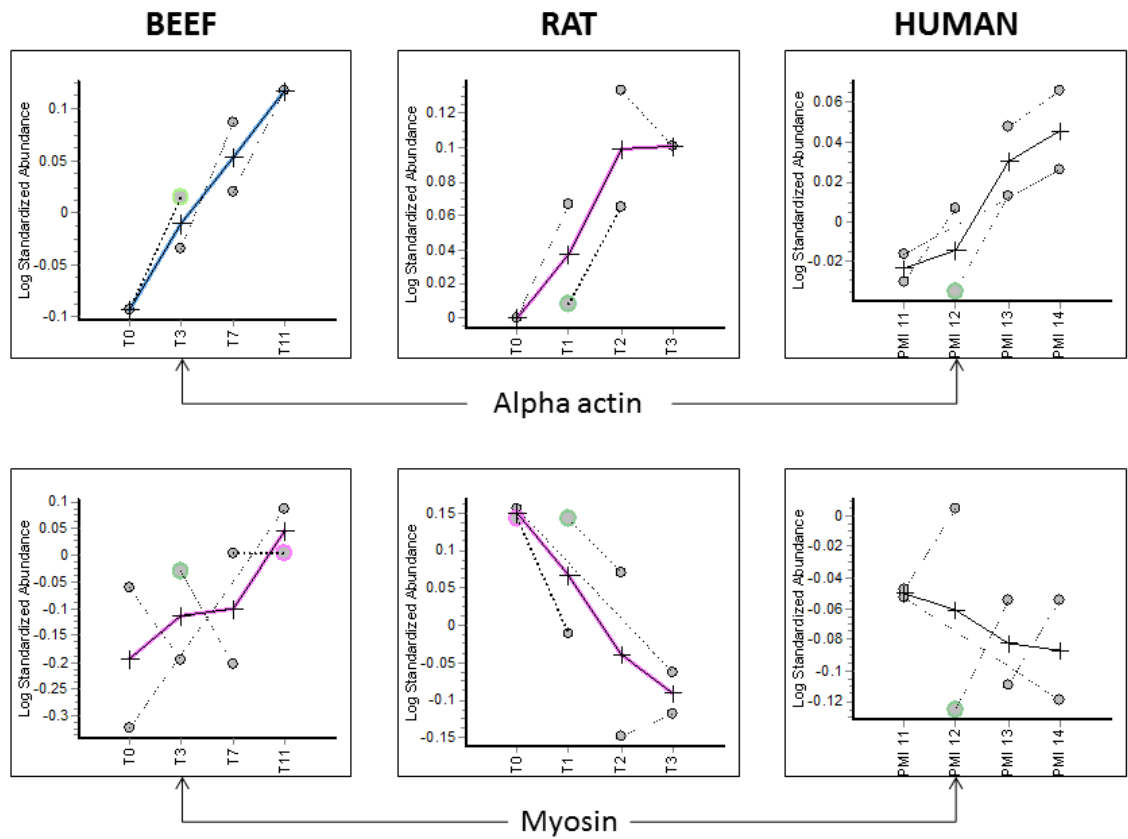


**Figure 3-11. Overview of the two types of protein found in all of the investigated species. Each row represents different protein type – alpha actin (top row) and myosin (bottom row). The graphs are also separated into three columns according to their species (indicated on top of each column – beef, rat, human from left to right). PMI and letter T followed by a number on the x-axis indicate PMI in days. Y-axis shows the log standardised pixel volume of the protein spots. The dots represent the volume of each protein spot. The dashed lines connect the spots compared on 1 gel. The + sign shows the mean value between samples from the same time point.**



### 3.3.3.3 Subject 5

The proteomics approach was successfully applied to human tissue from Subject 2 and revealed more possible biomarker candidates. However, this was only tested in a single human subject, which of course needs further confirmation. It seemed most logical to test another human cadaver, which had been decomposing for a similar amount of time. Two other subjects fulfilled that criteria, subject 3 (female) and 5 (male). The PMI overlap was better with the female, however, it was the only female cadaver included in the study as well as the only subject who did not die of natural causes (suicide). As a potential 'outlier' it would be difficult to interpret any collected data, as the effect of the cause of death on the decomposition process and any changes in the proteome is unknown. Therefore, the male subject was selected for the second analysis and comparison.

Four out of the five collected tissue samples for this individual were included in the analysis (PMI of 12, 13, 14 and 15 days). In the previous experiments, two replicate samples from each time point were analysed. In this case, in order to obtain a more reliable statistical representation of the results, three replicates of each sample were used, increasing the number of gels used in this experiment to 7 gels (six DiGE + one prep gel). Additionally, the proteins identified in beef and rat tissue were often repeating in different spots, as the proximity of the selected spots was not considered while selecting ones to pick. Therefore, in this analysis the positioning of the spots was taken into account, in order to include various proteins from different parts of the gel. Finally, a full advantage was taken of the use of an automated spot picker - not limiting the number of protein spots picked. As a result, seventy eight protein spots of interest were selected and picked. Figure 3-13 shows an image of one of the gels from this experiment highlighting the selected protein spots (including their spot numbers). All of the selected proteins showed increasing or decreasing trends over the investigated time period, very often nearly linear. Figure 3-14 shows nine graphs of proteins which were considered to be the most promising candidates out of the 78 selected spots.

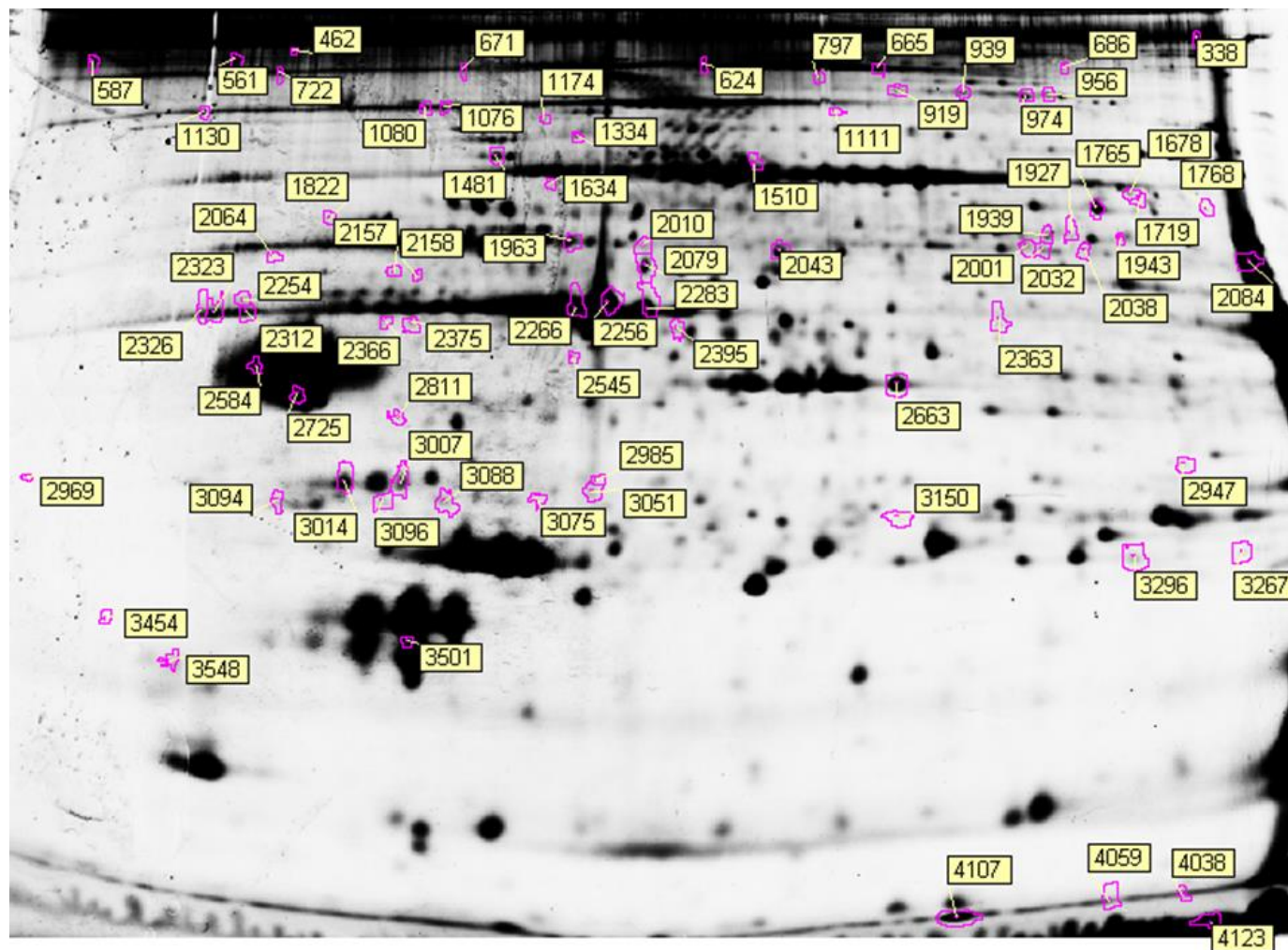
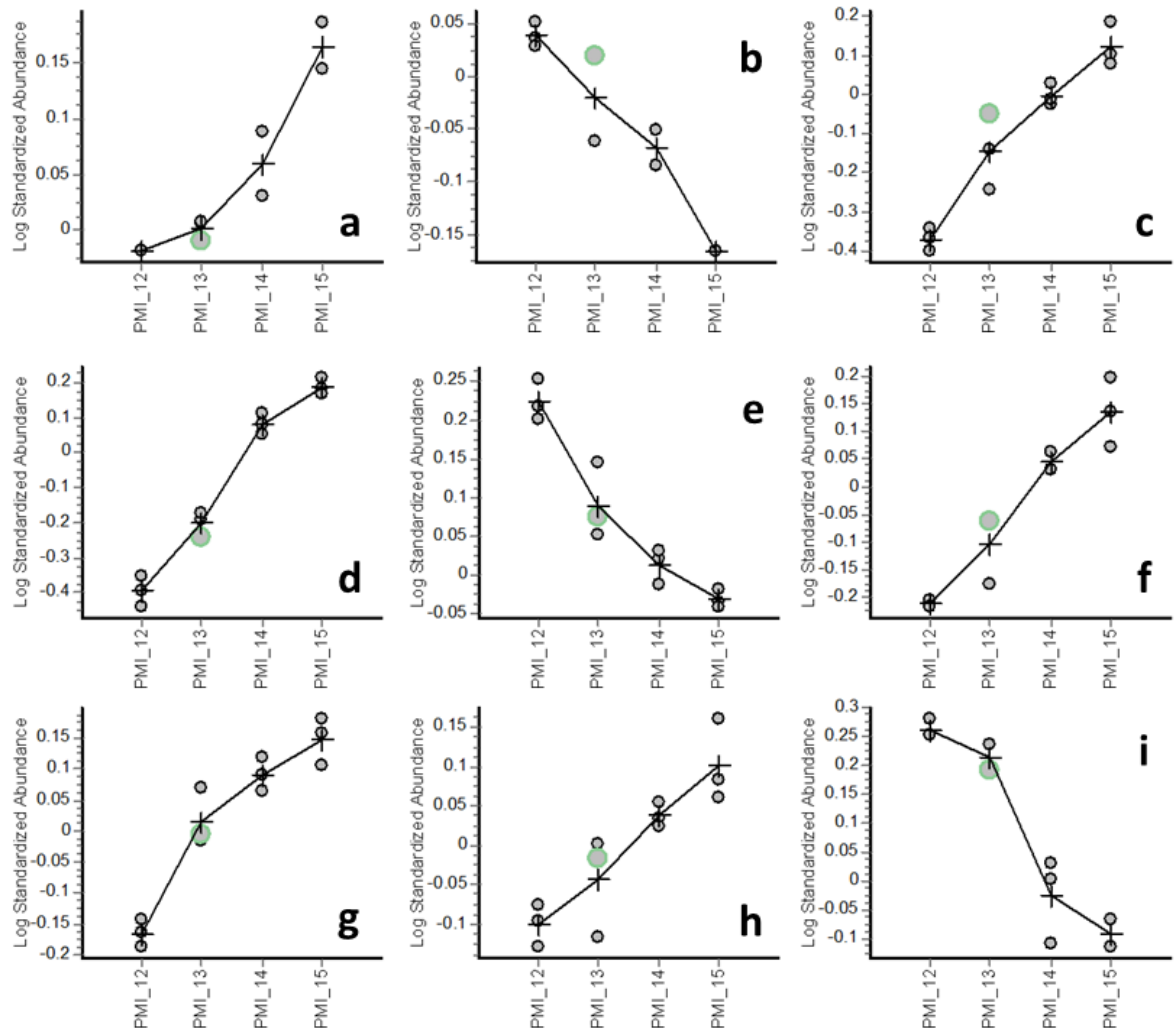


Figure 3-13. Image of a DiGE gel showing all of the 78 proteins of interest and their spot numbers (human tissue, subject 5). One of six DiGE gels included in this experiment. This image represents sample PMI 13 (13 days PM) labelled with Cy5 and scanned with red laser (633nm). All of the spots were successfully picked, but only two spots were identified through mass spectrometry (2256 and 2725) due to contamination issue. These spots of high volume were identified as actin and tropomyosin, respectively. Proteins were separated using pH gradient 4-7 (from left to right).



**Figure 3-14. Proteins of interest identified through 2DE experiment in human tissue (subject 5).**  
**Corresponding spot numbers: A – 338, B – 686, C – 919, D – 956, E – 1963, F – 2366, G – 2395, H – 3007, I – 3296.** The x-axis represents PMI, PMI\_12, PMI\_13, PMI\_14 and PMI\_15 correspond to 12, 13, 14 and 15 days PM, respectively. Y-axis shows the log standardised pixel volume of the protein spots (only spots which were included in the statistical evaluations were included in the graph). The dots represent the volume of each protein spot. The + sign shows the mean value between samples from the same time point, which are connected with a line to show the trend across the time course.

The selected protein spots of interest were analysed using LC-MS, in order to identify them. However, the result of the analysis was very puzzling as the majority of the 78 picked spots were identified as one protein - vimentin. This could not be a correct result since by definition, the proteins in the gel were separated out based on their weight and pI, and therefore it is highly unlikely to have the same protein in so many different parts of the gel. This indicates that the gel pieces were contaminated in some way with vimentin. The samples were re-analysed and finally, re-extracted again from the gel spots which were kept after initial extraction to test these results. Unfortunately, results of both of these analyses confirmed the contamination, which led to the conclusion that the contamination came from the gel itself, even before the LC-MS analysis.

Due to the sample contamination issue, it was impossible to identify the proteins of interest from this experiment. However, there were two very abundant spots, which were identified as actin and tropomyosin (spot no 2256 and 2725 in Figure 3-13, respectively) in all of the three tests. The contamination is still present in these spots; however, contrary to all of the other 76 results, in this case the proteins were much more abundant than vimentin. Additionally, their match scores and sequence coverage were quite high (see Figure 3-15), which suggested they were definitely present in these spots. Finally, they were picked from areas of the gel where the presence of these proteins could be expected. On the other hand, these areas contained a large pool of poorly resolved proteins, therefore, it is possible that more than one protein would be present and it would be very difficult to state which protein caused the observed change in abundance over PM time (Figure 3-15).

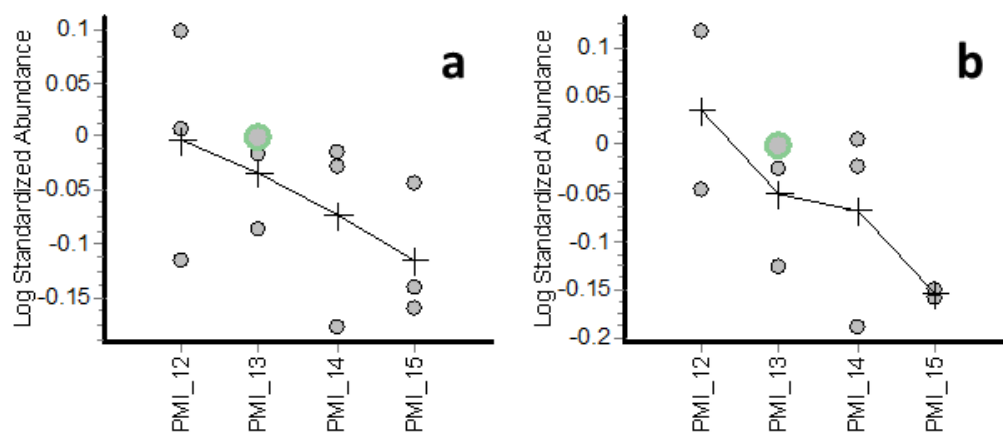


**Figure 3-15. Graphs representing change in protein abundance of spots identified as actin and tropomyosin in human tissue (subject 5).**

**Graph a – alpha actin (spot no: 2256, accession no: gi|4501881, T-test: 0.2, fold change: -1.19, mascot score: 633, sequence coverage: 46%), graph b – tropomyosin alpha (spot no: 2725, accession no: gi|49660014, T-test: 0.12, fold change: -1.32, mascot score: 608, sequence coverage: 53%).** The x-axis represents PMI: PMI\_12, PMI\_13, PMI\_14 and PMI\_15 correspond to 12, 13, 14 and 15 days PM, respectively. Y-axis shows the log standardised pixel volume of the protein spots (only spots which were included in the statistical evaluations were included in the graph). The dots represent the volume of each protein spot. The + sign shows the mean value between samples from the same time point, which are connected with a line to show the trend across the time course.

### 3.4 Discussion

The aim of this experiment was to identify possible protein biomarkers in muscle tissue, which could help to estimate PMI. The hypothesis was that certain proteins would show a predictable change in abundance with increasing PMI. Upon death, homeostasis ceases. Tissues that are no longer supplied with oxygen and nutrients are unable to maintain the intra and intercellular compartmentalisation that is required for controlled metabolism. However, many enzymes remain active and biochemical pathways will proceed, albeit in an increasingly chaotic manner. The proteome will be modified by the activity of the many enzymes that can modify proteins, by cleaving or modifying the polypeptide chain, and these changes may be evident in 2DE analysis through changes in the protein spot map that is observed. Thus, a protein that is cleaved by a protease activity will show decreased abundance as the amount of unmodified protein remaining is reduced. The products of this cleavage may show increased abundance, providing they are sufficiently large to be resolved on the gel, and sufficiently stable to accumulate. Alternatively, a protein may be rapidly degraded so that none of the intermediate products of degradation accumulate to detectable levels. Thus, an untargeted proteomics approach may allow identification of a number of polypeptides that show a steady increasing or decreasing trend over time post-mortem. Characterisation of these proteins by mass spectrometry may identify the gene product from which they originated, potentially highlighting a marker for time since death.

Three different tissue types were tested, beef steak, rat and human muscle tissue (biceps femoris). Proteins of interest were successfully identified in all three species. However, the proteins of interest varied between them. The protein spots in the case of beef tissue were hand-picked, which limited the number of identified proteins (25 out of 105). Nine proteins were selected as possible biomarker candidates, based on the graphical representation of how their levels change with time (Figure 3-2). These included heat shock protein beta 6, troponin T, myosin 7, actin, heat shock protein beta 1, myosin light chain 6B, pyruvate dehydrogenase E1 and desmin. Out of these, heat shock protein beta 6, troponin T and actin showed nearly linear relationships with PMI. The former two showed a decreasing trend and the latter increasing. In the case of rat tissue the PMI range was a lot shorter than in the other tissue types;

however, the experiment used intact cadavers, which were more likely to resemble an authentic decomposition process than an isolated piece of meat. In this case 40 spots of interest were picked using an automated spot picker, which yielded 22 different protein IDs. Again, the 9 best candidates were selected as shown in Figure 3-8, including myomesin-1, myosin-binding protein C (fast-type), myosin-binding protein C (slow-type), girdin-like isoform X1, glycogen phosphorylase, organic anion transporter K8, heat shock protein 90kDa alpha, alpha-actinin-3 and dnaK-type molecular chaperone hsp72-ps1. None of these matched the top 9 proteins identified in beef tissue, although actin and myosin were both identified in the two types of tissue. Finally, human muscle was also tested, 44 spots of interest were picked and 31 out of the 44 spots were identified. These 31 spots contained 24 unique proteins as alpha-actin and alpha-actinin were identified in a number of spots. The top 9 proteins selected were alpha-actinin-2 isoform 1, gelsolin isoform b, Chain A - Crystal Structure Of A Heat Shock 70kda Protein 2, Chain B - Crystal Structure Of A Complex Of Sse1p And Hsp70, serum albumin, mutant desmin, alpha-actin, heat shock protein beta 1, ATP synthase subunit d (mitochondrial isoform a). Again, these were very different results, with the exception of actin and heat shock protein. Myosin-7 was also identified, as in the case of beef tissue, but was not included in the top 9 choices (Figure 3-10). Tissue collected from a second human test subject was also tested, however, this analysis failed due to contamination.

Similarities were observed among all three species. Actin and myosin proteins were identified as proteins of interest in all three mammals (Figure 3-11). Actin and myosin serve as building blocks for the muscle structure and are also involved in muscle contraction, as well as in the formation of rigor mortis post-mortem. Actin seems the most likely candidate for a PMI biomarker. It was not only identified in all three tissue types, but more importantly, a similar pattern of increase was seen in all three mammals. The fact that it is one of the most abundant proteins in muscle makes it fairly easy to detect and a good biomarker candidate. Myosin is also a strong candidate, although it showed similar trends in only two out of three tissue types (rat and human), but nonetheless, it was selected as possible marker in all three. Heat shock proteins could also be good candidates as PMI biomarkers. Different members were identified from this class of proteins in different tissue types (with the exception of heat shock protein

beta 1 which was identified in both human and beef samples). However, they share similarities in their function. They are called stress-induced proteins, which help to maintain regular cellular conditions in times of stress (Campbell & Reece 2005). Cellular death would initiate a stress management response in tissues. They were previously identified as possible markers for post-mortem myofibrillar changes (Jia, Hildrum, et al. 2006) and degradation (Balan et al. 2014) in muscle tissue.

The 2DE proteomics approach, used in this study, is a gel based separation technique, which allows comparison of the proteome changes between two samples. It separates intact proteins as well as protein fragments, and is very sensitive to modifications that might result in changes in SDS-binding (apparent molecular weight) or native charge. For example, post-translational modification may result in a change in the charge of a protein. This is evident in the case of Troponin T (beef) and alpha-actinin (human, e.g. see Figure 9, spot numbers 1063, 1064, 1076, 1077, 1106 and 1107, with the last two showing an increase). The spots identified as these proteins are aligned horizontally along the gel, which suggests the same MW, but different pI. The collected data also shows evidence of proteolysis, which results in protein fragments with different molecular weights. As large proteins break down, smaller protein fragments will appear, for example, alpha-actinin identified in rat tissue (see Figure 3-4; spot numbers 1386, 1392 levels decreasing and 1568 increasing). The protein spot showing an increasing trend is situated slightly lower in the gel than the spots showing decreasing trends. This indicates that they have different MWs and the fragments which are lower down are smaller as the smaller proteins move easier and faster down the gel. A general idea of how the charge and molecular weight are separated/positioned within a 2DE gel can be obtained from Figure 3-16. Other, commonly used techniques like western blots or enzyme assays employ a targeted approach and are less sensitive to the complex changes in the proteome. They use protein-specific antibodies, which bind selectively to the protein of interest. In the case of western blots, the proteins are only separated based on their molecular weight (Mahmood & Yang 2012). However, the 2DE approach does have its limitations. For example, only two samples can be compared on one gel. This can be adapted to compare more samples at once

through the use of multiple gels and standards. However, this significantly increases the complexity and the costs of such experiments.

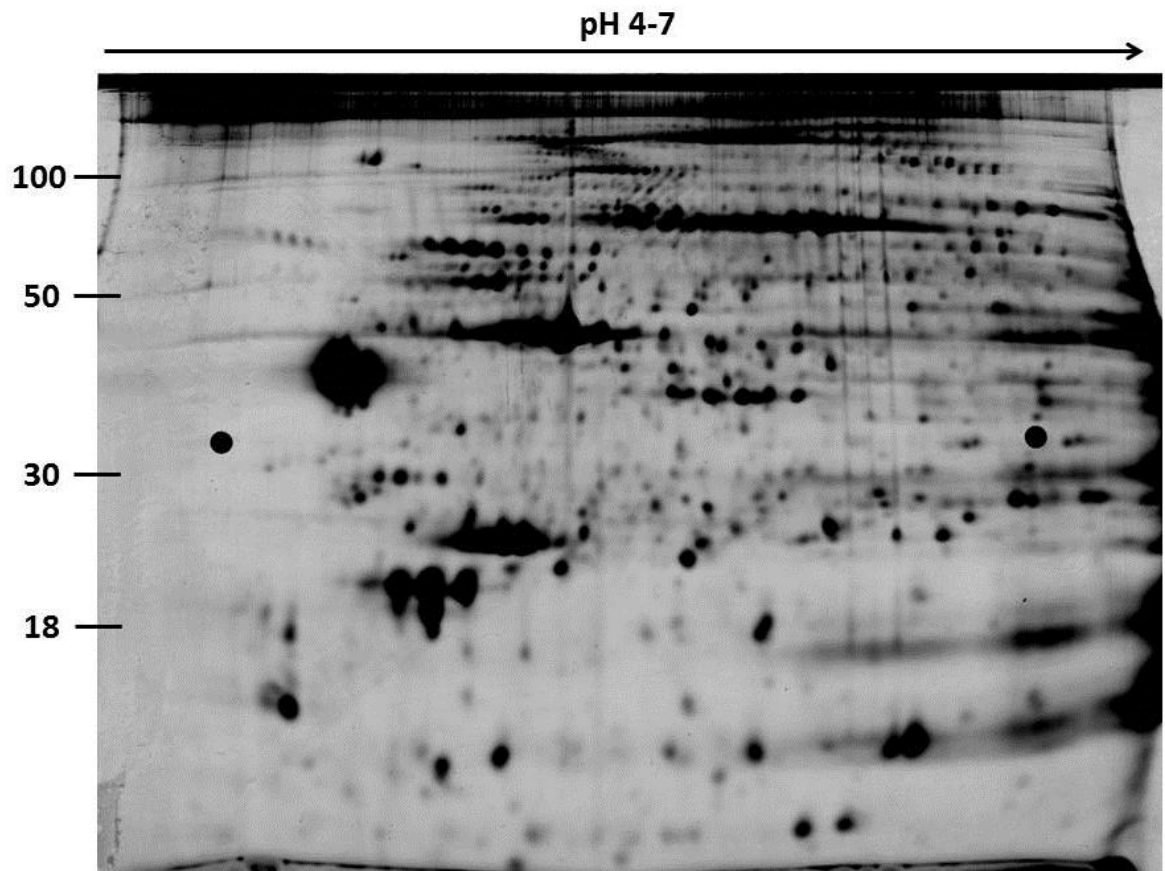


**Figure 3-16.** General representation of how molecular weight and pH are distributed in a standard 2DE gel.

The pH ranges from 4 to 7 from the left hand side of the gel to the right. The weight distribution occurs from top to bottom of the gel with the larger proteins on top, getting smaller towards the bottom of the gel. The numbers on the left indicate a rough scale of molecular weight in kDa.

Another limitation of this untargeted approach stems from the complexity of the sample, which causes problems with the reproducibility of the results. The proteome is very complex, consisting of thousands of large molecules which can also be easily transformed and modified to fulfil various roles in the organism, adding uncounted possibilities and protein combinations. Unless the proteins are somehow fractionated to look at a subset of the proteome, it is very difficult to obtain reproducible results between different experiments.

Protein fragmentation seen in this experiment may be caused by a process called proteolysis - various changes occurring post-mortem, which lead to loss of structural integrity of muscle tissue. After death, the blood flow ceases, which means there is no more oxygen delivered to the cells. The cells attempting to

carry on normal function, switch to anaerobic energy metabolism, i.e. glycolysis. This leads to build up of lactic acid in muscle tissue and in turn, lowers the pH (Koochmaraie 1992). This, combined with the gradually decreasing temperature of the body, initiates the decomposition process including proteolysis. The process of post-mortem proteolysis has been researched in the past, however, mainly with respect to muscle tenderisation in meat production. Nonetheless, this process would undoubtedly be occurring in skeletal tissue of any mammal, with differences in the extent and the rate of the process, which depends on the post-mortem conditions (e.g. temperature). Three proteolytic systems have been investigated with respect to post-mortem proteolysis: the calpain system, the lysosomal cathepsins and the multicatalytic proteinase complex (MCP) (Koochmaraie & Geesink 2006; Nowak 2011; Lian et al. 2013). However, it is believed that it is the calpain system which is mainly, if not solely, responsible for proteolytic degradation of skeletal muscle. The calpain system is activated by high levels of free calcium ( $\text{Ca}^{2+}$ ) in tissue. During life, the  $\text{Ca}^{2+}$  levels are low, which ensures the system is inactive. However, after death the levels of free calcium increase as it is released from mitochondria and sarcoplasmic reticulum (due to changes in pH and temperature conditions). At the same time, low pH inhibits the activity of calpastatin, which is a natural calpain inhibitor. Calpains cleave proteins titin, nebulin, filamin, desmin and Troponin-T (Hufflonergan & Beekman 1996). Actin and myosin are cleaved by lysosomal proteases (cathepsins) (Goll et al. 1983). Once the muscle filaments are degraded into smaller peptide fragments, they can then be further degraded to amino acids by the lysosomes or by the MCP system (Goll et al. 1992). There are two main modes of protease action, which separates them into exo- or endoproteases. Exopeptidases (e.g. some lysosomes) attack the N- or C-terminus of the peptide chain and cleave it one amino acid at a time. Endopeptidases (e.g. calpains) cleave the peptide chain in the middle, therefore creating smaller peptides.

Proteomic analysis of post-mortem muscle is most often carried out in order to establish how different factors affect meat tenderisation (Yates et al. 1983; Anderson et al. 2012; Picard et al. 2014) and how to improve the quality of aged meat (Frylinck et al. 2013). However, a few researchers tried to find a link between the post-mortem changes in muscle and PMI. A few studies, by Sabucedo *et al.* (Sabucedo & Furton 2003), Pittner *et al.* (Pittner et al. 2015)

and two by Kumar *et al.* (Kumar, Ali, Singh, et al. 2015; Kumar, Ali, Bhattacharya, et al. 2015) pointed towards troponin as a possible PMI biomarker. The former study investigated cardiac Troponin I (cTnI) and the other three, cardiac troponin T (cTnT) in porcine (Pittner et al. 2015) and human tissue. All studies reported degradation of troponin with a linear relationship over time. Geesink and Koohmaraie also reported degradation of troponin T (TnT), while investigating the proteolysis process in post-mortem lamb tissue (Geesink & Koohmaraie 1999) and Lametsch *et al.* identified two different fragments of TnT in aged pig meat (Lametsch et al. 2002). The fragments were of slightly different sizes, 43 and 38 kDa, where the larger fragment decreased in abundance over time and the smaller one increased. This is similar to the present study, as TnT was identified in three different spots and showed both increasing and decreasing trends. However, contrary to Lametsch's results, the size of the protein fragments was the same, but the pI differed slightly. This would indicate proteins with different post-translational modifications, which can behave differently. In this study, troponin was only detected in beef tissue and was not selected in the results for rat or human tissue. Nevertheless, it is a very strong candidate for a PMI biomarker. It is already a known marker of myocardial damage (Osuna et al. 1998; Ellingsen & Hetland 2004; Zhu, Ishikawa, Michiue, Li, Zhao, Oritani, et al. 2006; Zhu, Ishikawa, Michiue, Li, Zhao, Kamikodai, et al. 2006; Everett et al. 2015).

Another two studies by Xiao and Chen (Xiao & Chen 2005) and Liu *et al.* (Y. Liu et al. 2008) looked at the degradation of actin post-mortem. The former used the western blotting technique to test the presence of actin and tubulin in rat liver, up to 18 days post-mortem. They reported that they were able to detect actin up to 8 days PM and that it was not detectable from 10 days onwards. Additionally, they detected beta-tubulin up to 2 days PM and stated it was not visible 4 days after death. The second group looked at actin in various organs and tissues up to 72 h PM. They concluded that actin was gradually degrading with time at various rates, depending on the tissue. They suggested actin could be used for time since death estimation. These results disagree with the data obtained in this study. Actin was identified in all three species investigated in this experiment in multiple protein spots for each, and all but one actin spot (beef tissue) showed actin increasing in abundance after death. Additionally, the

human tissue from subject 2 was collected between 11 and 14 days PM and actin was still detectable. These findings agree with the study of Lametsch *et al.* where an increase in actin levels was also observed (Lametsch *et al.* 2002). These differences could arise from the different tissue types used. Hepatic tissue used in the study by Xiao and Chen is very enzymatically rich; therefore, it degrades more rapidly than muscle tissue. Additionally, both of these studies used western blot technique, whereas 2DE was used in this and Lametsch's study.

Two other proteins, myosin and heat shock protein were identified in the present study as proteins of interest. To the best of the author's knowledge, neither of them has previously been suggested as a potential PMI biomarker. However, their degradation, or the lack thereof, has been looked at as a part of the investigation of the post-mortem proteolysis process. According to Geesink and Koohmaraie, myosin heavy chain shows very little degradation from 0 to 56 days post-mortem while myosin light chain remains unchanged in this time period in lamb muscle (Geesink & Koohmaraie 1999). Tuttle *et al.* also reported that the levels of myosin heavy chain remain unaffected over the period of up to 7 days PM in rabbit tissue (Tuttle *et al.* 2014). On the other hand, Lametsch *et al.* reported an increase in the abundance of this protein post-mortem in pig meat (Lametsch *et al.* 2002). The results of the present study agree with the last-mentioned publication. Myosin heavy chain was detected in human tissue and an increase was observed over time and the same was seen for myosin light chain identified in beef. Myosin binding protein C (both fast and slow type) was identified in rat tissue and it was seen that the slow type accumulates over time while the fast type degrades. This is contrary to the findings of Di Luca *et al.* where the authors reported that the fast type of myosin binding protein C increases in abundance in porcine muscle over time since death (Di Luca *et al.* 2013).

Various types of heat shock proteins (HSPs) were identified previously in aged meat, for example pork (Di Luca *et al.* 2013) and beef (Jia, Hollung, *et al.* 2006). Additionally, one study by Tavichakorntrakool *et al.* looked at PM changes in human muscle tissue and heat shock protein 27 kDa (otherwise known as heat shock protein beta 1) was among the proteins which were reported to be altered after 48 h PM (Tavichakorntrakool *et al.* 2008). All of these studies showed that

HSPs degrade with increasing time since death. This is in agreement with the results obtained for beef and rat tissue in this study. However, in human tissue, heat shock protein beta-1 was identified and appeared to be increasing in level over time.

### **3.5 Conclusion**

The untargeted proteomics approach successfully allowed the detection and identification of a number of proteins which change in abundance post-mortem. Skeletal muscle tissue from three different species, cow, rat and human, was tested. Proteins from the myosin, actin and heat shock families were identified as proteins of interest in all three cases. However, only actin showed similar increasing trends in all three, which makes it the strongest candidate as a PMI biomarker. Additionally, evidence of post-mortem proteolysis and protein fragmentation was observed. Due to the complexity of the proteome and the limitations of the methodology used it was not possible to fully develop this method for PMI estimation. However, this study created a great starting point for further research. The next step would require using one of the targeted approaches to test the above candidates in larger cohorts of test subjects.

## 4 METABOLOMICS (LC-MS)

### 4.1 Introduction

“Omics” approaches, such as proteomics and metabolomics, have led to the identification of biomarkers that are diagnostic or prognostic for disease states (Pena et al. 2015; LeWitt et al. 2013; Fedele et al. 2013; González-Domínguez et al. 2014; Blasco et al. 2014; Manna et al. 2015). This chapter deals with metabolomics (for proteomics see Chapter 3). Untargeted metabolomics can report on the relative abundance of a broad range of small molecules (such as amino acids, oligopeptides, sugars, bile acids and fatty acids) in any biological system of interest (Clarke & Haselden 2008). In the present study, an untargeted comparative metabolomics analysis was applied to search for molecular markers that evolve with predictable kinetics over time since death. The analytical methods most commonly employed for metabolomics are liquid chromatography-mass spectrometry (LC-MS), nuclear magnetic resonance (NMR) and gas chromatography-mass spectrometry (GC-MS). These techniques allow identification and quantitation of low molecular weight metabolites (up to ~1000 Da) (Clarke & Haselden 2008).

Various metabolites have previously been investigated for utility in PMI estimation. Harada *et al.* investigated the changes in levels of specific metabolites (lactate, alanine, pyruvate and glucose) in animal organs and tissues (liver, kidney, spleen, brain, heart and dorsal muscle) and found a correlation between PMI and levels of lactate and pyruvate in heart and muscle tissue (Harada et al. 1984). Sparks *et al.* presented a linear relationship between 3-methoxytyramine (3-MT) and PMI in the dorsal putamen (Sparks et al. 1986). The authors also concluded that this relationship varies with the cause of death. In cases where the cause of death was attributed to a heart disease, 3-MT was negatively correlated with PMI, while being positively correlated in cases with other causes of death. Three other studies reported metabolites that evolve over time in post-mortem sheep brain (Ith et al. 2002; Scheurer et al. 2005; Musshoff et al. 2011). Free trimethylammonium (fTMA), propionate and butyrate were found in all three investigations, among other compounds emerging post-mortem. Ith *et al.* also included human brain in the study and found similarities between the decomposition of human and sheep brain (Ith et al. 2002).

Banaschak *et al.* investigated the post-mortem changes in pig brain (Banaschak *et al.* 2005), and also identified fTMA in their study, as well as creatinine, lactate, acetate, alanine and succinate. More recently, Mao *et al.* showed a correlation between PMI and the breakdown products of ATP in rat brain, kidney and spleen (Mao *et al.* 2013). Meanwhile, Donaldson *et al.* discussed increasing concentrations of hypoxanthine, ammonia, NADH and formic acid in rat, pig and human blood post-mortem (Donaldson & Lamont 2013). Kang *et al.* was one of the first groups to utilise a global mass-spectrometry based metabolomics approach (as opposed to metabolite assays) in time since death estimation (Kang *et al.* 2012). Metabolites extracted from rat livers over the first 48 hours post-mortem were analysed by UPLC/Q-TOF MS. Statistical analysis of the data yielded 15 potential biomarker candidates, including various polysaccharides, steroids, nucleosides, amino acids and more.

This section shows the development of an LC-MS metabolomics approach to address PMI in beef and rat models, and the application of this approach to human cadavers with known PMI.

## 4.2 Methodology

Sample collection, preparation and analysis were as described in Chapter 2.

## 4.3 Results

Metabolites of interest were selected primarily because they showed a predictable and steady rate of change with PMI, as well as the confidence in the metabolite identification. Furthermore, selected metabolites showed similar trends between the tested human subjects as well as the animal (beef, rat) tissue and reinforced the confidence in selected compounds as markers. Metabolites of interest identified in rat and human tissue included skatole (3-methylindole), xanthine, n-acetylneuraminate, 1-methylnicotinamide, choline phosphate, uracil and a number of amino acids (see Table 4-1) with tyrosine, threonine and lysine being the most promising candidates.

**Table 4-1. List of all identified metabolites of interest in rat and human tissue. KEGG ID – number corresponding to a given metabolite in Kyoto Encyclopedia of Genes and Genomes (Kanehisa 1995), RT – retention time, Metabolite ID code – suggested coding system for reporting confidence of metabolite identification (Sumner et al. 2014). HRMS – high resolution mass spectrometry; superscript '1' means a normal full scan mass spectrum; subscript 'a' indicates the spectrum was matched to an authentic standard; subscript 'lib' indicates a spectral match to a reference library; R<sub>ta</sub> signifies retention time matched identifications (high confidence); the remaining ones are putatively identified.**

Metabolite name	Elemental formula	KEGG ID	Detected Mass	RT (min)	Metabolite ID code
L-Arginine	C <sub>6</sub> H <sub>14</sub> N <sub>4</sub> O <sub>2</sub>	C00062	174.1116	25.79	HRMS <sup>1</sup> <sub>a</sub> , R <sub>ta</sub>
L-Histidine	C <sub>6</sub> H <sub>9</sub> N <sub>3</sub> O <sub>2</sub>	C00135	155.0696	14.59	HRMS <sup>1</sup> <sub>a</sub> , R <sub>ta</sub>
L-Leucine	C <sub>6</sub> H <sub>13</sub> NO <sub>2</sub>	C00123	131.0946	10.12	HRMS <sup>1</sup> <sub>a</sub> , R <sub>ta</sub>
L-Lysine	C <sub>6</sub> H <sub>14</sub> N <sub>2</sub> O <sub>2</sub>	C00047	146.1055	24.39	HRMS <sup>1</sup> <sub>a</sub> , R <sub>ta</sub>
L-Methionine	C <sub>5</sub> H <sub>11</sub> NO <sub>2</sub> S	C00073	149.0511	10.83	HRMS <sup>1</sup> <sub>a</sub> , R <sub>ta</sub>
L-Phenylalanine	C <sub>9</sub> H <sub>11</sub> NO <sub>2</sub>	C00079	165.079	9.54	HRMS <sup>1</sup> <sub>a</sub> , R <sub>ta</sub>
L-Proline	C <sub>5</sub> H <sub>9</sub> NO <sub>2</sub>	C00148	115.0633	11.96	HRMS <sup>1</sup> <sub>a</sub> , R <sub>ta</sub>
L-Threonine	C <sub>4</sub> H <sub>9</sub> NO <sub>3</sub>	C00188	119.0583	13.52	HRMS <sup>1</sup> <sub>a</sub> , R <sub>ta</sub>
L-Tryptophan	C <sub>11</sub> H <sub>12</sub> N <sub>2</sub> O <sub>2</sub>	C00078	204.09	10.94	HRMS <sup>1</sup> <sub>a</sub> , R <sub>ta</sub>
L-Tyrosine	C <sub>9</sub> H <sub>11</sub> NO <sub>3</sub>	C00082	181.0739	12.2	HRMS <sup>1</sup> <sub>a</sub> , R <sub>ta</sub>
L-Valine	C <sub>5</sub> H <sub>11</sub> NO <sub>2</sub>	C00183	117.079	11.68	HRMS <sup>1</sup> <sub>a</sub> , R <sub>ta</sub>
Putrescine	C <sub>4</sub> H <sub>12</sub> N <sub>2</sub>	C00134	88.1001	21.97	HRMS <sup>1</sup> <sub>a</sub> , R <sub>ta</sub>
Xanthine	C <sub>5</sub> H <sub>4</sub> N <sub>4</sub> O <sub>2</sub>	C00385	152.0334	9.03	HRMS <sup>1</sup> <sub>a</sub> , R <sub>ta</sub>
Choline Phosphate	C <sub>5</sub> H <sub>14</sub> NO <sub>4</sub> P	C00588	183.0662	17.52	HRMS <sup>1</sup> <sub>a</sub> , R <sub>ta</sub>
Uracil	C <sub>4</sub> H <sub>4</sub> N <sub>2</sub> O <sub>2</sub>	C00106	112.0273	7.985	HRMS <sup>1</sup> <sub>a</sub> , R <sub>ta</sub>
L-Asparagine	C <sub>4</sub> H <sub>8</sub> N <sub>2</sub> O <sub>3</sub>	C00152	132.0535	14.48	HRMS <sup>1</sup> <sub>a</sub>
L-Aspartate	C <sub>4</sub> H <sub>7</sub> NO <sub>4</sub>	C00049	133.0375	14.0	HRMS <sup>1</sup> <sub>a</sub>
L-Cysteine	C <sub>3</sub> H <sub>7</sub> NO <sub>2</sub> S	C00097	121.0198	13.09	HRMS <sup>1</sup> <sub>lib</sub>
L-Glutamate	C <sub>5</sub> H <sub>9</sub> NO <sub>4</sub>	C00025	147.0532	9.59	HRMS <sup>1</sup> <sub>a</sub>
L-Serine	C <sub>3</sub> H <sub>7</sub> NO <sub>3</sub>	C00065	105.0426	14.97	HRMS <sup>1</sup> <sub>a</sub>
Cadaverine	C <sub>5</sub> H <sub>14</sub> N <sub>2</sub>	C01672	102.1157	22.08	HRMS <sup>1</sup> <sub>lib</sub>
Indole	C <sub>8</sub> H <sub>7</sub> N	C00463	117.0579	10.59	HRMS <sup>1</sup> <sub>lib</sub>
Skatole	C <sub>9</sub> H <sub>9</sub> N	C08313	131.0735	10.94	HRMS <sup>1</sup> <sub>lib</sub>
N-acetylneuraminatate	C <sub>11</sub> H <sub>19</sub> NO <sub>9</sub>	C00270	309.1061	12.23	HRMS <sup>1</sup> <sub>a</sub>
1-methylnicotinamide	C <sub>7</sub> H <sub>8</sub> N <sub>2</sub> O	C02918	136.0637	24.5	HRMS <sup>1</sup> <sub>lib</sub>

### 4.3.1 Beef tissue

The preliminary investigation using a beef steak sample resulted in putative identification of 2068 metabolites using the pHILIC method and 2309 using the HILIC method (for spreadsheets including all of the collected data see Appendices V and VI, pHILIC and HILIC respectively). Both columns are used for separation of polar and hydrophilic compounds (Loukas & Dotsikas 2011). However, the former column is more appropriate for basic conditions and the second for acidic conditions, so that some chemical classes are better separated in one system compared with the other. For example, organic acids will be

better separated by pHILIC chromatography, and biogenic amines (e.g. decomposition products) using HILIC chromatography. pHILIC and HILIC chromatography are thus complementary separation methods in LC-MS metabolomics.

A variety of compounds showed either increasing or decreasing patterns of change. Figure 4-1 shows an example of four different metabolites with interesting patterns of change over the investigated period.

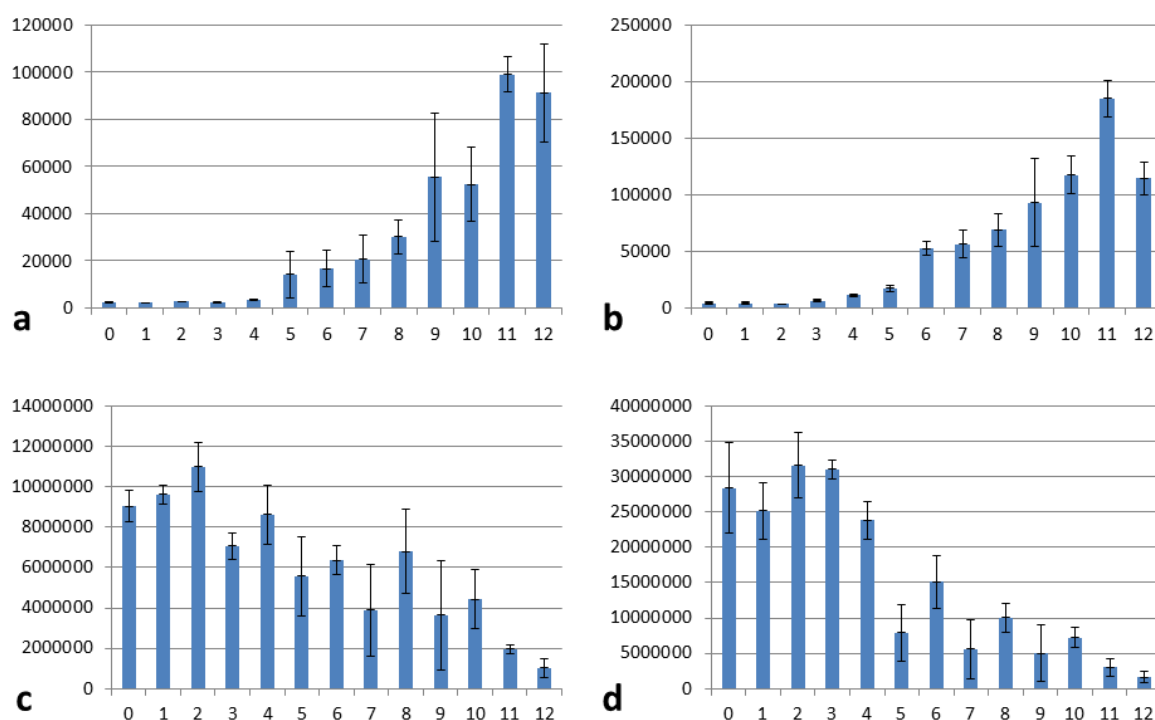


**Figure 4-1. Examples of metabolites identified in trial beef study.**

The graphs show as follows: a – n-acetyl-beta-alanine, b – purine, c – glutathione, d – choline. Muscle sample was aged over thirteen days: y-axis represents average instrument response (arbitrary units), the analysis included three technical replicates (three sections taken from one piece of tissue) of each sample, x-axis represents PMI (days). Error bars indicate standard deviation calculated from average instrument response.

#### 4.3.1.1 Decomposition products

This untargeted metabolomics approach resulted in a large amount of data, necessitating a methodical strategy of analysis. Therefore, based on information gained from the literature, certain classes of compounds were selected as possible PMI biomarkers. In the first instance, commonly known decomposition products like putrescine, cadaverine, indole and skatole were investigated (Vass 2001). They are formed by bacterial breakdown of amino acids after death, however, they are also present in living tissue (Wishart et al. 2013). Cadaverine is a product of lysine metabolism, putrescine of arginine and proline metabolism

and both indole and skatole are produced from tryptophan. The above compounds, as they are biogenic amines, were expected to be identified using the HILIC method of separation. However, only indole was detected this way. It was also detected using the pHILIC method along with putrescine and cadaverine. Neither of the decomposition products detected using the pHILIC method showed any obvious trend of change (see Figure 4-2a, b and c). On the other hand, indole detected using the HILIC method showed a steadily increasing pattern starting from the 3rd day post-mortem (see Figure 4-2d). This is a more reliable result since the HILIC column is more suitable for the separation of biogenic amines.

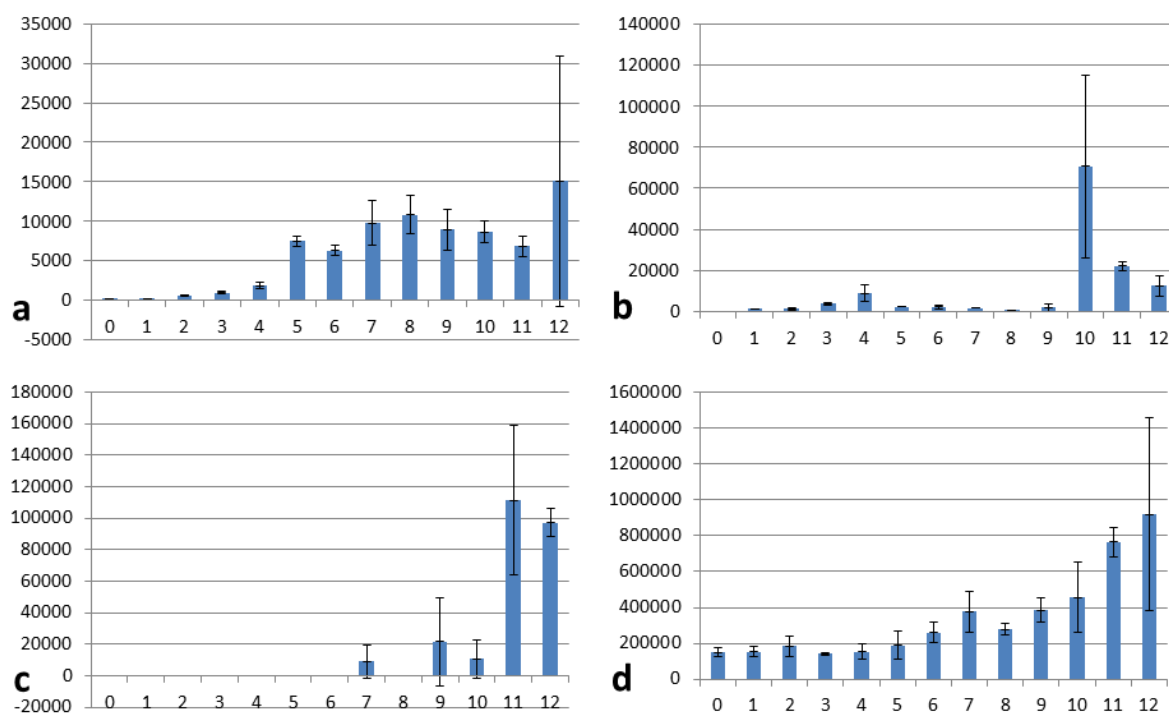


**Figure 4-2. Decomposition products identified in beef tissue.** The graphs represent: a – putrescine, b – cadaverine, c – indole (pHILIC), d – indole (HILIC). Y-axis are showing average instrument response (N=3), x-axis are showing PMI (days). Error bars indicate standard deviation calculated from average instrument response. The analysis included three technical replicates of each sample.

#### 4.3.1.2 Amino acids

Since the decomposition products did not yield a clear pattern, other compounds were investigated. Proteogenic amino acids were among the metabolites which were identified with the highest confidence; therefore, they were also looked at as potential candidates. All 20 of these amino acids were detected in beef tissue. In general, most of them showed increasing trends, however, not consistently over the whole investigated period. Two of the amino acids,

glutamine and alanine, showed decreasing trends contrary to the others. Figure 4-3 shows 14 out of the 20 detected amino acids which were identified with high confidence. Tryptophan, threonine, methionine, leucine and phenylalanine started to increase after the 5th day PM. Aspartate showed a general increasing trend throughout the investigated period. Glycine, glutamate, proline, serine and cysteine increased until the 9th or 10th day post-mortem and then started to decrease. Valine increased until the 3rd day PM and showed a fairly constant level from day 6 onwards. Arginine did not show a clear pattern of change (not shown). From the presented amino acids, serine, cysteine, threonine, methionine and alanine showed very clear and consistent changes over time.

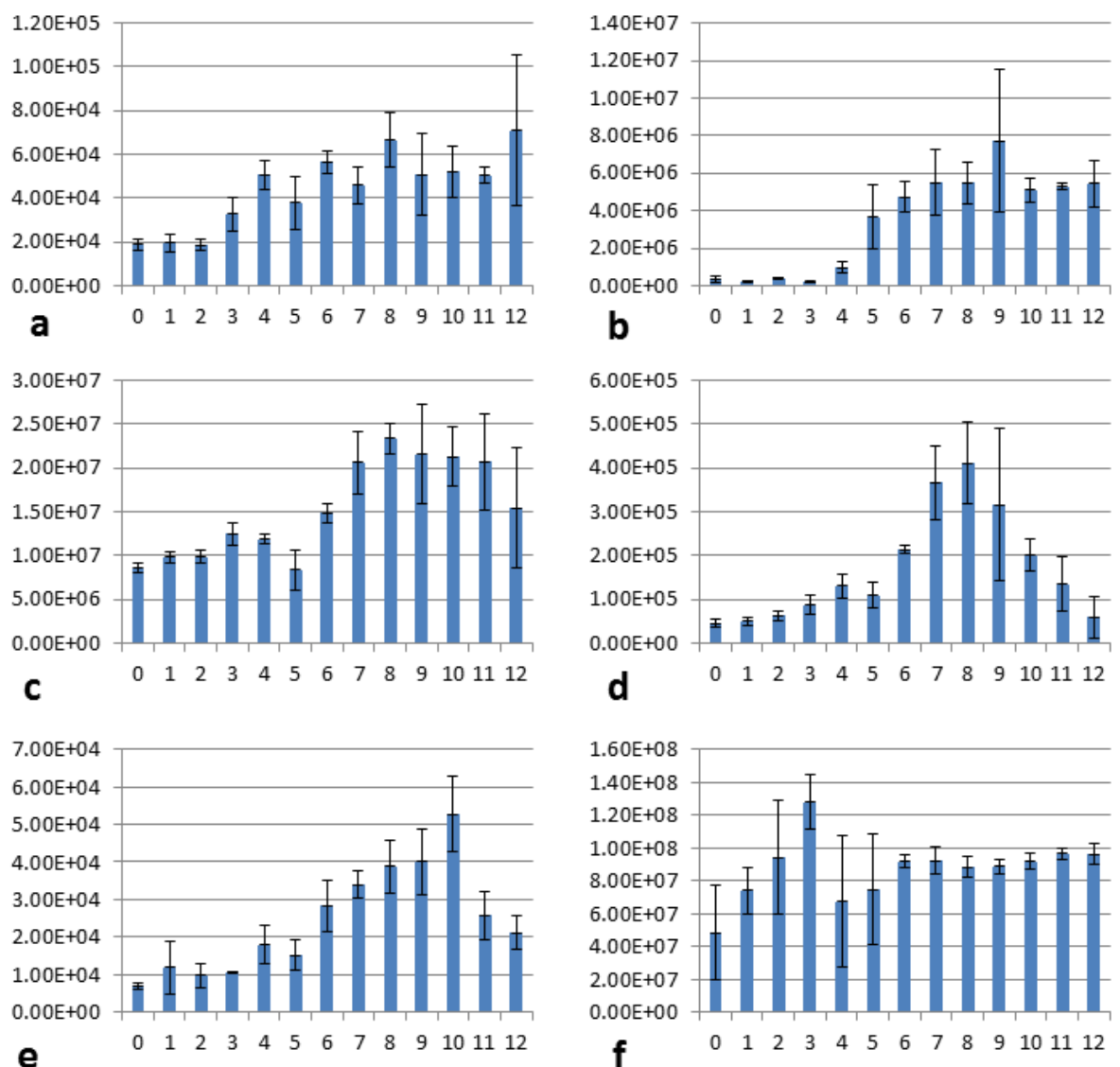


**Figure 4-3. Patterns of change observed in the identified amino acids (beef tissue).** The graphs represent: a – glycine, b – glutamate, c – proline, d – serine, e – cysteine and f – valine. Amino acids shown in graphs a-e show an increase until 9th or 10th day PM and then decrease. Valine increases for the first 3 days PM. Y-axes signify the average instrument response (arbitrary unit) and x-axes PMI (days). Error bars were calculated from standard deviation based on three technical replicates used for each time point.

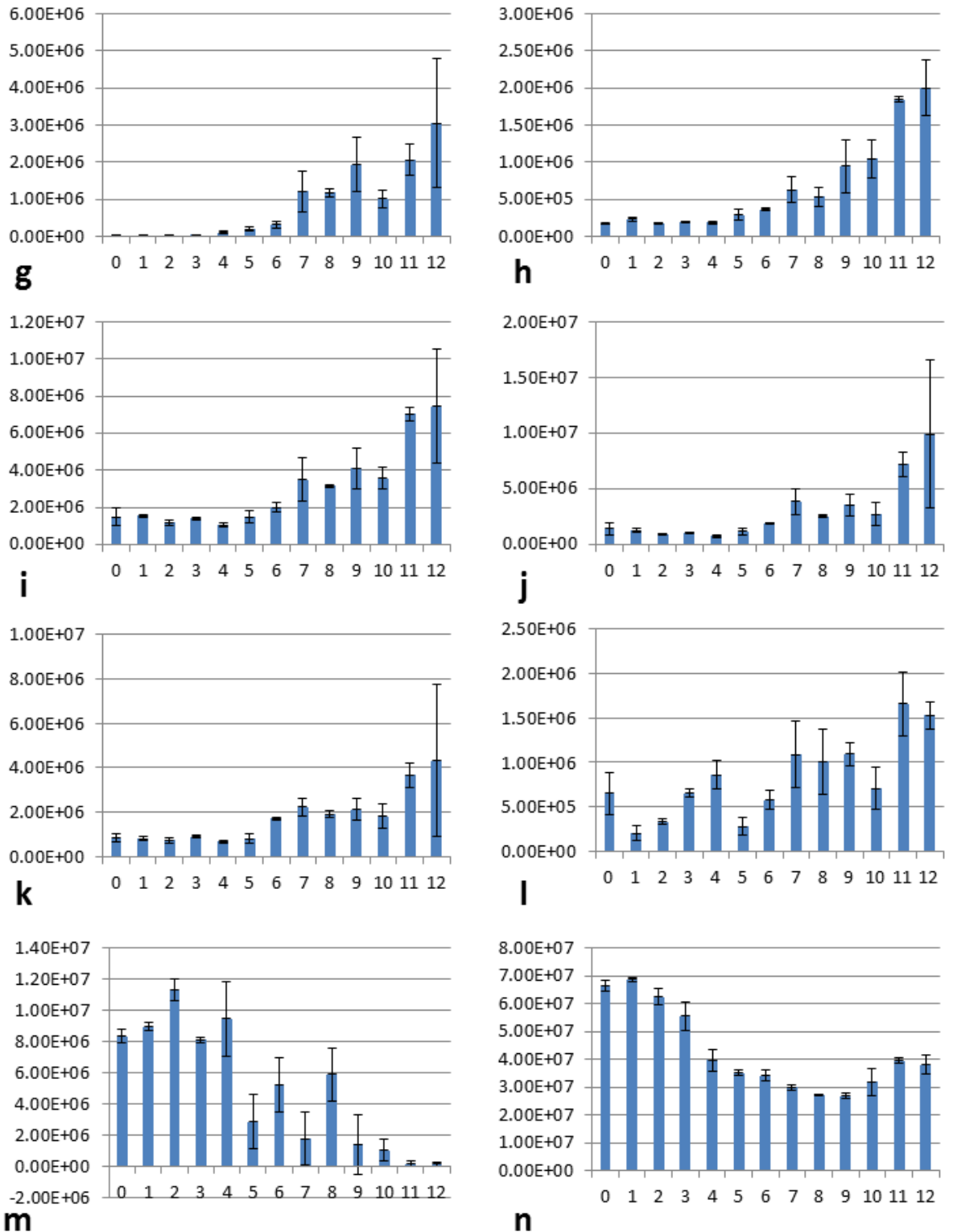


**Figure 4-3.** Continued from previous page.

The graphs represent: g – tryptophan, h – threonine, i – methionine, j – leucine, k – phenylalanine, l – aspartate, m – glutamine, n – alanine. Amino acids in graphs g-k show an increase from about day 5 onwards. Aspartate shows a general increasing trend throughout the investigated PMI. Glutamine and alanine show a decreasing trend. Y-axes signify the average instrument response (arbitrary unit) and x-axes PMI (days). Error bars were calculated from standard deviation based on three technical replicates used for each time point.

The amino acids showed promising results and could potentially serve as PMI biomarkers. In general, most of them showed increasing patterns with PMI. However, an isolated piece of tissue cannot fully represent the complexity of the decomposition process occurring in an intact cadaver. Therefore, after completing method development using a beef steak sample, the study was extended to include rat cadavers as an animal model. The methodology was shown to be well suited for the intended purpose. Hence it was followed by a more controlled study with intact cadavers, in order to give more insight into the reproducibility and reliability of amino acids as potential markers.

### **4.3.2 Rat tissue**

Muscle samples were obtained from 8 rats at 0, 24, 48 and 72 h PM (two rats dissected at each time point). Metabolites were extracted and analysed using an untargeted LC-MS approach. Both pHILIC and HILIC methods of separation were used. This approach allowed the detection and putative identification of 1753 metabolites in pHILIC and 1080 in HILIC (Appendices VII and VIII contain IDEOM spreadsheets with all of the detected metabolites using pHILIC and HILIC, respectively). The majority of the detected molecules were classified as peptides (separated into peptides, di-, tri- and tetra-peptides) and lipids (including fatty acyls, glycerolipids, glycerophospholipids, polyketides, prenols, sphingolipids, sterol lipids and gangliosides). Smaller groups included metabolites involved in amino acid, carbohydrate and nucleotide metabolism. Additionally, large numbers of identified metabolites remained unclassified as members of any particular metabolisms or pathways (479 in pHILIC and 270 in HILIC method). Figure 4-4 and Figure 4-5 show the percentage of the metabolites which were successfully classified.

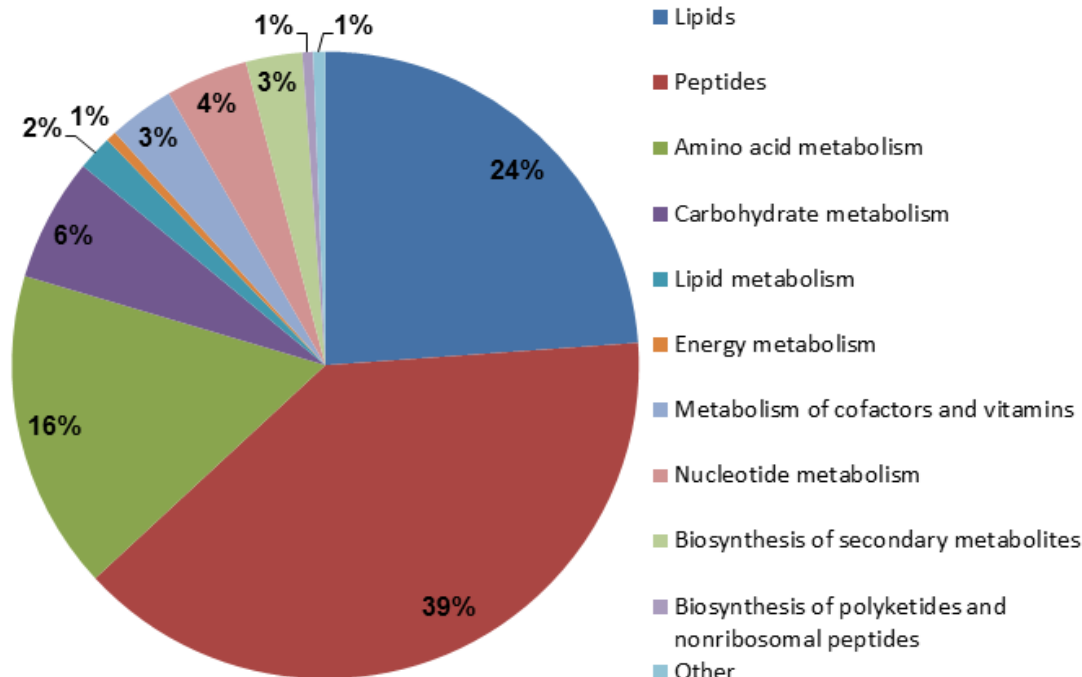


**Figure 4-4.** Graph representing the classes of compounds identified through the pHILIC method in rat tissue.

1753 metabolites were detected using the pHILIC method, out of which 1274 were classified into above groups by IDEOM (Creek et al. 2012). Values presented show the percentage of the total of classified compounds. Metabolites labelled as ‘other’ were classified as xenobiotics and medium components. Peptides group includes single, di-, tri- and tetra-peptides. Lipids group includes fatty acyls, glycerolipids, glycerophospholipids, polyketides, prenols, sphingolipids and sterol lipids.

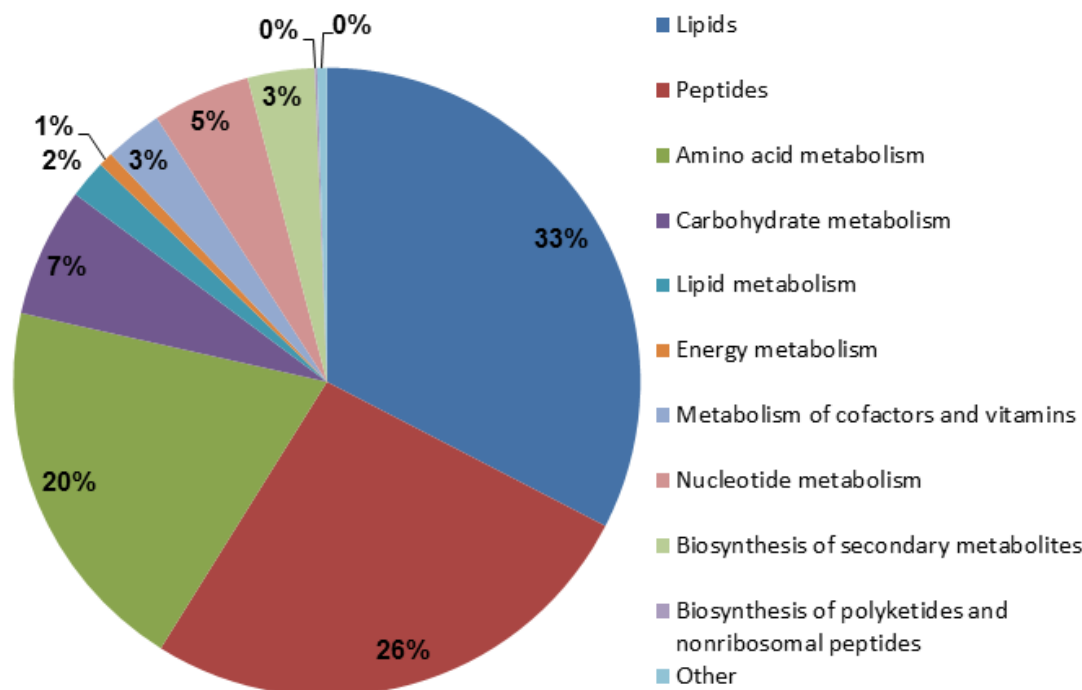


**Figure 4-5.** Graph representing the classes of compounds identified through the HILIC method in rat tissue.

1080 metabolites were detected using the pHILIC method, out of which 810 were classified into the above groups by IDEOM (Creek et al. 2012). Values presented show the percentage of the total of classified compounds. Metabolites labelled as ‘other’ were classified as xenobiotics and medium components. Peptides group includes single, di-, tri- and tetra-peptides. Lipids group includes fatty acyls, glycerolipids, glycerophospholipids, polyketides, prenols, sphingolipids and sterol lipids and gangliosides.

#### 4.3.2.1 Amino acids

Nineteen out of 20 of the proteogenic amino acids were detected in the rat muscle. Iso-leucine was indistinguishable from leucine, as these two compounds are isomers and eluted together. Similar to the data obtained from beef tissue, sixteen of them showed steadily increasing patterns over time since death. The remaining three (glycine, alanine and glutamine) showed less change over the investigated time period. Figure 4-6 shows the changes observed in eleven of those amino acids, which were identified with high confidence.

Among all of the detected amino acids, cysteine showed the highest rate of increase, nearly 22-fold by the third day post-mortem. However, it is not shown in Figure 4-6 as a potential biomarker candidate as the calculated error at one of the time points was very high. Leucine and aspartate increased 13-fold in that time, followed by valine with a 10-fold increase. Most of the other amino acids increased between 4 and 8-fold with proline increasing at the slowest rate of 2-fold change over the same time period and arginine and lysine 3-fold.

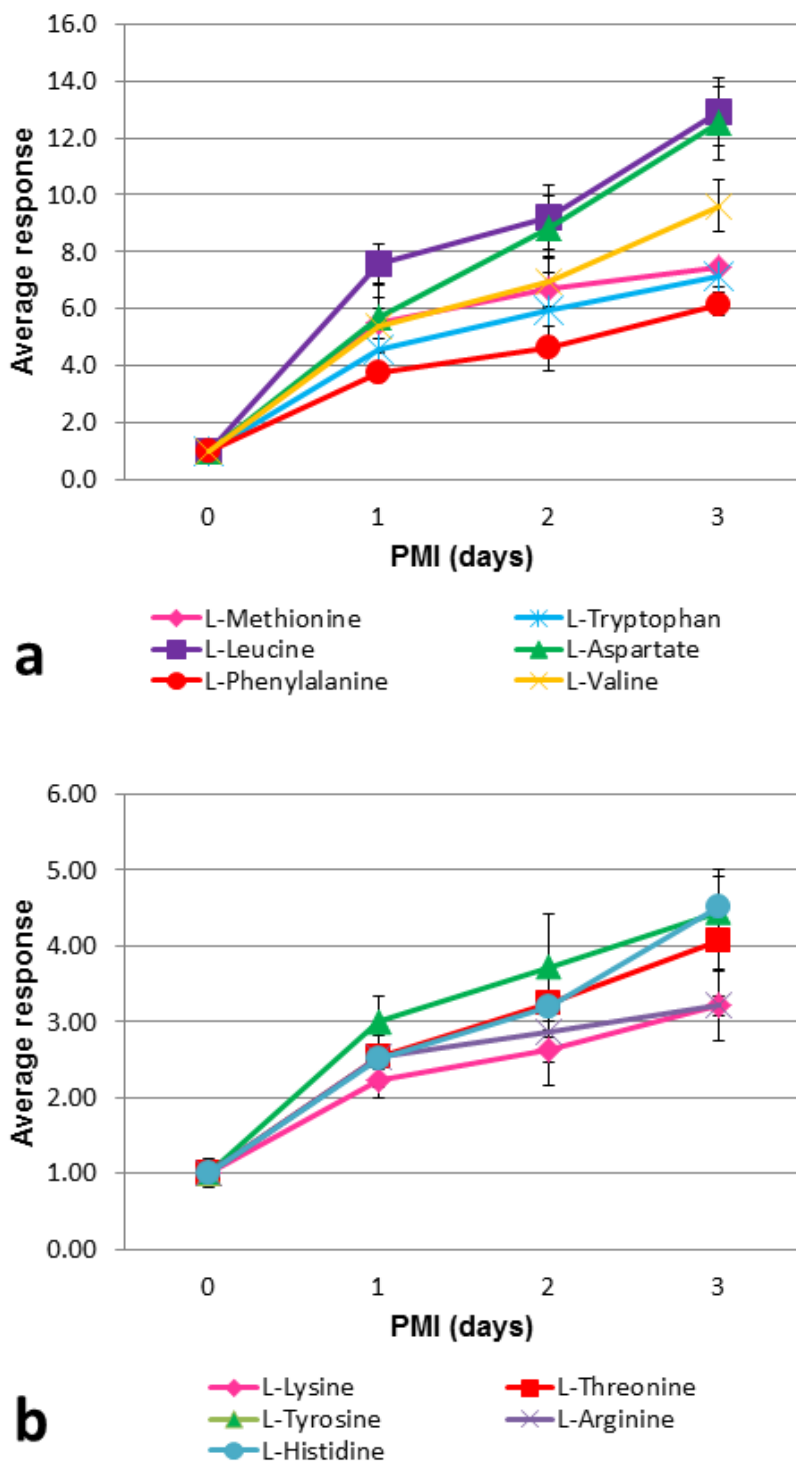


**Figure 4-6.** Change in levels of eleven amino acids with increasing time since death in rat tissue.

Graph a shows changes in levels of methionine, leucine, phenylalanine, tryptophan, aspartate and valine. Graph b shows lysine, tyrosine, histidine, threonine and arginine. Average instrument response (arbitrary unit) was normalised to time 0 and plotted against time. Error bars indicate standard deviation calculated from average instrument response. Two rats were analysed per time point, both right and left leg being sampled for each rat (N=4).

Additionally, since two rat cadavers were sampled at each time point, their metabolite levels were compared to each other. The absolute levels of the metabolites differed; however, the rates of increase of four amino acids (histidine, lysine, proline and asparagine) showed similarities between different rats (see Figure 4-7).

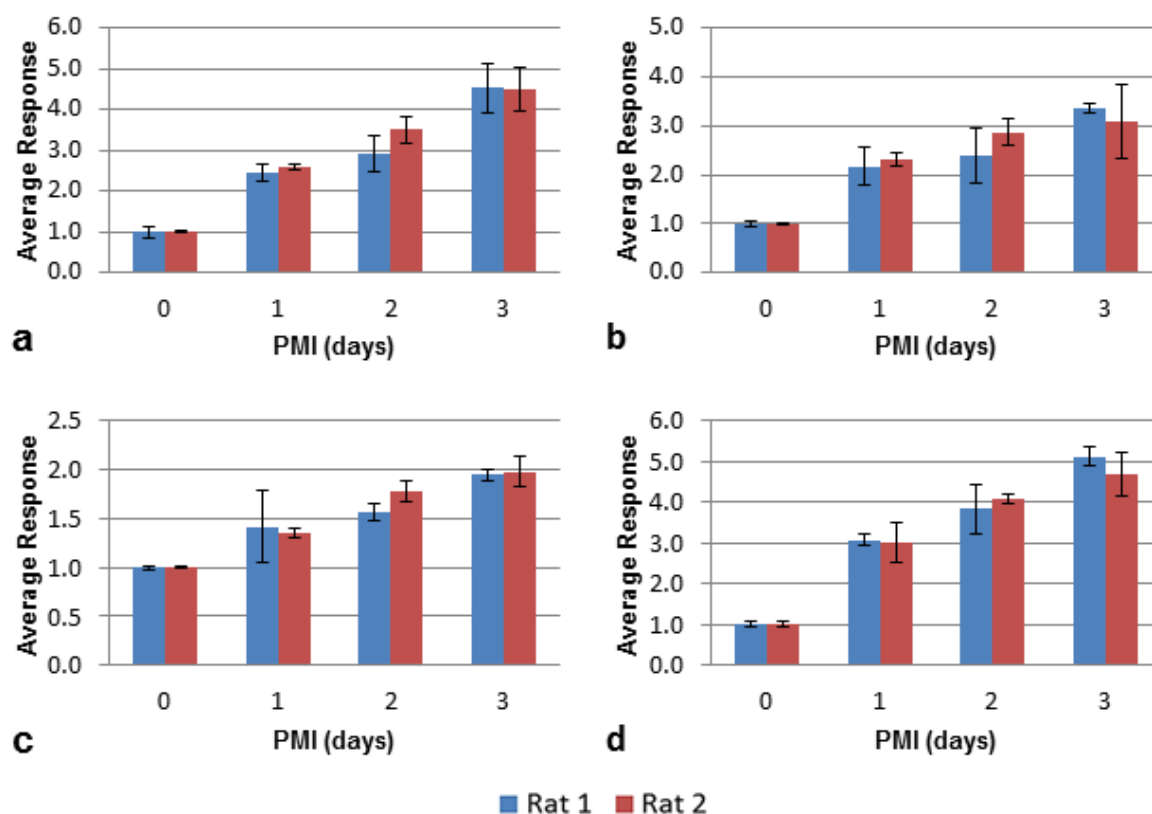


Figure 4-7. Amino acids which show similar instrument response for two rats sampled at the same PMI.

Graphs show the following amino acids: a – histidine, b – lysine, c – proline and d – asparagine. Two rats were dissected at each time point, the average response for both was normalised to time 0 at each PMI and compared. Error bars indicate standard deviation calculated from average instrument response. Left and right biceps femoris samples were treated as technical replicates for each rat (N=4).

#### 4.3.2.2 Decomposition products

Biogenic amines such as cadaverine, putrescine, indole and skatole, are well known decomposition products (Vass 2001). Contrary to the results obtained using beef tissue, all of these compounds were detected using the HILIC method, with the exception of skatole (pHILIC). Additionally, the compounds showed a clear trend which was not the case with beef. Putrescine, skatole and indole were found to be increasing with time since death while cadaverine, unexpectedly, decreased (Figure 4-8). The first three aforementioned

compounds increased approximately 4-, 7- and 8-fold, respectively. Cadaverine decreased by about 3-fold.

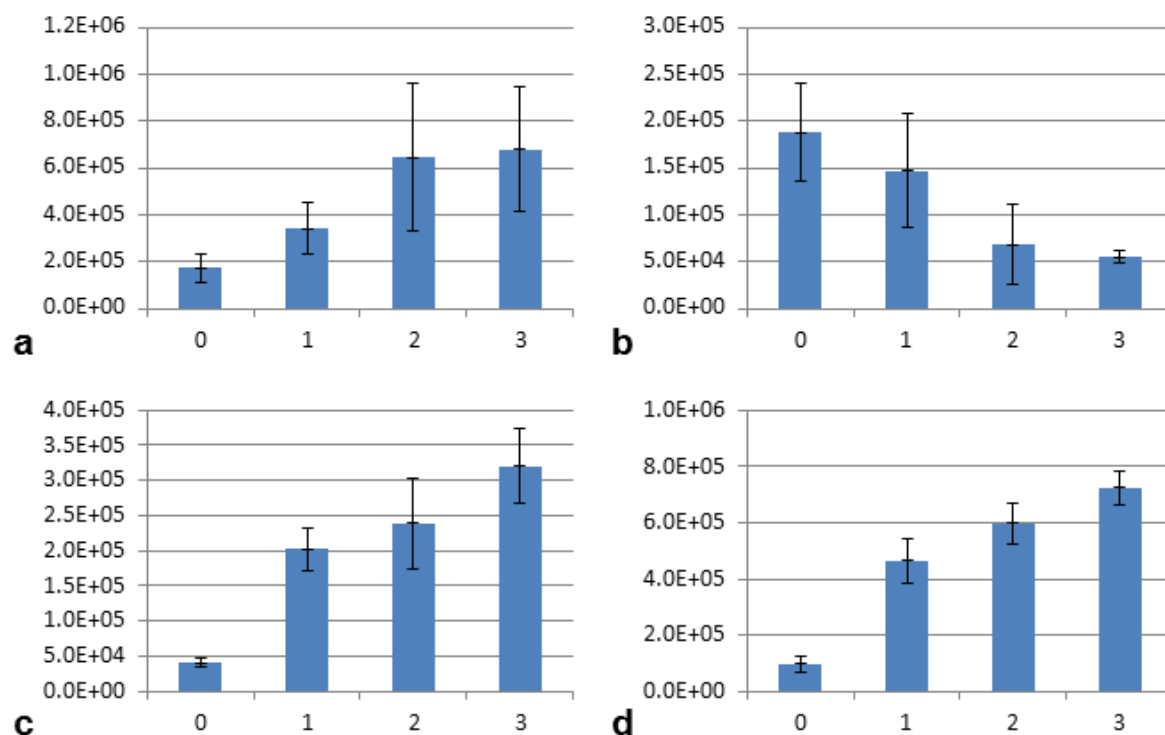


**Figure 4-8. Patterns of change of identified decomposition products with increasing time since death in rat tissue.**

Graphs show a mean instrument response (N = 4) with error bars to indicate the standard deviation: a – putrescine, b – cadaverine, c – indole and d – skatole. Y-axes represent instrument response, x-axes show days since death.

#### 4.3.2.3 Other metabolites

Five new compounds of interest were selected in rat tissue, based on their steady increasing changes over time as well as on the confidence in the compound identification: xanthine (purine metabolism), n-acetylneuraminic acid (derivative of neuraminic acid), uracil (pyrimidine metabolism), choline phosphate (glycerophospholipid metabolism) and 1-methylnicotinamide (metabolite of nicotinamide) (Wishart et al. 2013). Xanthine displayed the most significant increase of approx. 58-fold over three days post-mortem. N-acetylneuraminic acid and uracil showed a slower, but still significant, rate of increase - approximately 24- and 15-fold, respectively. Choline phosphate and 1-methylnicotinamide also increased consistently over the investigated period (see Figure 4-9).

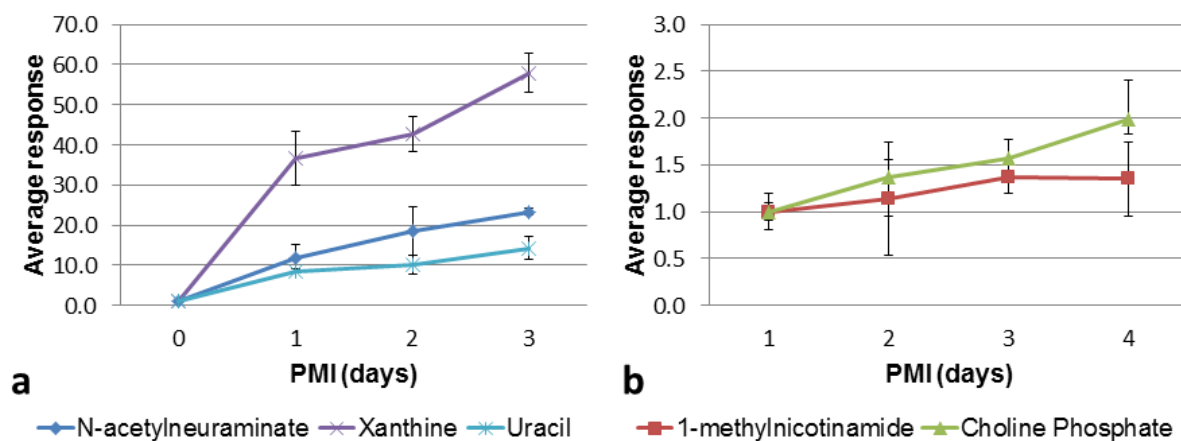


**Figure 4-9. Metabolites that increase in rat tissue with increasing PMI.** Graphs represent: a – xanthine (approx. 58-fold increase), n-acetylneuraminate (approx. 24-fold), uracil (approx. 15-fold) and b – choline phosphate (approx. 2-fold), 1-methylnicotinamide (approx. 1.4-fold). Means and standard deviations (shown by the error bars) were calculated from data collected from muscle of both right and left legs of two individual rats. The metabolites above, with the exception of 1-methylnicotinamide, were identified by matching to a reference standard.

### 4.3.3 Human tissue

The end goal of this research was to devise a PMI estimation method that could be used by forensic scientists in the investigation of fatalities. Therefore, the results obtained using the animal models were tested in human muscle in the final stages of the project. The human tissue was prepared and analysed in the same way as the rat tissue, with the exception of data processing. In the case of rat tissue, the data for all cadavers was analysed collectively and rats dissected at the same time point were treated as biological replicates in single analysis. Whereas, due to the high variability of the individual human cadavers (cause of death, age, sex, diet, environmental exposure since death, etc.), the data collected for each individual was processed as an individual time course to demonstrate changes in the metabolome in comparison to baseline. On average, for each human subject, 998 metabolites were detected and putatively identified using the pHILIC and 991 using the HILIC separation methods. Appendices IX, XI, XIII, XV, XVII and XIX show metabolites detected using pHILIC separation for subjects 1, 2, 3, 4, 5 and 6, respectively. Appendices X, XII, XIV, XVI, XVIII and XX show metabolites analysed using the HILIC method for subjects 1, 2, 3, 4, 5 and 6, respectively.

### 4.3.3.1 Amino acids

As was the case for rat tissue, generally increasing patterns were observed for most of the amino acids, for all of the tested human cadavers, with the exception of subject 1. Figure 4-10 shows an example of how the levels of one of the amino acids of interest (leucine) change over time for all of the subjects.

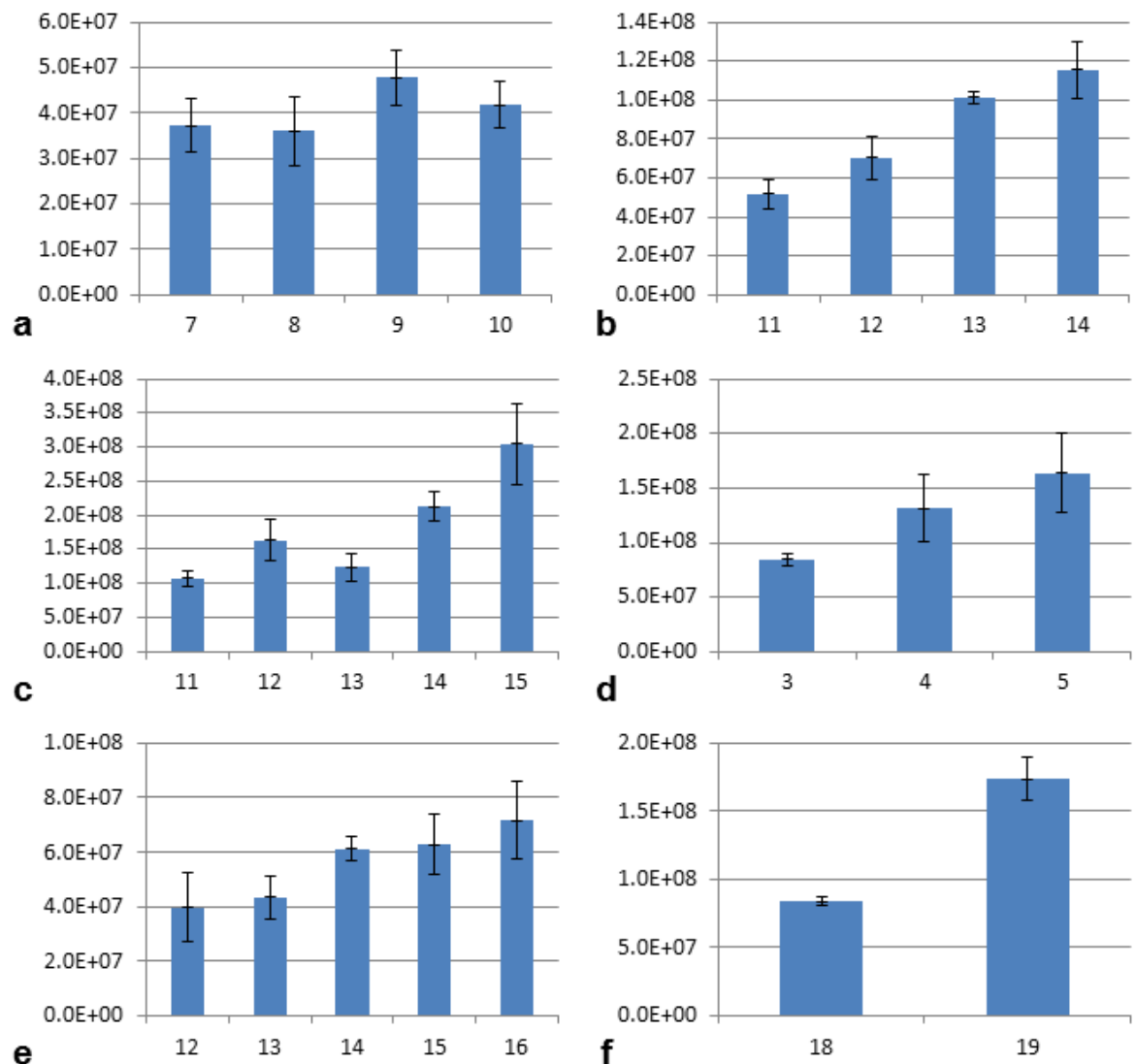


**Figure 4-10.** An example of how the levels of a single metabolite (leucine) change over time for all of the investigated subjects.

The graphs represent: a – subject 1, b – 2, c – 3, d – 4, e – 5 and f – 6. A steady increasing pattern can be seen for all of the subjects, with exception of subject 1. The levels of this amino acid go up irrespective of the temperature that the body was stored at (subjects 4 and 6 were stored outdoors). Y-axes represent instrument response and X-axes show time since death (days). Error bars indicate standard deviation calculated from average instrument response. The analysis included three technical replicates of each sample.

Similar trends were observed for nearly all of the proteogenic amino acids with the exception of glutamine and alanine, which did not show much change. Not every metabolite shared the same pattern in every single test subject, however,

leucine (Figure 4-10), tryptophan, tyrosine, threonine, lysine, phenylalanine and aspartate showed steady increases for all. The quantitative changes in amino acid levels were more variable between human individuals than between rats (as shown in Figure 4-6).

Although similar trends were observed in all subjects, it was difficult to draw conclusions based on this particular set of subjects, due to differences in storage conditions of the cadavers as well as their different PMIs. The measured levels of amino acids for subjects 2, 3 and 5 (who were of similar age and PMI) were normalised to PMI 12 in each subject (the first common time point for all of the three subjects). Four amino acids (glutamate, histidine, methionine and threonine) show similar rates of increase for the two male subjects, while lysine and tyrosine show an overlap for subjects 3 and 5 - female and male respectively (see Figure 4-11). Cysteine and serine show an overlap for all three subjects (see Figure 4-12). This finding is in agreement with data collected from rat cadavers, especially for histidine and lysine which showed similar rates of increase between different rat subjects.

Among the amino acids, tyrosine, threonine and lysine showed the most consistent increase over time between different individuals. Additionally, as mentioned above, they show similar rates of change for subjects around the same age and PMI, suggesting they are promising candidates for time since death biomarkers.

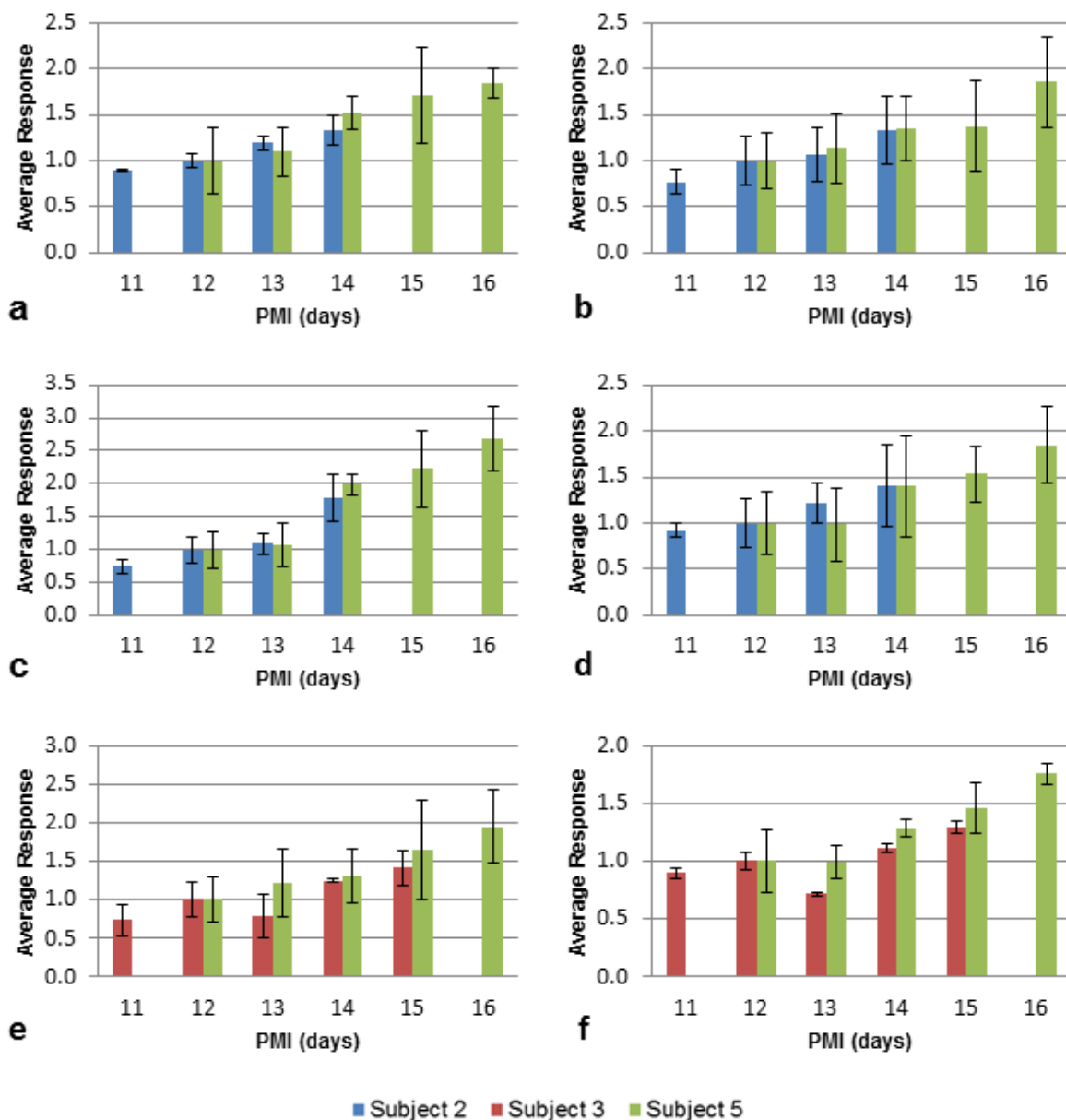


**Figure 4-11. Amino acids which show similar trend of increase over time for different subjects at the same PMI.**

Metabolites shown above: a – glutamate, b – histidine, c – methionine, d – threonine (two male subjects) e – lysine and f – tyrosine (male and a female). The average response for each subject was normalised to PMI 12 (first mutual time point for all subjects). Error bars indicate standard deviation calculated from average instrument response. The analysis included three technical replicates of each sample.

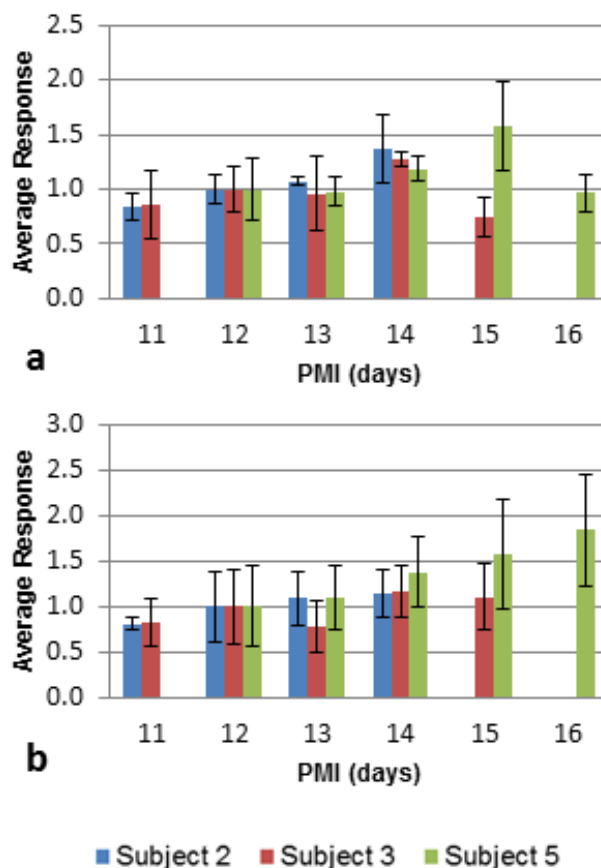


**Figure 4-12. Amino acids which show similar trend of increase over time for three different subjects at the same PMI.**

The graphs represent: a – cysteine, b – serine. The results for each amino acid were normalised to PMI 12 (first mutual time point for all subjects). Error bars indicate standard deviation calculated from average instrument response. The analysis included three technical replicates of each sample.

#### 4.3.3.2 Phenylalanine assay

Amino acids are among the most promising candidates for time since death biomarkers. Ideally, the method of quantification of these metabolites should be quick and easy, in order to facilitate its routine use. Therefore, the use of commercially available amino acid enzymatic assay kits was tested, to see if similar results can be achieved as by means of mass spectrometry. Five specific amino acid assay kits were available from a regular supplier (Sigma-Aldrich, UK): alanine, aspartate, glutamate, glutamine and phenylalanine. Alanine and glutamine were not included in the list of the metabolites of interest, therefore these were excluded. Aspartate, glutamate and phenylalanine show consistent trends with PMI in rat tissue, and phenylalanine also showed a similar trend in human tissue, so a phenylalanine assay kit was selected for initial testing.

Two assays were carried out to test what volume and dilution of the tissue extract should be used, so that it would fit within the calibration range

(described in detail in the methods section). After these tests there was only enough reagent left to carry out one test, including two of the human subjects - 2 and 5. Those two subjects were selected due to coincidental similarities between them - both male and around the same age. The levels of different metabolites were compared between them in the previous section and showed similarities. The enzymatic assay readings obtained from these two subjects are shown in Table 4-2.

**Table 4-2. Phenylalanine assay reading of samples obtained from human subjects 2 and 5. Row A includes the readings of the phenylalanine standard (in duplicate) at concentrations ranging from 0 to 1nmole. Columns 1 and 5 contain sample blanks of each sample. Rows B1-3, C1-3, D1-3 and E1-3 contain samples collected from subject 2: PMI 11, 12, 13 and 14, respectively. Rows F1-3, G1-3, H1-3, B5-7 and C5-7 contain samples collected from subject 5: PMI 12, 13, 14, 15 and 16, respectively. All samples were pipetted in duplicate with exception of sample blanks (not enough reagents left).**

<>	1	2	3	4	5	6	7	8	9	10	11	12
A	5351	4976	11926	9392	18545	14294	21927	23675	21806	27154	28953	32448
B	29195	42039	38272		23915	25093	32080					
C	25166	43777	38778		11842	18639	15635					
D	34948	38277	35156									
E	27204	30862	42859									
F	15865	21999	28001									
G	22602	27337	32765									
H	16139	27188	27449									

The duplicate readings obtained for the phenylalanine standard were averaged and plotted against the expected concentration. This graph is shown in Figure 4-13.

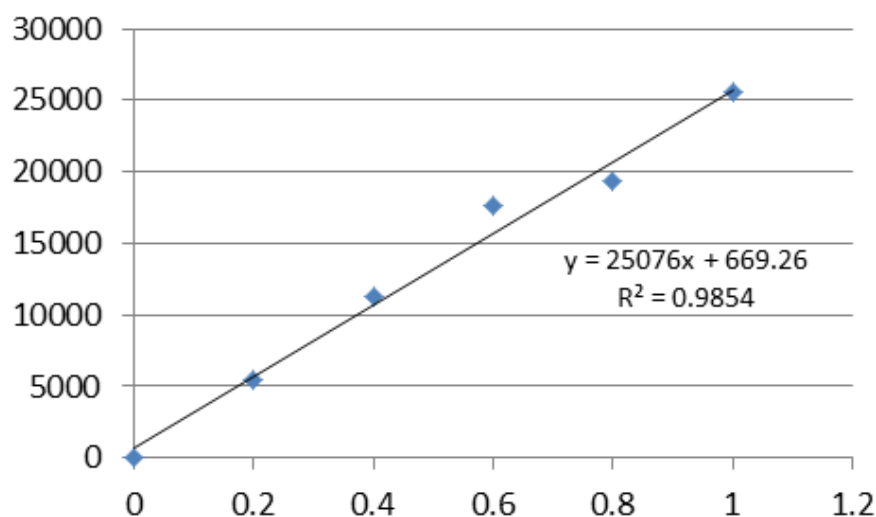


**Figure 4-13. Graph representing the standard curve for the phenylalanine enzymatic assay. Y axis represent the average instrument reading (based on duplicate measurements), x axis shows the expected amount of phenylalanine (nmole). Best fit line was created based on the plotted points. The equation for this line and the  $R^2$  value are also displayed.  $R^2$  represents how well the trend line is matched with the points – the closer to 1, the better the match.**

The equation shown in Figure 4-13 was used to calculate the amount of phenylalanine present in each sample. The results of these calculations are presented in Table 4-3.

**Table 4-3. The amount of phenylalanine present in the samples (subjects 2 and 5), calculated using the standard curve.**

**Average reading – mean result of two readings per each sample, reading minus blank – the number obtained by taking away the blank from average reading for every sample, phenylalanine – the amount of phenylalanine calculated with the curve equation.**

	PMI	Average reading	Reading minus blank	Phenylalanine (nmole)
Subject 2	11	40156	34992	1.4
	12	41278	36114	1.4
	13	36717	31553	1.2
	14	36861	31697	1.2
Subject 5	12	25000	19837	0.76
	13	30051	24888	0.97
	14	27319	22155	0.86
	15	28587	23423	0.91
	16	17137	11974	0.45

As the protocol stated, the average result obtained for the blank in the standard curve was taken away from the readings for all of the standards and samples. The results of this calculation for all of the samples are shown in Table 4-3. The protocol also suggested that a sample blank may be used to correct for background interference. Since it was not crucial to include the sample blank in the assay this step was omitted from the calculations. Unfortunately, the reading for subject 2 took the amount of phenylalanine higher than the top standard in the curve, which meant it could not be accurately quantified.

The concentration of phenylalanine present in the sample could be calculated using the amount of phenylalanine measured by the assay. This was done using a simple formula presented in Equation 4-1.

$$C = \frac{S_a}{S_v}$$

**Equation 4-1. Formula used to calculate the concentration of phenylalanine in the sample. Where  $S_a$  = Amount of phenylalanine in unknown sample (nmole) from standard curve,  $S_v$  = sample volume ( $\mu$ l) added to the wells, C = concentration of phenylalanine in the sample.**

Since the amount of phenylalanine in the samples collected from subject 2 was too high to be measured by the standard curve, only the concentrations of phenylalanine in samples collected from subject 5 were calculated. The results of this calculation are presented in Table 4-4.

**Table 4-4. The concentration of phenylalanine present in samples collected from subject 5. Concentration calculated using the amount of phenylalanine measured experimentally by the phenylalanine assay. PMI – post-mortem interval.**

Subject 5	
PMI	Phenylalanine (nmole/ $\mu$ l)
12	0.015
13	0.019
14	0.017
15	0.018
16	0.0090

The above concentrations were then plotted on a graph to see how the concentration changed with increasing time since death. This is shown in Figure 4-14a. Figure 4-14b shows the levels of phenylalanine measured using the standard metabolomics pipeline (LC-MS). The trends represented in those two graphs should be similar as they show the same metabolite measured in the same tissue samples. However, this is not the case. The levels of phenylalanine measured by the enzymatic assay show no particular trend with increasing time since death, while the ones measured by liquid-chromatography show an increasing trend.

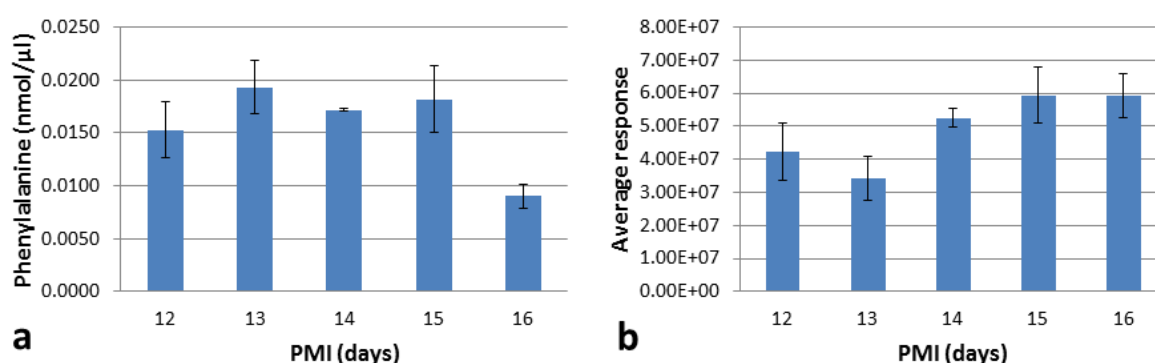


**Figure 4-14. Comparison of phenylalanine levels measured using two different methods (subject 5).**

Figure a – phenylalanine concentrations measured in all samples using the enzymatic assay, b – levels obtained through LC-MS analysis (average instrument response normalised to the first time point in the series). Error bars indicate standard deviation calculated from: a – duplicate reading, b – three technical replicates used for each sample.

The concentration of phenylalanine for subject 2 could not be calculated as the amount of the metabolite was not within the range of the standard curve. However, the average readings for this subject were also plotted on a graph in order to get an illustration of what the trend looked like and how it compared to what was measured using the LC-MS method. This is displayed in Figure 4-15.

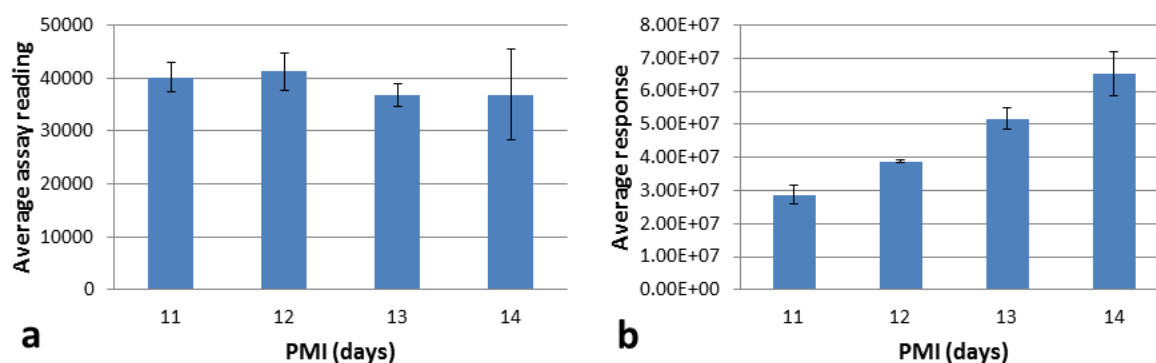


**Figure 4-15. Comparison of phenylalanine levels measured using two different methods (subject 2).**

**Figure a – average phenylalanine enzymatic assay reading for all of the samples (measured in duplicate), b – levels obtained through LC-MS analysis (average instrument response normalised to the first time point in the series). Error bars – standard deviation calculated from: a – duplicate reading, b – three technical replicates used for each sample.**

As in the case of subject 5, the trend emerging from phenylalanine levels measured using the assay is different than one seen from the LC-MS data (Figure 4-15). The latter displays a clear and steady increasing pattern, while the former does not seem to change at all. However, the phenylalanine responses for all of the samples tested for this subject are too saturated to measure its concentration and draw any valid conclusions.

#### 4.3.3.3 Other metabolites

The known decomposition products cadaverine, putrescine and indole, which showed promising changes in rat tissue did not show such changes in human tissue. In some cases they were not even detected at all. However, another decomposition product (skatole), was consistently identified in five out of the six tested subjects. Furthermore, it showed increasing patterns in 4 of them (with the exception of subject 1).

As in the case of rat tissue, a number of metabolites showed steady increasing patterns between the tested subjects (xanthine, choline phosphate, uracil, n-acetylneuraminic acid and 1-methylnicotinamide). General increasing patterns were

observed for all of the forementioned metabolites, for all of the tested cadavers, with the exception of subject 4. In the case of subject 4 only xanthine and skatole showed a slowly increasing pattern. However, in this case tissue collection was only possible at three time points and the cadaver was stored outdoors. N-acetylneuraminate showed the highest rate of increase over time for 5 out of the 6 subjects (with the exception of subject 3). Figure 4-16 shows the changes observed in the levels of these metabolites for all of the subjects. Additionally, since the PMIs of the investigated cadavers varied and were scattered from as little as 3 days post-mortem to 19 days after death, a general idea can be obtained of how these metabolites changed in levels throughout this period. They increased in all cases but subject 4, suggesting that these metabolites increase in level later in the post-mortem period (between 7 and 19 days post-mortem).

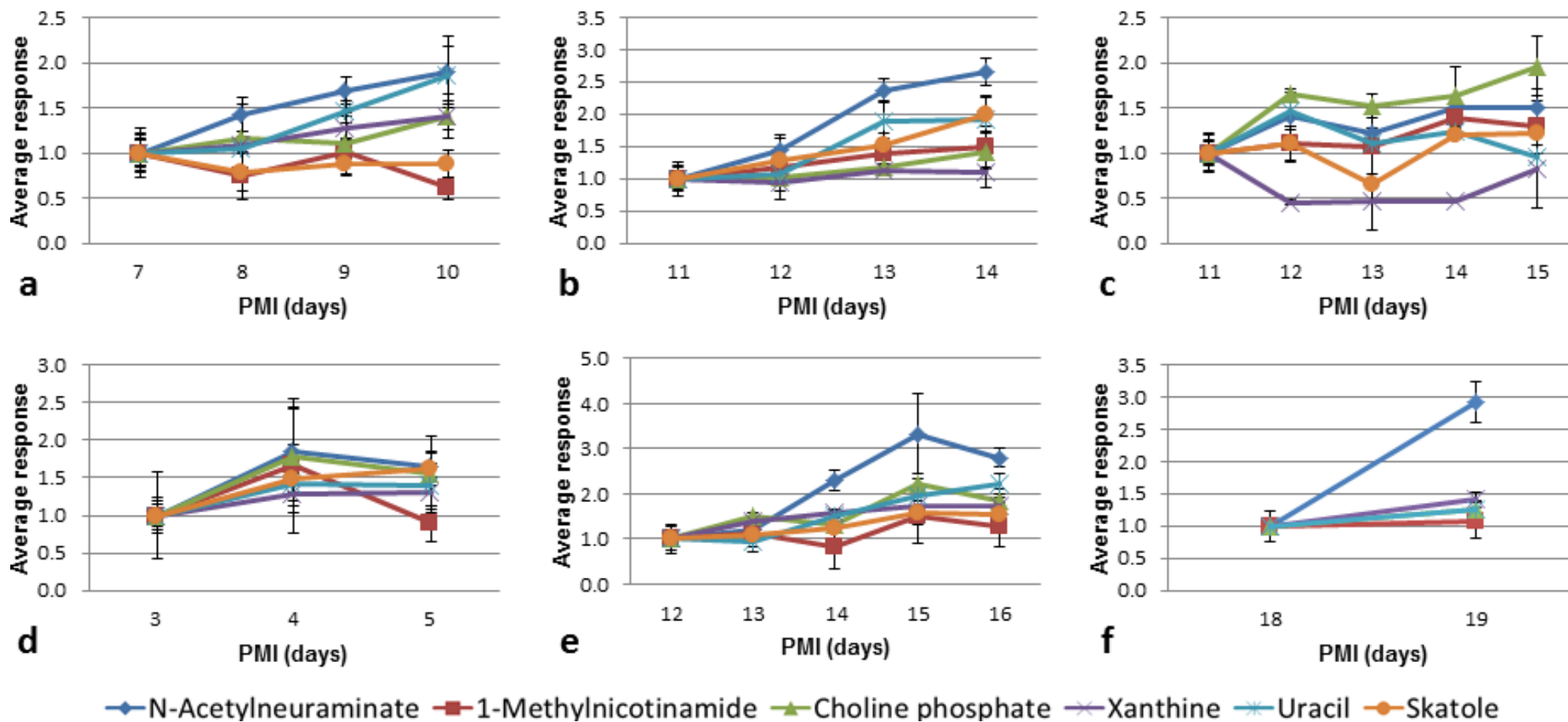


Figure 4-16. Graphs showing PMI changes in human cadavers of levels of metabolites of interest (n-acetylneuraminatate, 1-methylnicotinamide, choline phosphate, xanthine and uracil).

Data shown for all of the human cadavers tested: a – subject 1, b – subject 2, c – subject 3, d – subject 4, e – subject 5 and f – subject 6. Skatole was not detected in data collected for subject 6. Cadavers 4 and 6 were kept outdoors. Error bars indicate standard deviation calculated from average instrument response. The analysis included three technical replicates of each sample.

#### 4.3.4 PMI calculations

Post-mortem interval is most often reported as the amount of time which has passed since death. However, the ambient temperature at which the cadaver decomposes has a significant effect on the rate of decomposition. Therefore, the PMI calculation is sometimes corrected to include the temperature measurement. For example, Vass *et al.* reported PMI values in Cumulative Degree Hours (CDH) (Vass et al. 2002). To allow for comparison of the results presented in this thesis with existing literature, the PMIs of the subjects included in this study were also presented in CDH (see Table 4-5). CDH was calculated according to Vass *et al.* by using a 12 h temperature cycle to describe the advancement of the decomposition process. The temperature ( $^{\circ}\text{C}$ ) at 12 h intervals is averaged and cumulatively added to obtain CDH. For example, if the temp reached  $25^{\circ}\text{C}$  at 12 in the afternoon and  $15^{\circ}\text{C}$  at 12 at night, then the CDH for that 24 h period would equal to  $(25 + 15)/2 = 20$  for the first 12 h and then  $(15 + 25)/2 = 20$  for the following 12 h. This summarised  $(20 + 20)$  gives a CDH of 40. For human cadavers, calculations were based on the assumption that storage was at  $4^{\circ}\text{C}$  at the medical examiner's office prior to receipt at FACTS. At FACTS the temperature for the refrigerated cadavers was constant ( $45^{\circ}\text{F} \approx 7.2^{\circ}\text{C}$ ) and for the outdoor subjects the weather data was recorded. CDH for rats was included for the purpose of comparison with shorter PMIs. For the rodent model the temperature was controlled ( $20^{\circ}\text{C}$ ).

**Table 4-5. Sampling times for rat and human subjects included in this study as Post-Mortem Interval (PMI) and Cumulative Degree Hours (CDH).**

PMIs in days and their corresponding CDH values for all time points (calculated according to Vass *et al.* (Vass *et al.* 2002)). Subjects 1-6 refer to human individuals. Rats were stored at ambient temperature (20°C), human subjects 4 and 6 outdoors and others were refrigerated during the sampling period. X indicates that there were no more data points collected for this particular subject.

	Unit	Time point 1	Time point 2	Time point 3	Time point 4	Time point 5
Rats	PMI	0	1	2	3	X
	CDH	0	40.0	80.0	120.0	X
Subject 1	PMI	7	8	9	10	X
	CDH	81.6	96.0	110.4	124.8	X
Subject 2	PMI	11	12	13	14	X
	CDH	88.0	102.4	116.8	131.2	X
Subject 3	PMI	11	12	13	14	15
	CDH	107.2	121.6	136.0	150.4	164.8
Subject 4	PMI	3	4	5	X	X
	CDH	137.4	178.9	222.4	X	X
Subject 5	PMI	12	13	14	15	16
	CDH	108.8	123.2	137.6	152.0	166.4
Subject 6	PMI	18	19	X	X	X
	CDH	144.0	186.0	X	X	X

## 4.4 Discussion

This experiment aimed to discover potential metabolite biomarkers for PMI estimation. Beef steak was used as test sample to develop and optimise the methodology, followed by testing in rat and human cadavers. An untargeted metabolomics approach allowed the identification of a number of metabolites which showed potential as PMI biomarkers. Testing carried out using rat cadavers resulted in a number of putative markers, mainly proteogenic amino acids. Nearly all of the identified amino acids showed a steady rate of increase during the first 72 h after death. Protein degradation may explain many of the changes observed in this study. Since protein synthesis will cease in dead tissue, the pool of free amino acids does not deplete. The loss of homeostasis that accompanies death will rapidly compromise membrane functions that are actively maintained, leading to breakdown of cellular and subcellular compartmentalisation. The many proteases that are sequestered in living tissue will gain unregulated access to protein substrates and the resulting proteolysis will break down proteins into peptides and, ultimately, amino acids.

Well known decomposition products, cadaverine, putrescine, skatole and indole also showed promising patterns of change. The latter three compounds increased over time but cadaverine, surprisingly, decreased. It is possible that the decomposition was not sufficiently advanced for this particular polyamine to increase in level. Additionally, it is a metabolite of lysine, which showed one of the slowest rates of increase among the amino acids observed.

Five other metabolites were also identified as possible biomarkers: xanthine (purine base), uracil (pyrimidine found in RNA), choline phosphate (precursor of choline in glycerophospholipid metabolism), n-acetylneuraminic acid (otherwise known as sialic acid, derivative of amino sugar neuraminic acid) and 1-methylnicotinamide (metabolite of nicotinamide) (Wishart et al. 2013). Levels of these compounds increased with time since death. Xanthine is formed from hypoxanthine, which in turn can be formed from inosine. The level of inosine increased rapidly from a low level, within the first 24 hours post-mortem in rat tissue and started to fall after that. This coincided with a rapid increase in hypoxanthine and xanthine within the same time period, which might suggest that this pathway is still active for some time after death and that inosine is converted to hypoxanthine and xanthine. This was also observed in two other studies in porcine and avian vitreous humour (Gardiner et al. 1989) and rat and human brain (Kovács et al. 2005). Xanthine can also be formed through DNA degradation, i.e. guanine deamination (Lindahl 1993). However, this is a less likely scenario as guanine levels also show an increase in the collected data. DNA degradation can also be responsible for an increase in uracil levels, through cytosine deamination (Lindahl 1993). However, this reaction is alkali catalysed and the pH of a decaying body is more likely to be acidic. Additionally, the levels of cytosine also show an increase post-mortem; therefore, uracil formation is likely to be a result of a different pathway. For example, uridine monophosphate (UMP) leads to formation of uridine and uridine is converted to uracil, which could explain the uracil increase, as UMP levels decreased and uridine remained fairly constant.

The increase in levels of the three remaining compounds is a bit more difficult to explain. Choline phosphate is a precursor of choline, but it can also be formed from choline, through a reverse reaction catalysed by choline phosphokinase (Dawson 1955). However, this reaction requires ATP to proceed, which is absent

in dead tissue. Another pathway leading to the formation of choline phosphate is from phosphodimethyl ethanolamine, which was not detected in this study, so cannot be commented upon. N-acetylneuraminic acid (sialic acid) was suggested as an indicator of muscle damage (Iwata et al. 2013). Sialic acid is present in the sarcolemma of skeletal muscle (for a muscle composition diagram see chapter 1) and it was proposed that as a result of muscle damage cytosolic enzymes are released into the extracellular space. One of these enzymes, sialidase, removes sialic acid from the sarcolemma. It is possible that this process could occur post-mortem as enzymes are released from the decomposing muscle tissue. Finally, it was shown that 1-methylnicotinamide is involved in the regulation of NAD content in cells and at the same time, recovery of ATP (Hoshino et al. 1984). As ATP is being used up in dying cells, the 1-methylnicotinamide could be synthesised from nicotinamide as a compensation mechanism.

These findings were also tested using human tissue at various stages of decomposition, where subject selection, cause of death and ante- and post-mortem environment could not be controlled. Nonetheless, the data collected using human subjects broadly agrees with the data obtained from rats. The same compounds were identified in most of the cadavers, showing similar trends. The only exceptions were decomposition products - cadaverine, putrescine and indole did not show significant changes in human tissue, perhaps because microbial colonisation of the larger human skeletal muscles is delayed compared with rats. On the other hand, skatole, showed increasing trends in human tissue. Additionally, certain amino acids (especially histidine and lysine) showed comparable rates of increase between different rat and human subjects. The absolute levels of these molecules may vary, but given the same conditions (i.e. temperature at which the decomposition occurs), they follow similar decomposition trends. The cadavers were stored at the same temperature at the time of sampling. This provided a controlled environment which resulted in similarities in the decomposition rates of these individuals. Lysine, tyrosine and threonine show the most potential for becoming biomarkers among the three species.

Furthermore, since amino acids are among the candidates for biomarkers of PMI, the use of a commercial amino acid enzymatic assay for this purpose was put to the test. The optimisation of the sample preparation for the assay was slightly

problematic, as the levels of phenylalanine in muscle tissue were unknown, and they had to fit within a small range (0 - 1 nmole) of the standard curve. An appropriate sample dilution was experimentally tested; however, when two different subjects were tested the levels of only one of them were within the calibration range. Metabolite levels vary from person to person, which might make this approach impractical as these differences can be large and require the optimisation of the extraction protocol for each of the tested subjects. This hinders the ease and speed of use of the assay as a test method. Additionally, the trends resulting from the enzymatic assay measurements did not agree with the trends seen in the LC-MS data. The LC-MS data was not quantitative; however, a similar trend of increase should be expected. The mass spectrometry approach offers higher sensitivity and reproducibility than the enzymatic assay, hence more reliable results. However, it would be impractical to use MS as a method of PMI estimation. It was used for biomarker discovery, with the aim of finding a marker which can then be tested with a high throughput assay. Finally, the homogeneity of the sample could be an issue. It is very difficult to say if the same amount of phenylalanine is present in every part of the muscle. This cannot be controlled; however, in this case sample size would make a difference. The weight of tissue sample used for the assay is very small 20mg, as opposed to 0.5g used for the extraction for LC-MS analysis. To summarise, at this stage of the investigation, the commercially available amino acid assays do not seem suitable for the purpose of PMI estimation. Amino acids show a great potential as PMI markers, however, more time is required to develop this test using available assays or analysers.

Amino acids have previously been suggested as possible markers in PMI estimation. In agreement with this study, increasing levels of amino acids were reported in various post-mortem specimens: vitreous humour (Patrick & Logan 1988a; Girela et al. 2008), cerebrospinal fluid (Kärkelä & Scheinin 1992; Girela et al. 2008), blood (Donaldson & Lamont 2014; Sato et al. 2015) and brain (Ith et al. 2011). Perry *et al.* presented a post-mortem increase in levels of various amino acids in rat and human brain samples (up to 48 h after death) (Perry et al. 1981). The investigators described a rapid increase in levels of most of the proteogenic amino acids within 24-48 h post-mortem, with the exception of glutamate. The levels of this amino acid remained unchanged over the

investigated PMI, which is contrary to our findings, that glutamate levels increase post-mortem. This difference could be explained by the involvement of glutamate in metabolic synthesis of GABA (gamma-aminobutyric acid) in brain, which would cause its depletion. On the other hand, the hydrolysis of proteins and GSH (glutathione) would contribute to increasing levels which added together might leave the levels of glutamate unchanged overall. It is possible that the first pathway does not occur in muscle tissue, or at least not to the same extent as in brain, so protein hydrolysis would be the primary contributor to increasing glutamate levels measured in this study.

Vass *et al.* investigated various compounds in different post-mortem organs and tissues, including muscle tissue (Vass *et al.* 2002). Similar to our findings in human tissue, this group found the most commonly known decomposition products (cadaverine and putrescine) not to be suitable for time since death determination due to their variability. The authors describe various amino acids as good biomarker candidates. However, according to their findings, muscle tissue can only be used to determine PMI longer than 300CDH. To put this into context, subject 2 was sampled between 88 and 131.2 CDH (11-14days PM) and subject 3 107.2 and 164.8 CDH (11-15 days PM). This is contrary to our findings, as we found amino acids to be useful biomarkers at earlier PMIs. Additionally, we found lysine to be one of the most promising biomarker candidates, while Vass *et al.* did not find it a consistent indicator of time since death, in any of the analysed types of tissue.

To our knowledge, xanthine, uracil, choline phosphate, n-acetylneuraminate and 1-methylnicotinamide have not previously been suggested as possible PMI markers. Lendoiro *et al.* presented an LC-MS/MS method of PMI estimation based on the measurement of hypoxanthine levels in vitreous humour (Lendoiro *et al.* 2012). The method was also validated to quantify levels of xanthine, however, not as a potential marker. Another study by Kovacs *et al.* showed increasing levels of both xanthine and uracil during first 24 h post-mortem in rat and human brains (Kovács *et al.* 2005). These findings are in agreement with the data presented in this thesis. However, PMI determination was not the scope of their investigation.

Muscle tissue has rarely been the focus in PMI research; however, it has great potential as a forensic specimen. Superficial muscle tissue is very easy to collect and is less emotive than sampling of internal organs for the next of kin. Additionally, it is more stable post-mortem than other organs or body fluids. As demonstrated in this study, it can be easily applied in PMI investigations. Various compounds show a steady increase over time, with threonine, tyrosine and lysine showing the most potential. However, more work is required to validate these results. The next step would be to apply targeted analysis in a larger cohort of subjects to test the selected metabolites. Quantification of the levels of these compounds would allow for a thorough statistical evaluation of the data and possibly a mathematical model for the estimation of PMI in muscle tissue. Importantly, instrumentation and workflows for the quantification of amino acids in samples are well developed and are ubiquitous in clinical biochemistry laboratories.

## **4.5 Conclusion**

The complexity of the decomposition process makes the PMI estimation difficult. This study demonstrates how the newly emerging field of metabolomics can advance this area of forensic research. In agreement with previous studies, we found a positive correlation between the levels of proteogenic amino acids and increasing time since death. Additionally, we discovered six new metabolites of interest in PMI investigation. Lysine, threonine and tyrosine show the most potential to become PMI markers in muscle tissue, however, more time and testing is required to develop these markers further.

## 5 METABOLOMICS (GC-MS)

### 5.1 Introduction

Gas-chromatography (GC) coupled with mass spectrometry is a tool growing increasingly popular in the field of metabolomics. It might not be chosen as often as LC-MS, as it is limited to the detection of volatile compounds and non-volatile metabolites must thus be derivatised prior to GC analysis. However, when analysing low molecular weight compounds, GC-MS is highly sensitive, efficient, reproducible and quantitative. Additionally, it is capable of obtaining highly reproducible compound fragmentation patterns which allows building comprehensive reference libraries for compound identification, that can be used by different laboratories (Garcia & Barbas 2011).

The objective of an untargeted metabolomics approach is to create a detailed metabolic profile of an organism, as well as giving the opportunity to find any changes and differences on a molecular level, when the state of that organism changes for any reason (i.e. disease state). The versatility of this approach can be used in various areas of research - food, nutrition, systems biology, drug discovery and mode of action (Lee et al. 2016; Petersson et al. 2015; Zhang et al. 2015), but most frequently it is used to discover new biomarkers, both diagnostic and prognostic (Surowiec et al. 2015; Yi et al. 2006; Jiye et al. 2005; Kloet et al. 2012; Kenny et al. 2005; Wu et al. 2011). GC-MS is a perfect tool for this task, however, best results are obtained when orthogonal approaches are used to complement each other (Fanos et al. 2014). Therefore, this chapter describes how the GC-MS metabolic profiling approach has been successfully applied in PMI biomarker research and how two different approaches (LC-MS and GC-MS) can be used together to get a better insight into biological processes occurring after death.

Metabolic markers of PMI previously presented in the literature have been discussed in the previous chapter (chapter 4). The most relevant publications will be presented in the discussion section of this chapter.

## 5.2 Methodology

Sample derivatisation and analysis using GC-MS was carried out by Stefan Weidt, mass spectrometry technologist at Glasgow Polyomics - rat tissue at the Thermo facility in Runcorn, UK and human tissue at Glasgow Polyomics. In both cases the Trace 1310 gas chromatograph coupled with a QExactive-GC mass spectrometer (Thermo Scientific) was used. Sample preparation, analysis and instrumentation used were described in Chapter 2. Sample collection, extraction and the processing of the collected GC-MS data was carried out by the author of this thesis.

### 5.2.1 Peak identification, average response calculation and presentation for relative quantification

Raw MS-data was processed using Trace Finder 4.0 software (Thermo Fisher). The software compiled a list of detected peaks for each of the study groups (rat, human - each subject separately) and also matched the detected peaks against compounds present in the reference library (NIST - The National Institute of Standards and Technology). Peaks of interest were selected based on the graphical representation of the change in the level of the compound over time. Unidentified compounds or those with an unlikely library match were not considered. As the software did not calculate the error associated with these levels, a list of response areas for all samples for each peak of interest was obtained from the software. Samples collected at each time point were analysed in three technical replicates. Therefore the mean and standard deviation of the area response were calculated for each time point. Finally, the average values for all time points were normalised to time point 0, to compare how much each of the samples differ from time 0 and each other (fold change). All of these calculations were carried out in Microsoft Excel, where the graphs representing the data were also created. These were obtained by plotting the average response (either normalised or not, as required) against time, including the associated error with each sample ( $\pm$  standard deviation). The spreadsheets with the above calculations are attached in Appendices XXI and XXII for rat and human samples, respectively.

## 5.3 Results

Gas chromatography-mass spectrometry was used to test two out of three species included in this study, rat and human. Beef tissue, used for method development in case of LC-MS analysis, was not subjected to GC-MS analysis, in order to focus the remaining period of the project on sample sets which showed promising results in the LC-MS analysis. A number of metabolites of interest were detected in both cases, however, unlike LC-MS results, the list of selected compounds differed slightly between species. Certain compounds, i.e. proteogenic amino acids were highlighted in both the LC and GC-MS parts of the study. Also, the GC-MS analysis revealed a few additional compounds of interest, including non-proteogenic amino acids as well as compounds involved in the purine and pyrimidine pathways.

### 5.3.1 Rat tissue

Biceps femoris muscle was collected from 8 rats, two at a time, over a period of 4 days (time 0 - right after death, 24 h, 48 h and 72 h after death). Muscle tissue was extracted, derivatised and analysed using an untargeted GC-MS approach. The data collected yielded 22 metabolites of interest, which are presented in Table 5-1. 901 peaks were detected in total, across 4 time points and 148 of these peaks were putatively identified. However, these included ambiguous identifications, where the matched compound was not silylated. Given that the samples were derivatised before analysis, the detected compounds of interest should occur in a silylated form (addition of one or more  $\text{Si}(\text{CH}_3)_3$  groups). This reduced the number of possible compounds of interest further. The final criterion for a metabolite of interest was increasing or decreasing abundance over the investigated PMI. Based on this, 22 compounds were selected as possible biomarker candidates. These included 17 amino acids, 13 proteogenic and 4 non-proteogenic, and hexanoic acid (carboxylic acid), uracil (pyrimidine metabolism), hypoxanthine, adenine (purine metabolism) and glucosamine (carbohydrate metabolism).

**Table 5-1. List of metabolites of interest as PMI biomarkers selected in rat tissue.**

**Peak ID** – identifier given to each peak by the software, **RT** – retention time, **Monoisotopic mass** – fragment masses used to identify the compound, **NIST (The National Institute of Standards and Technology)** – mass spectral reference library used to identify the peaks. The compounds present in the sample were silylated prior to analysis, which is represented in the elemental composition, although omitted from the compound name.

Peak ID	RT (min)	Monoisotopic Mass	NIST	Elemental Composition
peak @ 6.22 173.10	6.22	173.099289	Hexanoic acid	C <sub>9</sub> H <sub>20</sub> O <sub>2</sub> Si
peak @ 8.35 218.10	8.35	218.10289	L-Tryptophan	C <sub>17</sub> H <sub>28</sub> N <sub>2</sub> O <sub>2</sub> Si <sub>2</sub>
peak @ 9.16 158.14	9.16	158.136017	L-Leucine	C <sub>12</sub> H <sub>29</sub> NO <sub>2</sub> Si <sub>2</sub>
peak @ 9.46 158.14	9.46	158.136017	L-Isoleucine	C <sub>12</sub> H <sub>29</sub> NO <sub>2</sub> Si <sub>2</sub>
peak @ 10.03 241.08	10.03	241.08226	Uracil	C <sub>10</sub> H <sub>20</sub> N <sub>2</sub> O <sub>2</sub> Si <sub>2</sub>
peak @ 10.36 204.12	10.36	204.123459	Serine	C <sub>12</sub> H <sub>31</sub> NO <sub>3</sub> Si <sub>3</sub>
peak @ 10.70 218.14	10.70	218.138794	Cystathionine	C <sub>19</sub> H <sub>46</sub> N <sub>2</sub> O <sub>4</sub> SSi <sub>4</sub>
peak @ 11.20 160.08	11.20	160.078812	L-Aspartate	C <sub>10</sub> H <sub>23</sub> NO <sub>4</sub> Si <sub>2</sub>
peak @ 11.26 248.13	11.26	248.13182	Alanine	C <sub>12</sub> H <sub>31</sub> NO <sub>2</sub> Si <sub>3</sub>
peak @ 12.40 176.09	12.40	176.092484	L-Methionine	C <sub>11</sub> H <sub>27</sub> NO <sub>2</sub> SSi <sub>2</sub>
peak @ 12.85 220.10	12.85	220.100769	L-Cysteine	C <sub>12</sub> H <sub>31</sub> NO <sub>2</sub> SSi <sub>3</sub>
peak @ 13.61 246.13	13.61	246.134262	L-Glutamate	C <sub>10</sub> H <sub>24</sub> O <sub>2</sub> NSi <sub>2</sub>
peak @ 13.69 218.10	13.69	218.103378	L-Phenylalanine	C <sub>15</sub> H <sub>27</sub> NO <sub>2</sub> Si <sub>2</sub>
peak @ 14.11 234.12	14.11	234.116287	Homocysteine	C <sub>13</sub> H <sub>33</sub> NO <sub>2</sub> SSi <sub>3</sub>
peak @ 14.17 188.09	14.17	188.092194	Asparagine	C <sub>13</sub> H <sub>32</sub> N <sub>2</sub> O <sub>3</sub> Si <sub>3</sub>
peak @ 15.65 265.09	15.65	265.093567	Hypoxanthine	C <sub>11</sub> H <sub>20</sub> N <sub>4</sub> O <sub>2</sub> Si <sub>2</sub>
peak @ 16.17 174.11	16.17	174.11293	N-Acetyl-L-Lysine	C <sub>17</sub> H <sub>40</sub> N <sub>2</sub> O <sub>3</sub> Si <sub>3</sub>
peak @ 16.23 218.10	16.23	218.102722	L-3-Methylhistidine	C <sub>13</sub> H <sub>27</sub> N <sub>3</sub> O <sub>2</sub> Si <sub>2</sub>
peak @ 16.31 264.11	16.31	264.109619	Adenine	C <sub>11</sub> H <sub>21</sub> N <sub>5</sub> Si <sub>2</sub>
peak @ 16.83 203.12	16.83	203.115646	Glucosamine	C <sub>24</sub> H <sub>61</sub> NO <sub>5</sub> Si <sub>6</sub>
peak @ 16.88 156.12	16.88	156.120346	L-Lysine	C <sub>18</sub> H <sub>46</sub> N <sub>2</sub> O <sub>2</sub> Si <sub>4</sub>
peak @ 17.04 218.10	17.04	218.103378	L-Tyrosine	C <sub>18</sub> H <sub>35</sub> NO <sub>3</sub> Si <sub>3</sub>

The samples were collected at early PMIs, at relatively short intervals of 24 h apart. However, the post-mortem changes occurring in the tissue samples could be seen simply by the comparison of total ion chromatograms (TICs) of samples collected at different time points. The TIC is a chromatogram which contains of all of the GC peaks detected in the sample. Figure 5-1 displays four TICs, each from one of the samples collected at each of the four time points, arranged with increasing PMI for the purpose of comparison.

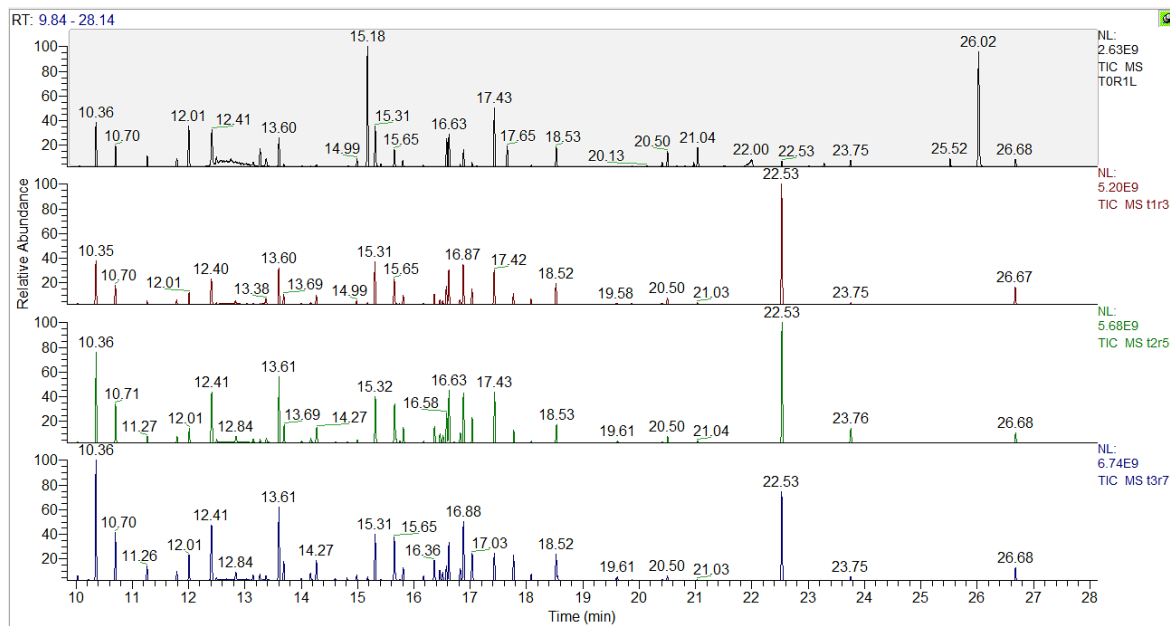


**Figure 5-1. Comparison of TICs obtained from analysis of rat tissue samples collected at each time point.**

**TIC – total ion chromatogram. Starting from the top of the image, first chromatogram corresponds to sample collected at time 0, second chromatogram corresponds to sample collected at day 1, third and fourth correspond to days 2 and 3, respectively. Sections between 10 to 28 min of the chromatograms are shown, with the highest abundance of peaks. Total run time was 36 min. Four samples were collected and analysed for each time point, chromatograms for only one out of four are displayed. Samples were analysed in full scan mode. Top chromatogram is greyed out as it was selected at the time when the screen shot was taken. This image was created using Xcalibur Qual Browser (Thermo).**

Clear differences can be seen between the chromatograms in Figure 5-1. Certain peaks became more intense with increasing PMI and others became less intense or even disappeared. This is highlighted further, using a shorter run time interval to make the differences clearer, in Figure 5-2. The abundances between the replicates of each sample differed slightly, with varying degrees of variation between time points. The coefficient of variation (%CV), which is a measure of the degree of variability with respect to the average of the data set, varied from 0.06 to 0.53 for the relative abundance of the peaks. However, even considering the variance between the replicates, still a general increase was observed across the time points. The peaks of interest presented in Figure 5-2 were submitted to the NIST mass spectral reference library for identification. The compounds were matched to glycine, serine, threonine, thiourea, oxo-proline, glutamate and lysine, with most of the peaks increasing in intensity over time.

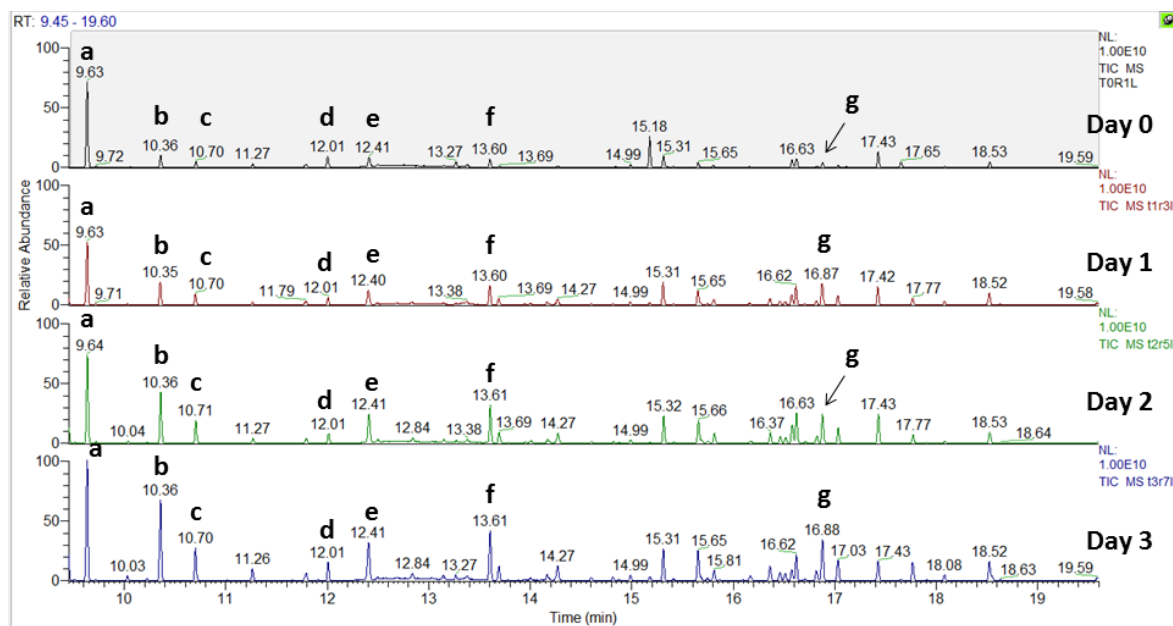


**Figure 5-2. Comparison of selected peaks in the TIC's of samples collected at each time point (rat tissue).**

TIC – total ion chromatogram. Chromatograms were labelled with their corresponding time points on the right-hand side of each chromatogram. Sections between 9.5 and 20 min of the chromatograms are shown to highlight peaks of interest. Total run time was 36 min. The highlighted peaks correspond to the following compounds (matched in the NIST database): a – glycine, b – serine, c – cystathionine, d – thiourea, e – methionine, f – glutamate, g – lysine. Four samples were collected and analysed for each time point, chromatograms for only one out of four are displayed. Samples were analysed in full scan mode. Top chromatogram is greyed out as it was selected at the time when the screen shot was taken. This image was created using Xcalibur Qual Browser (Thermo).

Some of the peaks highlighted in Figure 5-2 were later included in the list of compounds of interest in Table 5-1. Not all of the peaks discussed above were included in this list as the final list was created based on the results obtained from the data processed with the TraceFinder software. Glycine (RT 9.63) and thiourea (RT 12.01) were not incorporated in the final list.

### 5.3.1.1 Amino acids

Amino acids comprised the majority (17 out of 22) of the metabolites of interest. Thirteen of them were proteogenic amino acids, which were highlighted as compounds of interest through LC-MS analysis (Chapter 4). Figure 5-3 shows the detected changes of these thirteen compounds with increasing PMI. Apart from the listed compounds, glutamine was also detected, but did not show a clear trend with PMI. The remaining 6 proteogenic amino acids were not detected, however, the GC analysis allowed separation of two isomers, leucine and isoleucine, which was not possible with the LC-MS method used.

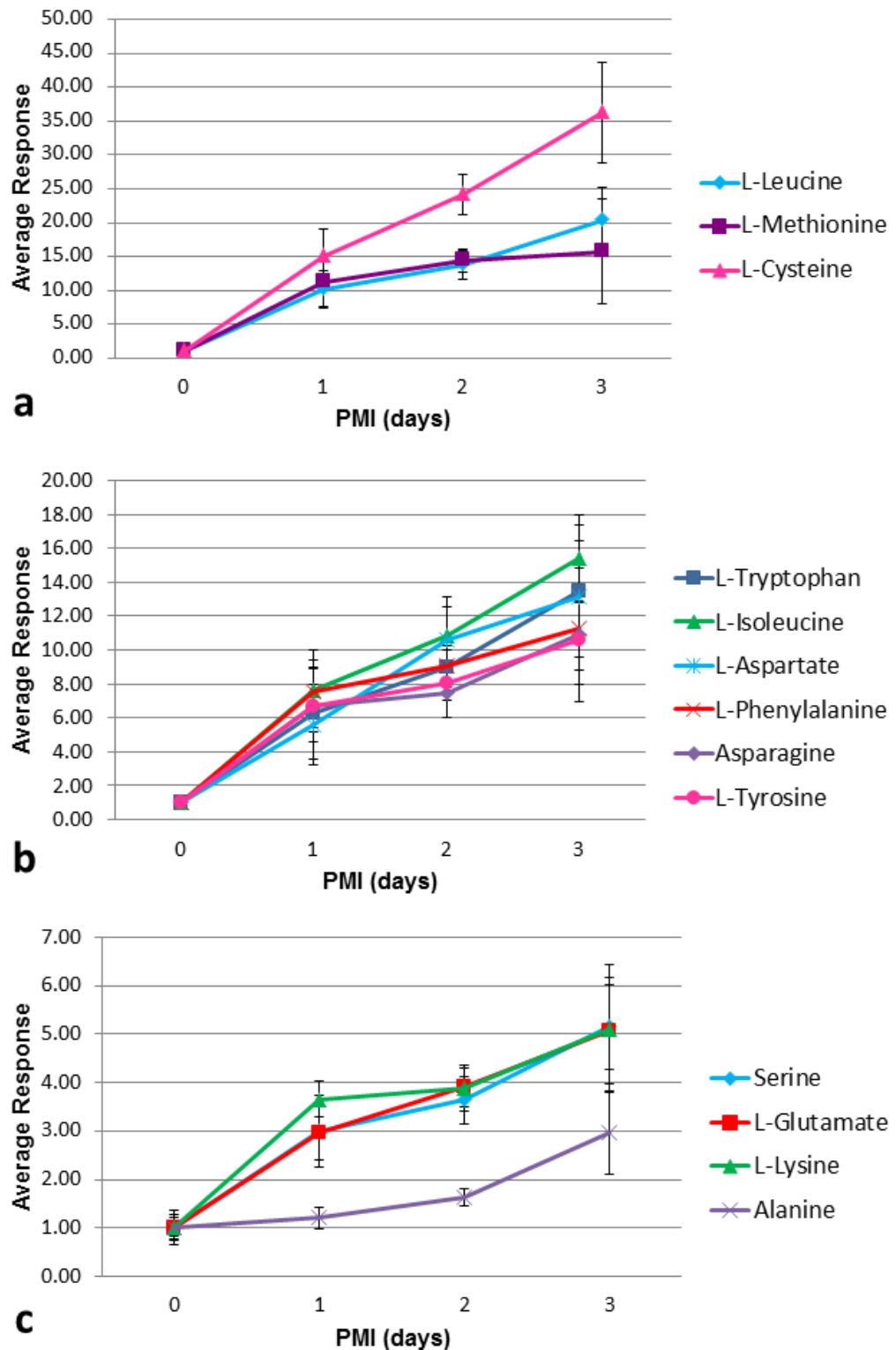


**Figure 5-3.** Change in levels of thirteen proteogenic amino acids with increasing time since death in rat tissue.

Graph a shows changes in levels of leucine, methionine and cysteine. Graph b shows tryptophan, isoleucine, aspartate, phenylalanine, asparagine and tyrosine. Graph c shows serine, glutamate, lysine and alanine. Average instrument response (arbitrary units) was normalised to time 0 and plotted against time. Error bars indicate standard deviation calculated from average instrument response. Two rats were analysed per time point, both right and left leg being sampled for each rat (N=4).

Cysteine displayed the highest rate of increase of about 36-fold, followed by leucine at 20-fold. The majority of the amino acids (methionine, tryptophan,

isoleucine, aspartate, phenylalanine, asparagine and tyrosine) increased between 10- and 15-fold. Serine, glutamate and lysine all increased by about 5-fold, with alanine showing the smallest increase of around 3-fold.

Most of the amino acids listed above were already highlighted as compounds of interest through the LC-MS experiment, with two exceptions. First, isoleucine and leucine were not discriminated by liquid chromatography. Second, alanine did not show a clear pattern of change with PMI in LC-MS analysis. Surprisingly, it showed a clear increasing pattern over time in the results of this experiment. The changes observed for this compound using the two different chromatography methods are compared in Figure 5-4.

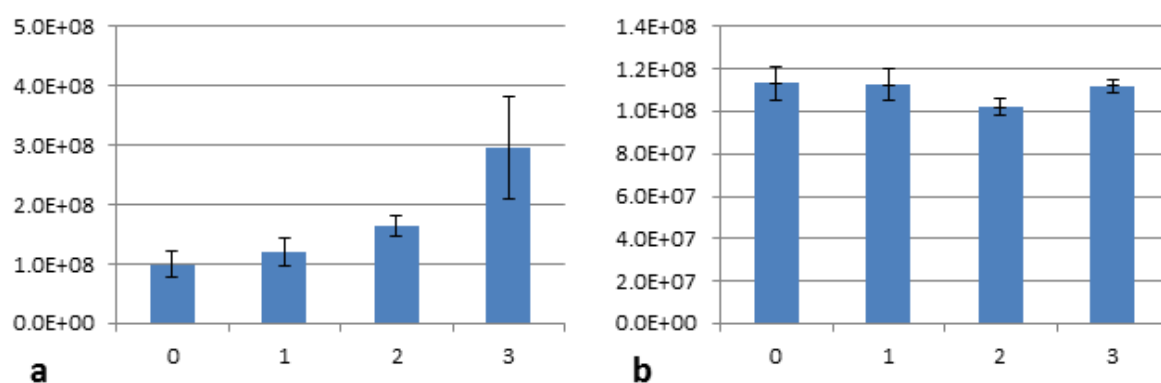


**Figure 5-4. Change in levels of Alanine detected using two different methods, GC-MS (a) and LC-MS (b).**

Alanine was one of the metabolites of interest detected in rat tissue via GC-MS. Here, results of GC-MS analysis are compared with those obtained by LC-MS analysis of the same tissue extracts. Y-axes represent average instrument response (N=4), x-axes show time since death (days). Error bars indicate standard deviation calculated from average instrument response.

Additionally, four other, non-proteogenic amino acids were selected as metabolites of interest, cystathionine, homocysteine, n-acetyl-L-lysine and L-3-methylhistidine. Cystathionine and homocysteine are involved in cysteine synthesis from serine (Kanehisa 1995). N-acetyl-lysine is an acetylated form of lysine and is a common post-translational modification of intact proteins. 3-Methylhistidine is produced as a result of methylation of actin and myosin, two of the main building blocks of muscle tissue (Wishart et al. 2013). The trends of change observed for these compounds are presented in Figure 5-5. All of their levels increase over time by approximately 5-fold. The LC-MS results for these compounds can be seen in Figure 5-6.

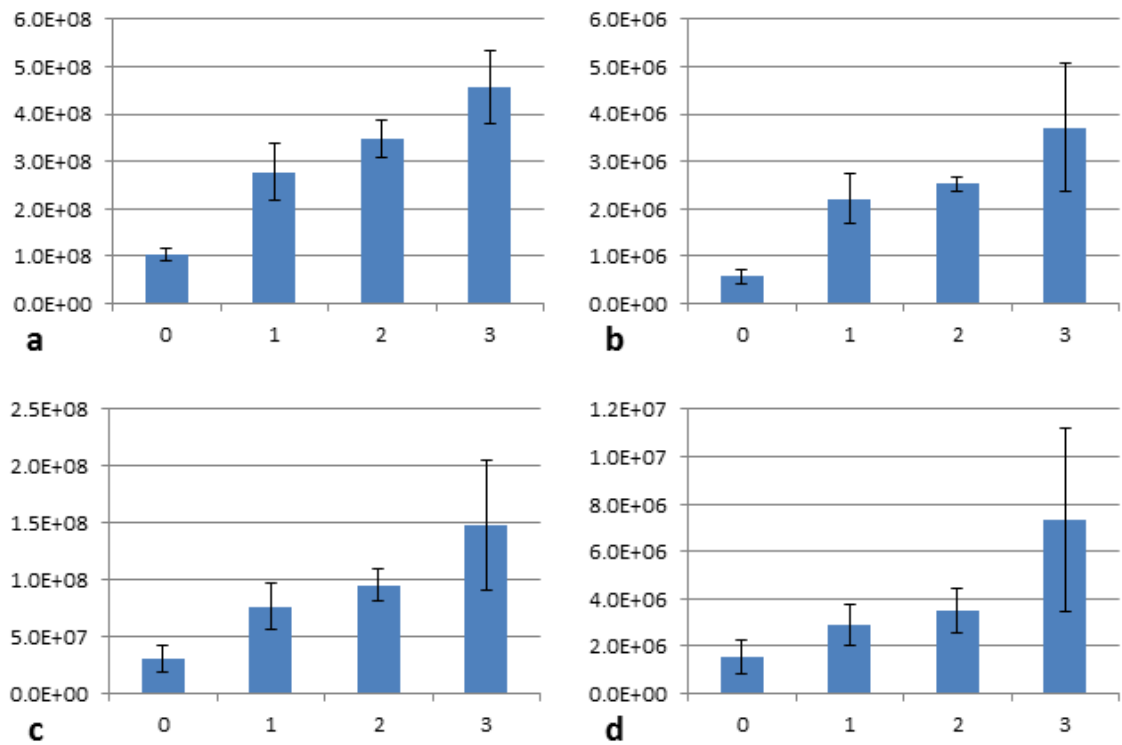


**Figure 5-5. Change in levels of non-proteogenic amino acids of interest with increasing time since death in rat tissue. Graphs show the mean instrument response (N = 4) with error bars to indicate the standard deviation: a – cystathionine, b – homocysteine, c – N-acetyl-L-lysine and d – L-3-methylhistidine, detected using GC-MS. Y-axes represent instrument response, x-axes show days since death.**

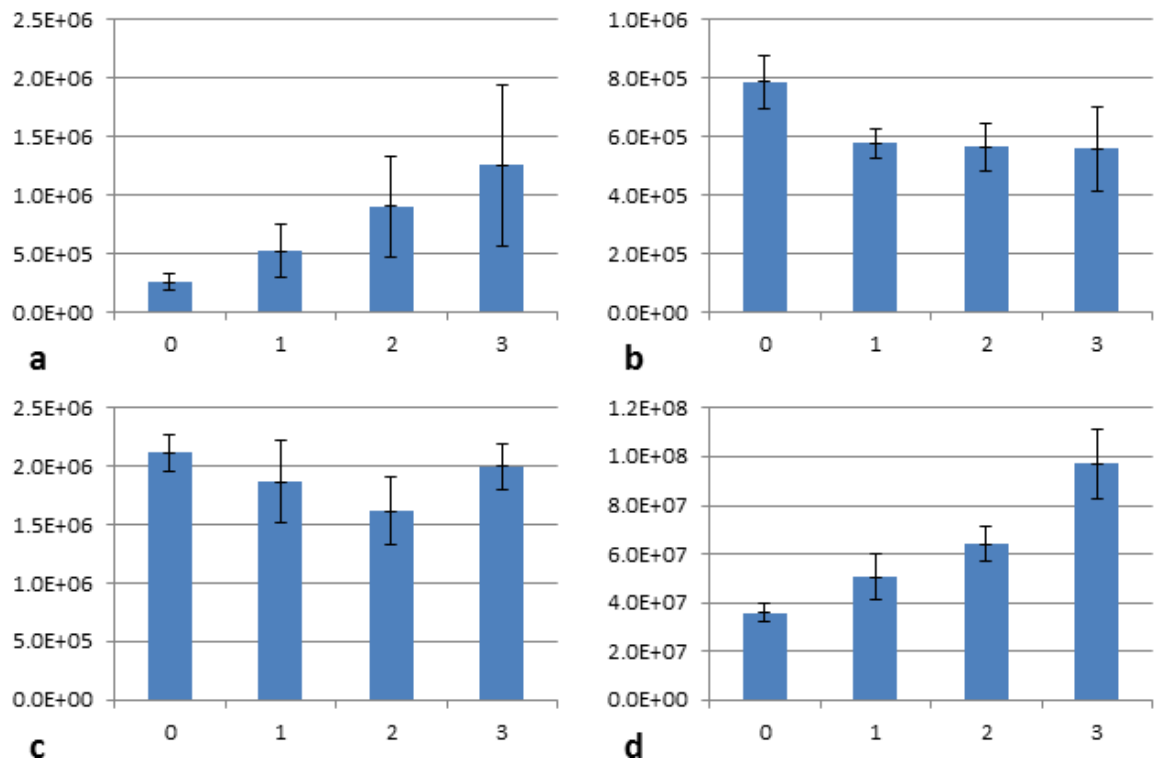


**Figure 5-6. Non-proteogenic amino acids of interest compared with LC-MS results. Compounds detected in the GC-MS analysis were also found in the LC-MS analysis and presented here for comparison. The above graphs represent: a – cystathionine, b – homocysteine, c – N-acetyl-L-lysine, d – L-3-methylhistidine detected using LC-MS. Y-axes represent average instrument response (N=4), x-axes show time since death (days). Error bars indicate standard deviation calculated from average instrument response.**

Unlike the proteogenic amino acids, the compounds shown in Figure 5-5 did not present themselves as metabolites of interest in the LC-MS analysis. For the purpose of comparison, the list of metabolites detected in the LC-MS analysis was searched for these compounds. They were also detected using the other method, however the results differed slightly. In the LC-MS data cystathionine and 3-methylhistidine also show steadily increasing trends. However, homocysteine and N-acetyl-lysine do not show much change over the investigated period, which disagrees with the GC-MS data.

### **5.3.1.2 Other metabolites**

The GC-MS approach not only confirmed that amino acids are strong PMI biomarker candidates, but also allowed the identification of several additional prospective markers. Five other metabolites, hexanoic acid (carboxylic acid, otherwise known as caproic acid (Wishart et al. 2013)), uracil (pyrimidine metabolism), glucosamine (carbohydrate metabolism), hypoxanthine and adenine (purine metabolism), also showed promising changes with increasing PMI. The first four of the aforementioned compounds showed an increasing trend over time (see Figure 5-7), while adenine decreased (see Figure 5-8). This compound also showed the smallest rate of change, as its level only decreased by about half over the investigated time period. Glucosamine showed the highest rate of increase of about 43-fold. The level of uracil increased about 18-fold, followed by hypoxanthine with about 12-fold increase. Hexanoic acid showed the slowest rate of increase among all of the metabolites of interest of about 2.5 fold. Uracil was also highlighted as a possible marker in the LC-MS data.

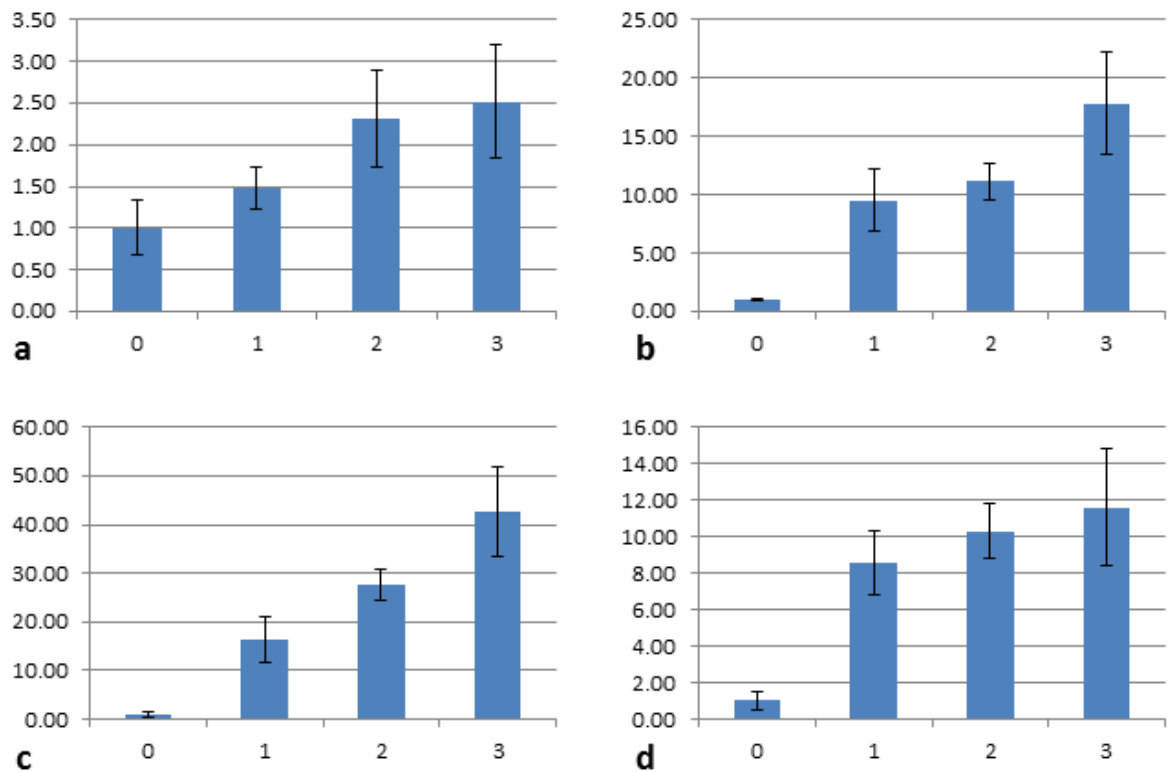


**Figure 5-7. Metabolites that increased in rat tissue with increasing PMI.** Graphs represent: a – hexanoic acid, b – uracil, c – glucosamine, d – hypoxanthine. Y-axes represent average instrument response (N=4), x-axes show time since death (days). Error bars indicate standard deviation calculated from average instrument response.

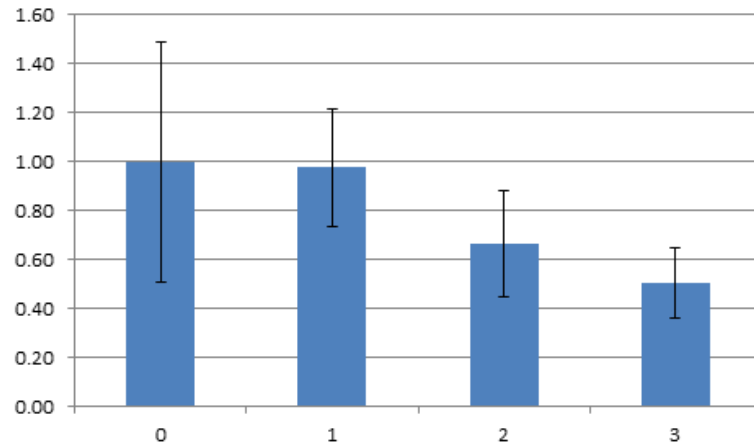


**Figure 5-8. Adenine showed a decreasing trend in rat tissue with increasing PMI.** Graph shows a mean instrument response (N = 4) with error bars to indicate the standard deviation. Data collected using GC-MS. Y-axes represent instrument response, x-axes show days since death.

Again, the data obtained through the GC-MS approach was compared with the LC-MS as all but one of the compounds (uracil) were not previously highlighted as possible markers. Figure 5-9 shows a comparison between the trends of change of uracil, hexanoic acid, hypoxanthine and adenine through both approaches. Glucosamine was not included as the LC-MS results for this compound were inconclusive, both increasing and decreasing trends were

observed. The other four compounds of interest, presented in Figure 5-9 show very similar, if not identical trends.

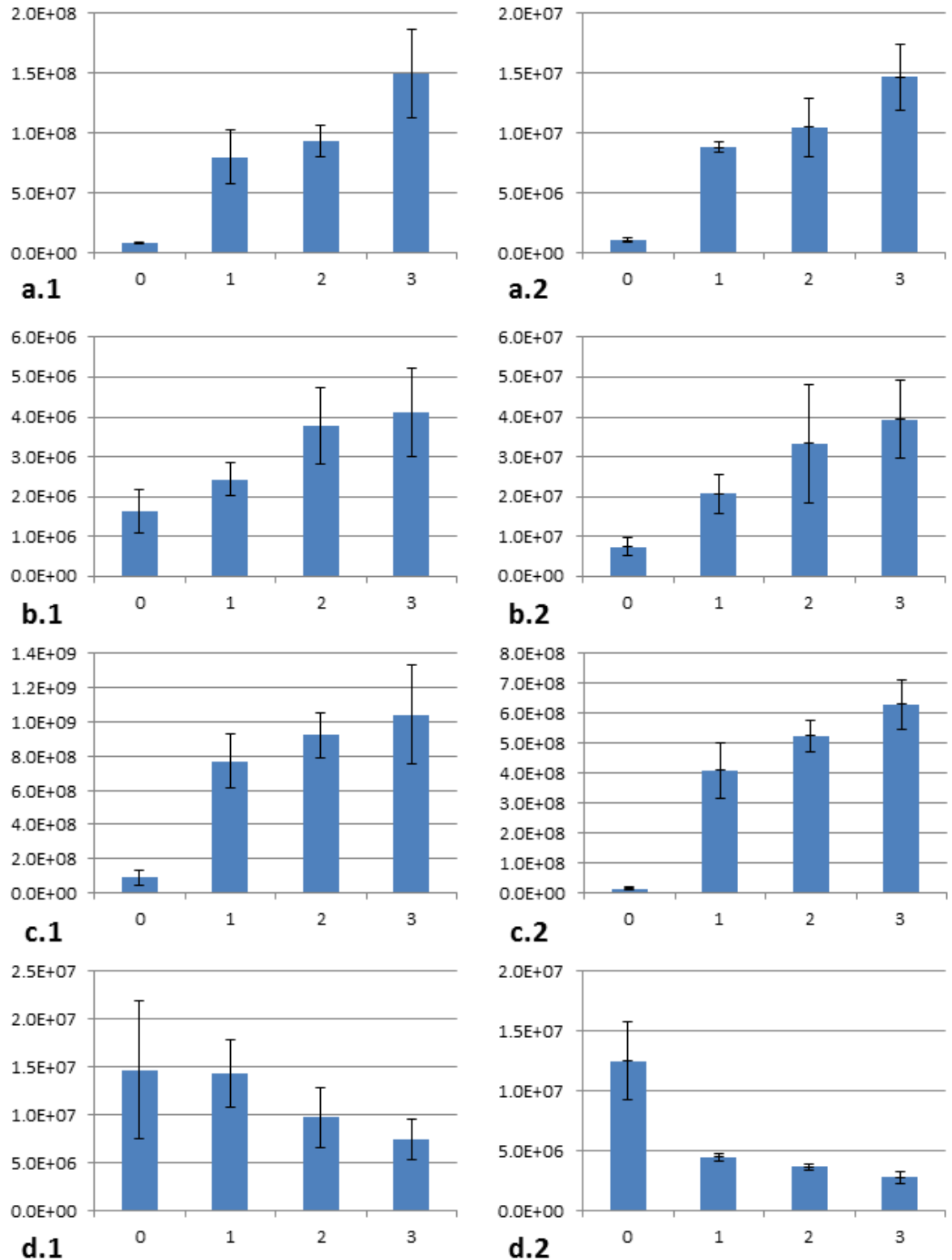


**Figure 5-9. Comparison of changes in metabolites of interest based on GC-MS and LC-MS results.**

Compounds detected in the GC-MS analysis (indicated by .1) were also found in the LC-MS analysis and presented here for comparison (indicated by .2). The above graphs represent: a – uracil, b – hexanoic acid, c – hypoxanthine, d – adenine. Y-axes represent average instrument response (N=4), x-axes show time since death (days). Error bars indicate standard deviation calculated from average instrument response.

### 5.3.2 Human tissue

Aliquots of human tissue samples, previously extracted for LC-MS analysis (Chapter 4), were derivatised and analysed at Glasgow Polyomics. However, human samples were analysed using a newly set up GC-MS instrument (Q Exactive GC system, Thermo Scientific). Initially, samples collected from subjects 2, 3 and 5 were analysed as a test (referred to as batch 1). These subjects were selected as the cadavers were kept at the same temperature and their PMIs were overlapping. Samples collected from subjects 4 and 6 (stored outdoors, referred to as batch 2) were run separately on a different occasion, after further method improvements. Samples collected from subject 1 were not analysed in this study. Additionally, apart from the tissue extracts, a mixture of various amino acids (see Chapter 2) at different concentrations was analysed within the two batches. This was carried out in order to create a calibration curve, which would enable absolute quantification of the amino acids detected in the test samples. An internal standard was added to all of the samples and calibrators to make this possible (the method is described in detail in Chapter 2). However, when the internal standard is not considered, relative quantification can also be carried out. Both relative and absolute quantifications of this data will be discussed in separate sections below.

#### 5.3.2.1 Relative quantification

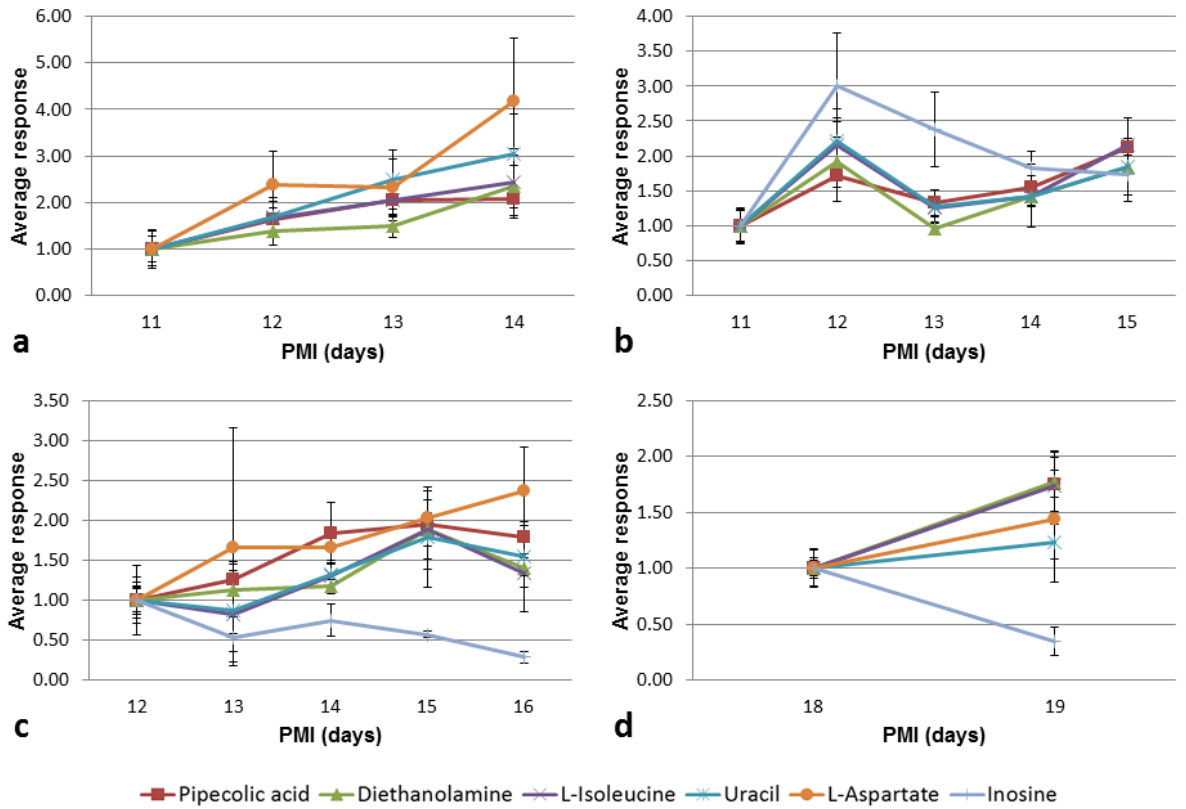
Data was collected for 5 out of 6 human subjects included in this study. Data collected for each individual was processed separately. The average response, fold changes across the time courses and standard deviations were calculated as described in section 5.2.1 of this chapter. The selection criteria applied to choose metabolites of interest were the same as in the case of rat tissue (compounds showing a clear trend of change over time, which were matched through the NIST library search to a likely match in a silylated form). A separate list of compounds of interest was created for each of the subjects. The list for subject 2 was created first and contained 19 metabolites of interest. The subsequent lists for the other subjects contained smaller numbers of possible markers, but also highlighted some additional markers not observed in subject 2. Selected compounds did not always show the same trends between subjects and in some cases, the peaks detected in one subject were not detected in the

others. To obtain a clearer view of any changes that were consistent across all of the tested subjects, the lists were combined into a colour coded chart in Table 5-2. Twenty four metabolites were selected and are presented in Table 5-2. Among them, there are 16 amino acids, of which 13 are proteogenic. The remaining seven compounds are pipercolic acid (metabolite of lysine), diethanolamine (otherwise DEA, organic chemical compound), uracil (pyrimidine metabolism), malic acid (TCA cycle intermediate), glycerate-3-phosphate (glycolysis intermediate), benzoic acid (carboxylic acid), hypoxanthine and inosine (purine metabolism) (Wishart et al. 2013). Table 5-2 shows how each of the compounds behaved for each of the subjects. Compounds which increased with PMI were labelled with blue and those which decreased with green. Darker shades of these two colours were used if the peak ID did not match the listed compound in the subject. A purple colour was used if the metabolite level remained constant. A yellow colour indicates that the peak did not show any particular trend with time and red if the peak was not detected in a subject. Ideally, it is desirable to see compounds which increased or decreased in all of the tested subjects (i.e. blue or green colour all across the table). This can be observed for one of the selected compounds, diethanolamine. Another four compounds were very close to this result, showing similar trends for 4 out of 5 tested subjects. These were pipercolic acid, isoleucine, uracil and aspartate. Another compound worth pointing out is inosine, the only metabolite that showed a decreasing trend in 3 out of 5 subjects. These top 6 metabolites of interest are displayed in Figure 5-10, which shows their change over time for subjects 2, 3, 5 and 6. Subject 4 was not included in this figure, as only two out of the top 6 compounds (diethanolamine and aspartate) showed a steadily increasing trend in this subject. These two compounds can be seen in Figure 5-11. Additionally, only 4 out of the 24 metabolites of interest detected in human tissue showed any consistent trend for subject 4 (diethanolamine, aspartate, 5-oxo-proline and glycerate-3-phosphate). On the other hand, in the case of subjects 2 and 6, promising patterns of change were shown by 19 and 20 out of the 24 selected biomarker candidates, respectively (see Table 5-2).

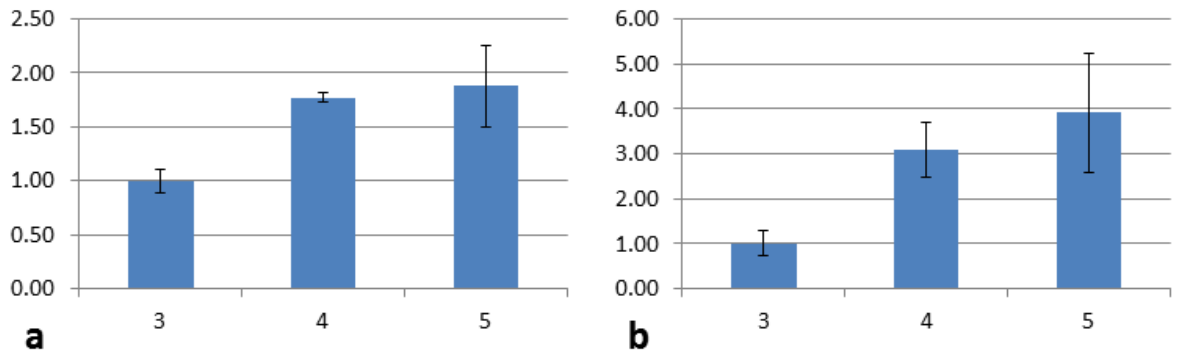
**Table 5-2. Metabolites of interest selected in human tissue.**

Table shows a list of selected metabolites and how their levels change over time in all of the tested subjects. Colours indicate the type of change observed, darker shades of colours indicate that the peak ID did not match the listed compound i.e. light and dark blue colour indicate an increasing pattern, but ID differs for dark blue. Same applies to green, indicating a decrease. Yellow – no clear pattern was observed, purple – level did not change and red – peak was not detected. Peak ID – identifier assigned by the software, RT – retention time, NIST – mass spectral library used to identify peaks. The compounds present in the sample were silylated prior to analysis, which is represented in the elemental composition, although omitted from the compound name.

Peak ID	RT (min)	Monoisotopic Mass	NIST	Elemental Composition	Subject 2	Subject 3	Subject 4	Subject 5	Subject 6
peak @ 6.90 158.14	6.90	158.135788	L-Leucine	C <sub>12</sub> H <sub>29</sub> NO <sub>2</sub> Si <sub>2</sub>					
peak @ 7.34 156.08	7.34	156.083969	Pipecolic acid	C <sub>12</sub> H <sub>27</sub> NO <sub>2</sub> Si <sub>2</sub>					
peak @ 7.75 218.10	7.75	218.102631	3-Hydroxy-tyrosine	C <sub>21</sub> H <sub>43</sub> NO <sub>4</sub> Si <sub>4</sub>					
peak @ 8.53 218.10	8.53	218.102921	Diethanolamine	C <sub>13</sub> H <sub>35</sub> NO <sub>2</sub> Si <sub>3</sub>					
peak @ 9.16 158.14	9.16	158.135895	L-Isoleucine	C <sub>12</sub> H <sub>29</sub> NO <sub>2</sub> Si <sub>2</sub>					
peak @ 9.28 174.11	9.28	174.11261	Glycine	C <sub>11</sub> H <sub>29</sub> NO <sub>2</sub> Si <sub>3</sub>					
peak @ 9.50 241.08	9.50	241.082321	Uracil	C <sub>10</sub> H <sub>20</sub> N <sub>2</sub> O <sub>2</sub> Si <sub>2</sub>					
peak @ 9.64 204.12	9.64	204.123459	Serine	C <sub>12</sub> H <sub>31</sub> NO <sub>3</sub> Si <sub>3</sub>					
peak @ 9.83 219.11	9.83	219.110336	L-threonine	C <sub>12</sub> H <sub>33</sub> NO <sub>3</sub> Si <sub>3</sub>					
peak @ 10.15 248.13	10.15	248.13176	Alanine	C <sub>12</sub> H <sub>31</sub> NO <sub>2</sub> Si <sub>3</sub>					
peak @ 10.51 189.11	10.51	189.112579	Malic acid	C <sub>13</sub> H <sub>30</sub> O <sub>5</sub> Si <sub>3</sub>					
peak @ 10.72 232.12	10.72	232.118301	L-Aspartate	C <sub>13</sub> H <sub>31</sub> NO <sub>4</sub> Si <sub>3</sub>					
peak @ 10.75 176.09	10.75	176.092422	L-Methionine	C <sub>11</sub> H <sub>27</sub> NO <sub>2</sub> SSi <sub>2</sub>					
peak @ 10.77 156.08	10.77	156.083969	5-Oxo-L-Proline	C <sub>11</sub> H <sub>23</sub> NO <sub>3</sub> Si <sub>2</sub>					
peak @ 10.97 220.10	10.97	220.100235	Cysteine	C <sub>12</sub> H <sub>31</sub> NO <sub>2</sub> SSi <sub>3</sub>					
peak @ 11.33 246.13	11.33	246.134048	Glutamate	C <sub>14</sub> H <sub>33</sub> NO <sub>4</sub> Si <sub>3</sub>					
peak @ 11.43 218.10	11.43	218.102631	L-Phenylalanine	C <sub>15</sub> H <sub>27</sub> NO <sub>2</sub> Si <sub>2</sub>					
peak @ 12.38 357.11	12.38	357.113159	Glycerate-3-phosphate	C <sub>15</sub> H <sub>39</sub> O <sub>7</sub> PSi <sub>4</sub>					
peak @ 12.45 265.09	12.45	265.093872	Hypoxanthine	C <sub>11</sub> H <sub>20</sub> N <sub>4</sub> OSi <sub>2</sub>					
peak @ 12.70 174.11	12.70	174.11261	N-Acetyl-L-Lysine	C <sub>17</sub> H <sub>40</sub> N <sub>2</sub> O <sub>3</sub> Si <sub>3</sub>					
peak @ 12.89 179.09	12.89	179.088638	Benzoic Acid	C <sub>10</sub> H <sub>15</sub> O <sub>2</sub> Si					
peak @ 13.03 156.12	13.03	156.120209	L-Lysine	C <sub>18</sub> H <sub>46</sub> N <sub>2</sub> O <sub>2</sub> Si <sub>4</sub>					
peak @ 13.12 218.10	13.12	218.102631	L-Tyrosine	C <sub>18</sub> H <sub>35</sub> NO <sub>3</sub> Si <sub>3</sub>					
peak @ 15.93 217.11	15.93	217.107498	Inosine	C <sub>22</sub> H <sub>44</sub> N <sub>4</sub> O <sub>5</sub> Si <sub>4</sub>					



**Figure 5-10.** Trends of change of the six metabolites of interest for subjects 2, 3, 5 and 6. The above graphs represent the change in levels of pipecolic acid, diethanolamine, isoleucine, uracil, aspartate and inosine for a – subject 2, b – subject 3, c – subject 5 and d – subject 6. Levels of inosine and aspartate for subjects 2 and 3, respectively, are not included as they did not show the same pattern and obscured the rest of the graph. Error bars indicate standard deviation calculated from average instrument response. The analysis included three technical replicates of each sample.



**Figure 5-11.** Metabolites showing increasing trend with PMI for subject 4. Graphs show the change in levels of a – diethanolamine and b – aspartate for subject 4, detected using GC-MS. Y-axes represent average instrument response, calculated from three technical replicates of each sample, x-axes show time since death (days). Error bars indicate standard deviation calculated from average instrument response.

The data described above were compared with data collected using the LC-MS approach. Diethanolamine was not detected by LC-MS and, as was the case for rat tissue, isoleucine was not separated from its isomer leucine. Pipecolic acid showed an increasing trend for only 2 out of 5 subjects, while uracil, aspartate and inosine showed very similar trends, increasing for the former two compounds and decreasing for the latter.

A few other compounds presented in Table 5-2 seem to be likely biomarker candidates. The amino acids alanine, methionine, phenylalanine, lysine, tyrosine and N-acetyl-lysine, as well as as benzoic acid, showed increasing trends for three out of the five tested subjects. Slightly less likely candidates are glutamate, glycine, serine, threonine and 5-oxo-proline, which showed promising trends only for two out of five tested subjects. Four of the remaining metabolites, glycerate-3-phosphate, malic acid, 3-hydroxy-tyrosine and cysteine showed conflicting trends among the tested subjects, while hypoxanthine was listed as a metabolite of interest only for subject 2. This result is surprising in comparison with the LC-MS results, in which tryptophan, tyrosine, threonine, lysine and phenylalanine showed steady increases for all tested individuals. On the other hand, aside from the proteogenic amino acids, neither of the selected compounds of interest showed any particular changes with PMI when separated using the pHILIC LC column. Additionally, benzoic acid and 3-hydroxytyrosine were not detected. However, benzoic acid was detected using the HILIC column and showed a general increasing trend for subjects 2, 5 and 6. N-acetyl-lysine also showed increasing trends for subjects 2 and 5 in the HILIC data.

Leucine, which showed the second highest rate of increase in rat tissue, remained virtually unchanged for all of the tested subjects (see Figure 5-12 for subjects 2, 3, 5 and 6). The levels oscillated around the value of the initial time point, with the other values only slightly exceeding 1-fold. This disagrees with the data collected through the LC-MS approach, where levels of leucine increased steadily over time for the same subjects (see Figure 5-13). For subject 2, levels of this metabolite increased just over 2-fold, for subject 3 nearly 3-fold, for subjects 4 and 5 slightly under 2-fold (graph not shown for subject 4) and 2-fold for subject 6. This is a moderately slow increase over time in comparison to other metabolites. Overall, a clear increasing trend can be seen in the LC-MS data, but this is not mirrored in the GC-MS set.

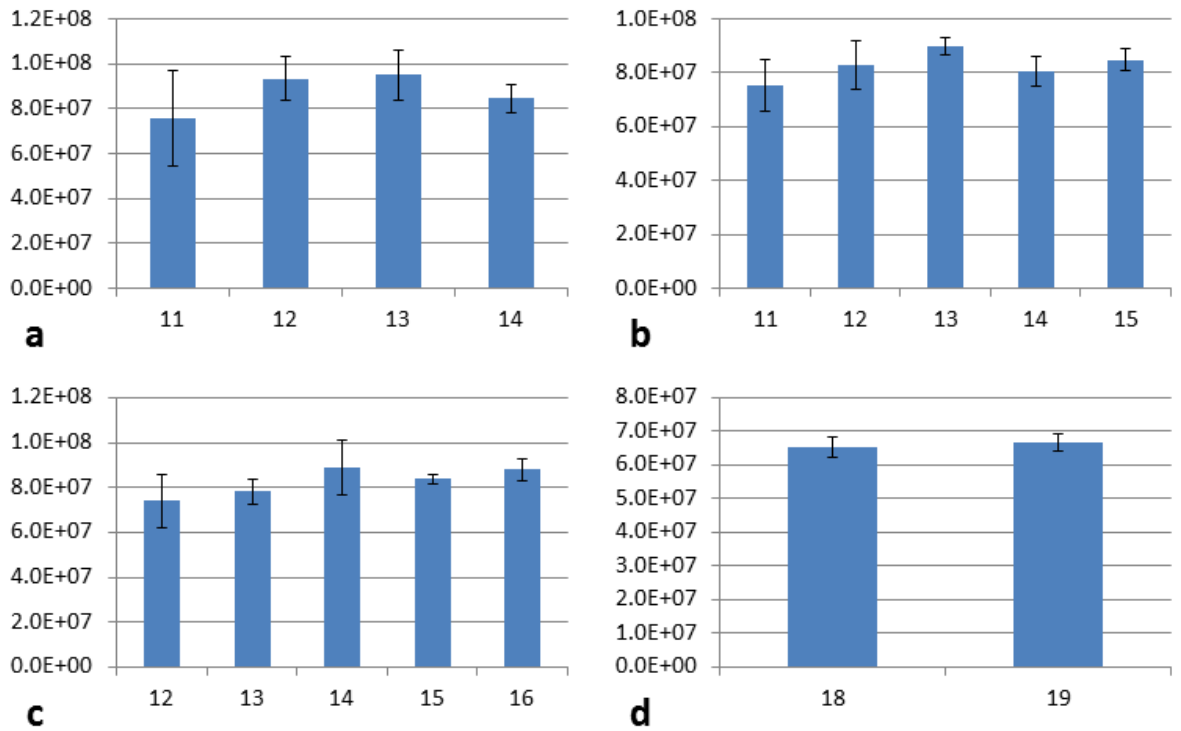


**Figure 5-12. Levels of leucine detected in human tissue by GC-MS.** Graphs represent levels of leucine detected over time for a – subject 2, b – subject 3, c – subject 5 and d – subject 6 using GC-MS. Y-axes represent average instrument response, calculated from three technical replicates of each sample, x-axes show time since death (days). Error bars indicate standard deviation calculated from average instrument response.

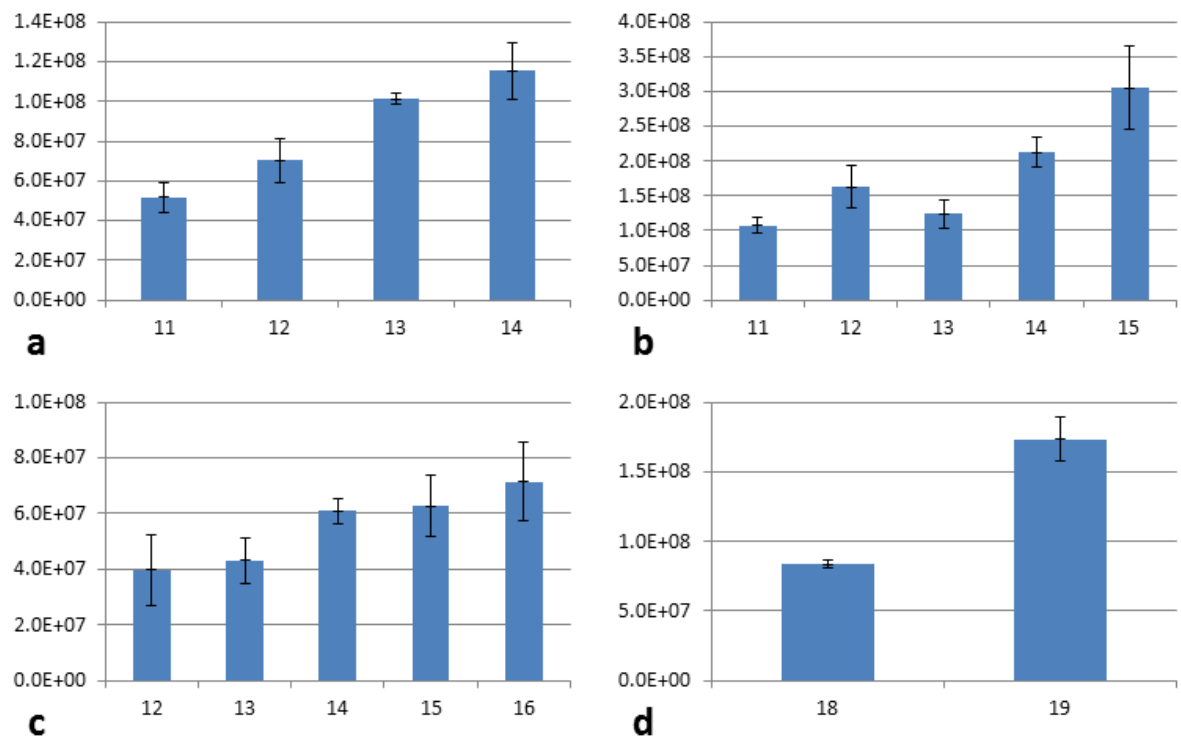


**Figure 5-13. Levels of leucine detected in human tissue by LC-MS.** Graphs represent levels of leucine detected over time for a – subject 2, b – subject 3, c – subject 5 and d – subject 6 using LC-MS. Y-axes represent average instrument response, calculated from three technical replicates of each sample, x-axes show time since death (days). Error bars indicate standard deviation calculated from average instrument response.

The data collected from human cadavers is very variable; however, it was possible to pinpoint certain compounds with the potential to become PMI biomarkers. Pipecolic acid, diethanolamine, isoleucine, uracil, aspartate and inosine showed the most potential out of the 24 compounds of interest. Additionally, aspartate and uracil were also among the compounds of interest selected in the rat study. Amino acids showed the most consistent changes among all of the different species tested using both LC and GC approaches; therefore, they were selected for absolute quantification in the final part of this study.

### **5.3.2.2 Absolute quantification**

The GC-MS approach was used to try to accurately quantify the amount of the amino acids present in PM samples, since they had been shown to have the highest potential to become PMI markers in this study so far. A mixture of amino acids at known concentrations was analysed along with the samples to provide a calibration curve. Twenty four different amino acids were included in the mix, mainly proteogenic amino acids with the addition of cystine, ornithine, hydroxyproline and homoserine. Figure 5-14 shows chromatograms of 14 out of the 24 amino acids included in the mix. The amino acids displayed in Figure 5-14 are the ones detected in the untargeted analysis described in section 5.3.2.1 of this chapter. Running these standards served not only as the basis for a calibration curve, but also the retention times of the peaks in the standards could be compared with those in the samples to confirm the identities of the compounds. Provided that the standard is analysed under the same conditions as the sample, the RT of each compound should remain the same and permit unambiguous compound identification. Two batches of samples were analysed on different days and the RTs of the compounds did not differ by more than 0.01min from batch to batch. Chromatograms in Figure 5-14 are shown to confirm the identities of the amino acids presented in Table 5-2 (section 5.3.2.1). RT comparison confirmed the identities of all but three of the 14 amino acids detected which had a reference standard. Leucine was identified at RT 6.90, while the standard eluted at 8.99 min and alanine was detected at 10.15 while the reference standard eluted at 7.25 min. The retention times of compounds might differ between different instruments as well as from batch to batch on the same instrument. The discrepancy in the retention times of the

aforementioned compounds might have been caused by running the human samples in two separate batches. Hydroxyproline eluted at the same time as the compound identified as 5-oxo-proline, which suggests it is more likely that it is hydroxyproline. However, these two compounds have very similar mass spectra (in the derivatised form). Amino acids have common fragments, which give rise to the same masses in their spectra. Usually, a few unique fragments can be identified, but this is not always the case. Manual comparison of the detected masses with the library records indicates 5-oxo-proline is a correct match.

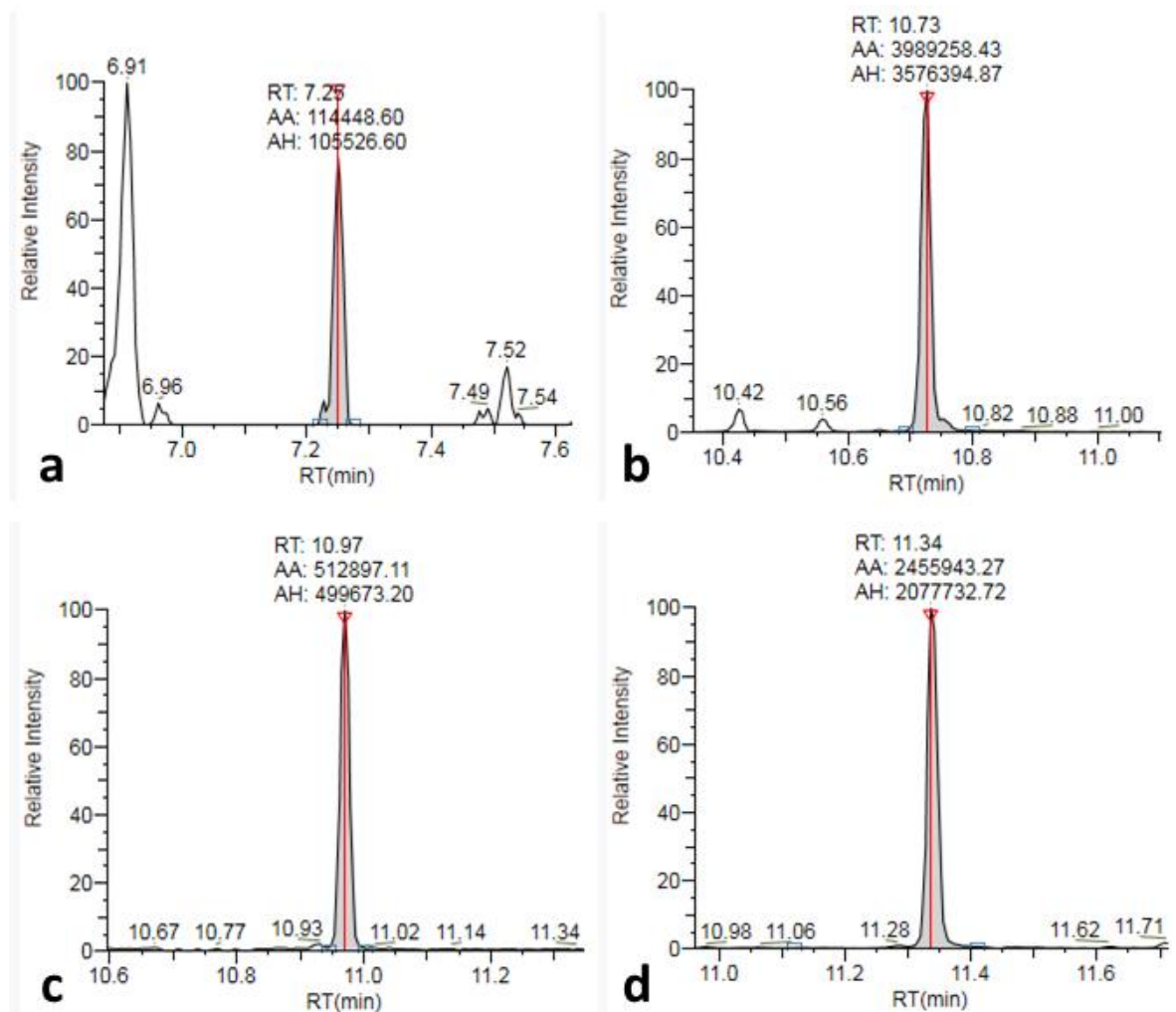


**Figure 5-14. Extracted ion chromatograms of selected amino acid standards.** The graphs above show the peaks and retention times of six amino acids: a – alanine, b – aspartate, c – cysteine, d – glutamate, which were included in the standards mix and run together with the human samples in batch 1. Y-axis shows the relative intensity, the most abundant peak visible in the window is assigned as 100 and the other peaks are scaled accordingly to that peak. RT – retention time in min (x-axis), AA – peak area, AH – absolute height of the peak.

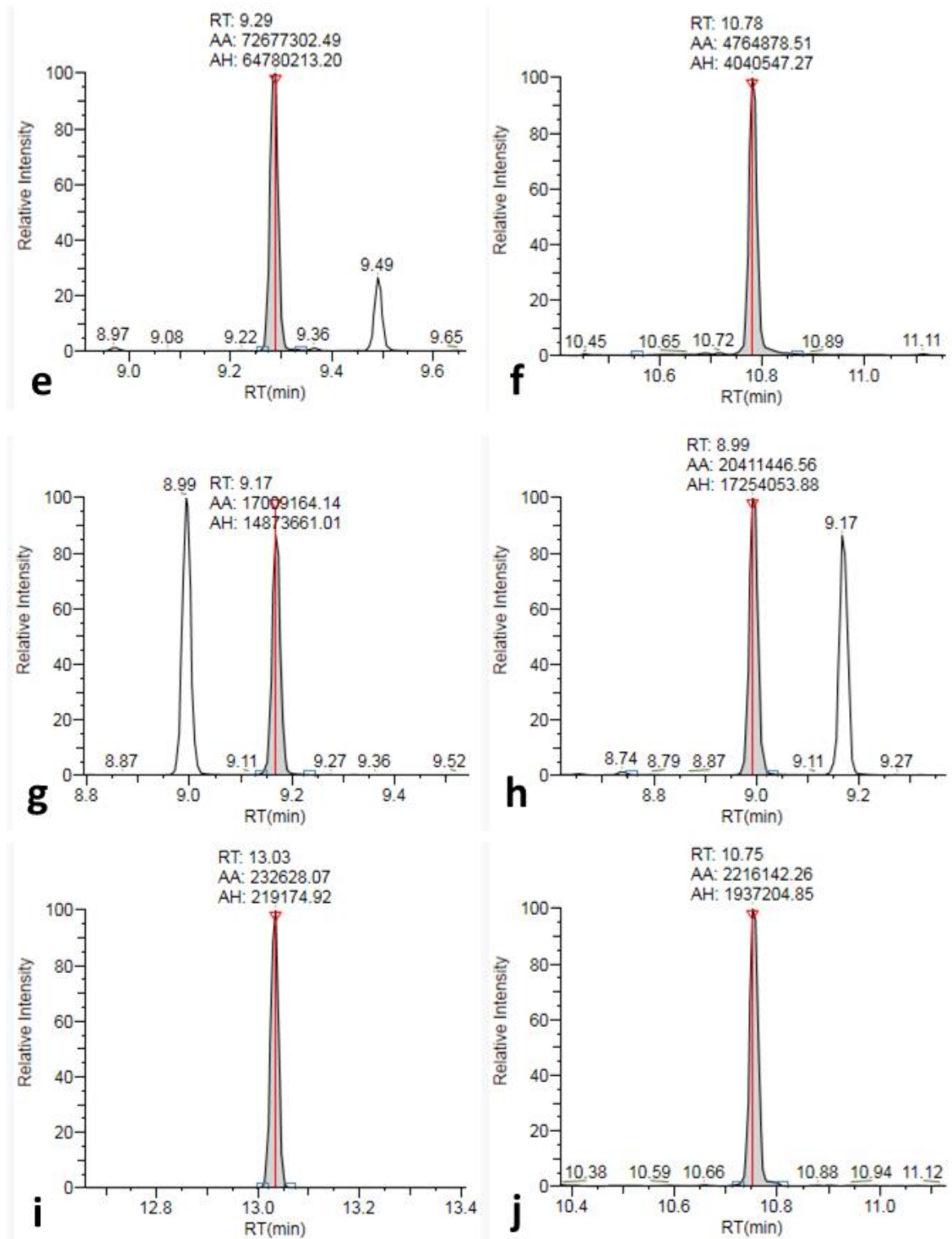


Figure 5-14. Continued from previous page.

The graphs above show the peaks and retention times of six amino acids: e – glycine, f – hydroxyproline, g – isoleucine, h – leucine, i – lysine, j – methionine, which were included in the standards mix and run together with the human samples in batch 1. Y-axis shows the relative intensity, the most abundant peak visible in the window is assigned as 100 and the other peaks are scaled accordingly to that peak. RT – retention time in min (x-axis), AA – peak area, AH – absolute height of the peak.

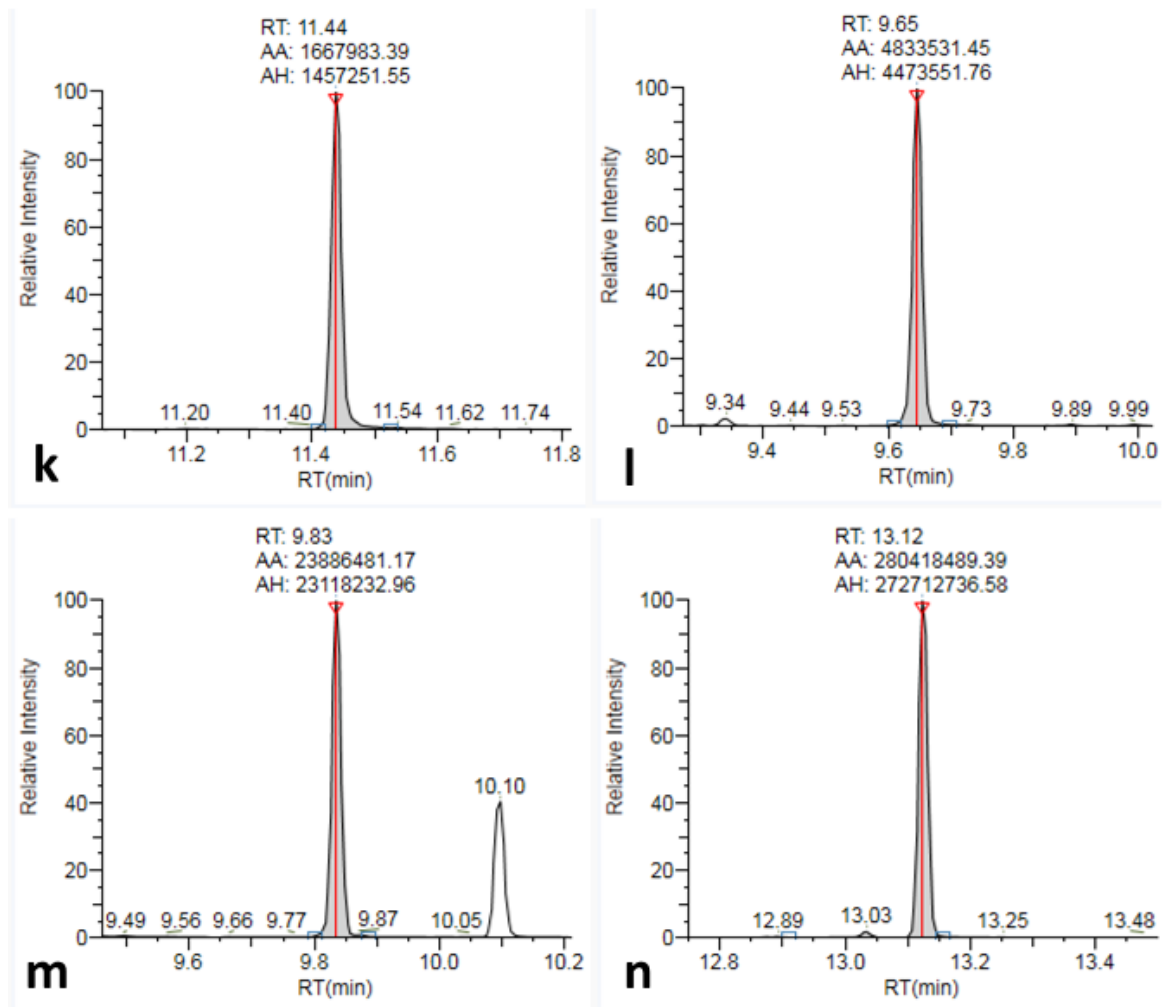
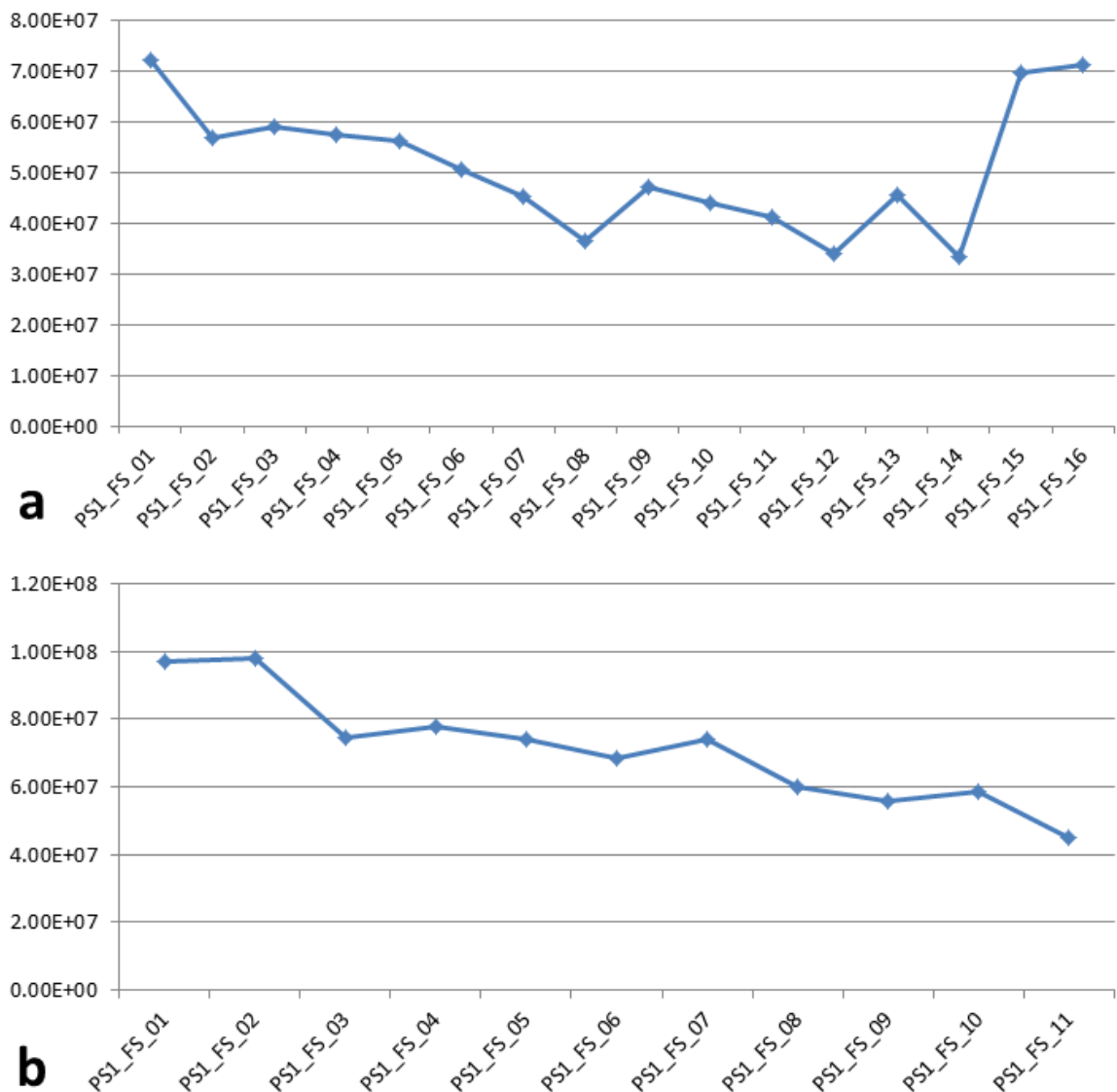


Figure 5-14. Continued from page 18.

The graphs above show the peaks and retention times of six amino acids: k – phenylalanine, l – serine, m – threonine and n – tyrosine, which were included in the standards mix and run together with the human samples in batch 1. Y-axis shows the relative intensity, the most abundant peak visible in the window is assigned as 100 and the other peaks are scaled accordingly to that peak. RT – retention time in min (x-axis), AA – peak area, AH – absolute height of the peak.

A pooled standard, an aliquot of each of the samples mixed together, is commonly included in analysis of large batches of metabolomics samples. This sample mix is injected a few times at the beginning of the run, to condition the system before analysis of the samples of interest, as well as at regular intervals throughout the batch as a check for reproducibility of the analysis. For this reason, a pooled standard was included in the analysis described in this chapter. The pooled standard was injected every 5 samples. The first six pooled standards were injected to condition the system at the start of the batch. The pooled standard was analysed 16 times in batch 1 and 11 times in batch 2. The instrument responses of the pooled standard were plotted on a graph to check for reproducibility across the batch (see Figure 5-15). The pooled standards were labelled in order of injection. In batch 1 the first standard shows much higher

response than the subsequent pooled standards. The remaining 5 conditioning pooled standards varied in response, showing a decreasing trend, however, they showed much less variation than the samples injected later on throughout the batch. In batch 1 the pooled standard was injected multiple times from a single aliquot. In order to address the issue of the high variation in the response of the control sample, separate aliquots were prepared for each injection in batch 2. This improved the pooled standard response across the batch; however, reproducibility issues are still apparent in the second batch.



**Figure 5-15.** Graph representing the pooled standard response across the batch. The response obtained for each pooled standard was plotted in the order of injection, for batch 1 (graph a) and batch 2 (graph b). Y-axis represents the response of each sample and x-axis contains the label given to each pooled standard with the numbers indicating the order in which these samples were injected. First 6 samples were injected at the beginning of the batch to condition the column.

Additionally, internal standards were added to all of the samples, calibrators and quality control samples (QC), to increase precision and accuracy of the

collected data (described in detail in chapter 2). Ideally, the internal standard used should be an isotopically labelled version of the target compound (Dunn et al. 2011). However, that complicates and significantly increases the cost of the analysis in the case of multiple target analytes (as in this case). Isotopically labelled compounds might not be available for each of the analytes. Therefore, three internal standards were used:  $^{13}\text{C}_6$ -glucose,  $\text{D}_{27}$ -myristic acid and scyllo-inositol. Both glucose and myristic acid were in a labelled form and scyllo-inositol, an isomer of inositol, does not naturally occur in mammalian tissue (MacRae & Ferguson 2005). This ensured that the detected levels of each internal standard would not be confused with levels of any of the compounds naturally occurring in the samples. In principle, the response of these three compounds should be the same in all of the samples, calibrators and quality control samples. Figure 5-16 and Figure 5-17 show the levels of response obtained for these compounds within the two batches run (subjects 2, 3 and 5 in batch 1 and subjects 4 and 6 in batch 2). Of course, small variation in the response between the samples was to be expected. However, in these analyses all three of the internal standards in both batches showed a very large variation of response across the samples.

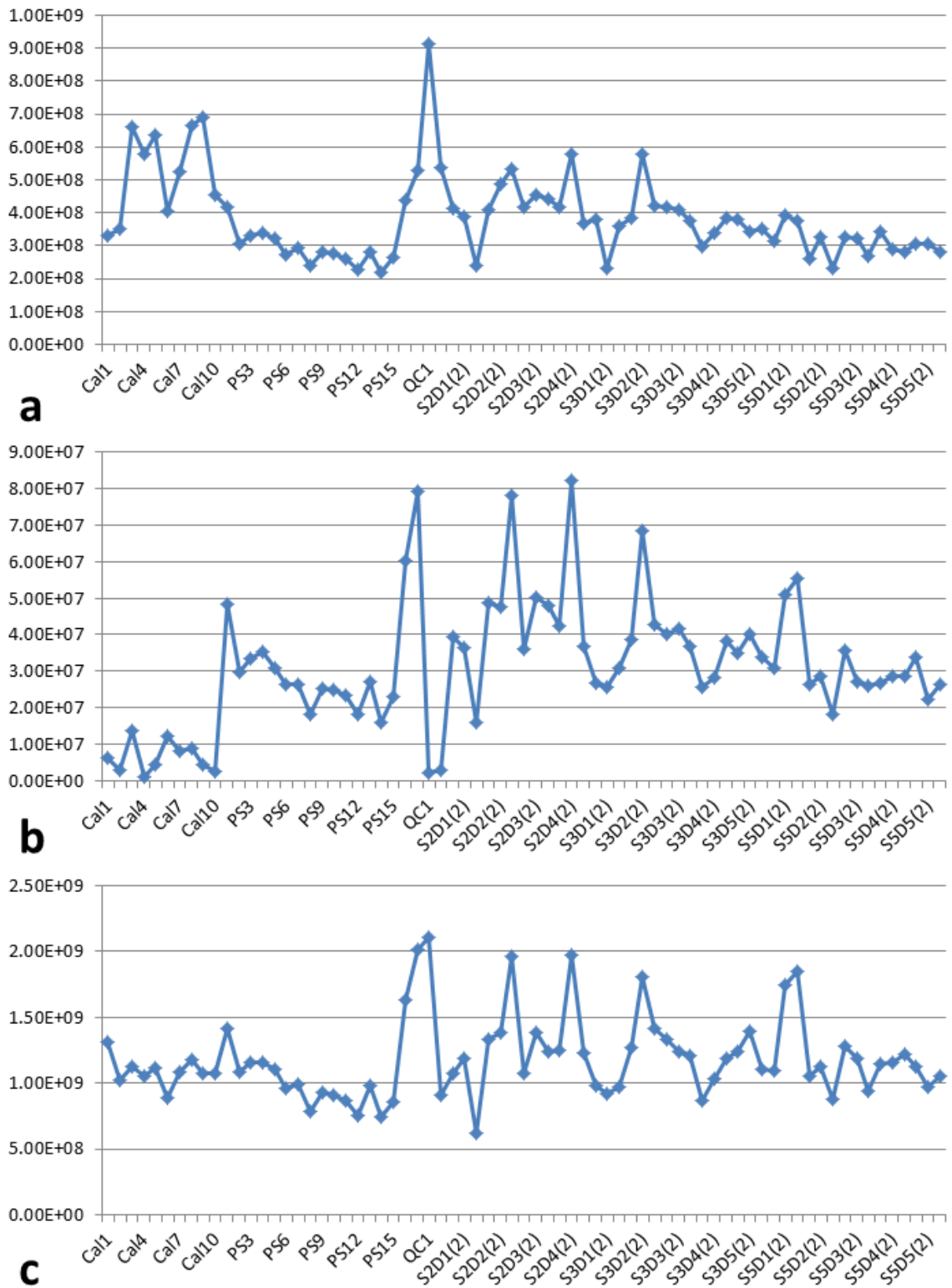


**Figure 5-16.** The responses of internal standards shown across the whole batch (batch 1). The graphs show the peak areas (y-axis) for each particular calibrator, QC, samples and pooled standards (x-axis) for three ISSs: a –  $^{13}\text{C}_6$ -glucose, b –  $\text{D}_{27}$ -myristic acid and c – scyllo-inositol. The labels in the y-axis indicate cal – calibrators (1-10), PS – pooled standards (1-17), QC – quality control samples (1-2) and SnDn – samples, where S stands for subject and D stands for the day (time point), n – number in the sample name. Due to high number of samples every third sample name is displayed in y-axis. Batch 1 included subjects 2, 3 and 5.

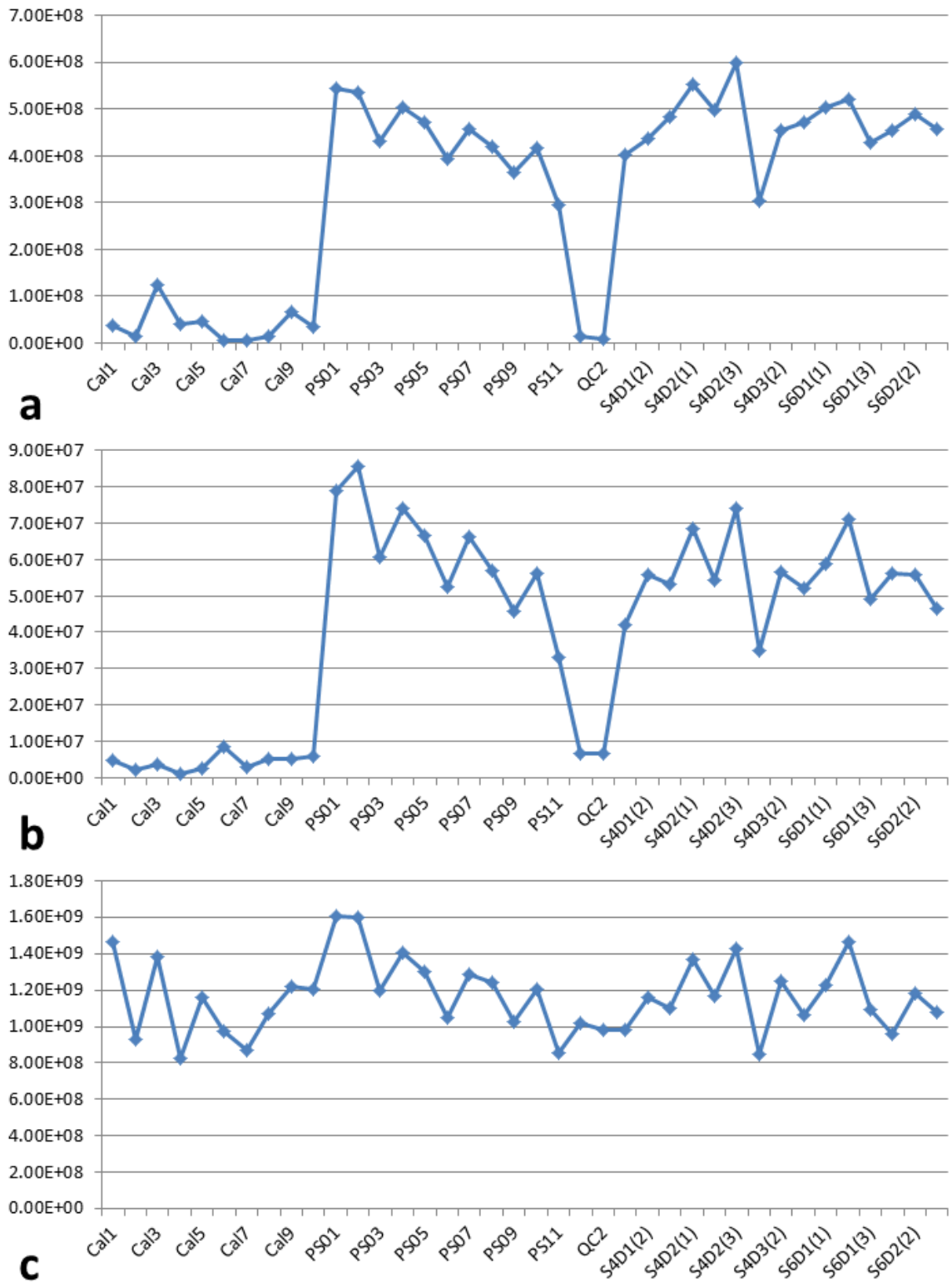


**Figure 5-17.** The responses of internal standards shown across the whole batch (batch 2). The graphs show the peak areas (y-axis) for each particular calibrator, QC, samples and pooled standards (x-axis) for three ISS: a –  $^{13}\text{C}_6$ -glucose, b –  $\text{D}_{27}$ -myristic acid and c – scyllo-inositol. The labels in the y-axis indicate cal – calibrators (1-10), PS – pooled standards (1-11), QC – quality control samples (1-2) and SnDn – samples, where S stands for subject and D stands for the day (time point), n – number in the sample name. Due to high number of samples every second sample name is displayed in y-axis. Batch 2 included subjects 4 and 6.

The calibration curve consisted of 10 different concentrations ranging from 4.6 nmole to 23 pmole. Table 5-3 shows the expected concentrations at which the

calibrators were prepared. Calibrators 6-10 were 1 in 10 dilutions of calibrators 1-5. This was done in order to expand the range of the calibration curve. As a result, calibrators 4 and 6 and 5 and 7 have the same concentration. Table 5-3 also shows the apparent concentrations of the calibrators calculated from the experimental data obtained. This was achieved by plotting the areas of the calibrators on a graph and describing the trend obtained with a mathematical (quadratic) equation. This equation was then used to calculate the apparent concentrations of the calibrators as well as the concentrations of the unknowns (amino acids in the human tissue samples). This data processing was carried out by Stefan Weidt using Xcalibur software.

**Table 5-3. Actual vs calculated concentrations of the calibrators.**

The table shows the actual concentrations at which the calibrators were prepared and the calculated concentrations obtained from the calibration curve (. % difference shows how close the calculated value is to the expected value in percentage, minus sign indicates the calculated value is smaller than the expected one. This data was collected for isoleucine, chosen as an example.

Sample ID	Concentration (nmole)	Calculated Concentration (nmole)	%Difference
Calibrator 1	4.545	4.556	0%
Calibrator 2	2.273	2.192	-4%
Calibrator 3	0.909	0.985	8%
Calibrator 4	0.455	0.607	33%
Calibrator 5	0.227	0.149	-34%
Calibrator 6	0.455	0.621	36%
Calibrator 7	0.227	0.098	-57%
Calibrator 8	0.091	0.030	-67%
Calibrator 9	0.045	0.006	-86%
Calibrator 10	0.023	-0.023	-202%

As can be seen in Table 5-3, large errors appear in the resulting calculated concentrations, even though the  $R^2$  value of the calibration curve was 0.998. A separate calibration curve was prepared for each of the amino acids included in the standard mix. A similar trend was observed in each case. Calibrators 1-5 (higher concentrations) were not far off the expected concentration of the standard, however, the calibrators on the lower end of the curve were very variable and with a large error. This was also observed in the case of the quality control samples. Two QC samples were run in each batch at two concentrations 1.591 and 0.159 nmole. These were mid-range concentrations between calibrators 1-5 and a 1 in 10 dilution of this value. The QC with the lower concentration failed for most of the amino acids included in the mix, while the

other QC passed. A threshold of 20% variation from the actual concentration was used as a cut-off value to determine if a QC passed or failed.

The reproducibility issue seen in the responses of internal and pooled standards as well as the error associated with the calibrators and QC samples puts the validity of the quantification into question. Nevertheless, the trends of change of detected metabolites were compared between the absolute and relative quantification results. An example comparison for leucine and glutamate is shown in Figure 5-18. The levels of leucine were quantitated within the lower range of the calibration and the trends seen differ from the trend obtained through relative quantitation. In the case of glutamate both graphs show an increasing pattern, however, slightly different. The levels of glutamate were quantitated within the higher range of the calibration which had a smaller error associated with it.

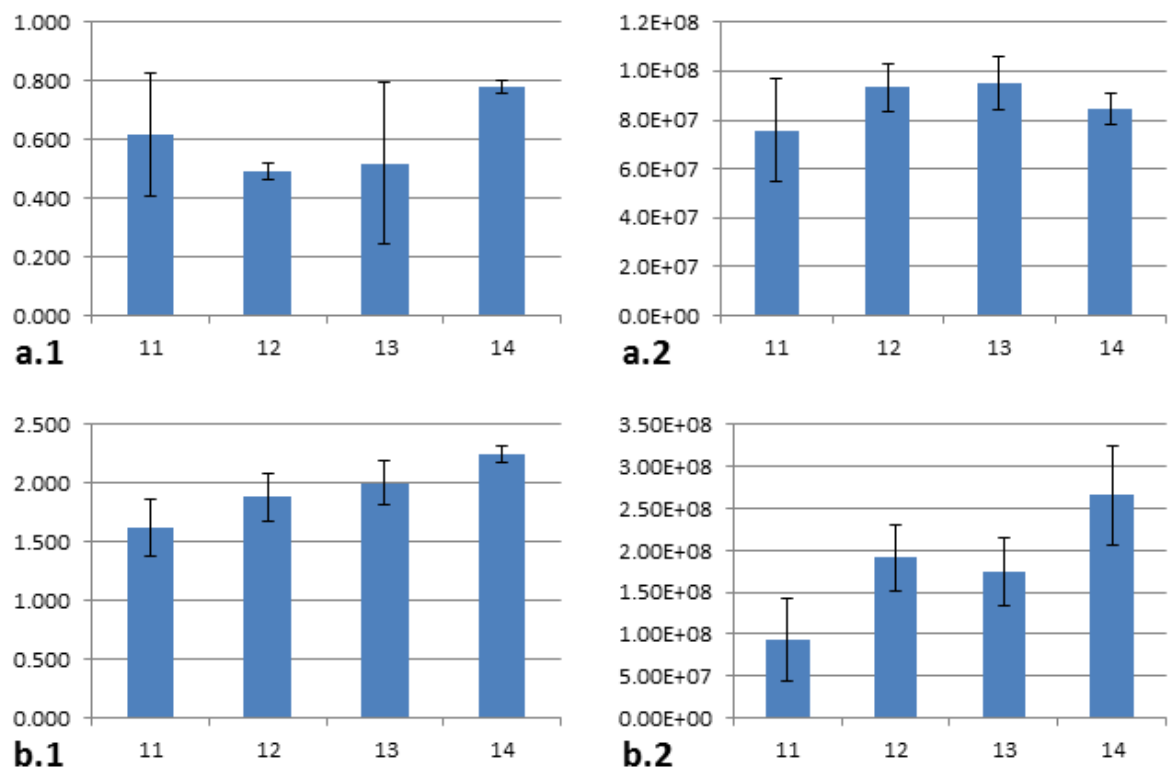


**Figure 5-18. Comparison of results obtained with absolute and relative quantification.** The above graphs show the trends of change detected for leucine (graphs a.1 and a.2) and glutamate (graphs b.1 and b.2). Graphs labelled with 1 (absolute quantification) represent the average calculated amount of the amino acids in nmole (y-axis in a.1 and b.1). Graphs labelled with 2 (relative quantification) show the average response detected for these compounds (y-axis in a.2 and b.2). In all four graphs the x-axis show PMI (days). Error bars show the standard deviation calculated from the average amount of the metabolites shown in the graphs (N=3). Three aliquots of each sample were used for analysis. Metabolite concentration was calculated using a calibration curve prepared with amino acid standards. Results shown were collected for subject 2.

The absolute quantification method needs improvement. However, the relative quantitation allowed the detection and identification of possible biomarker candidates. A number of amino acids, as well as uracil, hypoxanthine and n-acetyl-lysine were listed as metabolites of interest in both rat and human tissue.

## 5.4 Discussion

This part of the study aimed to apply a state-of-the-art GC-MS instrument in PMI biomarker research. Furthermore, a new method for absolute quantification of multiple amino acids was developed and tested. Two types of tissue were tested, rat and human. Relative quantification was carried out on the first and both relative and absolute quantification on the human data. Similar to the LC-MS approach described in chapter 4, an untargeted approach was also applied in this case. The results of this study confirmed that amino acids are the most likely candidates for PMI biomarkers. However, a few new metabolites were also added to the list of possible compounds, which were not considered before. Confirming the results of the LC-MS analysis, 11 proteogenic amino acids were detected and showed an increase with PMI in rat tissue: tryptophan, leucine, serine, aspartate, methionine, cysteine, glutamate, phenylalanine, asparagine, lysine and tyrosine. Additionally, alanine also showed an increasing trend, which was not apparent in the LC data, and isoleucine and leucine were successfully discriminated, as the GC approach allowed separating these isomers. The differences observed between leucine trends by GC-MS and LC-MS are most probably the result of its co-elution with isoleucine in the LC data. Furthermore, a few other, non-proteogenic amino acids were detected - homocysteine, cystathionine, n-acetyl-lysine and 3-methylhistidine. Interestingly, homocysteine and cystathionine are both involved in the cysteine synthesis pathway. Homocysteine reacts with acetyl-serine to give cystathionine and then cystathionine can be deaminated to form cysteine (see Figure 5-19). Cysteine showed the highest rate of increase among all of the amino acids, which could suggest that the two abovementioned reactions continue post-mortem. Of course, there are many other metabolic pathways which lead to cysteine formation, however, without detecting the compounds involved, it is impossible to say which could have any impact on cysteine accumulation post-mortem. On the other hand, both homocysteine and cystathionine also increase over time, although at a much lower rate. The rates of increase of these compounds are

comparable, about 5-fold, (see Figure 5-5), while cysteine increased about 35-fold. The large increase in cysteine level can be most probably attributed to a combination of a few different factors (protein degradation, compound decompartmentalization etc. as discussed in chapters 3 and 4), rather than simply metabolic synthesis. All three of these compounds act as intermediates in a few metabolic reactions, both synthesising them and using them for synthesis of other compounds. Cysteine, being one of the proteogenic amino acids would be probably more abundant in general.

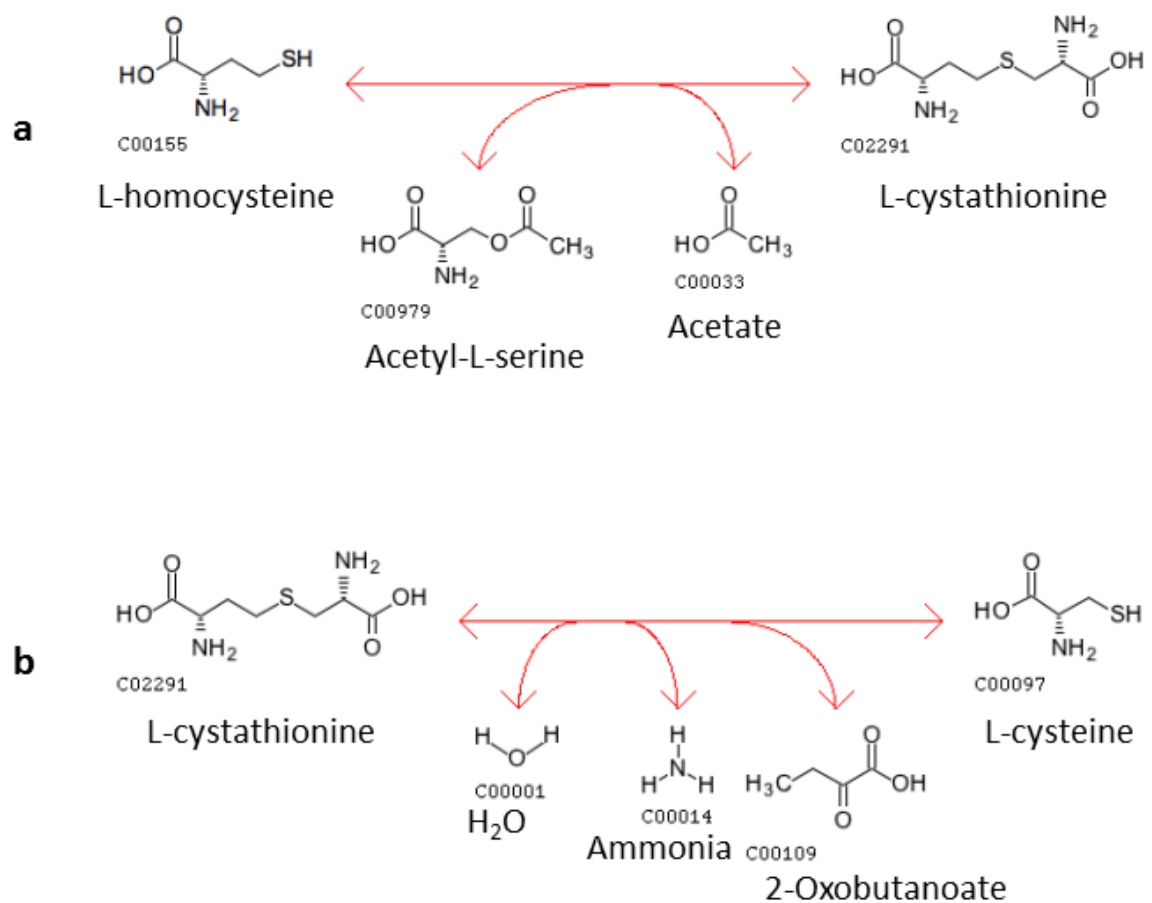


**Figure 5-19. Scheme showing two reactions involved in cysteine synthesis** (Kanehisa 1995). The figure shows the synthesis of cystathionine from homocysteine and acetyl-serine (a) and the synthesis of cysteine from cystathionine (b). The names of the compounds are placed below them. The number preceded by C under each compound, indicates its Kyoto Encyclopaedia of Genes and Genomes (KEGG) identification number (). The reactions included in the cysteine pathway are found in KEGG (Kanehisa 1995).

Interestingly, another amino acid of interest, 3-methylhistidine, is formed by methylation of actin and myosin (Wishart et al. 2013), which comprise muscle tissue and were selected as proteins of interest in the proteomic part of this study. Additionally, this compound is a known indicator of muscle degradation (Wang et al. 1998; Elia et al. 1981; Rathmacher et al. 1995). When muscle tissue

degrades, histidine present in the peptide chains of actin and myosin is methylated and excreted in urine (Elia et al. 1981). After the methylation occurs the compound is no longer used for protein synthesis. It is possible that after death, when bodily functions cease and the compound is not removed from the organism, it builds up in muscle tissue. This would make this compound a perfect candidate for PMI estimation, however, under carefully controlled dietary conditions, as meat intake can influence the amount of 3-methylhistidine present.

Five other compounds were selected as metabolites of interest in rat tissue: caproic acid (carboxylic acid (Wishart et al. 2013)), uracil (pyrimidine metabolism), glucosamine (carbohydrate metabolism), hypoxanthine and adenine (purine metabolism). All but one of these compounds, adenine, showed an increasing trend with PMI. Adenine decreased with time.

Human tissue was also tested for possible biomarkers with varying results from subject to subject. However, in general, various proteogenic amino acids showed the most promising changes, as was observed for rat tissue. Additionally, n-acetyl-lysine, uracil and hypoxanthine were also selected in both tissue types. On top of that, a few new compounds were added to the list: pipercolic acid, 3-hydroxy-tyrosine, diethanolamine, malic acid, 5-oxo-proline, glycerate-3-phosphate, benzoic acid and inosine. Out of all of the detected compounds of interest, the top six were picked, because they showed promising changes in most, if not all, of the tested subjects. These included pipercolic acid, diethanolamine, uracil, aspartate, isoleucine and inosine. A compound identified as diethanolamine showed a promising pattern of change, but this is likely a spurious identification as diethanolamine is not thought to be endogenous to the human body. In one of the subjects (subject 6) the diethanolamine peak was identified as indole-2-carboxylic acid. This is a more likely endogenous identification, however, less possible according to the database match. Further enquiry into the identity of this compound is required to present it as a possible biomarker. Uracil, aspartate and isoleucine are therefore the three most robust candidates based on the results from both human and rat tissue.

The results obtained through the GC-MS approach were compared with the results obtained using the LC-MS approach. In general the same trends of change

were observed when comparing results, with a few exceptions. For example, alanine (rat) and leucine (human) showed an increasing trend by GC-MS but by LC-MS the levels remain fairly constant over time. The differences seen between results could depend on the sensitivity of the instruments used, as well as on the correct identification of the compound. Many of the compounds presented here were putatively identified, especially in the case of GC rat data, where no standards were run within the batch. Additionally, LC chromatography suffers from ion suppression in which co-elution of different molecules or isomers affects the signal of the detected compound. In the case of LC analysis many compounds were identified with a few possible isomers. The resolution power of GC is better therefore; ion suppression is not an issue in this case. Furthermore, in the LC approach, many more compounds were detected and putatively identified in comparison with the GC data. This is most likely due to the fact that gas chromatography, as the name suggests analyses compounds in the gaseous state. Compounds which are not naturally volatile have to be derivatised before the analysis. However, a different range of compounds can be detected using this method, as the LC columns used in this study were specified to separate polar compounds. Derivatisation adds more steps into sample preparation, which can potentially bias quantitation to handling errors or sample loss. Also derivatisation efficiency comes into play. Compounds which have not derivatised efficiently will not be separated and detected. Furthermore, multiple derivatisation products can occur (i.e. Aspartate-2TMS and Aspartate-3TMS), which results in smaller numbers of different compounds detected. Therefore, sample preparation is crucial in GC experiments; reagents must be carefully selected and preparation method optimised. In the case of this experiment, especially in batch 1, there was not enough time to fully optimise the sample preparation. Certain stages of the preparation were carried out by a robot, which added appropriate aliquots of reagents to the samples. In theory, that should increase the reproducibility between the samples, however, that was not the case. The use of the robot was discontinued for this purpose. Smaller numbers of detected compounds means smaller numbers of possible biomarker candidates, but makes data analysis more straightforward. GC-MS proved an orthogonal approach that resulted in new biomarker candidates being added to the list. However, it must be kept in mind that there was limited time to carry out this analysis and the methods used require further optimisation. Even though

the analysis did not perform as well as it could, it was worth trying to carry out absolute quantification of the amino acids. The GC approach is better suited for this purpose as it does not suffer from ion suppression. Additionally, the fragmentation patterns obtained using an electron ionisation method give very reproducible fragmentation patterns, allowing compound identification through an established database. However, the molecular ion is often lost in the fragmentation. Knowing the molecular weight of a compound helps to limit the number of possible matches, which in this case is hindered. In LC fragmentation spectra the molecular ion is always present; however less structural information is obtained. Both approaches have their strengths and weaknesses, however, when combined, they can help to characterise a large part of the metabolome.

As mentioned above, the GC-MS approach gives the opportunity of absolute quantification of the metabolites present in the sample. Amino acids were selected for this part of the study as they seemed the most likely biomarker candidates, as seen in this and the previous chapter. This was the final part of the project, with not much time left for instrument and method optimisation, therefore the quantification was not successful. Reproducibility between the samples was an issue, which made the normalisation of the data very difficult. The internal standard used for this purpose was added to the samples post-extraction (ideally it should be added pre-extraction). As a result, it did not correct for the extraction efficiency, but it would have corrected for the derivatisation and injection efficiency. The sample was injected in a split mode with a small split ratio of 1:10. Split ratio is the ratio between the carrier gas flow rate and the split vent flow rate. This ratio should be carefully selected based on the capacity of the inlet liner, temperature of the liner and type of the solvent used. Any issues in the ratio of these factors can cause an issue with the sample flow and in turn with reproducibility. It was later observed (outside the scope of this study) that a higher split flow improved the reproducibility between the samples analysed using this instrument. The amino acid quantification was unsuccessful; however, considering the aim of this project, the absolute amount of the biomarker might not be necessarily required. Knowing the exact amount of the analyte in question would help to produce an accurate mathematical equation describing the change of this analyte with PMI. However, the levels of metabolites vary from person to person and therefore

this absolute amount will differ in each case. But if it was possible to find a metabolite for which the rate of change over time is similar between different people, this would prove more useful in PMI estimation, irrespective of the absolute amount of the analyte present.

As described in the previous chapter, various metabolites, including amino acids were previously suggested as potential markers for PMI (Vass et al. 2002; Patrick & Logan 1988a; Girela et al. 2008; Kärkelä & Scheinin 1992; Kang et al. 2012), however very few studies used a global metabolomics approach for this purpose (Hirakawa et al. 2009; Schmidt et al. 2014). The field of metabolomics is growing fast and GC-MS is becoming increasingly popular for this purpose. Similarly, more and more researchers show interest in PMI estimation and with the advancements and developments in the metabolomics field, they are trying new ways of approaching this issue. Donaldson and Lamont used a GC-MS based metabolomics approach to identify biomarkers in post-mortem blood (Donaldson & Lamont 2014). As a result they mainly listed proteogenic amino acids as possible candidates.

Sato *et al.* (Sato et al. 2015) and Kaszynski *et al.* (Kaszynski et al. 2016) both used very similar approaches to GC-MS metabolic profiling as that described here. The only difference is that both groups created mathematical PMI prediction models and here, an absolute quantification of various metabolites was attempted. Due to the limited amount of test subjects in the case of rat tissue, and the varying PMI scattered along a large time frame of 19 days in the case of human tissue, it was not possible to create an accurate prediction model from the data presented here. Sato *et al.* tested post-mortem rat plasma, while Kaszynski *et al.* muscle and serum of mice. Similar to the results presented here, both studies listed amino acids as metabolites of interest. Kaszynski *et al.* also listed hypoxanthine as a possible biomarker in muscle tissue. Hypoxanthine levels were previously correlated with PMI, however, measured in vitreous humour (Camba et al. 2014; Passos et al. 2009; Muñoz-Barús et al. 2010; Lendoiro et al. 2012; Muñoz Barús et al. 2002; Rognum et al. 1991) or blood (Donaldson & Lamont 2013). The previously mentioned study by Sato *et al.* also lists another metabolite of interest highlighted in this study, namely uracil (Sato et al. 2015). They list it as one of the metabolites detected, but they do not include it as one of the components of the PMI prediction model. To the best of

the author's knowledge, n-acetyl-lysine, the final metabolite of interest, has not been previously suggested as a potential marker for PMI.

## 5.5 Conclusion

This chapter demonstrated how state-of-the-art GC-MS technology can be successfully applied in PMI research. The absolute quantification method requires optimisation and validation but relative quantification was successfully applied. The approach further confirmed the results of the LC-MS analysis, pointing towards amino acids as the best candidates for PMI biomarkers, especially isoleucine, aspartate and n-acetyl-lysine. Additionally, a few new possible candidates were discovered: adenosine in rat, inosine in human and hypoxanthine in both tissue types. GC-MS is not without its challenges, but it has potential as a tool for metabolic profiling. Used in complement with the LC-MS approach (Chapter 4), GC-MS augments the process of biomarker discovery.

## 6 GENERAL DISCUSSION

Estimation of the post-mortem interval in the case of an unwitnessed or a hidden death is an extremely difficult task. The currently used methods present a rather short window of time (24-48 h) when this can be accurately assessed (Fatteh 1973). Throughout the years, many researchers have attempted to solve this issue, both by trying to improve already known methods, as well as by applying new and advanced techniques (Nelson 2000; Usumoto et al. 2010; Young et al. 2013; Vass et al. 2002), but with limited success. The decomposition of the human body is a very complicated process, which can be influenced by many different factors. The environment in which the body is decomposing (including temperature, humidity, substrate, local fauna and flora) and whether the body is clothed or buried, will affect how fast and in what way decomposition proceeds. However, it is not just the surroundings of the dead body that matter in the decomposition process. Many studies have evaluated the chemical and biological processes occurring after death (Sabucedo & Furton 2003; Zapico et al. 2014; Jia, Hildrum, et al. 2006), but interindividual differences in body composition, metabolism etc. are influenced by our genotype and lifestyle (diet, weight or possible disease state). All of these factors, which are important during life, may have a bearing on the processes occurring post-mortem and may thus influence estimation of time since death.

Trying to quantify or assess post-mortem changes in some way would require extensive studies, involving many test subjects, from various backgrounds, representing different groups of age, body shape, cause of death etc. Basically, it would require a large clinical study on dead bodies. However, each large clinical study also requires a negative control group. What kind of control group could be used in this case? Subjects where the samples were collected seconds after death, or from a living healthy individual? This is a very unique field of research which is limited by not only logistical but also ethical issues. Not many laboratories are equipped to store dead bodies or would be able to source any samples from them. This was one of the issues encountered at the very beginning of this project. Initially, it was possible to obtain neither animal nor human cadavers, which could be stored and sampled at various intervals. In the UK, pathologists examining the bodies of deceased only sample what is required to determine the cause of death. Cadavers which are donated to science usually

go to a university anatomy department and due to their ethical commitments, they do not allow any specimens to leave their laboratory. It would only be possible after the tissue was formalin fixed, which limits any further testing. A similar scenario was encountered at the animal unit, where potentially, rat cadavers could be sourced for the study. We were advised against storing the cadavers at our laboratory facilities and it was not possible to keep them for a prolonged length of time at the animal unit. Therefore, the initial testing was carried out using a piece of beef steak obtained from an abattoir. However, in the later stages of the project, thanks to co-operation with Dr Mark McLaughlin from the veterinary school at the University of Glasgow and Dr Daniel Wescott from Texas State University, we were able to source rat and human post-mortem tissue for testing.

Despite the initial problems with sourcing appropriate test subjects for sampling, the project was very successful. As hypothesized, a number of biological compounds were shown to increase or decrease post-mortem. This was demonstrated using established proteomics and metabolomics methodologies. These techniques allow detection and quantification of biomolecules in any given organism. Moreover, these techniques provide a snapshot of the proteome and metabolome of an organism in a given state. In this particular case, the project involved looking at changes occurring over time in post-mortem muscle tissue (biceps femoris).

Muscle tissue is not a commonly used specimen in forensic research. Blood, vitreous humour, urine or liver are more often used. Depending on the cause or circumstances of death, blood or urine might not always be available for sampling. Also, blood coagulates and settles down in lower parts of the body, therefore, it might not always be practical to obtain a representative blood sample. However, muscle is much easier to sample as it is situated just beneath the surface of the skin. It is highly unlikely that a muscle tissue sample will not be available. Additionally, muscle tissue is more stable post-mortem, i.e. it does not degrade as fast as, for example, liver, which is rich in enzymes that can accelerate decomposition (Vass 2001).

The proteomics approach was an obvious choice for the task. Muscle tissue sampled in this study is very protein rich. Protein degradation is known to be one

of the processes occurring in decaying tissue (Vass 2001). It has been thoroughly researched in the past, mainly in studies investigating meat tenderisation processes, aiming to improve its quality as food (Koochmaraie & Geesink 2006; Kemp & Parr 2012; Nowak 2011; Lametsch et al. 2002). However, this proteolysis process was later recognised as a possible key to PMI estimation (Poloz & O'Day 2009; Pittner et al. 2015). The study described in this thesis also showed clear evidence of protein degradation, as both small and large fragments of the same proteins were detected. The proteins most often suggested as possible PMI markers are troponin (Sabucedo & Furton 2003; Kumar, Ali, Singh, et al. 2015; Pittner et al. 2015) and actin (Lametsch et al. 2002; Y. Liu et al. 2008; Xiao & Chen 2005). The results of this study also point towards these two proteins as possible markers. However, troponin was only detected in beef tissue. Actin on the other hand was detected in all three species and showed similar trends for all. Out of all of the detected proteins, it is the strongest biomarker candidate. Two other proteins also appeared as very strong candidates: myosin and heat shock protein. All three of these proteins were detected in all three species, however, a few different types of heat shock protein were found. Apart from these three proteins, the results between the species varied considerably. The protein spots on electrophoresis gels picked for analysis were selected on the basis of the measured change in the protein level. However, this was limited by a number of factors in the 2DE approach, mainly the efficiency of the protein precipitation and separation, the quality and efficiency of the reagents used as well as the quality of the gel images. These and other factors can influence how the gel looks and how many protein spots can be detected by the software and successfully matched between the gels. This, as well as the nature of the untargeted approach, means that there is no guarantee that the results will be reproducible, which of course does not mean that for example troponin, does not behave in similar way in rat and beef tissue. It just has not been detected. In order to fully investigate the potential candidates discovered in this study, it should be followed by more experiments employing a targeted approach. This way the samples could be tested for particular proteins and any common trends could be investigated further.

The proteomics approach was very successful. The initial hypothesis was proven and potential protein PMI biomarkers were found. However, the 2DE approach

used is a very time consuming and expensive technique. A single 2DE experiment can take up to two weeks to complete from start to finish; therefore, it would be impractical to employ it as a routine tool of PMI estimation. Of course, this approach could be just the initial step of the biomarker discovery and once validated, other methods of detection could be used routinely, for example assays targeting specific proteins. This would require further testing to pinpoint a specific protein as a marker. Due to the complexity of the proteome, involving large numbers of potential protein types and modifications, this might be a challenging task. Additionally, proteins can be quite unstable and are susceptible to further degradation during the extraction process if inappropriately handled. Undoubtedly, when using muscle tissue as a test specimen, protein extraction will be required.

The extraction protocol for the LC-MS metabolomics approach was much shorter and did not involve as many steps as the protein extraction protocol. In the case of the GC-MS approach, sample derivatisation is required which adds more steps to the sample preparation. Metabolomics profiling aims to detect small molecules present in the sample, which is easier to carry out than detection and identification of large proteins. Hundreds or even thousands of compounds can be detected simultaneously in a single experiment and putatively identified through a search in a reference database. The identity of many of these compounds can also be verified through the inclusion of appropriate standards in the experiment, multiple compounds at a time. As a result, the metabolomics approach is perhaps better equipped to develop high throughput assays for biomarker detection.

As expected, the metabolomics study resulted in a number of possible biomarker candidates, mainly proteogenic amino acids, but also other products of amino acid metabolism, decomposition products, and metabolites involved in purine, pyrimidine and other pathways. Two different approaches were used in this case, liquid and gas chromatography, both coupled to mass spectrometry. The first approach yielded higher numbers of detected metabolites, most probably because the LC-MS protocol is a well-established and routinely used at Glasgow Polyomics, whereas, the GC-MS protocol was somewhat a trial run. Both methods pointed towards proteogenic amino acids as the best biomarker candidates and the results were very similar, yet not for all compounds. The similarities

between results from the two methods were quite reassuring and put more confidence into the obtained results. The GC-MS approach was slightly more problematic in terms of the sample preparation and method optimisation; however, it has a potential to offer high sensitivity and reproducibility. Additionally, fragmentation patterns are highly reproducible between different instruments, which gives the possibility to create public libraries (Garcia & Barbas 2011). These two approaches, where possible, are best used as complementary techniques. They can detect different classes of compounds which increases the experimental coverage of the metabolome. This was apparent in this study. The LC-MS approach yielded a large amount of data and many possible biomarker candidates, yet the GC-MS approach still managed to add to the list and certain compounds detected in the GC dataset were not present in the LC dataset.

Liquid and gas chromatography are both widely used in forensic laboratories for various purposes (e.g. toxicological analysis). Therefore, it would be quite feasible to implement a PMI estimation method based on one or both of these techniques. Ideally, however, it would be best to translate the developed method into a smaller, easy to use assay, for example ELISA (enzyme-linked immunosorbent assay), which could detect the levels of specific proteins or other markers. A quick assay would save a lot of time and significantly reduce the cost of the testing. Therefore, a commercially available amino acid assay (phenylalanine) was tested to see if it could be implemented as a new method of PMI estimation. Tissue from two human subjects was tested with this assay and even though tests were carried out to find an appropriate dilution of the extracted samples, levels for one of the subjects were outwith the calibration. Also the trends of change measured with the assay differed significantly from those measured with the LC-MS method. This could be due to cross-reactivity of tyrosine present in the sample. More work is required to further optimise the sample preparation and validate the method in order to improve the results of the assay. There was not enough time and reagents left in the kit to test all of the possible pre-treatment steps. Nevertheless, commercially available amino acid assays may well be suitable for this kind of testing.

Despite the initial difficulties with sourcing appropriate samples, the project progressed well. As intended, possible biomarker candidates were discovered,

through both proteomic and metabolomics approaches. The data collected confirmed some of the previous findings in the field and added a few new possible biomarker candidates. To the best of the author's knowledge, xanthine, uracil, choline phosphate, n-acetylneuraminate and n-acetyl-lysine, have not been previously suggested as PMI markers.

This project is the first step towards a new method of PMI estimation. To take this project further, more testing including more test subjects would be required to validate the results. However, it would be more useful to monitor the changes in bodies decaying at room temperature. Here, the facilities were limited; therefore, the bodies were kept in the fridge during testing. The decomposition process was still apparent, but it is unlikely that corpses being the subject of forensic investigation would be kept in refrigerated conditions until discovery. Additionally, if some of the cadavers would be kept outdoors, it would be best to find a better way of closing up the incision point or sample different sites of the muscle. Over 3 days, insects enter the incision, which made further sampling very difficult, if not impossible. Moreover, the activity of insect larvae present would influence the way the tissue decomposes. As a result, it might not be comparable to tissue decomposing under the skin. The same could be said about leaving the incision site opened over the few days of sampling as contact with oxygen will definitely influence the processes occurring in the tissue. Maybe various smaller sampling sites could be made on different days to avoid this or a needle muscle biopsy approach could be used. In this type of study it is of utmost importance to keep as many factors as possible constant, while sampling the same subjects at different time points.

The next step after further tests involving a larger number of test subjects would be targeted analysis involving the compounds of interest. The extraction method could potentially be improved to focus on certain groups of compounds, especially in the proteomics approach. All of the compounds of interest should be evaluated separately, as well as collectively, as perhaps a ratio between certain compounds would be a better indicator of PMI than a single compound alone. Targeted analysis would be the key; however, only semi-quantitative approaches will be useful. As discussed in the previous chapter, concentrations of the same compounds between different people will most certainly vary, therefore, similar trends or rates of change will be more useful to try to

establish any possible mathematical formulae describing these trends. Finally, after all of these compounds are appropriately verified and tested, the results of the study should be translated to a much faster and more easily applied approach. If this test was to be implemented in forensic mass-spectrometry laboratories, then a fast, high throughput, possibly automated approach would be the best. This project was the first step in a long process of implementing a new method of PMI estimation. However, it was a big step, bringing us closer to achieve this goal.

## Appendices

Please see the attached files.

- I. Supplementary data: List of proteins identified in the trial proteomics experiment (beef tissue) - Excel spreadsheet
- II. Supplementary data: List of proteins identified in the second proteomics experiment (beef tissue) - Excel spreadsheet
- III. Supplementary data: List of proteins identified in the 2DE proteomics experiment (rat tissue) - Excel spreadsheet
- IV. Supplementary data: List of proteins identified in the 2DE proteomics experiment (human tissue, subject 2) - Excel spreadsheet
- V. Supplementary data: Metabolomic dataset comparing all beef samples collected at various times post-mortem (LC-MS, pHILIC separation) - IDEOM macro-enabled spreadsheet
- VI. Supplementary data: Metabolomic dataset comparing all beef samples collected at various times post-mortem (LC-MS, HILIC separation) - IDEOM macro-enabled spreadsheet
- VII. Supplementary data: Metabolomic dataset comparing all rat samples collected at various times post-mortem (LC-MS, pHILIC separation) - IDEOM macro-enabled spreadsheet
- VIII. Supplementary data: Metabolomic dataset comparing all rat samples collected at various times post-mortem (LC-MS, HILIC separation) - IDEOM macro-enabled spreadsheet
- IX. Supplementary data: Metabolomic dataset comparing all samples collected from subject 1 (LC-MS, pHILIC separation) - IDEOM macro-enabled spreadsheet
- X. Supplementary data: Metabolomic dataset comparing all samples collected from subject 1 (LC-MS, HILIC separation) - IDEOM macro-enabled spreadsheet
- XI. Supplementary data: Metabolomic dataset comparing all samples collected from subject 2 (LC-MS, pHILIC separation) - IDEOM macro-enabled spreadsheet
- XII. Supplementary data: Metabolomic dataset comparing all samples collected from subject 2 (LC-MS, HILIC separation) - IDEOM macro-enabled spreadsheet
- XIII. Supplementary data: Metabolomic dataset comparing all samples collected from subject 3 (LC-MS, pHILIC separation) - IDEOM macro-enabled spreadsheet

- XIV. Supplementary data: Metabolomic dataset comparing all samples collected from subject 3 (LC-MS, HILIC separation) - IDEOM macro-enabled spreadsheet
- XV. Supplementary data: Metabolomic dataset comparing all samples collected from subject 4 (LC-MS, pHILIC separation) - IDEOM macro-enabled spreadsheet
- XVI. Supplementary data: Metabolomic dataset comparing all samples collected from subject 4 (LC-MS, HILIC separation) - IDEOM macro-enabled spreadsheet
- XVII. Supplementary data: Metabolomic dataset comparing all samples collected from subject 5 (LC-MS, pHILIC separation) - IDEOM macro-enabled spreadsheet
- XVIII. Supplementary data: Metabolomic dataset comparing all samples collected from subject 5 (LC-MS, HILIC separation) - IDEOM macro-enabled spreadsheet
- XIX. Supplementary data: Metabolomic dataset comparing all samples collected from subject 6 (LC-MS, pHILIC separation) - IDEOM macro-enabled spreadsheet
- XX. Supplementary data: Metabolomic dataset comparing all samples collected from subject 6 (LC-MS, HILIC separation) - IDEOM macro-enabled spreadsheet
- XXI. Supplementary data: Metabolites of interest detected in rat tissue using the GC-MS approach - Excel spreadsheet
- XXII. Supplementary data: Metabolites of interest detected in human tissue using the GC-MS approach - Excel spreadsheet

## List of References

- Abdallah, C., Dumas-Gaudot, E., Renaut & J. Sergeant, K., 2012. Gel-based and gel-free quantitative proteomics approaches at a glance. *International Journal of Plant Genomics*, 2012(Article ID 494572), p.17 pages. Available at:  
<http://www.pubmedcentral.nih.gov/articlerender.fcgi?artid=3508552&tool=pmcentrez&rendertype=abstract> [Accessed December 12, 2013].
- Adelson, L., Sunshine, I., Rushforth, N.B. & Mankoff, M., 1963. Vitreous potassium concentration as an indicator of postmortem interval. *Journal of Forensic Sciences*, 8(4), pp.503-14.
- Ahmad, Y. & Lamond, A.I., 2014. A perspective on proteomics in cell biology. *Trends in Cell Biology*, 24(4), pp.257-264. Available at:  
<http://dx.doi.org/10.1016/j.tcb.2013.10.010>.
- Alban, A., David, S.O., Bjorkesten, L., Andersson, C., Sloge, E., Lewis, S. & Currie, I., 2003. A novel experimental design for comparative two-dimensional gel analysis: Two-dimensional difference gel electrophoresis incorporating a pooled internal standard. *Proteomics*, 3, pp.36-44.
- Alibegović, A., 2014. Cartilage: A new parameter for the determination of the postmortem interval? *Journal of Forensic and Legal Medicine*, 27, pp.39-45. Available at:  
<http://linkinghub.elsevier.com/retrieve/pii/S1752928X14001528> [Accessed August 21, 2014].
- Anders, S., Kunz, M., Gehl, A., Sehner, S., Raupach, T. & Beck-Bornholdt, H.P., 2013. Estimation of the time since death--reconsidering the re-establishment of rigor mortis. *International Journal of Legal Medicine*, 127(1), pp.127-30. Available at:  
<http://www.ncbi.nlm.nih.gov/pubmed/22015934> [Accessed January 21, 2014].
- Anderson, M.J., Lonergan, S.M., Fedler, C.A., Prusa, K.J., Binning, J.M. & Huff-

- Lonergan, E., 2012. Profile of biochemical traits influencing tenderness of muscles from the beef round. *Meat Science*, 91(3), pp.247-254. Available at: <http://www.ncbi.nlm.nih.gov/pubmed/22386323> [Accessed January 7, 2014].
- Anderson, N.L. & Anderson, N.G., 1998. Proteome and proteomics: New technologies, new concepts, and new words. *Electrophoresis*, 19, pp.1853-1861.
- Arab, L., 2004. Individualized nutritional recommendations: do we have the measurements needed to assess risk and make dietary recommendations? *Proceedings of the Nutrition Society*, 63, pp.167-172.
- Aydin, B., Colak B., Balci, Y. & Demirüstü, C., 2010. Consistency of postmortem interval estimations of physicians using only postmortem changes of putrefied dead bodies. *The American Journal of Forensic Medicine and Pathology*, 31(3), pp.243-6. Available at: <http://www.ncbi.nlm.nih.gov/pubmed/20634667> [Accessed January 21, 2014].
- Balan, P., Kim, Y.H.B. & Blijenburg, R., 2014. Small heat shock protein degradation could be an indicator of the extent of myofibrillar protein degradation. *Meat Science*, 97(2), pp.220-222. Available at: <http://dx.doi.org/10.1016/j.meatsci.2014.01.019>.
- Balasooriya, B.A.W., St. Hill, C.A. & Williams, A.R., 1984. The biochemistry of vitreous humour. A comparative study of the potassium, sodium and urate concentrations in the eyes at identical time intervals after death. *Forensic Science International*, 26(2), pp.85-91. Available at: <http://www.ncbi.nlm.nih.gov/pubmed/6489885>.
- Banaschak, S., Rzanny, R., Reichenbach, J.R., Kaiser, W.A. & Klein, A., 2005. Estimation of postmortem metabolic changes in porcine brain tissue using <sup>1</sup>H-MR spectroscopy--preliminary results. *International Journal of Legal Medicine*, 119(2), pp.77-9. Available at: <http://www.ncbi.nlm.nih.gov/pubmed/15578198> [Accessed November 28,

2014].

- Bauer, M., Gramlich, I., Polzin, S. & Patzelt, D., 2003. Quantification of mRNA degradation as possible indicator of postmortem interval—a pilot study. *Legal Medicine*, 5(4), pp.220-227. Available at: <http://linkinghub.elsevier.com/retrieve/pii/S1344622303000853> [Accessed January 21, 2014].
- Beecher, C.W.W., 2003. The human metabolome. In G. G. Harrigan & R. Goodacre, eds. *Metabolic Profiling: its Role in Biomarker Discovery and Gene Function Analysis*. Kluwer Academic Publishers, pp. 311-319.
- Bilheux, H.Z., Cekanova, M., Vass, A.A., Nichols, T.L., Bilheux, J.C., Donnell, R.L. & Finochiarro, V., 2015. A novel approach to determine post mortem interval using neutron radiography. *Forensic Science International*, 251, pp.11-21. Available at: <http://linkinghub.elsevier.com/retrieve/pii/S0379073815000833>.
- Bisegna, P., Henßge, C., Althaus, L. & Giusti, G., 2008. Estimation of the time since death: sudden increase of ambient temperature. *Forensic Science International*, 176(2-3), pp.196-9. Available at: <http://www.ncbi.nlm.nih.gov/pubmed/18029125> [Accessed November 27, 2014].
- Blackstock, W.P. & Weir, M.P., 1999. Proteomics: quantitative and physical mapping of cellular proteins. *Trends in Biotechnology*, 17(3), pp.121-127.
- Blasco, H., Nadal-Desbarats, L., Pradat, P.F., Gordon, P.H., Antar, C., Veyrat-Durebex, C., Moreau, C., Devos, D., Mavel, S., Emond, P., Andres, C.R. & Corcia, P., 2014. Untargeted 1H-NMR metabolomics in CSF: Toward a diagnostic biomarker for motor neuron disease. *Neurology*, 82(13), pp.1167-1174.
- Bocaz-Beneventi, G., Tagliaro, F., Bortolotti, F., Manetto, G. & Havel, J., 2002. Capillary zone electrophoresis and artificial neural networks for estimation of the post-mortem interval (PMI) using electrolytes measurements in human

vitreous humour. *International Journal of Legal Medicine*, 116(1), pp.5-11.

- Boehm, J., Schmidt, U., Porsche, M., Veeck, J. & Schaefer, H.E., 2012. Post-mortem analysis of bone marrow osteoclasts using tartrate-resistant acid phosphatase staining: does histochemistry work and correlate with time since death? *Journal of Clinical Pathology*, 65(11), pp.1013-8. Available at: <http://www.ncbi.nlm.nih.gov/pubmed/22844067> [Accessed January 21, 2014].
- Bortolotti, F., Pascali, J.P., Davis, G.G., Smith, F.P., Brissie, R.M. & Tagliaro, F., 2011. Study of vitreous potassium correlation with time since death in the postmortem range from 2 to 110 hours using capillary ion analysis. *Medicine, Science, and the Law*, 51, pp.S20-3. Available at: <http://www.ncbi.nlm.nih.gov/pubmed/22021629> [Accessed April 8, 2014].
- Brion, F., Marc, B., Launay, F., Gailliedreau, J. & Durigon, M., 1991. Postmortem interval estimation by creatinine levels in human psoas muscle. *Forensic Science International*, 52, pp.113-120.
- Brooker, R.J., Widmaier, E.P., Graham, L.E. & Stiling, P.D., 2014. *Biology* 3rd ed., New York, NY: McGraw-Hill Education.
- Camba, A., Lendoiro, E., Cordeiro, C., Martinez-Silva, I., Calvo-Rodriguez, M.S., Vieira, D.N. & Munoz-Barus, J.I., 2014. High variation in hypoxanthine determination after analytical treatment of vitreous humor samples. *Forensic Science, Medicine, and Pathology*, 10(4), pp.627-33. Available at: <http://www.ncbi.nlm.nih.gov/pubmed/25119241> [Accessed November 21, 2014].
- Campbell, N.A. & Reece, J.B., 2005. *Biology* 7th ed. B. Wilbur et al., eds., San Francisco, CA: Benjamin Cummings, Pearson Education.
- Chandrakanth, H. V., Kanchan T., Balaraj, B.M., Virupaksha, H.S. & Chandrashekar, T.N., 2013. Postmortem vitreous chemistry--an evaluation of sodium, potassium and chloride levels in estimation of time since death (during the first 36 h after death). *Journal of Forensic and Legal Medicine*,

20(4), pp.211-6. Available at:  
<http://www.ncbi.nlm.nih.gov/pubmed/23622461> [Accessed November 25, 2014].

Clark, M.A., Worell, M.B. & Pless, J.E., 1997. Post-mortem changes in soft tissues. In W. D. Haglund & M. H. Sorg, eds. *Forensic taphonomy: the postmortem fate of human remains*. Boca Raton, Florida: CRC Press, pp. 151-60.

Clarke, C.J. & Haselden, J.N., 2008. Metabolic profiling as a tool for understanding mechanisms of toxicity. *Toxicologic Pathology*, 36, pp.140-147.

Cockle, D.L. & Bell, L.S., 2015. Human decomposition and the reliability of a “Universal” model for post mortem interval estimations. *Forensic Science International*, 253, p.136.e1-136.e9. Available at:  
<http://www.sciencedirect.com/science/article/pii/S037907381500211X%5Cnhttp://linkinghub.elsevier.com/retrieve/pii/S037907381500211X>.

Corradini, B., Alu, M., Radheshi, E., Gabbolini, V., Ferrari, F., Santunione, A.L. & Silingardi, E., 2015. Estimation of the time of death through the analysis of clock miRNAs expression in blood and vitreous humor. *Forensic Science International: Genetics Supplement Series*, 5, pp.e204-e206.

Cortes, C. & Vapnik, V., 1995. Support-Vector Networks. *Machine Learning*, 20, pp.273-297.

Creek, D.J., Jankevics, A., Burgess, K.E.V., Breitling, R. & Barrett, M.P., 2012. IDEOM: an Excel interface for analysis of LC-MS-based metabolomics data. *Bioinformatics*, 28(7), pp.1048-1049. Available at:  
<http://www.pubmedcentral.nih.gov/articlerender.fcgi?artid=3337394&tool=pmcentrez&rendertype=abstract> [Accessed May 29, 2014].

Creek, D.J., Jankevics, A., Breitling, R., Watson, D.G., Barrett, M.P. & Burgess, K.E.V., 2011. Toward global metabolomics analysis with hydrophilic interaction Liquid Chromatography-Mass Spectrometry: improved metabolite

identification by retention time prediction. *Analytical Chemistry*, 83, pp.8703-8710.

Cubbon, S., Bradbury, T., Wilson, J. & Thomas-Oates, J., 2007. Hydrophilic interaction chromatography for mass spectrometric metabonomic studies of urine. *Analytical Chemistry*, 79, pp.8911-8918.

Cuperlovic-Culf, M. & Culf, A.S., 2016. Applied metabolomics in drug discovery. *Expert Opinion on Drug Discovery*, 11(8), pp.759-770.

Dabbs, G.R., 2010. Caution! All data are not created equal: The hazards of using National Weather Service data for calculating accumulated degree days. *Forensic Science International*, 202, pp.e49-e52. Available at: <http://dx.doi.org/10.1016/j.forsciint.2010.02.024>.

Dawson, R.M.C., 1955. Phosphorylcholine in Rat Tissues. *Biochemical Journal*, 60(2), pp.325-328.

Dekeirsschieter, J., Verheggen, F.J., Gohy, M., Hubrecht, F., Bourguignon, L., Lognay, G. & Haubruge, E., 2009. Cadaveric volatile organic compounds released by decaying pig carcasses (*Sus domesticus* L.) in different biotopes. *Forensic Science International*, 189(1-3), pp.46-53. Available at: <http://www.ncbi.nlm.nih.gov/pubmed/19423246> [Accessed January 21, 2014].

Dekeirsschieter, J., Stefanuto, P.H., Brasseur, C., Haubruge, E. & Focant, J.F., 2012. Enhanced characterization of the smell of death by comprehensive two-dimensional gas chromatography-time-of-flight mass spectrometry (GCxGC-TOFMS). *PloS One*, 7(6), p.e39005. Available at: <http://www.pubmedcentral.nih.gov/articlerender.fcgi?artid=3377612&tool=pmcentrez&rendertype=abstract> [Accessed January 21, 2014].

Dhingra, V., Gupta, M., Andacht, T. & Fu, Z.F., 2005. New frontiers in proteomics research: A perspective. *International Journal of Pharmaceutics*, 299, pp.1-18.

Dinis-Oliveira, R.J., 2016. Metabolomics of Methylphenidate and Ethylphenidate: Implications in Pharmacological and Toxicological Effects. *European Journal of Drug Metabolism and Pharmacokinetics*, [Epub ahead of print].

Dokgöz, H., Arican, N., Elmas, I. & Fincanci, S.K., 2001. Comparison of morphological changes in white blood cells after death and in vitro storage of blood for the estimation of postmortem interval. *Forensic Science International*, 124(1), pp.25-31. Available at: <http://www.ncbi.nlm.nih.gov/pubmed/11741756>.

Domon, B. & Aebersold, R., 2010. Options and considerations when selecting a quantitative proteomics strategy. *Nature Biotechnology*, 28(7), pp.710-721. Available at: <http://dx.doi.org/10.1038/nbt.1661>.

Donaldson, A.E. & Lamont, I.L., 2013. Biochemistry changes that occur after death: potential markers for determining post-mortem interval. *PLoS One*, 8(11), p.e82011. Available at: <http://www.pubmedcentral.nih.gov/articlerender.fcgi?artid=3836773&tool=pmcentrez&rendertype=abstract> [Accessed January 7, 2014].

Donaldson, A. E. & Lamont, I.L., 2014. Metabolomics of post-mortem blood: identifying potential markers of post-mortem interval. *Metabolomics*, 11(1), pp.237-245. Available at: <http://link.springer.com/10.1007/s11306-014-0691-5> [Accessed January 20, 2015].

Dunn, W.B., Broadhurst, D., Begley, P., Zelena, E., Francis-McIntyre, S., Anderson, N., Brown, M., Knowles, J.D., Halsall, A., Haselden, J.N., Nicholls, A.W., Wilson, I.D., Kell, D.B., Goodacre, R. & HUSERMET Consortium, 2011. Procedures for large-scale metabolic profiling of serum and plasma using gas chromatography and liquid chromatography coupled to mass spectrometry. *Nature Protocols*, 6(7), pp.1060-1083.

Elia, M., Carter, A., Bacon, S., Winearls, C.G. & Smith, R., 1981. Clinical usefulness of urinary 3-methylhistidine excretion in indicating muscle protein breakdown. *British Medical Journal (Clinical Research ed.)*, 282(6261), pp.351-354.

- Ellingsen, C.L. & Hetland, O., 2004. Serum Concentrations of Cardiac Troponin T in Sudden Death. *The American Journal of Forensic Medicine and Pathology*, 25(3), pp.213-215.
- Eloh, K., Sasanelli, N., Maxia, A. & Caboni, P., 2016. Untargeted Metabolomics of Tomato Plants after Root-Knot Nematode Infestation. *Journal of Agricultural and Food Chemistry*, 64, pp.5963-8.
- Estracanholti, É.S., Kurachi, C., Vicente, J.R., Campos de Menezes, P.F., Castro e Silva Junior, O. & Bagnato, V.S., 2009. Determination of post-mortem interval using in situ tissue optical fluorescence. *Optics Express*, 17(10), pp.8185-8192.
- Everett, B.M., Brooks, M.M., Vlachos, H.E.A., Chaitman, B.R., Frye, R.L. & Bhatt, D.L., 2015. Troponin and Cardiac Events in Stable Ischemic Heart Disease and Diabetes. *N Engl J Med.*, 373(7), pp.610-620.
- Fan, L., Yin, M., Ke, C., Ge, T., Zhang, G., Zhang, W. & Zhou, X., 2016. Use of Plasma Metabolomics to Identify Diagnostic Biomarkers for Early Stage Epithelial Ovarian Cancer. *Journal of Cancer*, 7, pp.1265-72.
- Fanos, V., Caboni, P., Corsello, G., Stronati, M., Gazzolo, D., Noto, A., Lussu, M., Dessi, A., Giuffre, M., Lacerenza, S., Serraino, F., Garofoli, F., Serpero, L.D., Liori, B., Carboni, R. & Atzori, L., 2014. Urinary 1 H-NMR and GC-MS metabolomics predicts early and late onset neonatal sepsis. *Early Human Development*, 90 Suppl 1, pp.78-83.
- Fatfeh, A., 1973. *Handbook of Forensic Pathology*, Philadelphia: Lippincott.
- Fedele, T.A., Galdos-Riveros, A.C., de Farias e Melo, H.J., Magalhaes, A. & Maria, D.A., 2013. Prognostic relationship of metabolic profile obtained of melanoma B16F10. *Biomedicine & Pharmacotherapy*, 67(2), pp.146-156.  
Available at:  
<http://linkinghub.elsevier.com/retrieve/pii/S0753332212001059>.
- Finehout, E.J., Franck, Z., Relkin, N. & Lee, K.H., 2006. Proteomic analysis of

cerebrospinal fluid changes related to postmortem interval. *Clinical Chemistry*, 52(10), pp.1906-13. Available at: <http://www.ncbi.nlm.nih.gov/pubmed/16887899> [Accessed February 21, 2014].

Frylinck, L., Strydom, P.E., Webb, E.C. & du Toit, E., 2013. Effect of South African beef production systems on post-mortem muscle energy status and meat quality. *Meat Science*, 93, pp.827-837. Available at: <http://dx.doi.org/10.1016/j.meatsci.2012.11.047>.

Gallois-Montbrun, G.F., Barres, D.R. & Durigon, M., 1988. Postmortem interval estimation by biochemical determination in birds muscle. *Forensic Science International*, 37(3), pp.189-92.

Garcia, A. & Barbas, C., 2011. Gas Chromatography-Mass Spectrometry (GC-MS)-Based Metabolomics. *Methods in Molecular Biology*, 708, pp.191-204.

Gardiner, E.E., Newberry, R.C. & Keng, J.-Y., 1989. Postmortem Time and Storage Temperature Affect the Concentrations of Hypoxanthine, other Purines, Pyrimidines, and Nucleosides in Avian and Porcine Vitreous Humor. *Pediatric Research*, 26(6), pp.639-640.

Geesink, G.H. & Koohmaraie, M., 1999. Postmortem proteolysis and calpain/calpastatin activity in callipyge and normal lamb biceps femoris during extended postmortem storage. *Journal of Animal Science*, 77(6), pp.1490-1501.

German, J.B., Bauman, D.E., Burrin, D.G., Failla, M.L., Freake, H.C., King, J.C., Klein, S., Milner, J.A., Pelto, G.H., Rasmussen, K.M. & Zeisel, S.H., 2004. Metabolomics in the Opening Decade of the 21st Century : Building the Roads to Individualized Health. *The Journal of Nutrition*, 134, pp.2729-2732.

German, J.B., Roberts, M. & Watkins, S.M., 2003. Personal Metabolomics as a Next Generation Nutritional Assessment. *The Journal of Nutrition*, 133(12), pp.4260-4266.

- Gill-King, H., 1997. Chemical and ultrastructural aspects of decomposition. In W. D. Haglund & M. H. Sorg, eds. *Forensic taphonomy: the postmortem fate of human remains*. Boca Raton, Florida: CRC Press, pp. 93-104.
- Gillis, J.D., Price, G.W. & Prasher, S., 2016. Lethal and sub-lethal effects of triclosan toxicity to the earthworm *Eisenia fetida* assessed through GC-MS metabolomics. *Journal of Hazardous Materials*, [Epub ahead of time]. Available at: <http://dx.doi.org/10.1016/j.jhazmat.2016.07.022>.
- Girela, E., Villanueva, E., Irigoyen, P., Girela, V., Hernandez-Cueto, C. & Peinado, J.M., 2008. Free amino acid concentrations in vitreous humor and cerebrospinal fluid in relation to the cause of death and postmortem interval. *Journal of Forensic Sciences*, 53(3), pp.730-3. Available at: <http://www.ncbi.nlm.nih.gov/pubmed/18471224> [Accessed February 21, 2014].
- Goff, M.L., 2009. Early post-mortem changes and stages of decomposition in exposed cadavers. *Experimental and Applied Acarology*, 49(1-2), pp.21-36.
- Goll, D.E., Otsuka, Y., Nagainis, P.A., Shannon, J.D., Sathe, S.K. & Muguruma, M., 1983. Role of muscle proteinases in maintenance of muscle integrity and mass. *Journal of Food Biochemistry*, 7(3), pp.137-177.
- Goll, D.E., Thompson, V.F., Taylor, R.G. & Christiansen, J.A., 1992. Role of the calpain system in muscle growth. *Biochimie*, 74, pp.225-237.
- González-Domínguez, R., García-Barrera, T. & Gómez-Ariza, J.L., 2014. Metabolomic study of lipids in serum for biomarker discovery in Alzheimer's disease using direct infusion mass spectrometry. *Journal of Pharmaceutical and Biomedical Analysis*, 98, pp.321-326. Available at: <http://linkinghub.elsevier.com/retrieve/pii/S0731708514002635>.
- Goodacre, R., Vaidyanathan, S., Dunn, W.B., Harrigan, G.G. & Kell, D.B., 2004. Metabolomics by numbers: acquiring and understanding global metabolite data. *Trends in Biotechnology*, 22(5), pp.245-252.

- Gos, T. & Raszeja, S., 1993. Postmortem activity of lactate and malate dehydrogenase in human liver in relation to time after death. *International Journal of Legal Medicine*, 106, pp.25-9. Available at: <http://www.ncbi.nlm.nih.gov/pubmed/8398887>.
- Grabski, A.C. & Burgess, R.R., 2001. Preparation of protein samples for SDS-polyacrylamide gel electrophoresis: procedures and tips. *InNovations*, 13, pp.10-12.
- Griffiths, W.J. & Wang, Y., 2009. Mass spectrometry: from proteomics to metabolomics and lipidomics. *Chemical Society Reviews*, 38, pp.1882-1896.
- Häggsström, M., 2014. Medical gallery of Mikael Häggström 2014. *WikiJournal of Medicine* 1 (2). DOI:10.15347/wjm/2014.008. ISSN 2002-4436. Public Domain.
- Harada, M., Maeiwa, M., Yoshikawa, K. & Ohsaka, A., 1984. Identification and quantitation by <sup>1</sup>H-NMR of metabolites in animal organs and tissues. An application of NMR spectroscopy in forensic science. *Forensic Science International*, 24, pp.1-7.
- Hauther, K.A., Cobaugh, K.L., Meadows Jantz, L., Sparer, T.E. & DeBruyn, J.M., 2015. Estimating Time Since Death from Postmortem Human Gut Microbial Communities. *Journal of Forensic Sciences*, 60(5), pp.1234-1240.
- Henssge, C., 1988. Death time estimation in case work. I. the rectal temperature time of death nomogram. *Forensic Science International*, 38, pp.209-236.
- Henssge, C., Althaus, L., Bolt, J., Freisleder, A., Haffner, H.-T., Henssge, C.A., Hoppe, B. & Schneider, V., 2000. Experiences with a compound method for estimating the time since death: I. Rectal temperature nomogram for time since death. *International Journal of Legal Medicine*, 113, pp.303-319.
- Henssge, C., Madea, B., Krompecher, T. & Nokes, L., 2002. *The estimation of the time since death in the early postmortem period* 2nd ed. B. Knight, ed.,

London: Arnold Publishing.

- Hirakawa, K., Koike, K., Uekusa, K., Nihira, M., Yuta, K. & Ohno, Y., 2009. Experimental estimation of postmortem interval using multivariate analysis of proton NMR metabolomic data. *Legal Medicine*, 11, pp.S282-S285. Available at: <http://dx.doi.org/10.1016/j.legalmed.2009.02.007>.
- Hoerr, V., Duggan, G.E., Zbytnuik, L., Poon, K.H., Große, C., Neugebauer, U., Methling, K., Löffler, B. & Vogel, H.J., 2016. Characterization and prediction of the mechanism of action of antibiotics through NMR metabolomics. *BMC Microbiology*, 16(82). Available at: <http://dx.doi.org/10.1186/s12866-016-0696-5>.
- Hoffman, E.M., Curran, A.M., Dulgerian, N., Stockham, R.A. & Eckenrode, B.A., 2009. Characterization of the volatile organic compounds present in the headspace of decomposing human remains. *Forensic Science International*, 186, pp.6-13.
- Hoshino, J., Schluter, U. & Kroger, H., 1984. Nicotinamide methylation and its relation to NAD synthesis in rat liver tissue culture. Biochemical basis for the physiological activities of 1-methylnicotinamide. *Biochimica et Biophysica Acta*, 801, pp.250-258.
- Hubig, M., Muggenthaler, H., Sinicina, I. & Mall, G., 2011. Body mass and corrective factor: impact on temperature-based death time estimation. *International Journal of Legal Medicine*, 125(3), pp.437-44. Available at: <http://www.ncbi.nlm.nih.gov/pubmed/21286739> [Accessed November 26, 2014].
- Hubig, M., Muggenthaler, H. & Mall, G., 2015. Confidence intervals in temperature-based death time determination. *Legal Medicine*, 17(1), pp.48-51. Available at: <http://www.ncbi.nlm.nih.gov/pubmed/25205513> [Accessed November 25, 2014].
- Huff-lonergan, E.J. & Beekman, D.D., 1996. Proteolysis of specific muscle structural proteins by mu-calpain at low pH and temperature is similar to

degradation in postmortem bovine muscle. *Journal of Animal Science*, 74, pp.993-1008.

Hunter, W.G., Kelly, J.P., Mcgarrah, R.W., Khouri, M.G., Craig, D., Haynes, C., Ikayeva, O., Stevens, R.D., Bain, J.R., Muehlbauer, M.J., Newgard, C.B., Felker, G.M., Hernandez, A.F., Velazquez, A.F., Kraus, W.E. & Shah, S.H., 2016. Metabolomic Profiling Identifies Novel Circulating Biomarkers of Mitochondrial Dysfunction Differentially Elevated in Heart Failure With Preserved Versus Reduced Ejection Fraction: Evidence for Shared Metabolic Impairments in Clinical Heart Failure. *Journal of the American Heart Association*, 5(8), p.e003190.

Inoue, H., Kimura, A. & Tuji, T., 2002. Degradation profile of mRNA in a dead rat body : basic semi-quantification study. *Forensic Science International*, 130, pp.127-132.

Ishikawa, N., Nishida, A., Miyamori, D., Kubo, T. & Ikegaya, H., 2013. Estimation of postmortem time based on aorta narrowing in CT imaging. *Journal of Forensic and Legal Medicine*, 20(8), pp.1075-7. Available at: <http://www.ncbi.nlm.nih.gov/pubmed/24237823> [Accessed November 25, 2014].

Ith, M., Scheurer, E., Kreis, R., Thali, M., Dirnhofer, R. & Boesch, C., 2011. Estimation of the postmortem interval by means of (1) H MRS of decomposing brain tissue: influence of ambient temperature. *NMR in Biomedicine*, 24(January), pp.791-798.

Ith, M., Bigler, P., Scheurer, E., Kreis, R., Hofmann, L., Dirnhofer, R. & Boesch, C., 2002. Observation and identification of metabolites emerging during postmortem decomposition of brain tissue by means of in situ <sup>1</sup>H-magnetic resonance spectroscopy. *Magnetic Resonance in Medicine : Official Journal of the Society of Magnetic Resonance in Medicine / Society of Magnetic Resonance in Medicine*, 48(5), pp.915-20. Available at: <http://www.ncbi.nlm.nih.gov/pubmed/12418008> [Accessed January 21, 2014].

- Iwata, Y., Suzuki, O. & Wakabayashi, S., 2013. Decreased surface sialic acid content is a sensitive indicator of muscle damage. *Muscle and Nerve*, 47, pp.372-378.
- Janaway, R.C., Percival, S.L. & Wilson, A.S., 2009. Decomposition of human remains. In S. L. Percival, ed. *Microbiology and Aging. Clinical Manifestations*. New York, NY: Springer Science + Business Media, LLC, pp. 313-334. Available at: <http://link.springer.com/10.1007/978-1-59745-327-1> [Accessed February 26, 2014].
- Jashnani, K.D., Kale, S. a & Rupani, A.B., 2010. Vitreous humor: biochemical constituents in estimation of postmortem interval. *Journal of Forensic Sciences*, 55(6), pp.1523-7. Available at: <http://www.ncbi.nlm.nih.gov/pubmed/20666922> [Accessed April 8, 2014].
- Jensen, O.N., 2004. Modification-specific proteomics: characterization of post-translational modifications by mass spectrometry. *Current Opinion in Chemical Biology*, 8, pp.33-41.
- Jia, X., Hildrum, K.I., Westad, F., Kummen, E., Aass, L. & Hollung, K., 2006. Changes in Enzymes Associated with Energy Metabolism during the Early Post Mortem Period in Longissimus Thoracis Bovine Muscle Analyzed by Proteomics. *Journal of Proteome Research*, 5, pp.1763-1769.
- Jia, X., Hollung, K., Therkildsen, M., Hildrum, K.I. & Bendixen, E., 2006. Proteome analysis of early post-mortem changes in two bovine muscle types: *M. longissimus dorsi* and *M. semitendinosis*. *Proteomics*, 6(3), pp.936-944. Available at: <http://www.ncbi.nlm.nih.gov/pubmed/16372268> [Accessed January 7, 2014].
- Jiye, A. Trygg, J., Gullberg, J., Johansson, A.I., Jonsson, P., Antii, H., Marklund, S.L. & Moritz, T., 2005. Extraction and GC/MS Analysis of the Human Blood Plasma Metabolome. *Analytical Chemistry*, 77, pp.8086-8094.
- Kaddurah-Daouk, R., Kristal, B.S. & Weinshilboum, R.M., 2008. Metabolomics: A Global Biochemical Approach to Drug Response and Disease. *The Annual*

*Review of Pharmacology and Toxicology*, 48, pp.653-83.

- Kaliszan, M., Hauser, R. & Kernbach-Wighton, G., 2009. Estimation of the time of death based on the assessment of post mortem processes with emphasis on body cooling. *Legal Medicine (Tokyo, Japan)*, 11(3), pp.111-7. Available at: <http://www.ncbi.nlm.nih.gov/pubmed/19200767> [Accessed January 21, 2014].
- Kanehisa, M., 1995. Kyoto Encyclopedia of Genes and Genomes (KEGG). Available at: <http://www.genome.jp/kegg/>.
- Kanehisa, M. & Goto, S., 2000. KEGG: Kyoto encyclopedia of genes and genomes. *Nucleic Acids Research*, 28(1), pp.27-30.
- Kang, S., Kassam, N., Gauthier, M.L. & O'Day, D.H., 2003. Post-mortem changes in calmodulin binding proteins in muscle and lung. *Forensic Science International*, 131, pp.140-7. Available at: <http://www.ncbi.nlm.nih.gov/pubmed/12590053>.
- Kang, Y.-R., Park, Y.S., Park, Y.C., Yoon, S.M., JongAhn, H., Kim, G. & Kwon, S.W., 2012. UPLC/Q-TOF MS based metabolomics approach to post-mortem-interval discrimination: mass spectrometry based metabolomics approach. *Journal of Pharmaceutical Investigation*, 42(1), pp.41-46. Available at: <http://link.springer.com/10.1007/s40005-012-0006-7> [Accessed October 7, 2014].
- Kärkelä, J. & Scheinin, M., 1992. Tryptophan and biogenic amine metabolites in post-mortem human cisternal fluid: effects of post-mortem interval and agonal time. *Journal of the Neurological Sciences*, 107(2), pp.239-45. Available at: <http://www.ncbi.nlm.nih.gov/pubmed/1373441>.
- Karp, P.D., Riley, M., Paley, S.M. & Pellegrini-Toole, A., 2002. The MetaCyc Database. *Nucleic Acids Research*, 30(1), pp.59-61. Available at: <http://nar.oxfordjournals.org/content/30/1/59.short>.
- Kaszynski, R.H., Nishiumi, S., Azuma, T., Yoshida, M., Kondo, T., Takahashi, M.,

Asano, M. & Ueno, Y., 2016. Postmortem interval estimation : a novel approach utilizing gas chromatography / mass spectrometry-based biochemical profiling. *Analytical and Bioanalytical Chemistry*, pp.1-10.

Kawamoto, O., Michiue, T., Ishikawa, T. & Maeda, H., 2013. Comprehensive evaluation of pericardial biochemical markers in death investigation. *Forensic Science International*, 224(1-3), pp.73-9. Available at: <http://www.ncbi.nlm.nih.gov/pubmed/23196195> [Accessed February 21, 2014].

Kemp, C.M. & Parr, T., 2012. Advances in apoptotic mediated proteolysis in meat tenderisation. *Meat Science*, 92(3), pp.252-259. Available at: <http://dx.doi.org/10.1016/j.meatsci.2012.03.013>.

Kenny, L.C., Dunn, W.B., Ellis, D.I., Myers, J., Baker, P.N., GOPEC Consortium & Kell, D.B., 2005. Novel biomarkers for pre-eclampsia detected using metabolomics and machine learning. *Metabolomics*, 1(3), pp.227-234.

Kikuchi, K., Kawahara, K.-I., Biswas, K.K., Ito, T., Tancharoen, S., Shiomi, N., Koda, Y., Matsuda, F., Morimoto, Y., Oyama, Y., Takenouchi, K., Miura, N., Arimura, N., Nawa, Y., Arimura, S., Jie, M.X., Shrestha, B., Iwata, M., Mera, K., Sameshima, H., Ohno, Y., Maenosono, R., Tajima, Y., Uchikado, H., Kuramoto, T., Nakayama, K., Shigemori, M., Yoshida, Y., Hashiguchi, T. & Maruyama, I., 2010. HMGB1 : A new marker for estimation of the postmortem interval. *Experimental and Therapeutic Medicine*, 1, pp.109-111.

Kimura, A., Ishida, Y., Hayashi, T., Nosaka, M. & Kondo, T., 2011. Estimating time of death based on the biological clock. *International Journal of Legal Medicine*, 125(3), pp.385-91. Available at: <http://www.ncbi.nlm.nih.gov/pubmed/21069371> [Accessed January 21, 2014].

Kloet, F.M. Van Der, Tempels, F.W.A., Ismail, N., van der Heijden, R., Kasper, P.T., Rojas-Cherto, M., van Doorn, R., Spijksma, G., Koek, M., van der Greef, J., Makinen, V.P., Forsblom, C., Holthofer, H., Groop, P.H.,

Reijmers, T.H. & Hankemeier, T., 2012. Discovery of early-stage biomarkers for diabetic kidney disease using ms-based metabolomics (FinnDiane study). *Metabolomics*, 8, pp.109-119.

Kominato, Y., Kumada, K., Yamazaki, K. & Misawa, S., 1989. Estimation of Postmortem Interval Using Kinetic Analysis of the Third Component of Complement ( C3 ) Cleavage. *Journal of Forensic Sciences*, 34(1), pp.207-217.

Koohmaraie, M., 1992. The role of Ca(2+)-dependent proteases (calpains) in post mortem proteolysis and meat tenderness. *Biochimie*, 74, pp.239-245.

Koohmaraie, M. & Geesink, G.H., 2006. Contribution of postmortem muscle biochemistry to the delivery of consistent meat quality with particular focus on the calpain system. *Meat Science*, 74, pp.34-43.

Kovács, Z., Kekesi, K.A., Bobest, M., Torok, T., Szilagyi, N., Szikra, T., Szepesi, Z., Nyilas, R., Dobolyi, A., Palkovits, M. & Juhasz G., 2005. Post mortem degradation of nucleosides in the brain: comparison of human and rat brains for estimation of in vivo concentration of nucleosides. *Journal of Neuroscience Methods*, 148(1), pp.88-93. Available at: <http://www.ncbi.nlm.nih.gov/pubmed/16054224> [Accessed November 27, 2014].

Kumar, S., Ali, W., Bhattacharya, S., Singh, U.S., Kumar, A. & Verma, A.K., 2015. The effect of elapsed time on cardiac troponin-T ( cTnT ) degradation and its relation to postmortem interval in cases of electrocution. *Journal of Forensic and Legal Medicine*, 34, pp.45-49. Available at: <http://dx.doi.org/10.1016/j.jflm.2015.05.009>.

Kumar, S., Ali, W., Singh, U.S., Kumar, A., Bhattacharya, S., Verma, A.K., 2015. The effect of elapsed time on the cardiac Troponin-T (cTnT) proteolysis in case of death due to burn: A study to evaluate the potential forensic use of cTnT to determine the postmortem interval. *Science and Justice*, 55(3), pp.189-194. Available at: <http://dx.doi.org/10.1016/j.scijus.2014.12.006>.

- Lametsch, R., Roepstorff, P. & Bendixen, E., 2002. Identification of Protein Degradation during Post-mortem Storage of Pig Meat. *Journal of Agricultural and Food Chemistry*, 50, pp.5508-5512.
- Lange, N., Swearer, S. & Sturner, W.Q., 1994. Human postmortem interval estimation from vitreous potassium : an analysis of original data from six different studies. *Forensic Science International*, 66, pp.159-174.
- Larkin, B., Iaschi, S., Dadour, I. & Tay, G.K., 2010. Using accumulated degree-days to estimate postmortem interval from the DNA yield of porcine skeletal muscle. *Forensic Science, Medicine, and Pathology*, 6(2), pp.83-92. Available at: <http://www.ncbi.nlm.nih.gov/pubmed/19851896> [Accessed November 27, 2014].
- Lee, D.E., Lee, S., Jang, E.S., Shin, H.W., Moon, B.S. & Lee, C.H., 2016. Metabolomic Profiles of *Aspergillus oryzae* and *Bacillus amyloliquefaciens* During Rice Koji fermentation. *Molecules*, 21(773).
- Lendoiro, E., Cordeiro, C., Rodriguez-Calvo, M.S., Vieira, D.N., Suarez-Penaranda, J.M., Lopez-Rivadulla, M. & Munoz-Barus, J.I., 2012. Applications of Tandem Mass Spectrometry (LC-MSMS) in estimating the post-mortem interval using the biochemistry of the vitreous humour. *Forensic Science International*, 223(1-3), pp.160-4. Available at: <http://www.ncbi.nlm.nih.gov/pubmed/22981211> [Accessed January 21, 2014].
- Lenz, E.M. & Wilson, I.D., 2007. Analytical Strategies in Metabonomics. *Journal of Proteome Research*, 6, pp.443-458.
- LeWitt, P.A., Li, J., Lu, M., Beach, T.G., Adler, C.H., Guo, L. & the Arizona Parkinson's Disease Consortium, 2013. 3-hydroxykynurenine and other Parkinson's disease biomarkers discovered by metabolomic analysis. *Movement Disorders*, 28(12), pp.1653-1660. Available at: <http://doi.wiley.com/10.1002/mds.25555>.
- Li, W.-C., Kai-Jun, M., Ye-Hui, L., Ping, Z., Hui, P., Heng, Z., Hui-Jun, W., Duan,

- M. & Long, C., 2014. Postmortem interval determination using 18S-rRNA and microRNA. *Science & Justice*, 54(4), pp.307-10. Available at: <http://www.ncbi.nlm.nih.gov/pubmed/25002049> [Accessed November 21, 2014].
- Lian, T., Wang, L. & Liu, Y., 2013. A New Insight into the Role of Calpains in Post-mortem Meat Tenderization in Domestic Animals : A review. *Asian-Australasian Journal of Animal Sciences*, 26, pp.443-454.
- Lindahl, T., 1993. Instability and decay of the primary structure of DNA. *Nature*, 362, pp.709-715.
- Lindon, J.J.C., Holmes, E. & Nicholson, J.K., 2003. So what's the deal with metabonomics? *Analytical Chemistry*, 75(17), p.384A-391A. Available at: <http://ci.nii.ac.jp/naid/80016147705/>.
- Liu, Q., Sun, Q., Liu, Y., Zhou, L., Zheng, N. & Liu, L., 2009. Bioluminescent assay of microbial ATP in postmortem tissues for the estimation of postmortem interval. *Journal of Huazhong University of Science and Technology. Medical Sciences*, 29(6), pp.679-683. Available at: <http://www.ncbi.nlm.nih.gov/pubmed/20037806> [Accessed January 7, 2014].
- Liu, Q., Cai, X., Liu, Y., Zhou, L., Yi, S. & Liu, L., 2008. Spectrophotometric determination of trimethylamine-nitrogen in cadaver tissues for the estimation of late postmortem interval: a pilot study. *Journal of Huazhong University of Science and Technology. Medical Sciences*, 28(6), pp.630-3. Available at: <http://www.ncbi.nlm.nih.gov/pubmed/19107354> [Accessed November 27, 2014].
- Liu, Y., Kuai, J.X., Zhang, Y.W. & Wang, Y.Y., 2008. The relationship between the degradation of actin and the postmortem interval in rats. *Fa Yi Xue Za Zhi (Journal of Forensic Medicine)*, 24(3), pp.165-7.
- Loukas, Y.L. & Dotsikas, Y., 2011. HILIC-MS/MS for the determination of polar bioactive substances: representative applications in the fields of

pharmacokinetics and metabolic profiling. In P. G. Wang & W. He, eds. *Hydrophilic Interaction Liquid Chromatography (HILIC) and Advanced Applications*. Boca Raton, Florida: CRC Press, pp. 427-435.

Di Luca, A., Elia, G., Mullen, A.M. & Hamill, R.M., 2013. Monitoring post mortem changes in porcine muscle through 2-D DIGE proteome analysis of Longissimus muscle exudate. *Proteome Science*, 11(1), p.9. Available at: <http://www.pubmedcentral.nih.gov/articlerender.fcgi?artid=3639075&tool=pmcentrez&rendertype=abstract> [Accessed January 7, 2014].

MacRae, J.I. & Ferguson, M.A.J., 2005. A robust and selective method for the quantification of glycosylphosphatidylinositols in biological samples. *Glycobiology*, 15(2), pp.131-138.

Madea, B., 2005. Is there recent progress in the estimation of the postmortem interval by means of thanatochemistry? *Forensic Science International*, 151(2-3), pp.139-49. Available at: <http://www.ncbi.nlm.nih.gov/pubmed/15939145> [Accessed January 21, 2014].

Madea, B., Herrmann, N. & Henbge, C., 1990. Precision of estimating the time since death by vitreous potassium - comparison of two different equations. *Forensic Science International*, 46, pp.277-284.

Madea, B. & Rödiger, A., 2006. Time of death dependent criteria in vitreous humor: accuracy of estimating the time since death. *Forensic Science International*, 164(2-3), pp.87-92. Available at: <http://www.ncbi.nlm.nih.gov/pubmed/16439082> [Accessed January 21, 2014].

Mahmood, T. & Yang, P.C., 2012. Western blot: Technique, theory, and trouble shooting. *North American Journal of Medical Sciences*, 4(9), pp.429-434.

Manna, S.K., Thompson, M.D. & Gonzalez, F.J., 2015. Application of Mass Spectrometry-based metabolomics in identification of early noninvasive biomarkers of Alcohol-Induced Liver Disease using mouse model. *Advances in*

*Experimental Medicine and Biology*, 815, pp.217-238. Available at:  
<http://link.springer.com/10.1007/978-3-319-09614-8>.

Mao, S., Fu, G., Seese, R.R. & Wang, Z.-Y., 2013. Estimation of PMI depends on the changes in ATP and its degradation products. *Legal Medicine*, 15(5), pp.235-8. Available at: <http://www.ncbi.nlm.nih.gov/pubmed/23639682> [Accessed November 25, 2014].

Mao, S., Dong, X., Fu, F., Seese, R.R. & Wang, Z., 2011. Estimation of postmortem interval using an electric impedance spectroscopy technique: a preliminary study. *Science & Justice : Journal of the Forensic Science Society*, 51(3), pp.135-8. Available at: <http://www.ncbi.nlm.nih.gov/pubmed/21889110> [Accessed January 21, 2014].

Marshall, T.K. & Hoare, F.E., 1962. Estimating the time of death. The rectal cooling after death and its mathematical expression. *Journal of Forensic Sciences*, 7, pp.56-81.

Matuszewski, S., Konwerski, S., Fraczak, K. & Szafalowicz, M., 2014. Effect of body mass and clothing on decomposition of pig carcasses. *International Journal of Legal Medicine*, 128(6), pp.1039-48. Available at: <http://www.pubmedcentral.nih.gov/articlerender.fcgi?artid=4196037&tool=pmcentrez&rendertype=abstract> [Accessed November 21, 2014].

McNaught, A.D. & Wilkinson, A., 1997. *IUPAC. Compendium of Chemical Terminology (the "Gold Book")* 2nd ed., Oxford: Blackwell Scientific Publications.

Megyesi, M.S., Nawrocki, S.P. & Haskell, N.H., 2005. Using accumulated degree-days to estimate the postmortem interval from decomposed human remains. *Journal of Forensic Sciences*, 50(3), pp.618-626.

Michalczyk, M., Macura, R., Tesarowicz, I. & Banas, J., 2012. Effect of adding essential oils of coriander (*Coriandrum sativum* L.) and hyssop (*Hyssopus officinalis* L.) on the shelf life of ground beef. *Meat Science*, 90(3), pp.842-

850. Available at: <http://www.ncbi.nlm.nih.gov/pubmed/22153611>  
[Accessed January 7, 2014].

Mihailovic, Z., Atanasijevic, T., Popovic, V. & Milosevic, M.B., 2011. Could lactates in vitreous humour be used to estimate the time since death? *Medicine, Science and the Law*, 51(3), pp.156-160. Available at: <http://msl.sagepub.com/lookup/doi/10.1258/msl.2011.010124> [Accessed November 25, 2014].

Mitchell, S., Holmes, E. & Carmichael, P., 2002. Metabonomics and medicine: the Biochemical Oracle. *Biologist (London)*, 49(5), pp.217-21.

Montowska, M. & Pospiech, E., 2012. Myosin light chain isoforms retain their species-specific electrophoretic mobility after processing, which enables differentiation between six species: 2DE analysis of minced meat and meat products made from beef, pork and poultry. *Proteomics*, 12(18), pp.2879-89. Available at: <http://www.ncbi.nlm.nih.gov/pubmed/22851476>  
[Accessed June 18, 2014].

Morgan, C., Nokes, L.D.M., Williams, J.H. & Knight, B.H., 1988. Estimation of the post-mortem period by multiple-site temperature measurements and the use of a new algorithm. *Forensic Science International*, 39, pp.89-95.

Muggenthaler, H., Sinicina, I., Hubig, M. & Mall, G., 2012. Database of post-mortem rectal cooling cases under strictly controlled conditions: a useful tool in death time estimation. *International Journal of Legal Medicine*, 126(1), pp.79-87. Available at: <http://www.ncbi.nlm.nih.gov/pubmed/21538225> [Accessed November 26, 2014].

Muñoz-Barús, J.I., Rodríguez-Calvo, M.S., Suarez-Penaranda, J.M., Vieira, D.N., Cadarso-Suarez, C. & Febrero-Bande, M., 2010. PMICALC: an R code-based software for estimating post-mortem interval (PMI) compatible with Windows, Mac and Linux operating systems. *Forensic Science International*, 194(1-3), pp.49-52. Available at: <http://www.ncbi.nlm.nih.gov/pubmed/19926236> [Accessed January 7,

2014].

Muñoz, J.I., Suarez-Penaranda, J.M., Otero, X.L., Rodriguez-Calvo, M.S., Costas, E., Miguens, X. & Concheiro, L., 2001. A new perspective in the estimation of postmortem interval (PMI) based on vitreous. *Journal of Forensic Sciences*, 46(2), pp.209-14. Available at: <http://www.ncbi.nlm.nih.gov/pubmed/11714180>.

Muñoz Barús, J.I., Suarez-Penaranda, J.M., Otero, X.L., Rodriguez-Calvo, M.S., Costas, E., Miguens, X. & Concheiro, L., 2002. Improved estimation of postmortem interval based on differential behaviour of vitreous potassium and hypoxanthine in death by hanging. *Forensic Science International*, 125(1), pp.67-74.

Muñoz Barús, J.I., Febrero-Bande, M. & Cadarso-Suárez, C., 2008. Flexible regression models for estimating postmortem interval (PMI) in forensic medicine. *Statistics in Medicine*, 27(24), pp.5026-5038.

Musshoff, F., Klotzbach, H., Block, W., Traeber, F., Schild, H. & Madea, B., 2011. Comparison of post-mortem metabolic changes in sheep brain tissue in isolated heads and whole animals using <sup>1</sup>H-MR spectroscopy--preliminary results. *International Journal of Legal Medicine*, 125(5), pp.741-4. Available at: <http://www.ncbi.nlm.nih.gov/pubmed/20449751> [Accessed January 21, 2014].

Myburgh, J., L'Abbe, E.N., Steyn, M. & Becker, P.J., 2013. Estimating the postmortem interval (PMI) using accumulated degree-days (ADD) in a temperate region of South Africa. *Forensic Science International*, 229, p.165.e1-165.e6.

Nelson, E.L., 2000. Estimation of short-term postmortem interval utilizing core body temperature: a new algorithm. *Forensic Science International*, 109(1), pp.31-38. Available at: <http://linkinghub.elsevier.com/retrieve/pii/S0379073899002169>.

Nesvizhskii, A., Vitek, O. & Aebersold, R., 2007. Analysis and validation of

proteomic data generated by tandem mass spectrometry. *Nature Methods*, 4(10), pp.787-797. Available at: [citeulike-article-id:1708095%5Cnhttp://dx.doi.org/10.1038/nmeth1088](http://dx.doi.org/10.1038/nmeth1088).

Nicholson, J.K., Lindon, J.C. & Holmes, E., 1999. "Metabonomics": understanding the metabolic responses of living systems to pathophysiological stimuli via multivariate statistical analysis of biological NMR spectroscopic data. *Xenobiotica*, 29(11), pp.1181-1189. Available at: <http://www.tandfonline.com/doi/full/10.1080/004982599238047>.

Nowak, D., 2011. Enzymes in Tenderization of Meat - The System of Calpains and Other Systems - a Review. *Polish Journal of Food and Nutrition Sciences*, 61(4), pp.231-237. Available at: <http://www.degruyter.com/view/j/pjfn.2011.61.issue-4/v10222-011-0025-5/v10222-011-0025-5.xml>.

O'Farrell, P.H., 1975. High Resolution Two-Dimensional Electrophoresis of Proteins. *The Journal of Biological Chemistry*, 250(10), pp.4007-4021. Available at: <http://www.jbc.org/content/250/10/4007.short>.

Odriozola, A., Riancho, J.A., de la Vega, R., Agudo, G., Garcia-Blanco, A., de Cos, E., Fernandez, F., Sañudo, C. & Zarrabeitia, M.T., 2013. miRNA analysis in vitreous humor to determine the time of death: a proof-of-concept pilot study. *International Journal of Legal Medicine*, 127(3), pp.573-8. Available at: <http://www.ncbi.nlm.nih.gov/pubmed/23254460> [Accessed April 8, 2014].

Oliver, S.G., Winson, M.K., Kell, D.B. & Baganz, F., 1998. Systematic functional analysis of the yeast genome. *Trends in Biotechnology*, 16, pp.373-378.

OpenStax, 2013. *OpenStax, Anatomy & Physiology*,

Osuna, E., Perez-Carceles, M.D., Alvarez, M.V., Noguera, J. & Luna, A., 1998. Cardiac troponin I (cTn I) and the postmortem diagnosis of myocardial infarction. *International Journal of Legal Medicine*, 111(4), pp.173-176.

- Passos, M.L.C., Santos, A.M., Pereira, A.I., Santos, J.R., Santos, A.J.C., Saraiva, M.L.M.F.S. & Lima, J.L.F.C., 2009. Estimation of postmortem interval by hypoxanthine and potassium evaluation in vitreous humor with a sequential injection system. *Talanta*, 79(4), pp.1094-9. Available at: <http://www.ncbi.nlm.nih.gov/pubmed/19615515> [Accessed April 8, 2014].
- Patrick, W.J. & Logan, R.W., 1988a. Free amino acid content of the vitreous humour in cot deaths. *Archives of Disease in Childhood*, 63, pp.660-662.
- Patrick, W.J. & Logan, R.W., 1988b. Free amino acid content of the vitreous humour in cot deaths. *Archives of Disease in Childhood*, 63, pp.660-662.
- Pena, M.J. , de Zeeuw, D., Mischak, H., Jankowski, J., Oberbauer, R., Woloszczuk, W., Benner, J., Dallmann, G., Mayer, B., Mayer, G., Rossing, P. & Heerspink, H.J.L., 2015. Prognostic clinical and molecular biomarkers of renal disease in type 2 diabetes. *Nephrology Dialysis Transplantation*, 30, p.iv86-iv95. Available at: <http://ndt.oxfordjournals.org/lookup/doi/10.1093/ndt/gfv252>.
- Perkins, D.N., Pappin, D.J., Creasy, D.M. & Cottrel, J.S., 1999. Probability-based protein identification by searching sequence databases using mass spectrometry data. *Electrophoresis*, 20(18), pp.3551-67.
- Perper, J.A., 2006. Time of death and changes after death, Part 1: Anatomical Considerations. In W. U. Spitz, ed. *Medicolegal investigation of death: Guidelines for the application of pathology to crime investigation*. Springfield, Illinois: Charles C. Thomas Publishing, pp. 87-127.
- Perry, T.L., Hansen, S. & Gandham, S.S., 1981. Postmortem changes of amino compounds in human and rat brain. *Journal of Neurochemistry*, 36(2), pp.406-410.
- Petersson, S. V., Linden, P., Moritz, T. & Ljung, K., 2015. Cell-type specific metabolic profiling of *Arabidopsis thaliana* protoplasts as a tool for plant systems biology. *Metabolomics*, 11, pp.1679-1689.

- Picard, B., Gagaoua, M., Micol, D., Cassar-Malek, I., Hocquette, J.-F. & Terlouw, C.E.M., 2014. Inverse Relationships between biomarkers and beef tenderness according to contractile and metabolic properties of the muscle. *Agricultural and Food Chemistry*, 62, pp.9808-9818.
- Pittner, S., Monticelli, F.C., Pfisterer, A., Zissler, A., Sanger, A.M., Stoiber, W. & Steinbacher, P., 2015. Postmortem degradation of skeletal muscle proteins: a novel approach to determine the time since death. *International Journal of Legal Medicine*. Available at: <http://link.springer.com/10.1007/s00414-015-1210-6>.
- Pittner, S., Ehrenfellner, B., Monticelli, F.C., Zissler, A., Sanger, A.M., Stoiber, W. & Steinbacher, P., 2016. Postmortem muscle protein degradation in humans as a tool for PMI delimitation. *International Journal of Legal Medicine*, [Epub ahead of print].
- Pla, A., Lemus, L., Valenzuela, A. & Villanueva, E., 1986. Postmortem Activity of the Key Enzymes of Glycolysis. *Z Rechtsmed*, 97, pp.49-59.
- Poloz, Y.O. & O'Day, D.H., 2009. Determining time of death: temperature-dependent postmortem changes in calcineurin A, MARCKS, CaMKII, and protein phosphatase 2A in mouse. *International Journal of Legal Medicine*, 123, pp.305-14. Available at: <http://www.ncbi.nlm.nih.gov/pubmed/19326139> [Accessed January 21, 2014].
- Prieto-Bonete, G., Perez-Carceles, M.D. & Luna, A., 2015. Morphological and histological changes in eye lens: Possible application for estimating postmortem interval. *Legal Medicine*, 17, pp.437-442. Available at: <http://dx.doi.org/10.1016/j.legalmed.2015.09.002>.
- Querido, D., 1990a. Double logarithmic, linear relationship between plasma sodium/potassium concentration ratio and postmortem interval during the 6 - 96 h postmortem period in rats. *Forensic Science International*, 44, pp.125-134.

- Querido, D., 1990b. Linearization of the relationship between postmortem plasma chloride concentration and postmortem interval in rats. *Forensic Science International*, 45, pp.117-128.
- Querido, D. & Phillips, M.R., 2001. Estimation of postmortem interval. Temperature-correction of extracellular abdominal impedance during the first 21 days of death. *Forensic Science International*, 116(2-3), pp.133-8. Available at: <http://www.ncbi.nlm.nih.gov/pubmed/11182264>.
- Rainy, H., 1868. On the cooling of dead bodies as indicating the length of time since death. *Glasgow Medical Journal*, 1, pp.323-30.
- Rathmacher, J.A., Flakoll, P.J. & Nissen, S.L., 1995. A compartmental model of 3-methylhistidine metabolism in humans. *The American Journal of Physiology*, 269(1 Pt 1), pp.E193-8. Available at: <http://www.ncbi.nlm.nih.gov/pubmed/7631776>.
- Rochfort, S., 2005. Metabolomics Reviewed: A new “omics” platform technology for systems biology and implications for natural products research. *Journal of Natural Products*, 68, pp.1813-1820.
- Rognum, T.O., Hauge, S., Oyasaeter, S. & Saugstad, O.D., 1991. A new biochemical method for estimation of postmortem time. *Forensic Science International*, 51(1), pp.139-46. Available at: <http://www.ncbi.nlm.nih.gov/pubmed/1752591>.
- Romanelli, M.C., Gelardi, M., Fiorella, M.L., Tattoli, L., di Vella, D. & Solarino, B., 2012. Nasal ciliary motility: a new tool in estimating the time of death. *International Journal of Legal Medicine*, 126(3), pp.427-33. Available at: <http://www.ncbi.nlm.nih.gov/pubmed/22370997> [Accessed November 25, 2014].
- Sabucedo, A.J. & Furton, K.G., 2003. Estimation of postmortem interval using the protein marker cardiac Troponin I. *Forensic Science International*, 134, pp.11-16. Available at: <http://linkinghub.elsevier.com/retrieve/pii/S037907380300080X> [Accessed

January 7, 2014].

- Sampaio-Silva, F., Magalhaes, T., Carvalho, F., Dinis-Oliveira, R.J. & Silvestre, R., 2013. Profiling of RNA degradation for estimation of post mortem interval. *PLoS One*, 8(2), p.e56507. Available at: <http://dx.plos.org/10.1371/journal.pone.0056507> [Accessed January 7, 2014].
- Santos Júnior, J.C., Mollo Filho, P.C., Guidugli, R.B.F., Nogueira Eberlin M., de Souza Passoa, G., Gomes de Silva, E., Arruda, M.A.Z. & Hoehr, N.F., 2014. Metals and (metallo)proteins identification in vitreous humor focusing on post-mortem biochemistry. *Metallomics*, 6, pp.1801-1807. Available at: <http://xlink.rsc.org/?DOI=C3MT00373F>.
- Sasaki, S., Tsunenari, S. & Kanda, M., 1983. The estimation of the time of death by non-protein nitrogen (NPN) in cadaveric materials. Report 3: Multiple regression analysis of NPN values in human cadaveric materials. *Forensic Science International*, 22(1), pp.11-22. Available at: <http://linkinghub.elsevier.com/retrieve/pii/0379073883901159>.
- Satelli, A. & Li, S., 2011. Vimentin as a potential molecular target in cancer therapy Or Vimentin, an overview and its potential as a molecular target for cancer therapy. *Cell Mol Life Sci.*, 68(18), pp.3033-3046.
- Sato, T., Zaitso, K., Tsuboi, K., Nomura, M., Kusano, M., Shima, N., Abe, S., Ishii, A., Tsuchihashi, H. & Suzuki, K., 2015. A preliminary study on postmortem interval estimation of suffocated rats by GC-MS/MS-based plasma metabolic profiling. *Analytical and Bioanalytical Chemistry*, 407(13), pp.3659-65. Available at: <http://link.springer.com/10.1007/s00216-015-8584-7>.
- Scheltema, R.A., Jankevics, A., Jansen, R.C., Swertz, M.A. & Breitling, R., 2011. PeakML/mzMatch: A file format, Java library, R library, and tool-chain for mass spectrometry data analysis. *Analytical Chemistry*, 83, pp.2786-2793.
- Scheurer, E., Ith, M., Dietrich, D., Kreis, R., Husler, J., Dirnhofer, R. & Boesch,

C., 2005. Statistical evaluation of time-dependent metabolite concentrations: estimation of post-mortem intervals based on in situ <sup>1</sup>H-MRS of the brain. *NMR in Biomedicine*, 18(3), pp.163-72. Available at: <http://www.ncbi.nlm.nih.gov/pubmed/15578674> [Accessed January 21, 2014].

Schmidt, T.M., Wang, Z.J., Keller, S., Heinemann, A., Acar, S., Graessner, J., Schoennagel, B.P., Adam, G., Fischer, R. & Yamamura, J., 2014. Postmortem <sup>31</sup>P magnetic resonance spectroscopy of the skeletal muscle: a -ATP/Pi ratio as a forensic tool? *Forensic Science International*, 242, pp.172-176. Available at: <http://dx.doi.org/10.1016/j.forsciint.2014.06.009>.

Shirley, N.R. & Wood, P.L., 2013. Lipidomics Analysis of Postmortem Interval: Preliminary Evaluation of Human Skeletal Muscle. *Metabolomics*, 3(3), p.127. Available at: <http://www.omicsonline.org/lipidomics-analysis-of-postmortem-interval-preliminary-evaluation-of-human-skeletal-muscle-2153-0769-3-127.php?aid=20119> [Accessed February 21, 2014].

Siddamsetty, A.K., Verma, S.K., Kohli, A., Puri, D. & Singh, A., 2014. Estimation of time since death from electrolyte, glucose and calcium analysis of postmortem vitreous humour in semi-arid climate. *Medicine, Science, and the Law*, 54(3), pp.158-66. Available at: <http://www.ncbi.nlm.nih.gov/pubmed/24166687> [Accessed November 25, 2014].

Singh, D., Prashad, R., Sharma, S.K. & Pandey, A.N., 2006. Estimation of postmortem interval from human pericardial fluid electrolytes concentrations in Chandigarh zone of India: log transformed linear regression model. *Legal Medicine*, 8, pp.279-87. Available at: <http://www.ncbi.nlm.nih.gov/pubmed/16978903> [Accessed November 27, 2014].

Smilde, A.K., Jansen, J.J., Hoefsloot, H.C.J., Lamers, R.J.A.N., van der Greef, J. & Timmerman, M.E., 2005. ANOVA-simultaneous component analysis (ASCA): A new tool for analyzing designed metabolomics data.

*Bioinformatics*, 21(13), pp.3043-3048.

- Smith, C.A., Want, E.J., O'Maille, G., Abagyan, R. & Suizdak, G., 2006. XCMS: processing mass spectrometry data for metabolite profiling using Nonlinear Peak Alignment, Matching, and Identification. *Analytical Chemistry*, 78(3), pp.779-787.
- Sparks, D.L., Slevin, J.T. & Hunsaker, J.C., 1986. 3-Methoxytyramine in the putamen as a gauge of the postmortem interval. *Journal of Forensic Sciences*, 31(3), pp.962-971.
- Statheropoulos, M., Agapiou, A., Zorba, E., Mikedi, K., Karma, S., Pallis, G.C., Eliopoulos, C. & Spiliopoulou, C., 2011. Combined chemical and optical methods for monitoring the early decay stages of surrogate human models. *Forensic Science International*, 210(1-3), pp.154-63. Available at: <http://www.ncbi.nlm.nih.gov/pubmed/21450424> [Accessed January 21, 2014].
- Statheropoulos, M., Agapiou, A., Spiliopoulou, C., Pallis, G.C. & Sianos, E., 2007. Environmental aspects of VOCs evolved in the early stages of human decomposition. *The Science of the Total Environment*, 385(1-3), pp.221-7. Available at: <http://www.ncbi.nlm.nih.gov/pubmed/17669473> [Accessed January 21, 2014].
- Statheropoulos, M., Spiliopoulou, C. & Agapiou, a, 2005. A study of volatile organic compounds evolved from the decaying human body. *Forensic Science International*, 153(2-3), pp.147-55. Available at: <http://www.ncbi.nlm.nih.gov/pubmed/16139103> [Accessed January 21, 2014].
- Sturner, W.Q., 1963. The vitreous humour: postmortem potassium changes. *The Lancet*, 1, pp.807-808.
- Sturner, W.Q. & Gantner, G.E.J., 1964. The postmortem interval. A study of potassium in the vitreous humor. *American Journal of Clinical Pathology*, 42, pp.137-44.

- Sumner, L.W., Lei, Z., Nikolau, B.J., Saito, K., Roessner, U. & Trengove, R., 2014. Proposed quantitative and alphanumeric metabolite identification metrics. *Metabolomics*, 10(6), pp.1047-1049. Available at: <http://link.springer.com/10.1007/s11306-014-0739-6>.
- Sun, T., Zhang, H., Yang, T. & Liu, L., 2013. Changes in ATP levels in rabbit blood and its application for estimation of the postmortem interval. *Journal of Huazhong University of Science and Technology. Medical Sciences*, 33(3), pp.452-6. Available at: <http://www.ncbi.nlm.nih.gov/pubmed/23771677> [Accessed November 25, 2014].
- Sun, T., Yang, T., Zhang, H., Zhuo, L. & Liu, L., 2014. Interpolation function estimates post mortem interval under ambient temperature correlating with blood ATP level. *Forensic Science International*, 238, pp.47-52. Available at: <http://www.ncbi.nlm.nih.gov/pubmed/24642264> [Accessed November 21, 2014].
- Surowiec, I., Orikiiriza, J., Karlsson, E., Nelson, M., Bonde, M., Kyamanwa, P., Karezni, B., Bergstrom, S., Trygg, J. & Normark, J., 2015. Metabolic Signature Profiling as a Diagnostic and Prognostic Tool in Pediatric Plasmodium falciparum Malaria. *Open Forum Infectious Diseases*, 2(2), pp.1-10.
- Sutherland, A., Myburgh, J., Steyn, M. & Becker, P.J., 2013. The effect of body size on the rate of decomposition in a temperate region of South Africa. *Forensic Science International*, 231(1-3), pp.257-262. Available at: <http://dx.doi.org/10.1016/j.forsciint.2013.05.035>.
- Swain, R., Kumar, A., Sahoo, J., Lakshmy, R., Gupta, S.K., Bhardwaj, D.N. & Pandey, R.M., 2015. Estimation of post-mortem interval: A comparison between cerebrospinal fluid and vitreous humour chemistry. *Journal of Forensic and Legal Medicine*, 36, pp.144-148. Available at: <http://dx.doi.org/10.1016/j.jflm.2015.09.017>.
- Swann, L.M., Forbes, S.L. & Lewis, S.W., 2010. Analytical separations of mammalian decomposition products for forensic science: a review.

*Analytica Chimica Acta*, 682(1-2), pp.9-22. Available at:  
<http://www.ncbi.nlm.nih.gov/pubmed/21056711> [Accessed January 21, 2014].

Swift, B., 2006. The Timing of Death. In G. N. Ruty, ed. *Essentials of Autopsy Practice: Current methods and modern trends*. Leicester, UK: Springer-Verlag London, pp. 189-214.

T'Kindt, R., Jankevics, A., Scheltema, R.A., Zheng, L., Watson, D.G., Dujardin, J.-C., Breitling, R., Coombs, G.H. & Decuypere, S., 2010. Towards an unbiased metabolic profiling of protozoan parasites: Optimisation of a Leishmania sampling protocol for HILIC-orbitrap analysis. *Analytical and Bioanalytical Chemistry*, 398(5), pp.2059-2069.

Tavichakorntrakool, R., Prasongwattana, V., Sriboonlue, P., Puapairoj, A., Pongskul, J., Khuntikeo, N., Hanpanich, W., Yenchitsomanus, P., Wongkham, C. & Thongboonkerd, V., 2008. Serial analyses of postmortem changes in human skeletal muscle: A case study of alterations in proteome profile, histology, electrolyte contents, water composition, and enzyme activity. *Proteomics. Clinical Applications*, 2(9), pp.1255-64. Available at: <http://www.ncbi.nlm.nih.gov/pubmed/21136921> [Accessed February 21, 2014].

Thierauf, A., Musshoff, F. & Madea, B., 2009. Post-mortem biochemical investigations of vitreous humor. *Forensic Science International*, 192(1-3), pp.78-82. Available at: <http://www.ncbi.nlm.nih.gov/pubmed/19729257> [Accessed January 7, 2014].

Tolstikov, V. V & Fiehn, O., 2002. Analysis of Highly Polar Compounds of Plant Origin: Combination of Hydrophilic Interaction Chromatography and Electrospray Ion Trap Mass Spectrometry. *Analytical Biochemistry*, 301, pp.298-307.

Tumram, N.K., Bardale, R.V. & Dongre, A.P., 2011. Postmortem analysis of synovial fluid and vitreous humour for determination of death interval: A comparative study. *Forensic Science International*, 204, pp.186-190.

Available at: <http://dx.doi.org/10.1016/j.forsciint.2010.06.007>.

- Tuttle, L.J., Alperin, M. & Lieber, R.L., 2014. Post-mortem timing of skeletal muscle biochemical and mechanical degradation. *Journal of Biomechanics*, 47, pp.1506-1509. Available at: <http://dx.doi.org/10.1016/j.jbiomech.2014.02.019>.
- Unlü, M., Morgan, M.E. & Minden, J.S., 1997. Difference gel electrophoresis: a single gel method for detecting changes in protein extracts. *Electrophoresis*, 18(11), pp.2071-7.
- Usumoto, Y., Hikiji, W., Sameshima, N., Kudo, K., Tsuji, A. & Ikeda, N., 2010. Estimation of postmortem interval based on the spectrophotometric analysis of postmortem lividity. *Legal Medicine*, 12(1), pp.19-22. Available at: <http://www.ncbi.nlm.nih.gov/pubmed/19962931> [Accessed January 21, 2014].
- Vanezis, P. & Trujillo, O., 1996. Evaluation of hypostasis using a colorimeter measuring system and its application to assessment of the post-mortem interval ( time of death ). *Forensic Science International*, 78, pp.19-28.
- Vass, A.A., 2001. Beyond the grave - understanding human decomposition. *Microbiology Today*, 28, pp.190-192.
- Vass, A.A., Barshick, S., Sega, G., Caton, J., Skeen, J.T., Love, J.C. & Synsteliën, J.A., 2002. Decomposition chemistry of human remains: a new methodology for determining the postmortem interval. *Journal of Forensic Sciences*, 47(3), pp.542-53. Available at: <http://www.ncbi.nlm.nih.gov/pubmed/12051334>.
- Vass, A.A., 2011. The elusive universal post-mortem interval formula. *Forensic Science International*, 204(1-3), pp.34-40. Available at: <http://www.ncbi.nlm.nih.gov/pubmed/20554133> [Accessed January 21, 2014].
- Wang, Z., Deurenberg, P., Matthews, D.E. & Heymsfield, S.B., 1998. Urinary 3-

methylhistidine excretion: association with total body skeletal muscle mass by computerized axial tomography. *Journal of Parenteral and Enteral Nutrition*, 22(2), pp.82-86. Available at:

<http://pen.sagepub.com/content/22/2/82.short>.

Warther, S., Sehner, S., Raupach, T., Puschel, K. & Anders, S., 2012. Estimation of the time since death: post-mortem contractions of human skeletal muscles following mechanical stimulation (idiomuscular contraction). *International Journal of Legal Medicine*, 126(3), pp.399-405. Available at: <http://www.ncbi.nlm.nih.gov/pubmed/22245837> [Accessed January 21, 2014].

Watkins, S.M. & German, J.B., 2002. Toward the implementation of metabolomic assessments of human health and nutrition. *Current Opinion in Biotechnology*, 13, pp.512-516.

Wehner, F., Wehner, H. & Schieffer, M.C., 1999. Delimitation of the time of death by immunohistochemical detection of insulin in pancreatic  $\beta$ -cells. *Forensic Science International*, 105, pp.161-169.

Wilkins, M.R., Sanchez, J., Gooley, A.A., Appel, R.D., Humphery-Smith, I., Hochstrasser, D.F. & Williams, K.L., 1995. Progress with Proteome Projects: Why all Proteins Expressed by a Genome Should be Identified and How To Do It. *Biotechnology and Genetic Engineering Reviews*, 13, pp.19-50.

Wingerd, B., 2014. *The human body: Concepts of anatomy and physiology* 3rd ed. D. Troy & L. Bonazzoli, eds., Baltimore, MD: Lippincott Williams & Wilkins.

Wingerd, B.D. & Stain, G., 1988. *Rat dissection manual*, Baltimore & London: The Johns Hopkins university press.

Wishart, D.S., Tzur, D., Knox, C., Eisner, R., Guo, A.C., Young, N., Cheng, D., Jewell, K., Arndt, D., Sawhney, S., Fung, C., Nikolai, L., Lewis, M., Coutouly, M.A., Forsythe, I., Tang, P., Shrivastava, S., Jeroncic, K., Stothard, P., Amegbey, G., Block, D., Hau, D.D., Wagner, J., Miniaci, J.,

- Clements, M., Gebremedhin, M., Guo, N., Zhang, Y., Duggan, G.E., MacInnis, G.D., Weljie, A.M., Dowlatabadi, R., Bamfort, F., Clive, D., Greiner, R., Li, L., Marrie, T., Sykes, B.D., Vogel, H.J. & Querengesser, L., 2007. HMDB: The human metabolome database. *Nucleic Acids Research*, 35(Database issue), pp.D521-D526.
- Wishart, D.S., Jewison, T., Guo, A.C., Wilson, M., Knox, C., Liu, Y., Djoumbou, Y., Mandal, R., Aziat, F., Dong, E., Bouatra, S., Sinelnikov, I., Arndt, D., Xia, J., Liu, P., Yallou, F., Bjorn Dahl, T., Perez-Pineiro, R., Eisner, R., Allen, F., Neveu, V., Greiner, R. & Scalbert, A., 2013. HMDB 3.0--The Human Metabolome Database in 2013. *Nucleic Acids Research*, 41(D1), pp.D801-D807. Available at: <http://nar.oxfordjournals.org/lookup/doi/10.1093/nar/gks1065>.
- Wu, H., Liu, T., Ma, C., Xue, R., Deng, C., Zeng, H. & Shen, X., 2011. GC/MS-based metabolomic approach to validate the role of urinary sarcosine and target biomarkers for human prostate cancer by microwave-assisted derivatization. *Analytical and Bioanalytical Chemistry*, 401, pp.635-646.
- Xia, J., Psychogios, N., Young, N. & Wishart, D.S., 2009. MetaboAnalyst: A web server for metabolomic data analysis and interpretation. *Nucleic Acids Research*, 37(Web Server issue), pp.W652-W660.
- Xia, J., Mandal, R., Sinelnikov, I.V., Broadhurst, D. & Wishart, D.S., 2012. MetaboAnalyst 2.0-a comprehensive server for metabolomic data analysis. *Nucleic Acids Research*, 40(Web Server issue), pp.W127-W133.
- Xiao, J.H. & Chen, Y.C., 2005. A study on the relationship between the degradation of protein and the postmortem interval. *Fa Yi Xue Za Zhi (Journal of Forensic Medicine)*, 21(2), pp.110-2.
- Yadav, J., Deshpande, A., Arora, A., Athawal, B.K. & Dubey, B.P., 2007. Estimation of time since death from CSF electrolyte concentration in Bhopal region of central India. *Legal Medicine*, 9(6), pp.309-13. Available at: <http://www.ncbi.nlm.nih.gov/pubmed/17616422> [Accessed November 21, 2014].

- Yates, L.D., Dutson, T.R., Caldwell, J. & Carpenter, Z.L., 1983. Effect of temperature and pH on the post-mortem degradation of myofibrillar proteins. *Meat Science*, 9(3), pp.157-179.
- Yi, L., He, J., Liang, Y.-Z., Yuan, D.-L. & Chau, F.-T., 2006. Plasma fatty acid metabolic profiling and biomarkers of type 2 diabetes mellitus based on GC / MS and PLS-LDA. *FEBS Letters*, 580, pp.6837-6845.
- Young, S.T., Wells, J.D., Hobbs, G.R. & Bishop, C.P., 2013. Estimating postmortem interval using RNA degradation and morphological changes in tooth pulp. *Forensic Science International*, 229(1-3).
- Zang, X.-H., Wu, Q.-H., Zhang, M.-Y., Xi, G.-H. & Wang, Z., 2009. Developments of Dispersive Liquid-Liquid Microextraction Technique. *Chinese Journal of Analytical Chemistry*, 37(2), pp.161-168. Available at: <http://linkinghub.elsevier.com/retrieve/pii/S1872204008600821> [Accessed January 7, 2014].
- Zapico, S.C., Menéndez, S.T. & Núñez, P., 2014. Cell death proteins as markers of early postmortem interval. *Cellular and Molecular Life Sciences: CMLS*, 71, pp.2957-62. Available at: <http://www.ncbi.nlm.nih.gov/pubmed/24297385> [Accessed November 25, 2014].
- Zhang, M., Wen, C., Zhang, Y., Sun, F., Wang, S., Ma, J., Lin, K., Wang, X., Lin, G. & Hu, L., 2015. Serum metabolomics in rats models of ketamine abuse by gas chromatography - mass spectrometry. *Journal of Chromatography B*, 1006, pp.99-103. Available at: <http://dx.doi.org/10.1016/j.jchromb.2015.10.037>.
- Zhu, B.L., Ishikawa, T., Michiue, T., Li, D.R., Zhao, D., Oritani, S., Kamikodai, Y., Tsuda, K., Okazaki, S. & Maeda, H., 2006. Postmortem cardiac troponin T levels in the blood and pericardial fluid. Part 1. Analysis with special regard to traumatic causes of death. *Legal Medicine*, 8(2), pp.86-93.
- Zhu, B.L., Ishikawa, T., Michiue, T., Li, D.R., Zhao, D., Kamikodai, Y., Tsuda,

K., Okazaki, S. & Maeda, H., 2006. Postmortem cardiac troponin T levels in the blood and pericardial fluid. Part 2: Analysis for application in the diagnosis of sudden cardiac death with regard to pathology. *Legal Medicine*, 8(2), pp.94-101.

Zubay, G.L., Parson, W.W. & Vance, D.E., 1995. *Principles of Biochemistry* E. M. Sievers & R. P. Steffek, eds., Dubuque, IA: Wm. C. Brown Publishers.